FTIR measurement of monomer fractions in dilute alcohol-acetone systems for the evaluation of the sPC-SAFT EoS

by

Francois Johan KRUGER

Thesis presented in partial fulfilment
of the requirements for the Degree

of

MASTER OF SCIENCE IN ENGINEERING
(CHEMICAL ENGINEERING)

in the Faculty of Engineering
at Stellenbosch University

Supervisor
Prof. A.J. Burger

December 2013

Declaration

By submitting this thesis electronically, I declare that the entirety of the work contained therein is my own, original work, that I am the sole author thereof (save to the extent explicitly otherwise stated), that reproduction and publication thereof by Stellenbosch University will not infringe any third party rights and that I have not previously in its entirety or in part submitted it for obtaining any qualification.

Francois Johan KRUGER

2013 / 09 / 20

Abstract

The simplified Perturbed-Chain Statistical Associating Fluid Theory (sPC-SAFT) is characterised by the dual advantages of decreased computational intensity, while remaining accurate for a variety of systems. Vapour-liquid equilibrium data are used to generate equation of state parameters. However, incorporating monomer fraction data into the parameter regression has long been advocated as a good, or even preferred, practice. Therefore, the monomer fraction data of dilute alcohol-acetone systems were analysed in this study. A small stainless steel sample vessel was constructed with temperature control, manual pressure control and a mechanism for liquid phase analysis via infrared spectroscopy.

The performance of the spectrometer was verified by comparison with the ethanol – n-hexane data of von Solms et al. (2007), after which new monomer fraction data were obtained for dilute solutions (between 0.01 and 1.5 mol%) of methanol, ethanol, 1-propanol and 2-propanol in acetone near 23 °C.

For dilute alcohol-acetone systems it was found that the propanols had the highest monomer fractions, and methanol the lowest. With increasing alcohol concentration, the monomer fractions decreased exponentially to values of 0.4 and 0.1 for methanol and the other alcohols respectively. The excess availability of hydrogen bond acceptors in the mixtures explains the equivalency observed for ethanol, 1-propanol and 2-propanol.

For dilute acetone-alcohol systems it was found that, especially for methanol and ethanol, there was a pronounced trend towards acetone monomer fractions of 1 at infinite dilution. For the acetone – 2-propanol system, a previously unrecorded monomer peak was observed and quantified. Acetone monomer fractions tended to decrease as alcohol chain-length increased, showing that acetone could more easily penetrate the hydrogen bond network of the solvent when the solvent-solvent bonds were weaker.

Monomer fraction data were compared to predictions for the sPC-SAFT scheme and parameters combinations published in the literature. The experimental data were accurately modelled using modified association parameters such that the solute associates strongly ($\varepsilon^{AB}\approx10^{3}$ $\kappa\approx1$), while the solvent parameters were decreased ($\varepsilon^{AB}\approx10^{2}$ $\kappa\approx10^{-3}$) to give a weakened solvent association effect. The difficulty for the dilute solute in penetrating the solvent bonding network appeared to be similar to the hydrophobic effect.

Two new association schemes were proposed for acetone, assigning a single (N) or two (2N) negative association sites to represent the oxygen valence electron pairs. These schemes showed relative success in modelling acetone as the solvent in the mixture, while not being able to predict acetone monomer fractions when acetone was the solute. For dilute acetone-alcohol systems, the data were best described using the 2B model for acetone, while the best choice of scheme for the alcohol varied from system to system.

For dilute alcohol-acetone mixtures it was generally found that a 2B-N model (with modified association parameters) provided the best fit to those experimental data. Accurate modelling below 0.1 mol% was difficult to attain with average errors decreasing to the order of 10% when this area was excluded. In this highly dilute region, not one of the models could describe the rapid change in (monomer fraction) gradient sufficiently while simultaneously offering accurate predictions over the entire experimental range.

Uittreksel

Die *sPC-SAFT* of *simplified Perturbed-Chain Statistical Associating Fluid Theory* toestandsvergelykings word wyd gebruik as gevolg van sy goeie akkuraatheid vir ‘n wye reeks sisteme, ten spyte van verminderde berekeningsintensiteit. Die parameters vir dié toestandsvergelyk word afgelei van fase-ewewig data, maar monomeer fraksie data word voorgestel vir die verbetering van (veral) die assosiasie parameters. Ten opsigte hiervan, was alkohol-asetoon sisteme bestudeer en hul monomeer fraksies gemeet. ‘n Staal reaktor was ontwerp (met ‘n temperatuurbeheerstelsel sowel as drukbeheer) om vloeistof monsters voor te berei vir analise d.m.v. infrarooi-spektroskopie.

Die akkuraatheid van die eksperimentele apparaat is bewys deur nabootsing van etanol – *n*-heksaan data van von Solms *et al.* (2007), waarna nuwe monomeer fraksie data gegenereer is vir verdunde mengsels (0.01 tot 1.5 mol%) van metanol, etanol, 1- en 2-propanol met asetoon by 23 °C.

Metanol monomeer fraksies het eksponensieël afgeneem na 0.4, terwyl etanol en propanol fraksies afgeneem het na ‘n gemene waarde van ongeveer 0.1. Hierdie tendens word toegeskryf aan ‘n oormaat van toeganklike waterstofbindingontvangers in hierdie mengsels.

Vir verdunde asetoon-alkohol sisteme is daar ‘n tendens, (veral vir verdunnings met metanol en etanol) vir die monomer fraksies om te neig na 1 by oneindige verdunning. ‘n Monomeer piek is ook waargeneem vir die asetoon – 2-propanol sisteem. Hierdie piek is nie voorheen gesien in ander studies nie en dit is ook die eerste keer wat sulke data gekwantifiseer is. Daar is bevind dat asetoon monomeer fraksies afneem soos alkohol kettinglengte toeneem.

Die gegenereerde monomeer fraksie data word vergelyk met verskeie *sPC-SAFT* parameterstelle vanuit die literatuur. Oor die algemeen, is die beraamde fraksie veel hoër as die eksperimentele data wanneer die 2B/3B/2C skemas met ‘n nie-assosiërende asetoon molekuul gemodelleer word. Wanneer die 2B parameters van von Solms *et al.* (2004) gebruik word, toon die beraming ‘n drastiese onderskatting van die data.

Om ‘n akkurate beraming van die monomeer fraksie data te kry, moet die assosiasie parameters van die opgeloste stof vermeerder word (met $\varepsilon^{AB}\approx10^{3}$ $\kappa\approx1$) terwyl die oplosmiddel s’n drasties verswak moet word (met $\varepsilon^{AB}\approx10^{2}$ $\kappa\approx10^{-3}$). Hierdie patroon kan vergelyk word met die hidrofobiese effek waar die kragte binne die oplosmiddel ‘n netwerk vorm wat die opgeloste stof uitstoot.

Twee nuwe assosiasie skemas word ook voorgestel vir asetoon waar onderskeidelik een (N) en twee (2N) negatiewe sones, wat die valenselektroonpare op die suurstofatoom voorstel, aan asetoon geheg word. Hierdie twee skemas het relatiewe sukses getoon in die modellering van verdunde alkohol-asetoon sisteme terwyl dit ‘n swak beskrywing van die verdunde asetoon-alkohol mengsels voorspel het. ‘n Gewysigde 2B asetoon skema gee ‘n goeie beskrywing van die eksperimentele data. In hierdie geval, is die keuse van alkohol skema minder belangrik, terwyl die waardes van die assosiasie parameters verminder moet word.

Vir verdunde alkohol-asetoon mengels word daar bevind dat ‘n 2B-N model met nuwe assosiasie parameters die beste passing van die eksperimentele data gee. Daar was ook bevind dat die modelle se akkuraatheid drasties afneem (met fout vermeerdering in die orde van 10%) wanneer die konsentrasie van die opgeloste stof minder as 0.1 mol% is.

Acknowledgements

The financial assistance of the National Research Foundation (NRF) towards this research is hereby acknowledged. Opinions expressed and conclusions arrived at, are those of the author and are not necessarily to be attributed to the NRF.

In the completion of this research, several individuals need to be thanked for their knowledge and/or support in various endeavours:

- Prof André Burger, for all your guidance at meetings and financial assistance from the department, without which none of this research could have been completed
- Dr Cara Schwarz, for the insightful discussions at meetings as well as all your assistance in acquiring many of the experimental apparatus
- Dr Paul Verhoeven, for all your invaluable assistance with respect to the FTIR experiments
- Mr LJ du Preez, for your help with designing the sample vessel and setting-up at the experimental apparatus at the Geology building
- *Messrs.* Jannie Barnard and Anton Cordier, for building the sample vessel and holder for the transmission cell
- Dr Riaan de Villiers, for helping to define the objectives of this study and always being available for consultation whether it be related to thermodynamics or programming
- Dr Bruce Bartlett, for your helpful discussions with respect to mathematical routines and the many tough squash games
- Dr Kiran Dellimore, for all the guidance with respect to managing post-graduate research and the many beers after, and at times during, squash
- Francois Roux, for the years of friendship and truly epic sporting battles through our shared burden of engineering studies – it is a distraction I could not have done without
- Johann Potgieter, for all the coffees and laughs, without which I would not have had the energy to complete this work

Finally I would also like to thank Cheree Rex-Marillier for all her love and support whilst I was completing this study. Without you I would not have been able to succeed. In the same breath I would also like to thank my mother, Elda, and father, Eugene, for all their encouragement and understanding.

Contents

List of figures

List of tables

Chapter 1: Introduction

1.1 Background

The Statistical Associating Fluid Theory (SAFT) is an equation of state (EoS) which was developed specifically to deal with the complexity of modelling associating compounds and systems. The SAFT formalism (or at least the chain and association terms within the SAFT formalism) finds its roots in a series of four papers authored by Wertheim (1984a) (1984b) (1986a) (1986b). The series is entitled *Fluids with Highly Directional Attractive Forces* and in it Wertheim develops a statistical thermodynamic model for fluids with a repulsive core and attractive sites capable of formation chains, which he termed the first-order thermodynamic perturbation theory (TPT) (Economou, 2002). TPT is very complex and lies beyond the scope of this investigation; a thorough discussion thereof can be found in the dissertation of Peery (2003).

A few years later, SAFT first appeared in the form by which it is recognised by today (Chapman et al., 1989) (Chapman et al., 1990). Soon after Chapman's version of SAFT was published, a slightly revised version of the formalism was published by Maciej Radosz (one of Chapman's co-workers) and Stanley Huang (1990). Their work contained parameters for more than 100 real fluids and became the more popular/accepted version of SAFT (in many sources it is shown as the original version) (Economou, 2002). Here it is referred to as SAFT-HR, although it is also known as CK-SAFT (Kontogeorgis & Folas, 2010, p.221). Here "CK" refers to Chen and Kreglewski who developed a modified square-well potential function, which simulates soft repulsion and was incorporated into SAFT as well as having been used earlier in the Boublik-Alder-Chen-Kreglewski (BACK) EoS (Yelash et al., 2005).

The original SAFT EoS is expressed in terms of the residual Helmholtz energy (a^r) and uses associated chains of hard spheres as its reference fluid (Chapman et al., 1989):

$$a^r = a^{seg} + a^{chain} + a^{assoc} \qquad \text{EQ 1.1}$$

The residual Helmholtz energy is written here as the sum of three parts: a^{seg} refers to the change in a^r due to interaction between segments e.g. Lennard-Jones (LJ) interactions; a^{chain} takes into account the effect the presence of covalent bonds between segments; and finally a^{assoc} accounts for specific site-site interactions which are representative of hydrogen bonds.

The segment term is resolved into two parts, consisting of a hard sphere reference (a^{hs}) and a perturbation, a dispersion force (a^{disp}) (Chapman et al., 1990). Hence:

$$a^r = \left(a^{hs} + a^{disp}\right) + a^{chain} + a^{assoc}$$

EQ 1.2

Chains are formed by super-imposing an infinitely strong association on the hard spheres to model covalent bonds. Segments are labelled from 1 to m in Figure 1. TPT specifies that type 1 may only bond to type 2, type 2 only to type 1 and 3 etc. The model in the figure also has two association sites, A and B. Note that it is not specified in TPT where these sites should be.

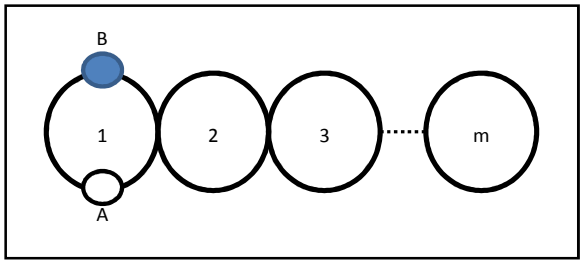

Figure 1: Model of a 2B type chain molecule e.g. alcohol. Reprinted (adapted) with permission from Chapman *et al.* (1990). Copyright 2012 American Chemical Society.

The use of an association scheme is implicitly incorporated in the development of all SAFT variants. The 2B association scheme (typical of alcohols) is shown in Figure 1, where A represents the two lone electron pairs on an oxygen atom and B represent the hydrogen atom in the O-H bond. The site A (electron donor) has the ability to associate with the hydrogen atom (site B – electron acceptor) of another alcohol molecule. The 2C association scheme (one electron donor site and one bipolar) was recently developed by de Villiers *et al.* (2011b) at Stellenbosch University and has shown promising applications in the description of mixtures containing alcohols.

While many modified SAFT equations considered different methods to model the various energy terms or change the type of reference fluid, the perturbed-chain SAFT (PC-SAFT) Gross and Sadowski (2001) incorporated a fundamental change in terms of how the reference is specified. A hard sphere reference, with a dispersion force, is again used. But the critical difference is that the hard spheres are formed into chains first, meaning that dispersion perturbation is applied to a chain fluid rather than a mixture of hard spheres.

This difference is highlighted in Figure 2, with the black circles representing hard spheres and the dotted line representing the dispersion force applied in each case.

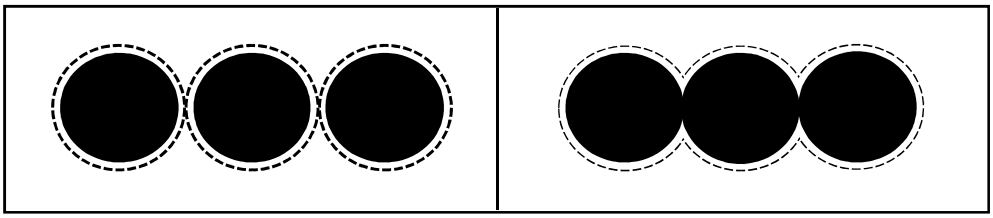

Figure 2: The main difference between SAFT (left) and PC-SAFT (right) is shown by dispersive hard spheres joined into chains (left), versus dispersive hard chains (right)

The first PC-SAFT paper was published in 2001 and only described non-associating compounds (Gross & Sadowski, 2001). It was later applied to associating compounds (Gross & Sadowski, 2002) and has become very widely used (Diamantonis & Economou, 2011). The simplified PC-SAFT (sPC-SAFT) was developed by von Solms *et al.* (2003) specifically to decrease the computational requirements.

Parameters are required for the various energy terms with the SAFT (and by extension, for the PC-SAFT) EoS. For non-associating compounds, three parameters pure component are required (Gross & Sadowski, 2001):

- m number of segments per chain
- σ temperature-independent segment diameter[1]
- ε_i the depth of the potential well[2]

For associating compounds, a further two pure component parameters are required (Chapman et al., 1989):

- ε^{AB} energy of association
- κ volume of association

These five parameters are usually fitted to pure component vapour pressure and liquid density data (Economou, 2002), but the addition of spectroscopic data have been considered as a preferred method for parameterization as early as the original SAFT formulation (Chapman et al., 1990).

[1] Sometimes parameter is given as the temperature-independent soft-core volume $\left(v^{\infty}\right)$ i.e. σ^3

[2] The symbol μ^0 is also used in SAFT-HR (Kontogeorgis & Folas, 2010, p.226)

Monomer fraction data are related to the concept of the unbonded fraction (X^A and X^B for scheme presented in Figure 2) developed within the association term of the SAFT formalism. Many sources advocate the use of spectroscopic data in this regard, but there are still surprisingly little data available for this application (Kontogeorgis & Folas, 2010, pp.202-203, 207). The majority of research of interest here has been done on alcohol-hydrocarbon systems (Asprion et al., 2001) (von Solms et al., 2007).

One obvious drawback of the original SAFT formulation is that polar interactions are not explicitly accounted for, but rather lumped in with the dispersion term (Economou, 2002) or qualitatively accounted for by the association term (Tan et al., 2008). To this end, terms have been developed to account explicitly for polar interactions: Jog and Chapman (1999) (JC) and Gross and Vrabec (2006) (GV). When the JC extension incorporated with PC-SAFT, the resultant EoS is referred to as the polar PC-SAFT (PCP-SAFT) EoS and requires the fraction of polar segment (χ_P) as an additional parameter (Jog et al., 2001). The GV extension to PC-SAFT is referred to as PC – Polar SAFT (PC-PSAFT) and requires the number of polar segments per molecule (n_p) which is usually set to 1 (Gross & Vrabec, 2006). The JC and GV terms were recently extended to the sPC-SAFT EoS by de Villiers *et al.* (2011a) to create the sPC-SAFT-JC and sPC-SAFT-GV equations of state.

Of specific interest to this investigation is the application whereby infrared (IR) spectroscopy is used to quantify hydrogen bonding (association) phenomena (Asprion et al., 2001) and how they can be applied within various sPC-SAFT frameworks. Spectroscopy can be used to calculate the relative concentrations of associating and non-associating species within a given system. Concentration data for the non-associating species (referred to as monomers) can be used to evaluate the performance of a SAFT EoS since monomer fractions are calculated indirectly in the a^{assoc} term. Therefore this link (between the SAFT association framework and experimentally determinable data) provides direct indication of EoS performance in describing hydrogen bonding, as well as an useful mechanism EoS parameters to be adjusted and optimised. By more accurately accounting for specific forces (e.g. dispersion, association and polar), an EoS can be optimised to the point where it not only accurately predicts the data sets to which the parameters were fitted, but also exhibits good predictive capabilities for systems and data sets to which it was not fitted.

SAFT related IR-studies have traditionally examined either pure water and alcohols, or a binary mixture of alcohols with alkanes. Acetone provides an interesting opportunity for study within this field. It is well known, for instance, that acetone (and chloroform) do not self-associate (or at least do so very weakly; Economou *et al.* 1991), but when mixed together they form a strongly associating

mixture (Kontogeorgis & Folas, 2010, pp.338-39). The hydrogen-bonding nature of acetone in a mixture with a strongly self-associating solvent, such as an alcohol, thus presents simultaneously a research opportunity and a thermodynamic modelling challenge.

1.2 Problem statement

The SAFT formalism in general and in particular the sPC-SAFT EoS (and the polar variation thereof) have shown great potential in the modelling of various complex systems (de Villiers et al., 2011a). These theories are however dependent on the existence of good data for their parameterisation. Spectroscopic data are especially useful for the parameterisation of association theories (as it directly describes the effects of association), but related data are very limited. Furthermore, the SAFT formalism is still very much in a development phase with promising new variations such as the 2C association scheme yet to be fully explored. A need therefore exists for not only reliable new spectroscopic data to be produced, but also for the evaluation of published parameters (derived for several of the sPC-SAFT variants) against this new data and the possible regression of new and improved EoS parameters.

1.3 Project aims and objectives

1.3.1 Overarching aim

This research is concerned with the evaluation of the following statement:

"The fraction of monomers present in various alcohol-acetone systems can be quantitatively determined by FTIR spectroscopy such that thermodynamic models may be evaluated within the sPC-SAFT framework."

It was attempted to either prove or disprove this statement by investigating the infrared spectra of these mixtures at constant temperature, with concentration as a variable. The spectral data will provide quantitative information as to the concentration of (nonhydrogen-bonded) monomers present in the mixture relative to the (hydrogen-bonded) polymeric species. These data can then be used to propose new regression parameters or association schemes with the sPC-SAFT framework. These new formulations can then be evaluated by performing a comparison between the new parameters and those obtained from regression using VLE data only.

1.3.2 Project objectives

The following objectives were met during this research:

- Validate the accuracy of the spectroscopic method by comparison with known results
- Determine whether the monomer fractions of both the alcohol and acetone may be determined by FTIR spectroscopy
- Use the monomer data to fit new association parameters within sPC-SAFT-framework
- Compare the relative performance of the new and old parameters

1.4 Significance of research

The success of this research could be seen as a step forward not only in the understanding of these systems and the intermolecular interactions of their components, but also the development of SAFT.

Consider the following quote (Jog et al., 1999b):

"SAFT offers advantages to industry today, but SAFT has not been fully optimized. In a sense, SAFT exists in a Redlich-Kwong form prior to transformation by a Soave or a Peng and Robinson. As recent theoretical extensions are applied and as researchers fine-tune the SAFT model, the predictive capabilities and range of applicability of the model will increase."

Despite significant work in the last *ca.* ten years, it would seem that this statement is still valid presently (Kontogeorgis & Folas, 2010, p.249). This research also adds to the relatively small, as stated by Kontogeorgis and Folas (2010, p.207), body of work involving the use of spectroscopic data for modelling of associating systems. Stimulating research in this specific field is of importance as the use of this data has been considered as the preferred method of parameterization even in the original SAFT formulation (Chapman et al., 1990).

Building the database of pure component and mixture parameters is seen as an important part in the development of the SAFT (Matzopoulos, 2010). By generating new spectroscopic data for methanol–, ethanol–, 1-propanol– and 2-proponal – acetone systems, the EoS can be evaluated in description of these very complex systems. These new data also presents the opportunity to develop new mechanisms within the SAFT framework for optimisation and improvement of the family of EoSs as a whole.

Chapter 2: Literature review

This literature review illustrates the theoretical basis for the experimental work and modelling endeavours described in this project. The initial focus is on the PC-SAFT EoS and its development. This relatively new branch of thermodynamics has seen many recent additions and the discussion leads naturally to association and hydrogen-bonding, specifically related to systems containing alcohols. Infrared spectroscopy is used to describe and quantify the association phenomena.

2.1 The Perturbed Chain Statistical Associating Fluid Theory

PC-SAFT was developed by Joachim Gross and Gabriele Sadowski (2000) (2001) (2002) in the early 2000s. The important departure from the original SAFT is that the PC-SAFT EoS uses a hard chain as reference, rather than the hard spheres in the original SAFT. The basis of what came to be known as the Perturbed Chain SAFT EoS was first seen in an article published by Joachim Gross and Gabrielle Sadowski (2000). The hard-chain reference was developed by incorporating the second-order perturbation theory of Barker and Henderson (1967) and using equivalent modified square-well potential to that developed by Chen and Kreglewski (1977) (Gross & Sadowski, 2001). The use of this reference fluid does however not drastically alter the structure of PC-SAFT compared to SAFT-HR, with only the dispersion term requiring modification (Diamantonis & Economou, 2011).

2.1.1 Development of PC-SAFT

Real substances were as described non-associating compounds with the formulation given in terms of the compressibility. The formulation for associating compounds was published a year later (Gross & Sadowski, 2002), giving the full equation as:

$$Z = Z^{id} + Z^{hc} + Z^{disp} + Z^{assoc}$$

EQ 2.1

where the superscripts represent the ideal, hard chain, dispersion and association contributions.

The formulation is shown in terms of the reduced residual Helmholtz free energy as (von Solms et al., 2003):

$$\tilde{a} = \frac{A}{NkT} = \tilde{a}^{id} + \tilde{a}^{hc} + \tilde{a}^{disp} + \tilde{a}^{assoc}$$

EQ 2.2

where A is the Helmholtz free energy [J]
$\tilde{a}^{type}$ is the reduced Helmholtz energy contribution of type
N is the number of molecules
k is Boltzman's constant [1.380 650 x10^{-23} J/K]
T is temperature [K]

The development of the terms in EQ 2.1 and EQ 2.2 is described below.

(A) The hard chain term

The hard chain reference is made up of two parts. It is a summation of the hard sphere and chain terms used in the original SAFT and SAFT-HR formulations. The hard sphere term is based on the Carnahan-Starling equation (Economou, 2002) while the chain term finds its roots in Wertheim's TPT (Diamantonis & Economou, 2011).

Pure component

Carnahan and Starling (1969) derived a compressibility equation for non-attracting rigid spheres. Ree & Hoover (1964) developed a Pade approximant given in the form of a reduced virial expansion. Carnahan and Starling then simplified the virial equation by postulating that the coefficients could be represented by a geometric series of integers. The resultant expression for the hard sphere contribution is shown here in terms of the reduced residual Helmholtz energy as (Economou, 2002):

$$\tilde{a}^{hs} = m\frac{4\eta - 3\eta^2}{(1-\eta)^2}$$

EQ 2.3

and the hard sphere compressibility as (Huang & Radosz, 1990):

$$Z^{hs} = m\frac{4\eta - 2\eta^2}{(1-\eta)^3}$$

EQ 2.4

where m is number of spherical elements per molecule
η is the reduced density

The reduced density is determined as a function of the closest-packed hard core volume:

$$\eta = \frac{\pi N_{AV}}{6}\rho m d^3$$
$$\Downarrow$$
$$\eta = 0.74048\rho m v^0$$

EQ 2.5

where ρ is the molar density
d is the temperature-dependent segment diameter
v^0 is the close-packed hard core volume
0.74048 is the packing factor of spheres

The definition of the temperature-dependent hard core diameter and volume, which is determined using the Barker-Henderson (1967) integral:

$$d = \int_0^{\sigma}\left[1-\exp\left(\frac{-u(r)}{kT}\right)\right]dr$$

EQ 2.6

where u(r) is the pair potential
r radial distance between segments

Chen & Kreglewski (1977) proposed a modified square-well potential, which approximates soft-repulsion:

$$u(r) = \begin{cases} \infty & r < \sigma - s \\ 3\varepsilon & \sigma - s \le r < \sigma \\ -\varepsilon & \sigma \le r < \lambda\cdot\sigma \\ 0 & r \ge \lambda\cdot\sigma \end{cases}$$

EQ 2.7

where s is set as 0.12σ
λ is the reduced well width

The repulsion step has a height parameter of 3ε and a width of 0.12σ, which empirically fitted for the description of smaller molecules such as short-chain alkanes (Yelash et al., 2005). Solving for EQ 2.6 and EQ 2.7, the temperature-dependent diameter is calculated as:

$$d_i = \sigma_i\left[1 - C\exp\left(\frac{-3\varepsilon_i}{kT}\right)\right]$$

EQ 2.8

$$v^0 = v^\infty \left[1 - C\exp\left(\frac{-3\varepsilon_i}{kT}\right)\right]^3$$

EQ 2.9

where C is assigned the value of 0.12
ε_i is the depth of the potential well [J]

C is set as specified, except for hydrogen, which is set as 0.241 (Economou, 2002).

The pure compound chain term is given by (Huang & Radosz, 1990):

$$\tilde{a}^{chain} = (1-m)\ln\left(g_{ii}^{hs}(\sigma_{ii})\right)$$

EQ 2.10

where g_{ii}^{hs} is radial distribution function of hard spheres

g_{ii} is the pair correlation function for the interaction of spheres in the mixture, evaluated at the contact point. g(d) is also referred to as the radial distribution function (RDF) and gives the factor by which the average density must be multiplied to attain the mean local density at a given point (Widom, 2002, pp.88-89, 102-103). EQ 2.10 reduces to (Huang & Radosz, 1990):

$$\tilde{a}^{chain} = (1-m)\ln\left(\frac{1-0.5\eta}{(1-\eta)^3}\right)$$

EQ 2.11

The chain term in terms of compressibility is:

$$Z^{chain} = (1-m)\frac{2.5\eta - \eta^2}{(1-\eta)(1-0.5\eta)}$$

EQ 2.12

Therefore, the hard chain term becomes:

$$\tilde{a}^{hc} = m\frac{4\eta - 3\eta^2}{(1-\eta)^2} - (m-1)\ln\left(\frac{1-0.5\eta}{(1-\eta)^3}\right)$$

EQ 2.13

$$Z^{hc} = m\frac{4\eta - 2\eta^2}{(1-\eta)^3} - (m-1)\frac{2.5\eta - \eta^2}{(1-\eta)(1-0.5\eta)}$$

EQ 2.14

Extension to mixtures

The first modification required for mixtures is to change the segment number (m) to a mean segment number. This is given by the following equation (Gross & Sadowski, 2001):

$$\bar{m} = \sum_i x_i m_i$$

EQ 2.15

The hard sphere contribution may be written in terms of the reduced Helmholtz energy (on a per segment basis) by using the full Carnahan-Starling equation, including Boublik (1970) & Mansoori *et al.* (1971) (Gross & Sadowski, 2001):

$$\tilde{a}^{hs} = \frac{A^{hs}}{N_{hs}kT} = \frac{1}{\xi_0}\left[\frac{(\xi_2)^2 + 3\xi_1\xi_2\xi_3 - 3\xi_1\xi_2(\xi_3)^2}{\xi_3(1-\xi_3)^2} - \left[\xi_0 - \frac{(\xi_2)^2}{(\xi_3)^2}\right]\ln(1-\xi_3)\right]$$

EQ 2.16

with

$$\xi_{k=0,1,2,3} = \frac{\pi N_{AV}}{6}\rho\sum_i x_i m_i d_{ii}^k$$

EQ 2.17

The radial distribution function for the chain term (in EQ 2.10) expands to:

$$g_{ij}^{hs} = \frac{1}{(1-\xi_3)} + \left(\frac{d_i d_j}{d_i + d_j}\right)\frac{2\xi_2}{(1-\xi_3)} + \left(\frac{d_i d_j}{d_i + d_j}\right)^2 \frac{2(\xi_2)^2}{(1-\xi_3)^3}$$

EQ 2.18

In terms of residual compressibility, the hard chain mixture is expressed as (Gross & Sadowski, 2001):

$$Z^{hc} = \frac{\xi_3}{(1-\xi_3)} + \frac{3\xi_1\xi_2}{\xi_0(1-\xi_3)^2} + \frac{3(\xi_2)^2 - \xi_3(\xi_2)^3}{\xi_0(1-\xi_3)^3}$$

EQ 2.19

(B) The dispersion term

As seen in Figure 2, the dispersion term accounts for the major development from SAFT to PC-SAFT. This term is developed as follows:

Pure component

The dispersion term is shown in terms of reduced residual Helmholtz energy: (Gross & Sadowski, 2001)

$$\tilde{a}^{disp} = \frac{A_1}{NkT} + \frac{A_2}{NkT}$$

EQ 2.20

with

$$\frac{A_1}{kTN} = -2\pi\rho m^2 \left(\frac{\varepsilon}{kT}\right)\sigma^3 I_1$$

EQ 2.21

$$\frac{A_2}{kTN} = -\pi\rho m\left(1 + Z^{hc} + \rho\frac{\partial Z^{hc}}{\partial\rho}\right)^{-1} m^2\left(\frac{\varepsilon}{kT}\right)^2 \sigma^3 I_2$$

EQ 2.22

The radial distribution functions are evaluated by:

$$I_1 = \int_1^\infty \tilde{u}(x)\, g^{hc}\left(m, x\frac{\sigma}{d}\right)x^2 dx$$

EQ 2.23

$$I_2 = \frac{\partial}{\partial\rho}\left[\rho\int_1^\infty \tilde{u}(x)^2\, g^{hc}\left(m, x\frac{\sigma}{d}\right)x^2 dx\right]$$

EQ 2.24

where

x		refers to the radial distance per segment (r/σ)
$\tilde{u}$		refers to reduced potential function (u(x)/ε)
$g^{hc}(m;x\frac{\sigma}{d})$		is the average segment-segment RDF

According to Gross & Sadowski (2000), the integrals in EQ 2.23 and EQ 2.24 have to be evaluated numerically and it is preferable to find simpler representations of these equations. By integration over the radius, expressions for I_1 and I_2 in terms of density (η) and segment number (m) may be obtained. Other authors, such as Gulati and Hall (1997), developed power series for $I_1(\eta, m)$ and $I_2(\eta, m)$ for specific cases such as the monomer (m=1) and dimer (m=2). Gross and Sadowski (2000) extended these results to the full range of densities and segment numbers by using:

$$I_1(\eta, m) = \sum_{i=0}^{6} a_i \eta^i$$

EQ 2.25

$$I_2(\eta, m) = \sum_{i=0}^{6} b_i \eta^i$$

EQ 2.26

with

$$a_i = a_{0i} + \frac{m-1}{m} a_{1i} + \frac{m-1}{m}\frac{m-2}{m} a_{2i}$$

EQ 2.27

$$b_i = b_{0i} + \frac{m-1}{m} b_{1i} + \frac{m-1}{m}\frac{m-2}{m} b_{2i}$$

EQ 2.28

42 model coefficients are required and these were fitted to pure component experimental data for *n*-alkanes. Experimental data enable the model parameters to correct for oversimplifications and errors introduced by the various model assumptions and approximations (Gross & Sadowski, 2001). The model constants for EQ 2.27 and EQ 2.28 are given in Table 1:

Table 1: Dispersion constants for PC-SAFT

i	a_{0i}	a_{1i}	a_{2i}	b_{0i}	b_{1i}	b_{2i}
0	0.9105631	-0.3084017	-0.0906148	0.7240947	-0.5755498	0.0976883
1	0.6361281	0.1860531	0.4527843	2.2382792	0.6995096	-0.2557575
2	2.6861348	-2.5030047	0.5962701	-4.0025849	3.8925673	-9.1558562
3	-26.547362	21.419794	-1.7241829	-21.003577	-17.215472	20.642076
4	97.759209	-65.255885	-4.1302113	26.855641	192.67226	-38.80443
5	-159.59154	83.31868	13.776632	206.55134	-161.82646	93.626774
6	91.297774	-33.746923	-8.672847	-355.60236	-165.20769	-29.666906

The hard chain compressibility term in EQ 2.22 reduces to:

$$\left(1 + Z^{hc} + \rho\frac{\delta Z^{hc}}{\delta\rho}\right) = \left(1 + m\frac{8\eta - 2\eta^2}{(1-\eta)^4} + (1-m)\frac{20\eta - 27\eta^2 + 12\eta^3 - 2\eta^4}{\left[(1-\eta)(2-\eta)\right]^2}\right)$$

EQ 2.29

Extension to mixtures

As per hard chain mixtures, the mean segment number replaces the segment number in EQ 2.29 to yield:

$$\left(1+Z^{hc}+\rho\frac{\delta Z^{hc}}{\delta\rho}\right)=\left(1+\bar{m}\frac{8\eta-2\eta^2}{(1-\eta)^4}+(1-\bar{m})\frac{20\eta-27\eta^2+12\eta^3-2\eta^4}{\left[(1-\eta)(2-\eta)\right]^2}\right)$$

EQ 2.30

The van der Waals one-fluid mixing rules are applied such that:

$$\frac{A_1}{kTN}=-2\pi\rho I_1(\eta,\bar{m})\sum_i\sum_j X_iX_jm_im_j\left(\frac{\varepsilon_{ij}}{kT}\right)\sigma_{ij}^3$$

EQ 2.31

$$\frac{A_2}{kTN}=-\pi\rho\bar{m}\left(1+Z^{hc}+\rho\frac{\delta Z^{hc}}{\delta\rho}\right)^{-1}\times I_2(\eta,\bar{m})\sum_i\sum_j X_iX_jm_im_j\left(\frac{\varepsilon_{ij}}{kT}\right)^2\sigma_{ij}^3$$

EQ 2.32

The following abbreviations commonly are used to shorten EQ 2.33 and EQ 2.34:

$$\overline{m^2\varepsilon\sigma^3}=\sum_i\sum_j X_iX_jm_im_j\left(\frac{\varepsilon_{ij}}{kT}\right)\sigma_{ij}^3$$

EQ 2.33

$$\overline{m^2\varepsilon^2\sigma^3}=\sum_i\sum_j X_iX_jm_im_j\left(\frac{\varepsilon_{ij}}{kT}\right)^2\sigma_{ij}^3$$

EQ 2.34

$$C_1=\left(1+Z^{hc}+\rho\frac{\delta Z^{hc}}{\delta\rho}\right)^{-1}$$

EQ 2.35

Interactions between unlike segments are evaluated using the Berthelot-Lorentz combinatory rules, with a binary interaction parameter sometimes used for the dispersion energy term. The Lorentz (1881) rule describes the average segment diameter by:

$$\sigma_{ij}=0.5\left(\sigma_i+\sigma_j\right)$$

EQ 2.36

The Berthelot (1898) rule is applied for a geometric mean of the energy terms:

$$\varepsilon_{ij}=\left(\varepsilon_i+\varepsilon_j\right)^{0.5}\left(1-k_{ij}\right)$$

EQ 2.37

In this case the Berthelot rule has incorporated a binary interaction parameter (k_{ij}) which may be used as additional fitted parameter.

(C) The association term

Wertheim's TPT provides a relatively simple manner in which to describe the residual Helmholtz energy in terms the monomer density, which is in-turn related to association strength. The hard chain and dispersion terms are described by three parameters (m, σ and ε), while the association term requires two more parameters (ε^{AA}, κ^{AA}) for each component. The association parameters can be determined either from spectroscopic data or, as is usually the case, fitted to VLE data.

The association model is shown here:

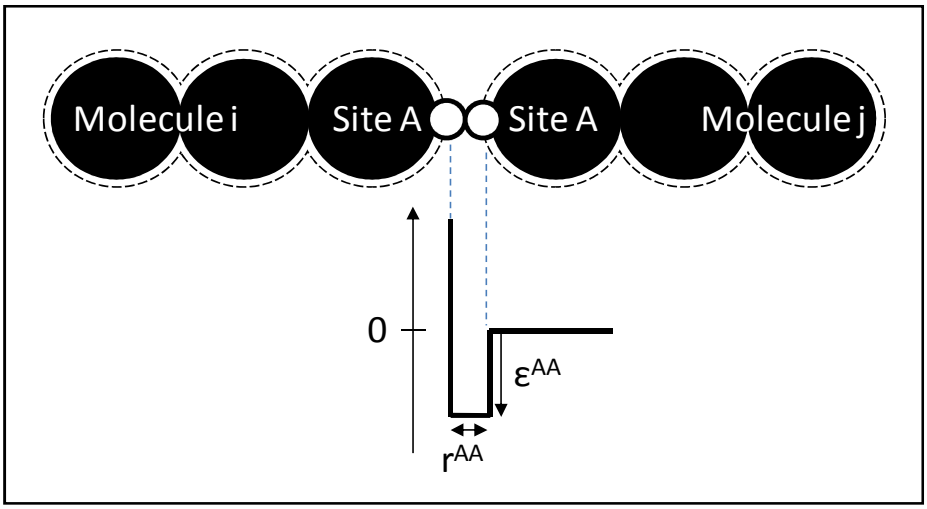

Figure 3: A model of associative bonding in SAFT. Reprinted (adapted) with permission from Chapman *et al.* (1990). Copyright 2012 American Chemical Society.

Figure 3 shows two chain molecules, i and j, each with an association site A. The association energy parameter, ε^{AA}, describes the depth of the square-well potential between the two A sites. The attraction potential is from the centre of one site to the centre of the other, given the association radius, r^{AA}, between the two sites. This radius related to the association volume parameter, κ^{AA}, described in the introduction. Associated chain or tree structures are allowed, but ring structures are not accounted for. Steric hindrance between association sites is also ignored (Chapman et al., 1990).

Pure component

The association term for pure components is calculated by (Chapman et al., 1990):

$$\tilde{a}^{assoc} = \sum_{A=1}^{M}\left[\ln X^A - \frac{X^A}{2}\right] + \frac{M}{2}$$

EQ 2.38

where M is number of association sites (per molecule)
X^A is the mole fraction of molecules not bonded at A,

and X^A is calculated by:

$$X^A = \left(1 + \sum_{B=1}^{M} \rho X^B \Delta^{AB}\right)^{-1}$$

EQ 2.39

where the summation is made over all sites which can bond with site A.

In EQ 2.39, Δ^{AB} is the association strength. It is calculated by (Chapman et al., 1990):

$$\Delta^{AB} = 4\pi F^{AB} \int_{d}^{r_c}\left[r^2 \Omega(r)\, g(r)^{seg}\right] dr$$

EQ 2.40

Here $4\pi r^2 \Omega(r)\, g(r)^{seg}\, dr$ represents the bonding-site-overlap volume element, with bonding assumed to occur at the contact point for hard spheres. Following the development of Huang and Radosz (1990), the integral is calculated by:

$$\Delta^{AB} = g(d)^{seg}\left[\exp\left(\frac{\varepsilon^{AB}}{kT}\right) - 1\right]\left(\sigma^3 \kappa^{AB}\right)$$

EQ 2.41

By approximating segments as hard spheres, the Carnahan-Starling hard sphere RDF can be used such that:

$$g(d)^{seg} \approx g(d)^{hs} = \frac{1 - 0.5\eta}{(1-\eta)^3}$$

EQ 2.42

Extension to mixtures

The association term for mixtures is as follows (Chapman et al., 1990):

$$\tilde{a}^{assoc} = \sum_i x_i \left[\sum_{A=1}^{M} \left[\ln X^{A_i} - \frac{X^{A_i}}{2} \right] + \frac{M_i}{2} \right]$$

EQ 2.43

where

$$X^{A_i} = \left(1 + N_{AV} \sum_j \sum_{B_j} \rho_j X^{B_j} \Delta^{A_i B_j} \right)^{-1}$$

EQ 2.44

In EQ 2.44 $\sum_{B_j}(\ )$ is summed over all sites for molecule j which can bond with site A on molecule i. $\sum_j(\ )$ is summed for all components in the mixture. The terms in EQ 2.44 are calculated using EQ 2.45 to EQ 2.47.

$$\rho_j = x_j \rho_{mix}$$

EQ 2.45

$$\Delta^{AB} = \sigma_{ij}^{\ 3} g_{ij} \left(\sigma_{ij} \right)^{seg} \kappa^{A_i B_i} \left[\exp\left(\frac{\varepsilon^{A_i B_i}}{kT} \right) - 1 \right]$$

EQ 2.46

$$\sigma_{ij} = 0.5 \left(\sigma_{ii} + \sigma_{jj} \right)$$

EQ 2.47

The Wolbach-Sandler (1998) combining rules are suggested for the cross-association strength and volume parameters (Gross & Sadowski, 2002):

$$\varepsilon^{A_i B_j} = 0.5 \left(\varepsilon^{A_i B_i} + \varepsilon^{A_j B_j} \right)$$

EQ 2.48

$$\kappa^{A_i B_j} = \left(\kappa^{A_i B_i} \kappa^{A_j B_j} \right)^{0.5} \left(\frac{\sqrt{\sigma_{ii} \sigma_{jj}}}{0.5 \left(\sigma_{ii} + \sigma_{jj} \right)} \right)^3$$

EQ 2.49

It can be shown that EQ 2.48 and EQ 2.49 are equivalent to using the geometric mean of the association strength i.e.:

$$\Delta^{A_iB_j} = \sqrt{\Delta^{A_iB_i}\Delta^{A_jB_j}}$$

EQ 2.50

EQ 2.50 is referred to as Elliott's Rule or ECR when the equivalent formulation is used in the Cubic-Plus-Association (CPA) equation of state (Kontogeorgis & Folas, 2010, pp.241, 264-5).

(D) Association schemes for 1-alkanols

The use of an association scheme is implicitly incorporated in the use of SAFT-type EoSs. Typical association schemes used for alcohols are shown in Table 2.

Table 2: Traditional association schemes for alcohols. Reprinted from Fluid Phase Equilibria, 296, G.M. Kontogeorgis *et al.*, Use of monomer fraction data in the parametrization of association theories, 219-229, Copyright 2012, with permission from Elsevier.

Species	Formula	Type	Site Fraction
Alcohol	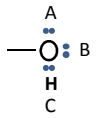	3B	$x^A=X^B;\ X^C = 2X^A-1;\ X_1=X^AX^BX^C$
	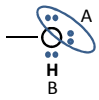	2B	$x^A=X^B;\ X_1=X^AX^B$
Water	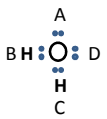	4C	$x^A=X^B=X^C=X^D;\ X_1=X^AX^BX^CX^D$
	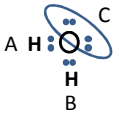	3B	$x^A=X^B;\ X^C = 2X^A-1;\ X_1=X^AX^BX^C$
	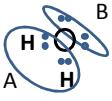	2B	$x^A=X^B;\ X_1=X^AX^B$

It has been shown that methanol is well described by a 3B scheme while heavier alcohols are better modelled using the 2B association scheme (von Solms et al., 2007). This difference is due to steric hindrance between larger alcohol molecules preventing all three sites from being used (Muller &

Gubbins, 2001). Recently, a new association scheme has been developed specifically to represent alcohols in alcohol-water systems (de Villiers et al., 2011b). The illustration of 2C scheme is shown in Figure 4.

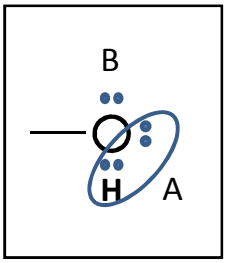

Figure 4: The 2C association scheme for alcohols in alcohol-water mixtures. Adapted with permission from de Villiers *et al.* (2011b). Copyright 2012 American Chemical Society.

The scheme makes a departure from the traditional 2B and 3B alcohol schemes by using one bipolar site (A in Figure 4) and one electron donor site (B in Figure 4). A bipolar site has the ability to bond with either a positive (electron acceptor) site or a negative (electron donor) site. The relations between the unbounded fraction are given by (de Villiers et al., 2011b):

$$X^B = \sqrt{X^A}$$

EQ 2.51

$$X^A = \frac{1}{6}\left\{-\frac{4}{\Delta\rho} + \frac{2\times 2^{1/3}}{\sqrt[3]{2\Delta^3\rho^3 + 27\Delta^4\rho^4 + 3\sqrt{3}\sqrt{\Delta^7\rho^7\left(4+27\Delta\rho\right)}}} + \frac{2^{2/3}\times\sqrt[3]{2\Delta^3\rho^3 + 27\Delta^4\rho^4 + 3\sqrt{3}\sqrt{\Delta^7\rho^7\left(4+27\Delta\rho\right)}}}{\Delta^2\rho^2}\right\}$$

EQ 2.52

The expression for X^A in EQ 2.52 is more complicated than for the 2B and 3B schemes. To illustrate this point, compare EQ 2.52 to X^A calculated from EQ 2.39 for the 2B and 3B schemes:

For the 2B scheme:

$$X^A = \frac{-1+\sqrt{1+4\rho\Delta}}{2\rho\Delta}$$

EQ 2.53

For the 3B scheme:

$$X^A = \frac{-(1-\rho\Delta)+\sqrt{(1+\rho\Delta)^2+4\rho\Delta}}{4\rho\Delta}$$

EQ 2.54

(E) Association schemes for acetone

Acetone does not self-associate, but does have the ability to cross-associate in a given mixture. Association schemes are typically assigned only to compounds that have the ability to self-associate. Von Solms *et al.* (2004) evaluated the physical properties of acetone to justify modelling it as a self-associating 2B molecule.

Table 3: Comparison of acetone parameters when modelled as a non-associating or associating compound

Model		m	σ [Å]	ε/k [K]	ε^{AB}/k [K]	κ	Reference	%AAD	
								P_{sat}	ρ_{liq}
PC-SAFT	-	2.77409	3.2557	253.406	-	-	Kouskoumvekaki *et al.* (2004)	0.99	1.95
PC-SAFT	2B	3.0925	3.0848	168.32	1321.2	0.9639	von Solms *et al.* (2004)	0.26	0.26

Table 3 shows the reported improvements when modelling acetone as an associating compound. The average absolute error percentage (%AAD) is improved by factors of almost 4 and 8 for saturated vapour pressure and liquid density predictions, respectively. Much improved binary VLE predictions are also obtained for systems such as the acetone-pentane system. Much of this improvement is attributed to association parameters accounting for the strong polar interactions observed in acetone, as is evidenced by the excellent phase equilibrium descriptions obtained by Jog *et al.* (2001) when adding a dipolar term.

Kontogeorgis & Folas (2010 pp. 338-341) describe the modelling options used for acetone in mixtures with chloroform. In this case neither component can self-associate and it was found that using the 2B scheme to describe acetone resulted in unsatisfactory phase behaviour models. The best results were obtained when assuming that acetone could only hydrogen bond with chloroform via ***both*** lone oxygen pairs.

2.1.2 Simplification to sPC-SAFT

The simplified PC-SAFT equation of state was introduced in 2003 (von Solms et al.) and is identical to PC-SAFT for pure components, with modifications being made only to the mixture terms. PC-SAFT had to be simplified in order to decrease the computational requirements of PC-SAFT without sacrificing physical accuracy. Another consideration may have been that a simpler EoS would be more accessible to a wider engineering audience. To this end, two modifications were introduced:

(A) Modification 1

The first modification pertains to the segment diameter. It is assumed that all the segments in the mixture have the same diameter, with the constraint that the new diameter must yield the same volume fraction as that of the mixture such that:

$$\eta = \xi_3 = \frac{\pi d^3}{6}$$

EQ 2.55

where the average diameter is given by:

$$d = \left(\frac{\sum_i x_i m_i d_i^3}{\sum_i x_i m_i} \right)^{1/3}$$

EQ 2.56

This radial distribution function (also implemented in the **chain and association mixture terms**) thus becomes:

$$g^{hs}(d) = \frac{1 - 0.5\eta}{(1-\eta)^3}$$

EQ 2.57

(B) Modification 2

In addition to simplifying the hard sphere RDF, a second modification is applied directly to the reduced residual Helmholtz energy such that the hard sphere term for mixtures is simplified.

$$\frac{a^{hs}}{RT} = \bar{m} \frac{4\eta - 3\eta^2}{(1-\eta)^2}$$

EQ 2.58

Similar combining rules are used, with one simplification to EQ 2.49 for the combined volume of association, given as the geometric mean of its constituent volumes (Grenner et al., 2007):

$$\kappa^{A_i B_j} = \sqrt{\kappa^{A_i B_i} \kappa^{A_j B_j}}$$

EQ 2.59

This mixing rule is referred to as CR-1 and is significantly less complex than the ECR formulation used by Gross and Sadowski (2002) in the PC-SAFT formulation. The use of ECR versus CR-1 does not drastically affect the results with the SAFT framework, as the segment diameter is not particularly sensitive to molecular type (Kontogeorgis & Folas, 2010, p.241).

When one or more of the components does not self-associate, but can cross-associate within a mixture e.g. an acetone-ethanol mixture, a different approach must be used. For both the ECR and CR-1 combining rules, the mixture volume of (cross-) association would necessarily become zero, thereby not accounting for cross-association. One strategy for resolving this problem was proposed by Folas *et al.* (2006) for the CPA EoS, which can be implemented with the SAFT framework as well. A modified CR-1 rule is proposed whereby cross-association volume parameter is fitted to phase equilibrium data while the cross-association strength parameter is calculated as per EQ 2.48.

2.1.3 Applications and limitations of PC-SAFT and sPC-SAFT

The applications of PC-SAFT and sPC-SAFT are presented here as a whole, as these "two" models are very closely linked, with many articles comparing them directly. Gross and Sadowski (2002) modelled a range of pure 1-alkanols from methanol to 1-nonanol using their original PC-SAFT formulation. Using newly calculated parameters they generated more accurate phase diagrams as compared to SAFT-HR. This is attributed to the improved description of dispersion. For ethanol, AAD% less than 1% were obtained for modelling pure liquid density and vapour pressure in the range 230 – 516 K, while the greatest deviation was seen for methanol (2.36% and 2.01% for vapour pressure and density). All alcohols were modelled with 2 association sites (2B scheme) and this is the likely reason for the greater observed deviation for methanol.

Methanol, ethanol, 1-propanol, 2-propanol and acetone were all incorporated in a study to compare the relative performance of PC-SAFT and sPC-SAFT (Kouskoumvekaki et al., 2004). While alcohol-acetone systems were not modelled directly, sPC-SAFT was able to more accurately model the binary phase equilibria of acetone in mixtures with complex polymers. PC-SAFT exhibited superior phase modelling when 1- and 2-propanol were used as a solvent in a polymer mixture. Grenner *et al.* (2007) used a novel approach for parameterization of sPC-SAFT for 1-alkanols ranging from ethanol to 1-hexadecanol. They derive generalized association parameters ε^{AB} and κ^{AB} of 2811.00 K and 0.0033 by calculating the geometric mean of each constant from the optimised values of each compound. With generalized association parameters, the physical parameters are fitted using functions linear in molar mass (M [g/mol]):

$$m = 0.0287M + 0.0749$$
$$m\sigma^3 = 1.6906M + 5.5449$$
$$m\frac{\varepsilon}{k} = 7.3107M + 91.577$$

EQ 2.60

Kontogeorgis *et al.* (2010) derived new CPA, NRHB and sPC-SAFT parameters for alcohols. A comparison was made between parameters derived with phase equilibrium data only and those with monomer fraction data incorporated into the regression algorithm. Tybjerg *et al.* (2010) derived sPC-SAFT-2B parameters for, amongst others, methanol by incorporating heat of vaporisation and compressibility factor data into their regression method along with the obligatory VLE data. These new 2B parameters provide improved modelling results compared to the older 3B parameters available in the literature. De Villiers *et al.* (2011b) derived new sPC-SAFT parameters for 1-alkanols with their 2C association scheme by incorporating heat of vaporisation data into the regression function. While the 2C scheme was developed and tested for water-alcohol systems, it would be interesting to evaluate its performance in other alcoholic mixtures. New parameters were also regressed within the 3B scheme for ethanol and 1-propanol (among others). The various developments shown are summarised in Table 4:

Table 4: (s)PC-SAFT literature parameters for various alcohols and association schemes

Model		m	σ [Å]	ε/k [K]	ε^{AB}/k [K]	κ	Reference	%AAD	
								P_{sat}	ρ_{liq}
Methanol									
PC-SAFT	2B	1.5255	3.23	188.9	2899.5	0.03518	Gross &Sadowski (2002)	2.36	2.01
sPC-SAFT	3B	3.5841	2.411	163.2	1795.8	0.1715	Kontogeorgis *et al.* (2010)	0.5	0.2
sPC-SAFT	3B [X]	2.4573	2.805	198.8	2009.1	0.0465	Kontogeorgis *et al.* (2010)	1	2.5
sPC-SAFT	2B	2.877	2.5763	164.91	2304.11	0.3608	Tybjerg *et al.* (2010)	0.44	1.61
sPC-SAFT	2B [X]	1.8538	3.099	225.2	2383.1	0.0402	Kontogeorgis *et al.* (2010)	1.0	2.5
sPC-SAFT	2C	2.100	2.7998	197.23	2535	0.823	de Villiers *et al.* (2011b)	0.52	0.37
Ethanol									
PC-SAFT	2B	2.3827	3.1771	198.24	2653.4	0.03238	Gross &Sadowski (2002)	0.99	0.79
sPC-SAFT	2B	1.23058	4.1057	316.91	2811.02	0.0033	Grenner *et al.* (2007)	1.12	2.2
sPC-SAFT	2B [X]	2.3352	3.214	209.2	2593.1	0.0267	Kontogeorgis *et al.* (2010)	0.2	0.7
sPC-SAFT	2C	2.3609	3.1895	207.56	2695.69	0.0327	de Villiers *et al.* (2011b)	0.18	0.21
1-Propanol									
PC-SAFT	2B	2.9997	3.2522	233.4	2276.8	0.01527	Gross &Sadowski (2002)	0.85	1.71
sPC-SAFT	2B	2.81484	3.3085	236.343	2370	0.01457	Kouskoumvekaki *et al.* (2004)	-	-
sPC-SAFT	2B	1.79963	3.9044	292.11	2811.02	0.0033	Grenner *et al.* (2007)	0.59	1.32
sPC-SAFT	2B [X]	1.9722	3.782	281.8	2722.8	0.0040	Kontogeorgis *et al.* (2010)	1	1.6
sPC-SAFT	2C	2.9537	3.2473	226.36	2448.02	0.0228	de Villiers *et al.* (2011b)	0.27	0.25
2-Propanol									
PC-SAFT	2B	3.0929	3.2085	208.42	2253.9	0.02468	Gross &Sadowski (2002)	0.7	1.25
sPC-SAFT	2B	3.05279	3.2088	204.214	2331	0.02642	Kouskoumvekaki*et al.* (2004)	-	-
sPC-SAFT	2B	1.79963	3.9044	269.29	2811.02	0.0033	Grenner *et al.* (2007)	1.62	1.63

It can be seen that the phase equilibrium description is generally improved when using sPC-SAFT as compared to PC-SAFT. Very good results, in terms of deviation from phase equilibrium data, have been obtained when using the 2B and 2C schemes over the range of alcohols considered here. Association schemes followed by "[X]" refer to those parameters derived by Kontogeorgis *et al.* (2010) where monomer fraction data were included in the regression algorithm. The [X] models here are slightly less accurate for VLE modelling, but provide more accurate descriptions for a wider range of properties.

2.1.4 Development of (s)PC-SAFT related to polar forces

Alcohols and acetone are considered in this study and thus polar interactions should also be considered. Many polar theories have been proposed in the literature, of which the following two have been deemed the most successful (de Villiers et al., 2011a):

- JG (Jog & Chapman, 1999) & (Jog et al., 2001)
- GV (Gross & Vrabec, 2006)

The JG and GV models have been incorporated into the PC-SAFT and sPC-SAFT framework to create the Polar PC-SAFT and PCP-SAFT, and the sPC-SAFT-JG and sPC-SAFT-GV models respectively. The development and equations of each model are briefly discussed here, while a more complete description may be found in the references mentioned above as well as in Tan *et al*. (2008).

Both models are built on a framework proposed by Walsh *et al.* (1992) for which multipolar interactions could be described in terms of a Padé approximant:

$$\tilde{a}^{polar} = \frac{\tilde{a}_2}{1 - \frac{\tilde{a}_3}{\tilde{a}_2}}$$

EQ 2.61

Here the subscripts refer to interactions between two and three molecules or segments. The two models are developed as follows:

(A) JC Polar term

Jog and Chapman used the model from EQ 2.61 and applied it dipolar chains by describing the two- and three-body interaction terms by expanding the expressions of Gubbins & Twu (1978):

$$\tilde{a}_2 = -\frac{2\pi}{9}\frac{\rho}{(kT)^2}\sum_i\sum_j x_i x_j m_i m_j x_{pi} x_{pj}\frac{\mu_i^2\mu_j^2}{d_{ij}^3} I_{2,ij}$$

EQ 2.62

$$\tilde{a}_3 = \frac{5\pi^2}{162}\frac{\rho^2}{(kT)^3}\sum_i\sum_j\sum_k x_i x_j x_k m_i m_j m_k x_{pi} x_{pj} x_{pk}\frac{\mu_i^2\mu_j^2\mu_k^2}{d_{ij}d_{jk}d_{ik}} I_{3,ijk}$$

EQ 2.63

where x_p the fraction of polar segments
μ is the segment dipole moment [D]

x_p is a fitted parameter which ideally should approximately be equal to 1/m for a chain molecule with one polar segment. The dipole moment can either be estimated from quantum mechanics, left as an adjustable parameter or the experimental value can be used. Here $I_{2,ij}$ and $I_{3,ijk}$ are integrated over the angular pair and triplet pair correlation functions respectively (Tan et al., 2008). The integrals are calculated analytically from Rushbrooke *et al.* (1973).

$$I_{2,ij} = \frac{1-0.3618\rho\bar{d}^3 - 0.3205\left(\rho\bar{d}^3\right)^2 + 0.1078\left(\rho\bar{d}^3\right)^3}{\left[1-0.5236\rho\bar{d}^3\right]^2}$$

EQ 2.64

$$I_{3,ijk} = \frac{1+0.62378\rho\bar{d}^3 - 0.11658\left(\rho\bar{d}^3\right)^2}{1-0.59056\rho\bar{d}^3 + 0.20059\left(\rho\bar{d}^3\right)^2}$$

EQ 2.65

with

$$\bar{d}^3 = \sum_i x_i m_i d_i^3$$

EQ 2.66

(B) GV Polar term

A second successful approach to modelling polar species was proposed by Gross & Vrabec (2006). Instead of introducing a new fitted parameter χ_p, it is simply defined as the ratio of dipolar segments to total segments such that EQ 2.61 is described by:

$$\tilde{a}_2 = -\frac{\pi\rho}{(kT)^2}\sum_i\sum_j x_i x_j \frac{n_{pi}n_{pj}}{m_i m_j}\frac{\mu_i^2\mu_j^2}{d_{ij}^3} I_{2,ij}$$

EQ 2.67

$$\tilde{a}_3 = -\frac{4\pi^2}{3}\frac{\rho^2}{(kT)^3}\sum_i\sum_j\sum_k x_i x_j x_k \frac{n_{pi}n_{pj}n_{pk}}{m_i m_j m_k}\frac{\mu_i^2\mu_j^2\mu_k^2}{\sigma_{ij}\sigma_{jk}\sigma_{ik}} I_{3,ijk}$$

EQ 2.68

where n_p the number of polar segments

Here $I_{2,ij}$ and $I_{3,ijk}$ are expressed as power series given by (Tan et al., 2008):

$$I_{2,ij} = \sum_{n=0}^{4}\left(a_{n,ij} + b_{n,ij}\frac{\varepsilon_{ij}}{kT}\right)\eta^n$$

EQ 2.69

$$I_{3,ijk} = \sum_{n=0}^{4} c_{n,ijk}\eta^n$$

EQ 2.70

where a, b and c are functions of chain length given by:

$$a_{n,ij} = a_{0n} + \frac{m_{ij}-1}{m_{ij}}a_{1n} + \frac{m_{ij}-1}{m_{ij}}\frac{m_{ij}-2}{m_{ij}}a_{2n}$$

EQ 2.71

$$b_{n,ij} = b_{0n} + \frac{m_{ij}-1}{m_{ij}}b_{1n} + \frac{m_{ij}-1}{m_{ij}}\frac{m_{ij}-2}{m_{ij}}b_{2n}$$

EQ 2.72

$$c_{n,ijk} = c_{0n} + \frac{m_{ijk}-1}{m_{ijk}}c_{1n} + \frac{m_{ijk}-1}{m_{ijk}}\frac{m_{ijk}-2}{m_{ijk}}c_{2n}$$

EQ 2.73

with m given by:

$$m_{ij} = \sqrt{m_i m_j}$$

EQ 2.74

$$m_{ijk} = \sqrt[3]{m_i m_j m_k}$$

EQ 2.75

The constants for EQ 2.71 to EQ 2.73 are given by Gross & Vrabec (2006) as:

Table 5: GV-polar model constants

i	a_{0i}	a_{1i}	a_{2i}	b_{0i}	b_{1i}	b_{2i}	c_{0i}	c_{1i}	c_{2i}
0	0.3043504	0.9534641	-1.161008	0.2187939	-0.5873164	3.4869576	-0.0646774	-0.9520876	-0.6260979
1	-0.1358588	-1.896383	4.5258607	-1.1896431	1.2489132	-14.915974	-14.915974	2.9924258	1.2924686
2	1.4493329	2.013118	0.9751222	1.1626889	-0.508528	15.372022	15.372022	-2.3802636	1.6542783
3	0.3556977	-7.3724958	-12.281038	0	0	0	0	-0.2701261	-3.4396744
4	-2.0653308	8.2374135	5.9397575	0	0	0	0	0	0

The constants in Table 5 were fitted to molecular simulation data for a 2-centre Lennard Jones fluid with the suggested restriction that $m_{ij(k)} \leq 2$ (Gross & Vrabec, 2006).

2.1.5 Selected applications of polar (s)PC-SAFT models

It has been shown that the incorporation of the JC di-polar term improves the predictive capabilities of SAFT-HR and PC-SAFT (Tan et al., 2008). Al-Saifi *et al.* (2008) tested the relative performance of the JC- and GV-models within the PC-SAFT framework and found that the JC-model generally performed better. The polar models were tested on binary alcohol-hydrocarbon, alcohol-alcohol, water-alcohol and water-hydrocarbon systems.

Table 6: Regressed parameters for various alcohols within polar association models

Model		m	σ [Å]	ε/k [K]	ε^{AB}/k [K]	κ	x_p	μ [D]	%AAD P_{sat}	%AAD ρ_{liq}
Methanol										
Polar PC-SAFT	2B	1.7266	3.1369	168.84	2585.9	0.06311	0.35128	1.7	0.43	0.47
PCP-SAFT		1.9708	2.9908	179.06	2465.9	0.06445			0.34	0.47
Ethanol										
Polar PC-SAFT	2B	2.2049	3.2774	187.24	2652.7	0.03363	0.29466	1.7	0.35	0.49
PCP-SAFT		2.4382	3.1477	191.37	2599.8	0.03481			0.36	0.29
1-Propanol										
Polar PC-SAFT	2B	2.6268	3.3918	219.13	2479.4	0.02096	0.26625	1.7	0.78	0.76
PCP-SAFT		2.8428	3.2928	225.7	2377.7	0.019			1.32	0.67
2-Propanol										
Polar PC-SAFT	2B	2.6856	3.38	199.1	2473.8	0.02237	0.26065	1.7	1.98	1.64
PCP-SAFT		2.685	3.38	212.32	2485.3	0.01552			1.85	1.79

For the parameters in Table 6, the number of polar segments (n_p) was not used an adjustable parameter. De Villiers *et al*. (2011a) suggested that it could be incorporated within the regression algorithm as one of the fitted parameters.

Polar PC-SAFT has been used to accurately describe phase diagrams of several binary ketone-alkane mixtures (Sauer & Chapman, 2003). Similar results were obtained by Tumakaka & Sadowski (2004) using the parameters in Table 7.

Table 7: Acetone parameters used by Tumakaka & Sadowski (2004) for polar and non-polar association theories

Model	m	σ [Å]	ε/k [K]	x_p	μ [D]
Polar PC-SAFT	2.187	3.6028	245.49	0.2969	2.72
PC-SAFT	2.891	3.2279	247.42	0	0

These polar PC-SAFT parameters were also implemented by De Villiers *et al.* (2011a) within the sPC-SAFT-JC model. Furthermore it was demonstrated that sPC-SAFT-JG described mixtures of polar compounds in alkanes are well, especially in the polar compound-rich region. It was found the sPC-SAFT-GV model more accurately described the alkane-rich region. The parameters in Table 8 were regressed for the sPC-SAFT-GV model:

Table 8: Acetone parameters used by de Villiers *et al.* (2011a) for the sPC-SAFT-GV model

Model	m	σ [Å]	ε/k [K]	n_p	μ [D]	%AAD P_{sat}	%AAD ρ_{liq}
sPC-SAFT-GV	2.786	3.228	210.14	1.4848	2.88	1.15	1.2

It should be noted that the number of polar segments (n_p) has been implemented as an adjustable parameter in the regression algorithm and acetone – *n*-hexane binary VLE data were also included. According to Tumakaka & Sadowski (2004) acetone has a dipole moment which is perpendicular to molecular axis, which is same alignment given within the JC-model (Al-Saifi et al., 2008). Conversely, the dipole moment exhibits axial alignment with the GV-model. This suggests that the JC-model may be better suited to modelling systems containing acetone.

2.2 Parameterisation of (s)PC-SAFT by monomer fraction data

The incorporation of monomer fraction data in the parameter regression algorithm has long been considered as a preferred method for obtaining the association parameters (ε^{AA}, κ^{AA}) (Chapman et al., 1989). Using this additional experimental data could result in better descriptions of hydrogen-bonding phenomena, without affecting the prediction accuracy for VLE (saturated liquid density and vapour pressure) (von Solms et al., 2007). The objective function for fitting all five parameters (EQ 2.76) is simply modified to incorporate monomer fraction data (Kontogeorgis et al., 2010).

$$SSE = \upsilon_1 \sum \left(\frac{P_{\exp} - P_{calc}}{P_{\exp}} \right)^2 + \upsilon_2 \sum \left(\frac{\rho_{\exp} - \rho_{calc}}{\rho_{\exp}} \right)^2 + \upsilon_3 \sum \left(\frac{X_{1,\exp} - X_{1,calc}}{X_{1,\exp}} \right)^2 \qquad \text{EQ 2.76}$$

The regression weights (v_i) are usually set equal to one such that an equal weighting is applied to each of the three data types.

2.2.1 Alcohol monomer fraction data in the literature

Monomer fraction data, especially pure component data, are quite limited (Kontogeorgis & Folas, 2010). Pure component monomer fraction data sources are given in Table 9.

Table 9: Pure alcohol monomer fraction data available for methanol, ethanol and 1-propanol

Alcohol	Source	Conditions
Methanol	Luck (1980)	-20°C to 360 °C
Ethanol	Luck (1986) in Moorthi & Nagata (1991)	-25 °C to 250 °C
1-Propanol	Lien (1972) in Moorthi & Nagata (1991)	15°C to 55 °C

Along with these pure component data sets, several binary data sets are available.

Table 10: Literature sources of binary monomer fraction data for alcohols in organic solvents.

Component 1	Component 2	Conditions	Author
Methanol	Hexane	Ambient	Martinez (1986)
Methanol	Acetone	27.3 °C	Max & Chapados (2005)
Propanol	Heptane	15-55 °C	Lien (1972)
Methanol	CCl4	20 °C	Prausnitz *et al.* (1999)
Pentanol Hexanol	Hexane	25, 35 °C	Gupta & Brinkley (1998)
Methanol Ethanol Pentanol	Hexane	Ambient (25 °C)	Asprion *et al.* (2001)
Propanol Hexanol	Hexane	25-40 °C	
Ethanol Propanol	Heptane		
Methanol Ethanol Propanol Pentanol Hexanol	Hexane	23.3 °C	Von Solms *et al.*(2007)

From Table 10 it is evident that monomer fraction data for alcohols are relatively limited, especially in terms of temperature. Non-associative solvents are generally used, with the notable exception being the methanol-acetone system. Max and Chapados (2005) do not explicitly calculate methanol monomer fractions, but do however provide interesting insights with respect to the hydrogen-bonding complexes formed.

(A) Comments on monomer fraction data in the literature

The data of Luck (1980) (1986) is also given in terms of fraction of free –OH groups. Von Solms *et al.* (2006b) show that this is the "fraction of nonbonded hydrogen atoms in the hydroxyl group". When using the 4C or 3B scheme, Luck's experimental values correspond to X^C (or X^D for 4C) and when using the 2B scheme it corresponds to X^B. The data of Luck has a further anomaly whereby the data of ethanol and methanol almost coincide with one another – this is very unlikely when considering the physical properties of these two fluids (Kontogeorgis et al., 2010).

2.2.2 Acetone monomer fraction data in the literature

No explicit monomer fraction data sets for acetone are available in literature, although spectroscopic studies have been done on the association of acetone in mixtures. Symons and Eaton (1985) measured dilute acetone solutions in several solvents and postulated that acetone monomers exist in solution with methanol. The monomer fraction was estimated as 0.10 for a 1% v/v (0.55% mole) solution at 25 °C. From their article it is not immediately evident which method was used in order to determine the monomer fraction value. This author suspects that the ratio of the peak heights were used as a 9:1 ratio is observed for the bonded and non-bonded peaks in Figure 5.

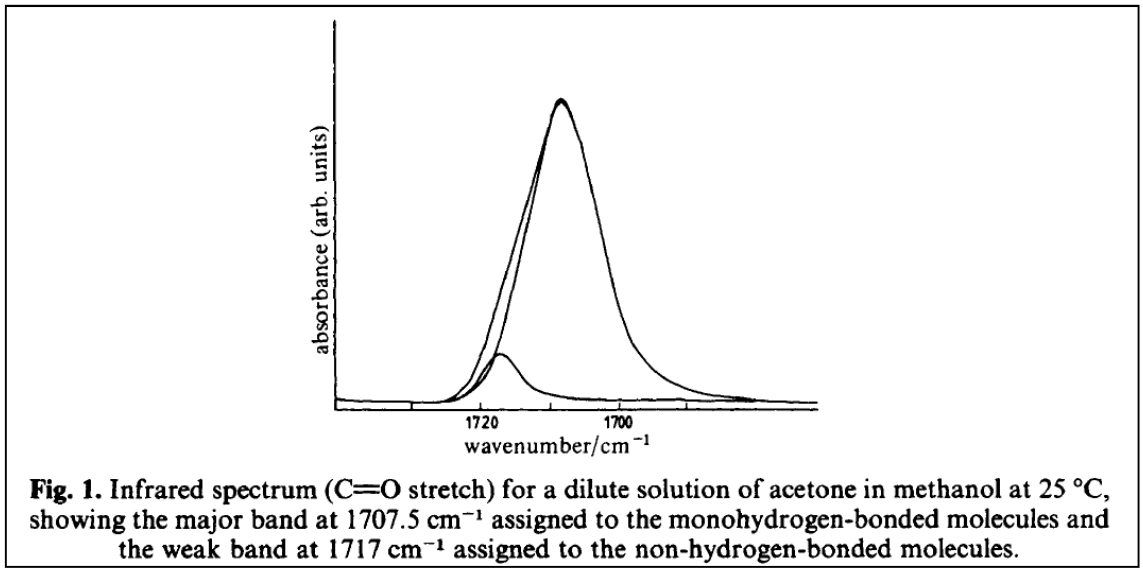

Fig. 1. Infrared spectrum (C=O stretch) for a dilute solution of acetone in methanol at 25 °C, showing the major band at 1707.5 cm^{-1} assigned to the monohydrogen-bonded molecules and the weak band at 1717 cm^{-1} assigned to the non-hydrogen-bonded molecules.

Figure 5: IR spectrum of a dilute acetone - methanol mixture at 25 °C. Symons M.C.R. & Eaton G., J. Chem. Soc., Faraday Trans1, 1985, 81, 1963-1977 - Reproduced by permission of The Royal Society of Chemistry

Max and Chapados (2005) also examined the acetone – methanol system (but at 27.3 °C) and used a spectral factor analysis to determine that 45.6% of acetone molecules appear as monomers in a dilute solution (0.3% mole). These monomer fraction values at infinite dilution are very different to those seen for alcohol – alkane systems, where the monomer fraction tends to one as the solute concentration tends to zero.

2.2.3 From monomer fraction data to SAFT modelling

The link between the SAFT EoS family and spectroscopic data is through the element X^A. It is important to realise that X^A is not a monomer fraction, but it is used to determine it (von Solms et al., 2007). The monomer fraction (X_1) is determined from the unbonded fractions ($X^{A, B,\cdots}$) as follows:

$$X_1 = \prod_{K=A,B,\ldots} X^K$$

EQ 2.77

Monomer fractions for alcohol-alkane mixtures have been measured, with the thermodynamic modelling done using the sPC-SAFT equation (von Solms et al., 2007). While the predictions are somewhat over-estimated, the trends are of the correct shape. It is shown that the pure component parameters and association schemes have a large effect on the predictions. An example of the modelling is shown in Figure 6.

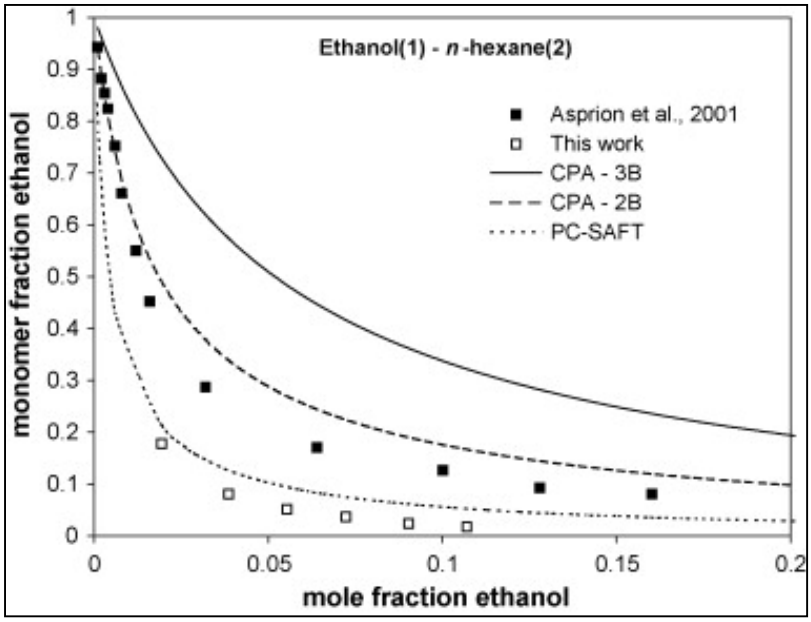

Figure 6: Monomer data and modelling with PC-SAFT(2B) for Ethanol in n-Hexane. Reprinted from Fluid Phase Equilibria, 261, N. von Solms *et al.*, Measurement and modelling of hydrogen bonding in 1-alkanol + *n*-hexane binary systems, 272-280, Copyright (2007), with permission from Elsevier.

In Figure 6, there is disagreement between the data of von Solms *et al.* (2007) and Asprion *et al.* (2001). It should be noted that there is a slight temperature difference, with the data measured at 23.3 °C (von Solms *et al.*) and 25 °C (Asprion *et al.*), but this does not account for the observed difference. The disagreement is mentioned by von Solms *et al.* (2007) but not discussed. Jensen and Kofod[3] (2005) attribute the difference in the literature monomer fraction data sets to the difference in the calculated absorption coefficients. A discussion on the difference between these two data sets can be found in the appendices (in Chapter 10.6).

[3]This reference refers to a report which was written as part of a master's thesis submitted at DTU and was obtained through private correspondence with Lars Jensen. This report is the source of the experimental data used by von Solms *et al.* (2007), which explains the seemingly inconsistent dates provided with the references.

2.3 Hydrogen bonding

Having completed an overview of the sPC-SAFT EoS and how monomer fraction data are used with it, the next step is to consider the driving force behind association (which is hydrogen bonding) and how it can be calculated.

Hydrogen bonding is a specific type of polar attraction that occurs when a hydrogen atom is bonded to a relatively small atom, which has a high electronegativity and a lone pair of valence electrons (Silberberg, 2003, p.434). While several atoms can partake in hydrogen-bonding interactions (e.g. C, N, O, F, P, S, Cl, Se, Br and I), most chemists only consider those interactions that are energetically stronger than the typical van der Waals interactions (Kollman & Allen, 1972).

2.3.1 Hydrogen bonding leading to the formation of clusters

For this investigation, the O-H bond in alcohols and the C=O bond in acetone are of special interest. Consider the following bond configurations in a mixture of ethanol and acetone:

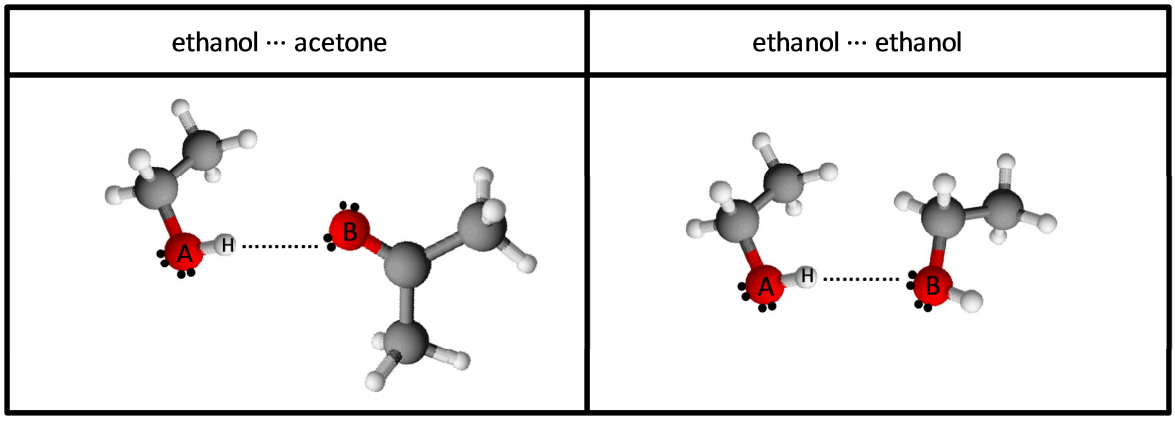

Figure 7: O-H···O complexes in acetone-ethanol mixtures

In Figure 7, the oxygen atoms labelled A are referred to as proton donors. The oxygen atoms labelled B are referred to as proton acceptors. The bond length between the donated proton and the proton acceptor is typically twice as large as the O-H bond and is temperature dependent (Chaplin, 2007). The normally monovalent hydrogen acts as a divalent atom and forms an O-H···O complex.

A complete definition with reference to the chemical bonding theory of Lewis is given here (Gilli & Gilli, 2009, p.25):

> "Hydrogen bonding occurs between a proton-donor group A – H and a proton-acceptor group B, where A is an electronegative atom O, N, S, X (F, Cl, Br, I) or C, and the acceptor

group is a lone pair of an electronegative atom or a π bond of a multiple bond (unsaturated) system. Generally, a H-bond can be characterized as a proton shared by two lone electron pairs."

A more developed H-bond description is given when incorporating the Bronsted-Lowry acid-base theory whereby an H-bond can be considered as a proton sharing two pairs of lone electrons, each on an electronegative atom of group (Gilli & Gilli, 2009, p.26). This gives the general form:

$$R - D^{-} : \cdots H^{+} \cdots : A - R'$$

H-bond complexes may become very large (especially in the solid phase). In alcohols, H–O···H–O hydrogen-bonding clusters form, where –OH groups can act as donors or acceptors (Tamenori et al., 2009). It is estimated that the average lifetime of hydrogen bonds are in the range 1 to 20 picoseconds (Chaplin, 2007). The formation of trimers dominates in alcohols at low temperatures (Tucker & Becker, 1973). For acetone clusters, it is shown that C=O···H–C donor-acceptor bonds form with stable cyclic dimers (Tamenori et al., 2009).

Co-opertivity (or non-additivity) is another important phenomenon in H-bonded networks. This occurs when a group of chemical bonds has a higher energy than the sum of the constituent bonds (Gilli & Gilli, 2009, p.81) which suggests that hydrogen co-operate with one another to form a bonded network. Co-opertivity in larger networked clusters may lead to an increase in hydrogen bonding strengths of as much as 270% (Luck, 1998).

When like molecules partake in hydrogen bonding, it is referred to as association and if the molecules are unlike, it is referred to as cross-association or solvation. A further result of hydrogen bonding is observed when a non-polar compound (e.g. an alkane) is mixed into a strongly hydrogen-bonded compound. The hydrogen-bonded molecules re-orientate themselves so as to maintain their hydrogen-bonded networks. This re-orientation leads to greater order compared to pure water. This phenomenon is entirely entropic is referred to as the hydrophobic effect (Kontogeorgis & Folas, 2010, pp.28-29).

Given the background knowledge of hydrogen-bonding shown here and the detailed discussions around hydrogen-bonding/association in relation to the SAFT formalism, it is necessary to examine the methods by which association data can be generated.

2.4 Infrared spectroscopy

Infrared spectroscopy is an energy absorption process where infrared light is passed through a given sample to determine the frequencies at which its constituent atoms are vibrating. It may be used for characterizing unknown samples and has long been the most common method used for identifying hydrogen bonds (Kollman & Allen, 1972).

2.4.1 Principles of infrared spectroscopy

The infrared spectrum is typically divided into three parts according to wavelengths (wavenumbers) and falls between microwaves and visible light (approximately from 100 to 10 000 cm^{-1}) in the electromagnetic spectrum. These three sections are the near-(NIR), mid- (MIR) and far-infrared (FIR) regions, with the MIR being the most important region for the quantitative analysis of organic compounds (Kellner et al., 1998, p.541) and has a range of 4000 to 600 cm^{-1} (2.5 to 15 µm) (Wetzel, 1998, p.141).[4]

The wavenumber ($\tilde{\nu}$) is defined as the inverse of wavelength (Nakamoto, 2008a, pp.2-3):

$$\tilde{\nu} = \frac{1}{\lambda}$$

EQ 2.78

At temperature above zero Kelvin, all matter is in a state of continuous vibration. When IR radiation at a given frequency is directed at a molecule, the molecule may absorb that radiation if one of the vibrations between its constituents (i.e. a molecular bond) is at the same frequency (Hsu, 1997, p.251). However, only bonds which have a dipole moment that varies with time can absorb infrared radiation (Pavia et al., 1996, p.16) and bonds that satisfy this criterion are said to be infrared active (Smith, 1998, p.10). When the absorption triggers an excitation from the ground energy state to the first excited energy state, this is referred to as a fundamental absorption or vibration. Fundamental vibrations usually occur in the MIR region. Overtones and combination bands also occur and these normally are visible in the near-infrared region. An overtone is a multiple of a fundamental vibration. Combination bands are either the sum or difference of fundamental vibrations and occur when multiple vibrations are excited simultaneously (Smith, 1998, p.14). A final type of band may appear due to the combination of a fundamental vibration with an overtone and this is referred to as Fermi resonance (Pavia et al., 1996, pp.19-20).

[4] The limits of the IR range vary from 100 to 14 000 cm^{-1} depending on which sources are consulted

2.4.2 Vibrational modes related to hydrogen bonding of alcohols

As this investigation is concerned with the hydrogen bonds of alcohols, the O-H vibrations are of interest. Consider the following O-H vibrations in an ethanol molecule:

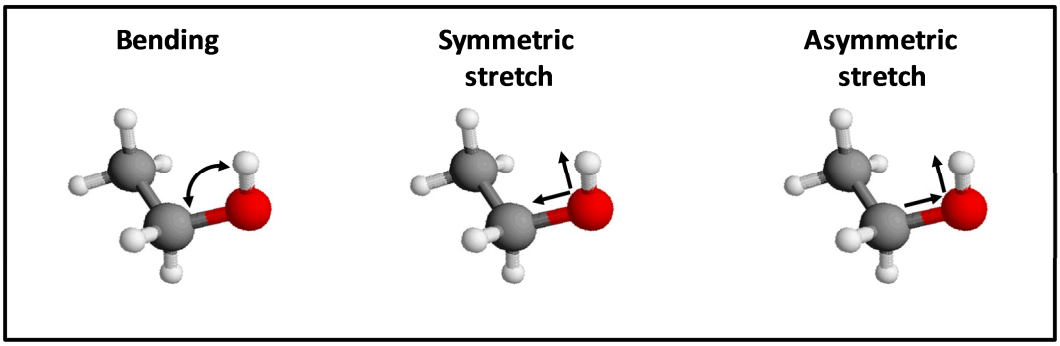

Figure 8: Basic (C-)O-H vibration modes in an ethanol molecule

Here we observe three modes of vibration: two stretching modes (symmetric and asymmetric) of the O-H and a bending motion of the C-O-H bond. The two stretching vibrations are of specific interest and appear in the range 3750-3200 cm^{-1}, the asymmetric stretch (v_3) having a higher frequency than the symmetric stretch (v_1) (Griffiths, 2005).

The O-H band has a very interesting property when it is diluted in a solvent. As the concentration of alcohol decreases, a second, very sharp peak begins to develop in the O-H band region. This peak, usually at 3700 – 3590 cm^{-1} (Kellner et al., 2004, p.774), is representative of the free O-H bonds, i.e. the O-H bonds that are not partaking in association (Pavia et al., 1996, p.47). It stands to reason that as the concentration decreases, the alcohol molecules in the mixtures become further removed from each other and therefore cannot associate with other alcohol molecules. This will be especially prevalent in a non-polar solvent where cross-association does not occur. The reason for the appearance of this peak is that hydrogen bonding decreases the strength of the O-H bond (Pavia et al., 1996, p.48). Therefore, a decrease in hydrogen bonding strengthens the O-H bond, which results in a shift to a higher frequency (wavenumber). There is some debate as to whether this band is in fact representative of the free O-H bonds (i.e. the monomers) with Czarnecki *et al.* (1998) attributing it to the terminal O-H bands in linear chains. More recent papers have shown that it is valid to assume that these bands are representative of the monomers (Asprion et al., 2001) (von Solms et al., 2006b) (von Solms et al., 2007).

2.4.3 Vibrational modes related to hydrogen bonding of acetone

As discussed in Section 2.3.1, the C=O bond for acetone acts as the H-bond donor. For liquid open-chain ketones, the harmonic C=O vibration absorbs between 1725 – 1705 cm^{-1} (Rao, 1963, p.193).

Nyquist (1990) studied several 1 % solutions of acetone in, amongst others, methanol, ethanol and 2-propanol. The C=O peaks reported near 1700 cm^{-1} are shown in Table 11.

Table 11: C=O peak positions for acetone in dilute alcoholic mixtures

Solvent	Peak	Shoulder
Methanol	1708.3	1716.2
Ethanol	1709.04	≈ 1717
2-Propanol	1710.31	-

In Table 11, the peak value represents the C=O bond that is hydrogen-bonded, while the shoulder is representative of C=O bonds not partaking in hydrogen-bonding. Max & Chapados (2005) found similar band positions for acetone in methanol:

- 1697 cm^{-1} representative of double-bonded acetone
- 1707.5 cm^{-1} representative of single-bonded acetone
- 1717 cm^{-1} representative of isolated acetone

The first overtone of the C=O bond peak also falls within the measurable range. For gas-phase acetone, this overtone band is located between 3455 and 3433 cm^{-1} (Guan et al., 2012). For pure liquid-phase acetone, the overtone appears at 3414 cm^{-1} (Dellepiane & Overend, 1966). These peaks overlap with O-H peaks, as identified by Max & Chapados (2005). Related to this study, the following spectral assignments are made for methanol in acetone:

- 3509 cm^{-1} representing methanol donating a single H-bond to acetone
- 3441 cm^{-1} representing methanol donating an H-bond to methanol
- 3340 cm^{-1} representing methanol accepting and donating H-bond

2.4.4 External factors influencing the v(O-H) band and hydrogen bonding

(A) Concentration

The effect of concentration on hydrogen bonding is determined by structural properties of the solvent and the solute. The two apparent cases for mixtures, solvation and the hydrophobic effect, are discussed in Section 2.3.1. For simple alcohols such as methanol (Dixit et al., 2002), ethanol and 1-propanol it has been shown (Adachi et al., 2002) that the hydrophobic effect dominates and it has been suggested that the methyl groups within the alcohols form clusters. The C-H···O interaction may be classified as hydrogen bonding, although this is still a topic of debate. Some scholars choose to define it as a van der Waals type interaction, since the bond energy is 4 kJ/mol. This energy may be enhanced by cluster formation (Chang et al., 2001). This effect also varies depending on the structure of the alcohol, with normal alcohols having a greater ability to form clusters than branched alcohols (Czarnecki & Wojtkow, 2004). Structure is further determinate of the monomer fraction due to the fact that monomer fractions increase as alcohol chain-length increases (von Solms et al., 2006b).

At higher alcohol concentrations, the hydrophobic effect becomes negligible. Here self-association and interactions between OH-groups dominate (Czarnecki & Wojtkow, 2004). Dissolved anions such as Cl^- have been shown to affect the v(O-H) band and thus it is important to avoid contamination (Rull, 2002).

Experimental work on *tert*-Butyl alcohol substantiates the idea of association of alcohols via the methyl groups. At very low alcohol concentrations, solute-solute interactions do not occur and the alcohol molecules appear in the monomeric form. The same study showed that water-water and alcohol-alcohol interactions were dominant in comparison to water-alcohol interactions in water-alcohol mixtures (Czarnecki & Wojtkow, 2004).

(B) Temperature

Temperature can also have a marked effect on absorption spectra, especially concerning the formation of inter- and intramolecular hydrogen bonds. The frequency shifts due to temperature are non-linear and very often the bandwidth is also affected (Peinado et al., 2006). It has been shown that for pure methanol (an associative compound) temperature has a slight effect on the extent of hydrogen bonding, but that the strength of hydrogen bonding is very sensitive to temperature variation (Czeslik & Jonas, 1999). Using two-dimensional correlation analysis (2D) NIR spectroscopy

for *sec*-Butanol, it has been shown that monomers increase with temperature, but at slower rate than the cyclic polymers disassociate (Czarnecki et al., 1998). The increase in monomer fraction with temperature is an expected result when one considers the effect of temperature increase at a molecular level.

(C) Pressure

It should be noted that hydrogen bonding increases with pressure and that pressure has a greater influence on the IR frequency than temperature (Desseyn et al., 2001). This is a logical result as higher pressure would force the molecules closer together, encouraging formation short-range hydrogen bonds. It has also been shown that this pressure dependence is dependent on the temperature (Okada et al., 2005).

2.4.5 Applications and difficulties of IR spectroscopy for hydrogen bonding analysis

For the purposes of this investigation, IR spectroscopy is used in the analysis and especially quantification of hydrogen bonding systems. For this to occur, the v(O-H) band must be seen in isolation. IR has a very good sensitivity in terms of viewing the v(O-H) band, so much so that it can differentiate between primary, secondary and tertiary alcohols due to the change in position of the narrow O-H stretch band between 3640 – 3540 cm^{-1} (Coates, 2000, p.10).

The MIR O-H stretching bands are very strongly affected by hydrogen bond co-operativity, which makes observation of the monomer band difficult. While some authors have advocated the superiority of NIR over MIR in the study of hydrogen bonding species (especially those involving water) it has been shown that the temperature dependence of the two regions is correlated and that concentration profiles generated from one spectral region may be used to resolve problems in another region (Libnau et al., 1994). Difficulties with the NIR spectrum are attributed to the weak intensity of the overtone bands associated with hydrogen bonding, as well as the complexity of the signal due to a multitude of combination bands and Fermi resonance phenomena (Rospenk & Zeegers-Huyskens, 1997). The use of 2D FT-NIR can resolve this complex signal, although it cannot provide quantitative information (Czarnecki et al., 1998).

2.5 Spectroscopic data analysis for alcohol solutions

2.5.1 Modelling of liquid spectra

IR spectra of liquids usually have a Lorentzian distribution, but peak symmetry is often spoilt by peak broadening (Dodd & DeNoyer, 2002). This broadening is due to disorder and introduces a Gaussian element into the peak character. Therefore, spectral peaks are often modelled using so-called Gauss-Lorentz (or Voigt) functions. The Voigt function is the superposition (or convolution) of a Lorentz function and Gauss function. Voigt profiles are a probability distribution and cannot be expressed analytically (Griffiths & de Haseth, 2007, p.11). For a full discussion on the Voigt function, consult Di Rocco *et al.* (2001) where a series expansion for this function is also given.

(A) Pseudo-Voigt profiles

A pseudo-Voigt peak is described by the following equation (Asprion et al., 2001) (Weisstein, 2002) (Weisstein, 2004):

$$A'\left(\tilde{\nu}\right)=\frac{A'_{\max}}{1+a^2\left(\tilde{\nu}-\tilde{\nu}_{\max}\right)^2}\exp\left[-b^2\left(\tilde{\nu}-\tilde{\nu}_{\max}\right)^2\right]$$

EQ 2.79

where
- $A'\left(\tilde{\nu}\right)$ is the calculated absorbance at wavenumber $\tilde{\nu}$
- $A'_{\max}$ is the maximum absorbance i.e. the height of the fitted peak
- $\tilde{\nu}_{\max}$ is the wavenumber at centre of the fitted peak
- a is the Lorentzian width
- b is the Gaussian width

EQ 2.79 cannot be integrated analytically, and therefore it is necessary to employ numerical integration to determine the area under the graph. For this, one may consider using Simpson's 3/8$^{\text{ths}}$ rule which uses for equally distributed points to calculate the integral (Chapra, 2008, pp.409-11):

$$\int_{x_1}^{x_4} f(x)dx \approx \frac{3h}{8}\left[f(x_1)+3f(x_2)+3f(x_3)+f(x_4)\right]$$

EQ 2.80

where
- h is the distance between each point
- $f(x_i)$ is the function value at x at point i

As long as the Gauss-Lorentz functions are relatively smooth and the value of h is small enough, the approximation of the area using EQ 2.80 will be accurate.

Another pseudo-Voigt function is given by the weighted summation (Griffiths & de Haseth, 2007, p.11):

$$A'\left(\tilde{\nu}\right)=\left(1-\alpha\right)\frac{A'_{\max}}{1+a^2\left(\tilde{\nu}-\tilde{\nu}_{\max}\right)^2}+\alpha A'_{\max}\exp\left[-b^2\left(\tilde{\nu}-\tilde{\nu}_{\max}\right)^2\right]$$

EQ 2.81

where α is called the Gaussian fraction and is usually less than 0.1 for most liquids.

These functions can be fitted to data with the Levenberg-Marquardt method (Dodd & DeNoyer, 2002), but other non-linear least square methods (e.g. Powell's Dog Leg method) could just as easily be implemented (see Madsen *et al.* (2004)).

(B) General peak-fitting considerations

The peaks can be fitted by using a range of mathematical modelling programs such as Origin (used by von Solms *et al.* (2007)), Matlab or freeware programs. It is however good practice to know how a spectrum is modified (i.e. which algorithms are used) and to have a good reason for doing so (Smith, 2011).

It is often useful to model a single peak by using two superimposed peaks. Furthermore, Dodd & DeNoyer (2002) make the following suggestions regarding peak-fitting:

- The most important peak parameter is location ($\tilde{\nu}_{\max}$)
- It is better to guess a narrow peak width (as opposed to a broad peak width)
- Data should never be smoothed before fitting
- It is usually better to estimate and remove baselines before modelling

Baseline modelling is a very important consideration whenever any spectral modelling is done. While baselines are treated as unwanted noise, there may often be a visible linear, exponential or hyperbolic trend (Dodd & DeNoyer, 2002). Baseline correction may also be done by simply joining the lowest points of a peak, usually in a reproducible manner (Stuart, 2004, p.51). This procedure is described graphically by Griffiths (2002) whereby the following two strategies are proposed for correcting the baseline of double peak:

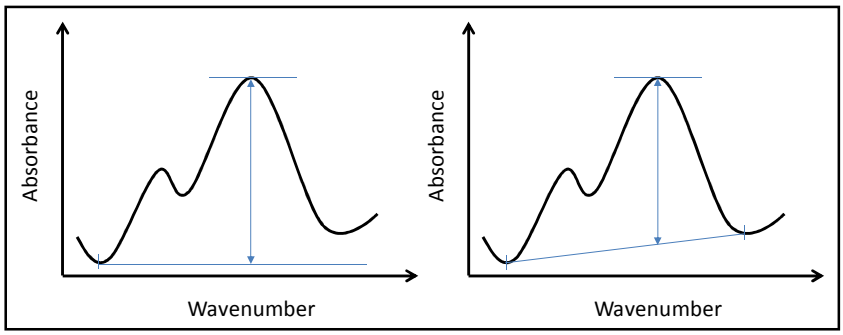

Figure 9: Two baseline correction strategies for a strong peak in a doublet [Redrawn from Griffiths (2002)]

In Figure 9, two strategies are shown viz. the single point method on the left and the tangent method on the right, where the goal is to find the peak absorbance of the strong band.

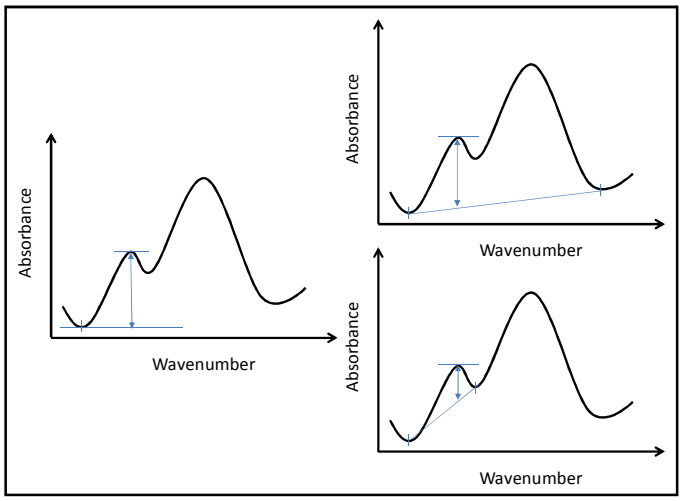

Figure 10: Baseline correction of a weaker absorption band in a doublet [Adapted from Griffiths (2002)]

In Figure 10 the single point method is shown for the weaker band on the left. When using the tangent method (on the right), there are now two possible tangents that can be used. The choice of method is very subjective and it is advisable to use the method which provides the best reproducibility (Griffiths, 2002).

Most spectrometers nowadays are accompanied with some form of analytical software which can perform automatic baseline corrections, but it is always important for the operator to observe carefully how the spectrum has changed (Dodd & DeNoyer, 2002). Griffiths (2002) also notes that it is very difficult for the automated software algorithms to distinguish between a broad real peak and a hump. Also, the baseline correction exercise is unnecessary for quantitative analysis and can be avoided by incorporating additional parameters into a partial least-squares (PLS) regression.

(C) Spectral subtraction

Spectral subtraction is a processing method whereby one removes unnecessary spectral features by subtracting a reference spectrum from the sample spectrum (Smith, 2011, pp.56-62). This process is relatively simple, but may not always obtain the desired results. Features common to the sample and reference spectra (e.g. non-interacting solvent peaks in a solvent subtraction) must be the same size and position in order for the subtraction to yield a zero baseline. Peaks larger than 0.8 absorbance units usually do not subtract well. Other spectral artefacts, such as derivative shaped peaks, may also occur.

A subtraction factor (in effect a scaling factor) may be used when a spectrum has a linear absorbance-concentration relationship (Griffiths & de Haseth, 2007, pp.201-03). This process can greatly simplify a spectrum and elucidate certain spectral features, but a good spectral subtraction is not always possible. Difference spectra should always be checked to ensure that they are sensible.

2.5.2 Method 1: Single low concentration calibration method

IR spectroscopy is what is referred to a secondary analysis technique i.e. a calibration must be done in order to develop a correlation between the intensity of a specific band and the parameter of interest – usually composition (Ismail et al., 1997, pp.108-09).

The calibration can be done by using a known mixture of very low alcohol content, where it may be assumed that only alcohol monomers appear. Asprion *et al.* (2001) suggest a lower limit of $x_{alcohol} = 0.001$ for IR spectroscopic investigations of alcohol solution, while Gupta and Brinkley (1998) detected a singular peak for 1-alcohols at $x_{alcohol} = 0.0007$. Therefore the total concentration of alcohol in the sample is represented by the monomer peak. The calibration is done using the Beer[5] law (von Solms et al., 2007):

$$A = \alpha C d \qquad \text{EQ 2.82}$$

where
- A is the integrated area of the absorbance peak [AU/cm]
- α is the absorption coefficient
- C is the concentration represented by the peak
- d is the cell pathlength through the sample [cm]

[5] Is more accurately called the Beer-Lambert-Bouguer law (Griffiths, 2002), but for the sake of brevity will be referred to as the Beer law

Pathlength is discussed in Section 2.5.5. The units of the absorption area are dependent on the units of concentration. Mole/mass fraction/percentage or molarity can all easily be implemented. Height may be used instead of area, but it is dependent on instrumental resolution (Griffiths, 2005) with the necessary adjustment made to the absorption coefficient. Once the absorption coefficient has been determined, it can be used to determine the concentration of monomers for the case when the total concentration is not representative of the monomer fraction. It must however be assumed that absorption coefficient is constant for the studied concentration range at each temperature (Gupta & Brinkley, 1998). This is a similar approach to the one used for the modelling of alcohol-alkane systems (von Solms et al., 2007), where the monomer peak was then fitted with a single Lorentz-Gauss peak. In their article, von Solms *et al.* mention a monomer peak around 3650 cm^{-1} but do not explicitly mention whether this peak position was constant throughout their fitting procedure.

2.5.3 Method 2: Multiple concentration calibration method

A more complex fitting procedure was followed by Asprion *et al.* (2001). The O-H stretch spectra are broken down into component parts by fitting multiple Lorentz-Gauss functions. When fitting multiple peaks, it is important to ensure that the fit doesn't become over-parameterised which can lead to non-unique results. Extraneous parameters also cause mathematical instability and overlapping peaks where one peak is taking all the signal power (Dodd & DeNoyer, 2002).

An example of the curve-fitting procedure is shown in Figure 11 where "Mo", "Di" and "Po" are used to denote the monomer, dimer and polymer peaks respectively.

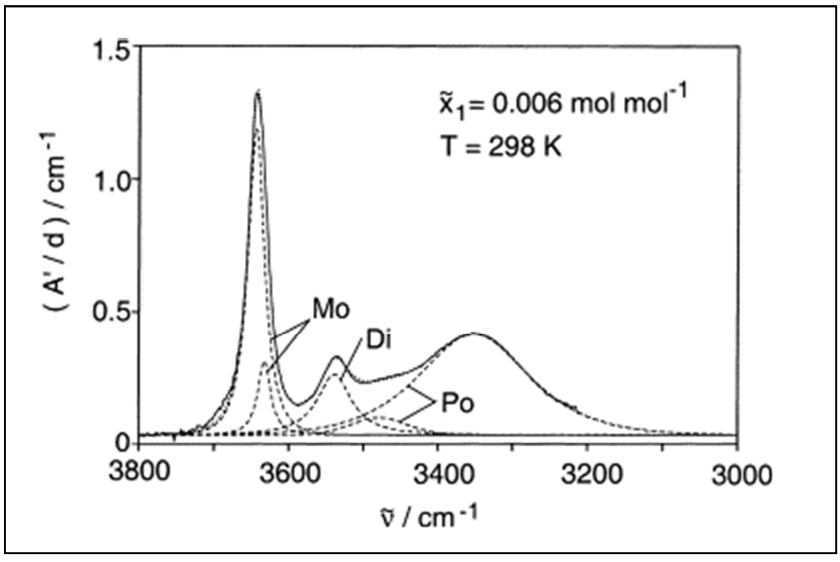

Figure 11: Fitted IR spectra for ethanol in ethanol in n-hexane. Reprinted from Fluid Phase Equilibria, 186, N. Asprion *et al.*, FT-IR spectroscopic investigation of hydrogen bonding in alcohol-hydrocarbon solutions, 1-25, Copyright 2012, with permission from Elsevier.

In Figure 11, the monomer and polymer peaks are asymmetrical and require fitting by two Gauss-Lorentz curves for each. The asymmetry in the monomer peak is most likely due to occurrence of rotational isomers and that of the polymer peak is due to the superposition of the many different bands described by this peak. These areas are combined to give the total area for a given band e.g. monomer. In their investigation, Asprion *et al.* (2001) fitted the parameters of all five curves to a single spectrum, where the monomer and dimer peaks were roughly the same size. The width and position parameters were then used as constants proceeding curve fits. The polymer peak parameters were not kept constant at higher concentrations, when the polymer peaks shifted to lower wavenumbers.

The low-concentration assumption cannot be made to determine the absorption coefficients of the dimer and polymer bands. By combining the Beer law (EQ 2.82) for each peak, a linear regression with at least three data points can determine the absorption coefficients by:

$$\tilde{c}_A = \frac{1}{d}\left(\sum_i \frac{A_i}{\alpha_i}\right)$$

EQ 2.83

where $\tilde{c}_A$ is the stoichiometric alcohol concentration
i is designated as monomer, dimer and polymer

It was found that this method tended to produce rather erratic values for the dimer coefficient due to the fact that no spectra exist where only dimers exist. This problem is however easily solved by minimising the following function, to solve for the absorption coefficients and equilibrium constants (Asprion et al., 2001):

$$\sum_j \sum_i \left(\frac{A_i}{\alpha_i d\tilde{c}_A} - \frac{c_i\left(\tilde{c}_A, \underline{K}\right)}{\tilde{c}_A} \right)^2$$

EQ 2.84

where $\underline{K}$ are the equilibrium constants
c_i are calculated from a thermodynamic model
j are the data points of an isothermal concentration series

In their discussion, Asprion *et al.* note that the choice of thermodynamic model had only a minor effect on the calculated absorption coefficients. For instance, a difference of 1.2% is reported for using the UNIQUAC model compared to an ideal solution for ethanol in *n*-hexane at 25 °C.

2.5.4 Considerations for maintaining the linearity of Beer's law

When considering Beer's law (EQ 2.82), it follows that as long as the absorption coefficient (α) and pathlength (d) remain constant, a proportional relationship will exist between the constituent concentration and the peak area it procedures. This proportionality is however only maintained under certain circumstances, with deviations occurring due to instrumental or sample effects (Hsu, 1997). Instrumental effects for FT spectrometers may include insufficient resolution and detector non-linearity, while sample effects may include chemical effects such as hydrogen bonding. For instance, the O-H peaks for diluted ethanol do not increase linearly with ethanol concentration, as the newly added molecules will not necessarily experience the same hydrogen bonding effects.

When absorbance is plotted against concentration, the graph is referred to as a Beer plot. When absorbance is plotted against pathlength, the graph is referred to as a Lambert plot. When a Lambert plot is linear, but the Beer plot is non-linear, the non-linearity of the Beer plot can be attributed to chemical effects such as association (Griffiths & de Haseth, 2007, pp.199-200). If the Lambert plot is also non-linear, it is due to instrumental effects. It is however impossible to distinguish between the electrical or optical problems based only on the Lambert plot.

Detector non-linearity is observed for Mercury Cadmium Telluride (MCT) detectors for strong absorption bands (Griffiths, 2002). This creates inaccuracies in the Beer law when absorption is above 0.2 absorption units. Methods, such as those proposed by Richardson *et al.* (1998) and Shao & Griffiths (2008), can be used to correct for this deviation.

Another very important factor to consider when using the Beer law to quantify spectroscopy data is that no air bubbles should be in the sample (Griffiths, 2002). These bubbles result in scatter of the incident rays and non-adherence to the Beer law.

2.5.5 Determination of cell path length (d) in Beer's Law

The pathlength of a transmission cell may be experimentally calculated by evaluating the interference pattern created when the sample cell is kept empty for both sample and background measurements. This sinusoidal pattern results from the interference between light travelling through the sample chamber and that which has internally reflected inside the chamber. The sample chamber pathlength (sample thickness) may be determined by (Griffiths & de Haseth, 2007, pp.253-55):

$$L = \frac{m}{2n(\nu_1 - \nu_2)}$$

EQ 2.85

Where m is the number of peak-to-peak fringes
n is the refractive index of the material between the reflecting surfaces
ν_1-ν_2 is the distance in wavenumbers over which m fringes are observed

2.6 Experimental spectroscopic methods

Two experimental methods were considered for this work viz. transmission FTIR and attenuated total reflectance (ATR) FTIR. Both methods can be operated on a single spectrometer. A schematic representation of the FTIR spectrometer used in this research is shown in Figure 12.

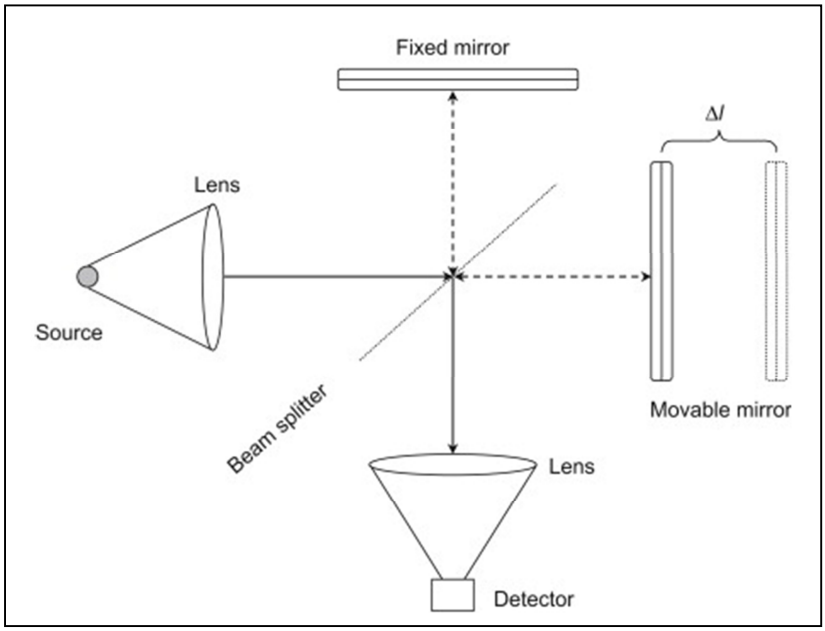

Figure 12: The basic components in an FTIR spectrometer. Reprinted from Infrared and Raman Spectroscopy, Peter Larkin, Elsevier Books, Copyright (2011), with permission from Elsevier

In Figure 12, the source creates IR radiation that passes through an aperture. The radiation is then split at the beam splitter, which divides it between the fixed and moving mirrors. The moving mirror creates a difference in the optical pathlengths between the two beams, which is a function of time. Both beams then either pass through the sample in transmittance mode, or are reflected against the sample in ATR mode. The beams then reach the detector, where the signal is processed as an interferogram. This very complex signal is Fourier transformed in real time to give the transmission spectrum as a function of wavenumber. The resolution of the spectrometer is determined by the amplitude of the motion of the moving mirror (Kellner et al., 1998).

2.6.1 Transmission FTIR

The difference between the transmission and ATR methods is seen at the sampling point. For the transmission mode, the IR radiation passes through sample held in a sample cell. The sample cell in its most basic form would consist of two optical materials separated by a spacer mounted in some form of a holder. The cell will usually also have Luer-lock fittings for sample injection – which may result in injection of air bubbles (Fabian & Vogel, 2002, p.59). Cells may be acquired as a sealed (window and spacer) unit with a fixed pathlength. Demountable cells are also available, where a range of spacers can be used to vary the pathlength (Specac, 2011)

(A) Transmission cell pathlength considerations

When using a transmission cell, the IR radiation passes through the sample and is absorbed. Absorption increases with pathlength. Thus it is important for the pathlength to be long enough to allow for sufficient absorption (i.e. be visible on the spectrum), but at the same time not be too long so that the spectrum becomes saturated (also see Section 2.6.3 for further discussions regarding saturation). Saturation may occur when the signal voltage is larger the maximum allowable voltage of the analog-to-digital converter (ADC). A saturated peak is clipped and has a flat-topped appearance (Griffiths & de Haseth, 2007, p.64). The pathlengths in Table 12 are prescribed for a given analyte concentration (Specac, 2011).

Table 12: Typical pathlengths used for given analyte concentration when using the Specac Omni Cell

Analyte concentration	Pathlength
> 10%	0.05 mm
10% - 1%	0.1 mm
1% - 0.1%	0.2 mm
< 0.1%	> 0.5 mm

The values in Table 12 can be used as rough guide for selecting transmission cell sizes.

(B) Transmission cell window selection considerations

Many IR window materials are available for transmission (and ATR) cells. As glass cannot be used for MIR spectroscopy, salt windows are usually used (Griffiths & de Haseth, 2007, pp.251-53). These include but are not limited to:

- NaCl
- KBr
- CaF_2
- ZnSe
- Sapphire

The most important parameters to consider, when selecting window material, are usually low wavenumber cutoff and refractive index. Von Solms *et al.* (2007) chose NaCl for the analysis of alcohol-alkane systems, except for systems containing methanol where sapphire windows were used.

In this investigation however, water-containing systems were also tested initially. For this reason NaCl was not considered as a viable window material – nor KBr. CaF_2 windows are virtually insoluble in water and as an additional advantage are also robust (Oliver, 2011).

2.6.2 Attenuated Total Reflectance FTIR

During an ATR measurement, the IR radiation travels through a crystal where it comes into contact with the sample during one or more total internal reflections (Fabian & Vogel, 2002, p.59). During the reflections, the IR beam partially absorbs into the sample.

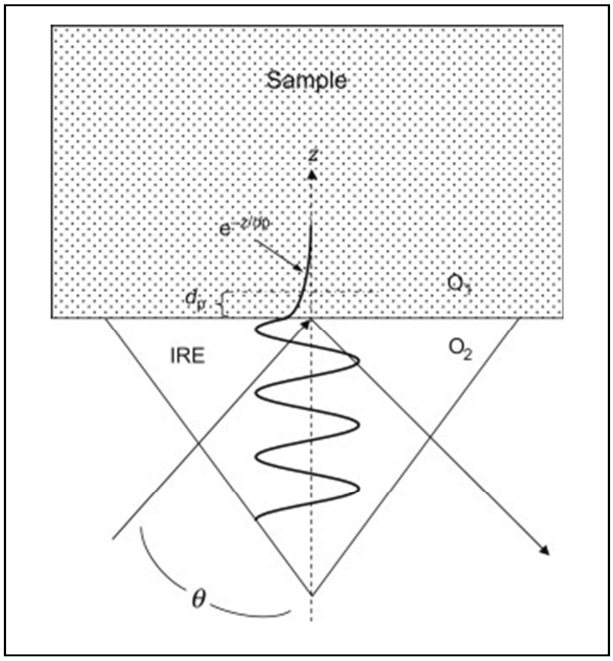

Figure 13: Mechanism for ATR-FTIR. Reprinted from Infrared and Raman Spectroscopy, Peter Larkin, Elsevier Books, Copyright (2011), with permission from Elsevier

In Figure 13, it can be seen that an ATR accessory has an internal reflection element (IRE), which allows the IR beam interact with the sample. The interaction results in an evanescent wave, which penetrates into the sample to a particular depth. The FTIR instrument then determines the spectrum that was absorbed by the sample by subtracting the reflected ray leaving the IRE from the incident ray which entered the IRE. The penetration depth (d_p) is defined by the following equation (Coates, 2001):

$$d_p = \frac{\lambda}{2\pi n_1 \sqrt{\sin^2\theta - n_{21}^2}}$$

EQ 2.86

where
- λ is the wavelength of the IR radiation
- n_1 is the refractive index of the IRE
- n_{21} is the ratio of refractive indices of the IRE and sample

For the most part these independent parameters can be controlled such that reproducible quantitative data can be obtained with ATR-FTIR.

ATR is considered a very practical solution for the analysis of liquids (Coates, 2001). It should also be noted that ATR accessories may make a spectral contribution to the FTIR instrument and thus it is good practice to take the background measurement with the accessory in place (Coates, 2001). It is

also preferable for an ATR probe not to be moved during an experimental study (Griffiths & de Haseth, 2007, p.200).

(A) ATR IRE selection considerations

In standard ATR probes, zinc selenide (ZnSe) is often used for the IRE crystal, due to its large spectral range (4000 – 650cm^{-1}), non-solubility in water and relative hardness. It is however attacked by strong acids and bases (Coates, 2001).

2.6.3 FTIR spectrometer components and operating parameters

This section contains a brief discussion on the various FTIR components that were manipulated during the spectral experiments completed in this study.

(A) Detectors

Two detector types were considered for this investigation:

- DGTS (deuterated triglycine sulphate)
- MCT (mercury cadmium telluride) (MCT-A High-D*)

In terms of basic application, the MCT detector is more sensitive, such that much finer definition may be attained for low concentration measurements. The disadvantage is however that peak saturation could occur at lower peak concentrations and MCT detector also needs to be cooled with liquid nitrogen in order to operate correctly whereas the DGTS detector can be operated at ambient conditions without a coolant.

(B) Aperture

From Figure 12, the aperture of spectrometer is related to IR beam leaving the source and can be thought of simply as an opening through which the IR beam must travel. The size of the aperture can be increased or decreased and it is used to control the angular size of the IR beam. This creates a point source effect which improves wavenumber accuracy and resolution. When the aperture size is too large, ADC saturation occurs, which creates non-linearity in the detector response. Aperture size also has a second trade-off consideration, whereby a larger aperture improves the signal-to-noise ratio and a smaller aperture results in better stability and accuracy. Generally, DGTS detectors can be operated with a larger aperture than a MCT detector (Thermo Fischer Scientific Inc., 2008).

It should also be noted that when using a sample cell, the cell itself may be the limiting aperture in the spectrometer setup (Griffiths & de Haseth, 2007, p.200). When this is the case, it is very important for the sample cell to be placed in exactly the same position relative to the IR beam.

2.7 Summary of literature review and selection of procedures

The SAFT framework has been developed from Wertheim's TPT specifically to account for association/hydrogen-bonding. The PC-SAFT equation of state (Gross & Sadowski, 2001) is a relatively recent development within the SAFT framework, whereby the dispersion term has been modified such that it is applied to hard chains rather than hard spheres. Von Solms *et al.* (2003) proposed further modifications to PC-SAFT (yielding the sPC-SAFT EoS) whereby the mixture terms were modified in order to decrease the computational complexity. In order to account for polar interactions, additional theories have also been developed. Two such theories are those developed by Gross & Vrabec (2006) and Jog & Chapman (1999). These terms have been incorporated into both PC-SAFT and sPC-SAFT, with successful applications for polar systems including alcohols and ketones.

Within all SAFT models, an association model must be specified for each component with a given mixture. These association models are typically based on physical characteristics of the molecules they represent. The 3B scheme (2 negative sites and 1 positive site) is typically used to model methanol, with the 2B scheme (1 negative, 1 positive) employed for ethanol onwards. The new 2C association mode was previously developed at Stellenbosch University (de Villiers et al., 2011b) and it has 1 negative and 1 bipolar site. The 2C scheme was developed specifically for modelling alcohol in solution with water, where very complex association interactions take place. This scheme should thus be suited for the purposes of modelling alcohol-acetone interactions. The 2B scheme has been assigned to acetone previously, partly to account for the polar interactions via the association framework.

The SAFT models include several parameters with generally three physical parameters, two for association and one for polar interactions. Adjustable parameters are usually fitted to pure component and VLE data, with some authors including other properties such as heat of vaporisation and monomer fraction data.

Monomer fraction data, traditionally quantitatively determined with IR spectroscopy, are found to be relatively sparse in the literature. Alcohol-acetone systems have been less well studied, in terms of monomer fractions (as opposed to in terms of spectroscopy) but two studies have calculated values of 0.10 and 0.456 as the acetone monomer fraction in a dilute solution with methanol.

From published monomer fraction data sets it is seen that the low concentration measurements are very important in terms of the calibration.

The O-H spectral peak (3700 – 3200 cm^{-1}) is seen to be representative of the hydrogen-bonding of alcohol, with the monomer peak in the region 3700 – 3590 cm^{-1}. Hydrogen-bonding in acetone takes places via the C=O bond. This bond is characterised by a spectral peak around 1710 cm^{-1} for acetone in alcohols, with a shoulder (representative of the acetone monomers) found nearer 1720 cm^{-1}.

From the literature review, it was determined that alcohol-acetone mixtures could be analysed in the spectral regions mentioned above, using a FTIR instrument in order to generate monomer fractions data. Two FTIR systems were considered, transmission and ATR, with transmission ATR shown to be more sensitive while ATR is more practical in the analysis of liquids. It was also concluded that a MCT detector would be more sensitive, while CaF_2 windows (for transmission FTIR) and ZnSe (for ATR-FTIR) would provide suitable spectral ranges for viewing both O-H and C=O bonds. Once the spectral data are obtained, it can be fitted with Gauss-Lorentz curves in order to determine the various peak areas to be used in the calibration and monomer fraction calculation.

Furthermore, the literature review reveals that there is a significant gap in terms of published binary monomer fraction data since very few cross-associating systems have been studied. Therefore, alcohol-acetone systems represent an excellent choice for this study, as both compounds can take part in hydrogen bonding. Generating monomer fraction data for such systems would provide an opportunity evaluate the performance of current association schemes and parameter sets, for both alcohols (2B/3B/2C) and acetone (2B), while also allowing the regression of new parameter sets.

Chapter 3: Materials & methods

From Chapter 1.3 it can be surmised that this project consists of two distinct phases, one experimental and the other theoretical. In Chapters 3 to 5, the focus is set upon describing the experimental phase of this research. Firstly, the experimental apparatus and methods are described (Chapter 3), secondly the accuracy of the experimental apparatus and analysis methods is verified (Chapter 4) and finally the experimental results are presented (Chapter 5).

The spectroscopic analyses were performed using an established spectrometer at the Geology Department of Stellenbosch University. The spectrometer is equipped such that it can analyse samples in two different modes viz. transmittance and ATR. For transmittance FTIR, the samples were presented in a sample cell, while for ATR-FTIR mode the samples were analysed in a specially designed vessel.

3.1 Nicolet 6700 FTIR spectrometer

A Nicolet 6700 spectrometer was used in these experiments. The spectrometer is fitted with a HeNe laser source and a KBr beamsplitter. The spectrometer comes standard with a DGTS detector, but is also fitted with a high definition MCT High-D* detector.

3.1.1 Spectrometer parameters and settings

For the spectrometer several of the settings could be varied, but it was found that the following parameter selections achieved the desired results for the given cases:

- For each liquid sample (irrespective of mode or detector selection):
  - Either 64 or 128 scans were recorded
  - a resolution of 4 cm^{-1} worked best for liquids, equating to a data spacing of 0.48 cm^{-1}
  - Happ-Genzel apodization and atmospheric suppression were also used
- For ATR mode:
  - Background spectra (256 scans) were taken at start of each experimental run
  - The spectral window set from 4000 to 650 cm^{-1}
  - H_2O suppression provided improved clarity in the O-H region

- For transmission mode:
    - Background scans were recorded after every sample using the same amount of scans as for the sample
    - The spectral window set from 4000 to 1100 cm^{-1}
- When using the DGTS detector:
    - Aperture was set to 75
    - Sample gain was set to 2
- When using the MCT detector:
    - Aperture was set to 12
    - Sample gain was set to 1

These parameters are provided for the express purpose of allowing the reader to replicate the experimental results on the given (or similar) device. But closer inspection of these settings also serves as an introduction to Chapter 5, where the comparative performance of the two modes and detector types are evaluated.

3.1.2 Transmission and ATR components

(A) Transmission cell specifications

The spectrometer operates in transmission mode with a Specac Omni Cell™ fitted with sealed CaF_2 windows.

Figure 14: Specac Omni Cell mounted in a custom-built baseplate

The cell is shown in Figure 14, where two CaF_2 sets, with a fixed pathlength specified at 0.2 and 0.5 mm respectively, were available. The sample window is held in place by four nuts between two plates and there are Luer lock injection ports. When injecting a sample, one should inject into the bottom port while allowing air to escape through the top port.

(B) ATR probe specifications

An immersion probe (DPR-207 from Axiom Analytical) was used in ATR mode. The accessory is used with a single elbow and is fitted with a 2-reflection ZnSe IRC. The ATR setup is seen in Figure 15:

Figure 15: Nicolet 6700 with a ZnSe ATR immersion probe attached

In Figure 15 one can see the probe attached to the spectrometer with a double elbow configuration. The probe can also be setup using a single elbow which will necessarily provide better signal strength due to the shorter pathlength and fewer reflections. The elbows are used to manipulate the probe toward the mixing vessel.

3.2 Sample presentation

3.2.1 ATR mode

A vessel was designed for the purpose of presenting the alcohol-acetone mixtures to the spectroscopic probe. The vessel specifications are provided Table 13 along with a schematic representation of the vessel internal arrangement in Figure 16.

Table 13: Mixing vessel specifications

Vessel Specifications	
Internal volume	15 - 40 mL
Volume/pressure control	Spring-loaded piston (manual)
Pressure relief valve	Swagelok SS OGM2 (manual)
Max. operating pressure	+/- 3 bar
Temperature control	Heating jacket (350 W)
Temperature measurement	PT 100 thermocouple
Max. operating temperature	+/- 100 °C
Seal type	NBR O-ring

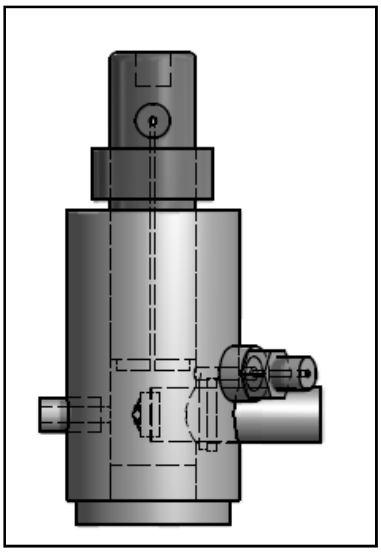

Figure 16: Internal arrangement of sample vessel

The sample is presented inside a hollowed out steel shaft, enclosed with a movable piston. The probe can be seen entering the mixing space from the right side in Figure 16 with an injection port above the probe entrance and a temperature probe port directly across it. The vessel is stirred using a magnetic stirrer.

Figure 17: Photo of the mixing vessel with ATR probe inserted

Figure 17 shows the mixing vessel with the ATR probe inserted on the right side. The piston (with a pressure gauge and valve attached) is seen extruding slightly above the metal frame and the magnetic stirring plate is seen below the vessel. The PT 100 probe is on the left and towards the back side of the vessel.

A schematic representation of the mixing vessel with all attachments is shown in Figure 18:

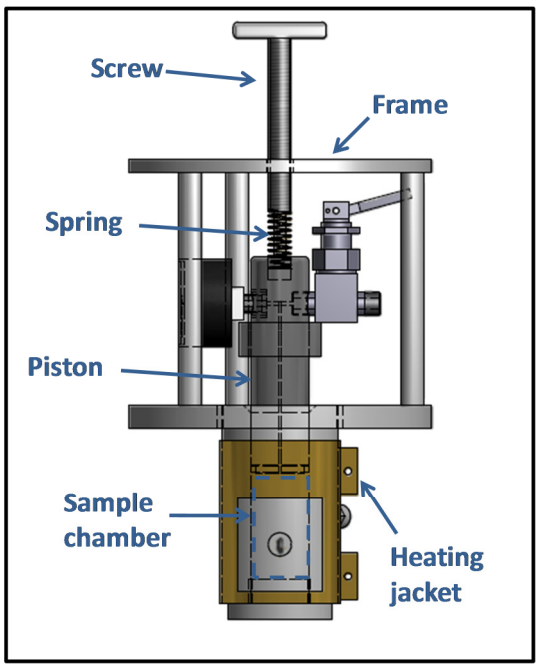

Figure 18: External arrangement of sample vessel

The piston is controlled by a spring-loaded screw. A Bordignon 4S10025 extra heavy duty spring (with a spring rate of 36.8 N/mm) allows the piston to move upwards in case of an excessive increase of pressure. The piston has spark-eroded 1 mm diameter hole which connects the sample chamber to a toggle valve.

The user can determine where the sample liquid level is located when the sample is initially loaded. This is done by opening the valve and moving the piston downwards until all the purge gas is forced out of the sample chamber. When liquid appears at the valve outlet, the valve is closed. The piston seals against the shaft with a nitrile O-ring. A Bourdon Tube Pressure gauge was installed in order to monitor the pressure within the vessel. More detailed schematics can be found in the appendices (Section 10.7).

3.2.2 Transmission mode

When using transmission mode, samples are prepared in the mixing vessel. A stainless steel shaft is used to seal the ATR probe entrance. Samples are extracted from the vessel and then injected into the sample cell (see Figure 14), which is placed inside the spectrometer for analysis.

3.3 Materials

The following chemicals were used in this investigation:

Table 14: Description of chemicals used in this investigation

Chemical	% Purity	% H_2O impurity	Company	Product number
Methanol	99.9	<0.02	Sigma-Aldrich	34885 Chromasolv®
Ethanol	99.8	<0.2	Sigma-Aldrich	34923 Spectranal®
1-Propanol	99.9	<0.05	Sigma-Aldrich	34871 Chromasolv®
2-Propanol	99.9	<0.05	Sigma-Aldrich	34863 Chromasolv®
Acetone	99.8	<0.2	Fluka	00568 (GC)
n-Hexane	99.0	<0.01	Sigma-Aldrich	52766

Maintaining a low water content is very important for this investigation, as water strongly hydrogen bonds and could thus corrupt the experimental data. Chemicals were bought in small batches in order to minimize atmospheric contamination between experiments. The acetone and *n*-hexane were also dried using molecular sieve (Fluka Analytical Molecular Sieve UOP Type 3A) and spectra of the pure chemical were taken before each experimental run to check whether any significant contamination had taken place.

3.4 Experimental procedure

3.4.1 Initial setup

- The baseline nitrogen purge line is switched on, set to 9 litres/min air (at 15 °C and 1.013 bar).
- If the MCT detector is used, liquid nitrogen is poured into the spectrometer to cool the detector.
- The experimental parameters for the spectrometer are set up (e.g. resolution, aperture etc.) and a bench alignment is done. Regular background scans are taken to determine the purging status and whether the ADC is saturated.
- The spectrometer is allowed to purge and the detector to cool down.
- If the ATR probe is used, it is inserted into the reactor and purged with technical grade nitrogen (Afrox 42-1E) for approximately 10 minutes, after which the probe is aligned.
- Meanwhile, the reactor temperature control is activated and set to a few degrees Celsius above the ambient temperature and is allowed to stabilise.

3.4.2 Solvent into mixing vessel

- The reactor is purged with nitrogen.
- The solvent is weighed on a Precisa® EP 920M (e=10mg, d=1mg).

- The sample is extracted from the container using a gas-tight Hamilton® syringe (typically 25ml), with the scale zeroed to the weight of the syringe, with measurements being taken.
- The solvent is injected into the reactor.
- The piston is then pushed down with the release valve open, to evacuate all the air from the reactor.

3.4.3 For ATR mode

- The background is taken with only the solvent in the reactor.
- Gradually increasing amounts of solute are added to the reactor.
- After each addition of solute, a suitable mixing time (typically 10 minutes – although tests show that 5 minutes is sufficient) is allowed before a spectral reading is taken.

3.4.4 Adding solute to the mixing vessel

- The solute is added to the vessel, using a 25uL or 100 µL gas-tight Hamilton® syringe.
- The solute is weighed on an OHAUS® Pioneer scale (e=1mg, d=0.1mg).
- The mixture is then allowed 10 minutes to mix, before a spectral measurement is made
- The temperature inside the mixing vessel is recorded on a spreadsheet along with the weights.

3.4.5 For transmission mode

- After the first batch of solute is added and allowed to mix, a 100 µL sample of the mixture is extracted from the mixing vessel.
- The vessel temperature is recorded.
- The sample is weighed before being injected into the transmission.
- Care is taken to remove bubbles from the transmission cell.
- The transmission cell is placed inside the spectrometer.
- After a 30 second wait, the sample is analysed.
- The temperature inside the spectrometer is measured using the handheld probe and recorded.
- The transmission cell is then removed and purged with pressurized nitrogen gas.
- The transmission cell is then either injected with pure solvent (ensuring that no gas bubbles are present) or left empty and then placed back in the spectrometer.
- After a 30 second wait, the background measurement is taken.

3.5 Experimental design

The experimental design consisted of three parts, with the first task being the determination of the optimal experimental parameters. This was followed by verification tests and finally data were measured for several dilute acetone-alcohol and alcohol-acetone systems.

3.5.1 Experimental parameters

The general parameters/settings are shown in Section 3.1.1 and were determined through non-specific experiments. The selection between transmission and ATR modes is tested through a specific experiment, whereby ethanol – *n*-hexane spectra were compared over similar concentration ranges, x_{EtOH} ε [0.0010; 0.0474] and [0.0018; 0.0424] for transmission and ATR modes respectively.

3.5.2 Verification tests

Following the determination of the optimal spectrometer operating settings, the detector linearity is established for detectors available. The C=O peak of acetone – *n*-hexane mixtures is collected for acetone mole fractions ranging from 0.0010 to 0.0302.

Literature data of von Solms *et al.* (2007) were reproduced in order to verify the accuracy of the experimental equipment. Ethanol – *n*-hexane system was chosen as a verification data set. Data were measured at 25.0 ± 0.5 °C with ethanol mole fractions ranging from 0.0036 to 0.0831.

3.5.3 New data collection

Finally, new data were collected for the following systems and conditions as listed in Table 15:

Table 15: Systems and conditions for experimental data measured in this work

Component 1	Component 2	mol% Comp 1	Temperature [°C]
Acetone	Methanol	0.018 - 0.468	23.2 ± 0.4
Acetone	Ethanol	0.016 - 0.544	23.2 ± 0.2
Acetone	1-Propanol	0.054 - 0.714	22.8 ± 1.0
Acetone	2-Propanol	0.0353 - 1.57	23.0 ± 0.6
Methanol	Acetone	0.016 - 0.861	23.3 ± 0.2
Ethanol	Acetone	0.092 - 0.747	24.8 ± 0.6
1-Propanol	Acetone	0.029 - 0.533	23.1 ± 0.4
2-Propanol	Acetone	0.062 - 0.892	23.3 ± 0.5

Chapter 4: Experimental verification & sample analysis

This chapter begins with a brief set of experiments, which consider various experimental parameters. These experiments are necessary to justify experimental parameter selections and to verify the accuracy of the experimental apparatus (Section 4.1). Included in this chapter is the experimental verification, which compares the data generated with our apparatus to the published data of von Solms *et al.* (2007) [referred to as "vS" throughout this chapter] and Asprion *et al.* (2001) [referred to as "As" throughout this chapter] for ethanol in *n*-hexane (Section 4.2). The verification data are followed by sample analyses, detailing the spectral processing methods used to calculate the monomer fractions for the acetone-alcohol (Sections 4.3) and alcohol-acetone (Section 4.4) systems.

4.1 Determination of optimal experimental parameters

In this section, two important experimental parameters are examined:

- Choice of ATR versus transmission modes
- Confirmation of detector linearity

4.1.1 Sample mode selection: ATR versus transmission

Two choices are available for sample presentation. ATR mode has a lower absorbance and thus can measure a wider range of concentrations. Since the measurements are made *in situ*, the temperature can be varied and controlled to 0.1 °C although the heat of mixing does present some complications in terms of maintaining the vessel temperature near or below the atmospheric temperature. With the experimental setup as described, transmission mode has a significant advantage in being able to measure very low concentrations due to strong signal strength.

Compare the following ethanol – *n*-hexane spectra for two similar concentration ranges:

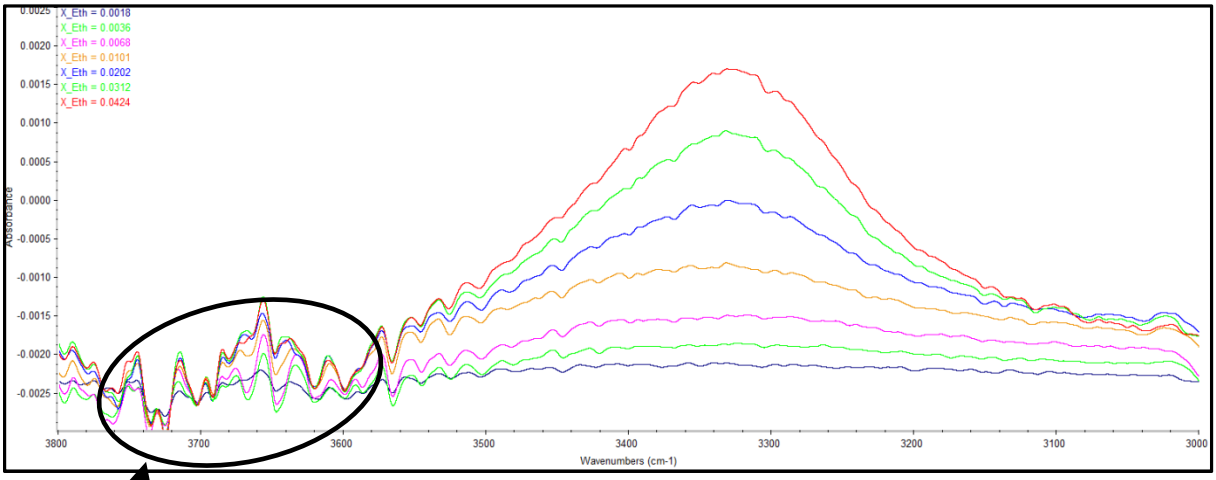

Figure 19: O-H peak spectra for dilute ethanol in n-hexane (x_{EtOH} ε [0.0018; 0.0424]) at 24.0 ± 0.5 °C collected in ATR mode using a MCT High-D* detector

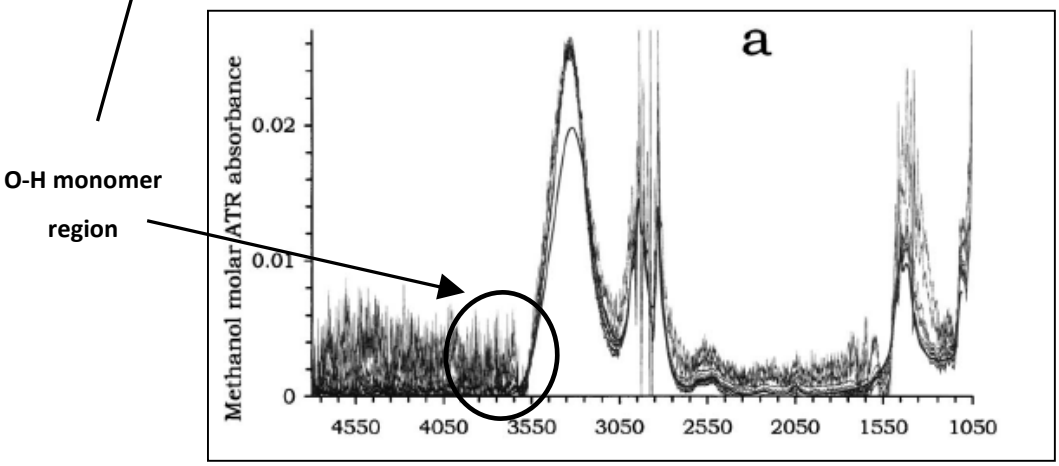

Figure 20: Methanol (x_{MeOH} ε [0.00; 0.25] in n-hexane) spectra collected with an ATR spectrometer. Reprinted with permission from J.-J.Max & C. Chapados, J. Chem. Phys 128 (2008) 224512.Copyright 2012, American Institute of Physics.

Figure 19 was achieved after months of optimisation with respect to several experimental variables (purge flow rate, aperture, optical velocity, spectral resolution, detector type, etc.) related to the configuration of the spectrometer. While Figure 20 was also collected using an ATR device, a DGTS detector was used in this case.

When looking at the monomer region (3700 – 3600 cm^{-1}) in Figure 20, there is a significant amount of noise relative to the size of monomer peak. The noise reduction seen in Figure 19 can probably be attributed to the use of the MCT High-D* detector, compared to the DGTS detector used by Max & Chapados (2008). As a secondary point Figure 19 also exhibits the excellent repeatability of FTIR, with four of the concentration points having repeated scans which lie atop one another.

The above findings show that the experimental apparatus provide excellent resolution in ATR-mode as compared to other studies found in the literature. These findings do however not aid in the selection between ATR and transmission modes for the experiments proposed in this work. For this decision, compare the spectra in Figure 19 to those collected using transmission mode in Figure 21.

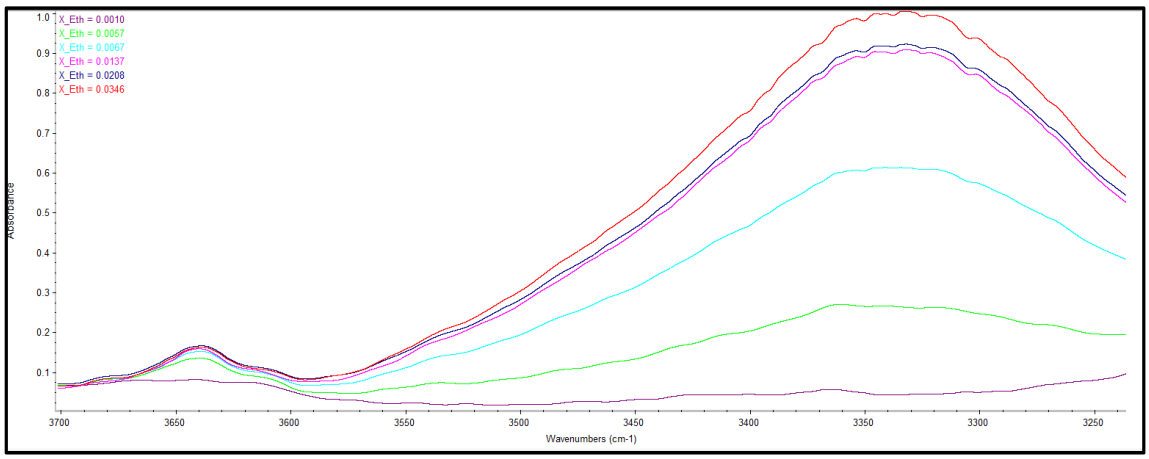

Figure 21: O-H peak spectra for dilute ethanol in n-hexane (x_{EtOH} ε [0.0010; 0.0346]) collected in transmission mode

The O-H peaks (monomer: near 3640 cm^{-1}, polymer: 3600 – 3300 cm^{-1}) are clearer in Figure 21 and the spectra are similar to those published by von Solms *et al.* (2007) and Asprion *et al.* (2001) groups. The O-H monomer peak is clearly visible around 3640 cm^{-1}, even at the low mole fraction of 0.0010. In comparison to the spectra collected in ATR mode, it is clear that transmission mode should be used for the quantification of the O-H monomer despite the fact that the ATR immersion probe offers greater flexibility and also more accurate temperature control (with the available experimental apparatus).

4.1.2 Confirmation of detector linearity in transmission mode

It is very important to establish whether the detector achieves a linear response for absorbance to concentration. As the greatest absorbance is achieved when using the MCT detector in transmission mode, the test of linearity is shown for this setup. For completeness, the linearity test for the ATR mode is given in the appendices (see Section 10.5) where C-O stretch peak at 1050 cm^{-1} is used.

For transmission mode, this peak cannot be used as it falls below the cut-off point of the CaF_2 windows in the transmission cell. The O-H peaks cannot be used either due to the obvious non-linear distribution of the concentration among the various hydrogen-bonding peaks. It was also found that C-H peaks absorb too strongly when operating in transmission mode. Therefore the final choice was

to use the C=O peak of acetone diluted in *n*-hexane, where AcO·$(Hex)_2$ complexes predominantly are formed and a single C=O peak appears at 1722 cm^{-1} (Max & Chapados, 2007).

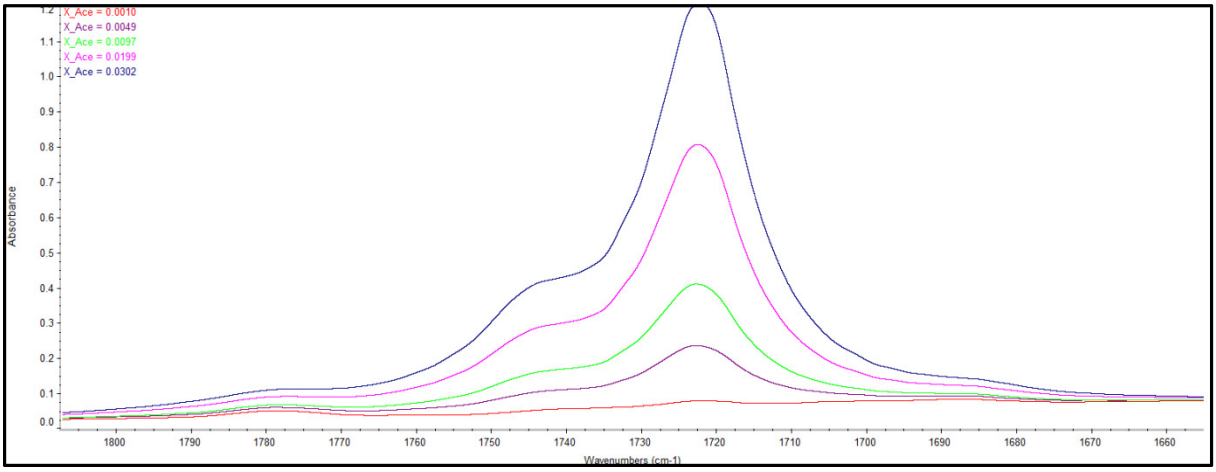

Figure 22: C=O peak at 1722 cm^{-1} for dilute mixtures of acetone (x ε [0.0010; 0.0302]) in *n*-hexane at 25.6 °C

In Figure 22, five spectra are shown. The C=O peak absorbs strongly at 1722 cm^{-1} with a maximum absorbance around 1.2 AU for the case x_{AcO} = 0.0302. Other spectral features are visible around 1780, 1745 and 1680 cm^{-1} and the spectra exhibit a negatively sloped linear baseline. This case provides not only a good test of detector linearity, but at the same time offers the opportunity to evaluate the peak-fitting methods. The raw spectra are baselined using their absorbance values at 1820 and 1660 cm^{-1}.

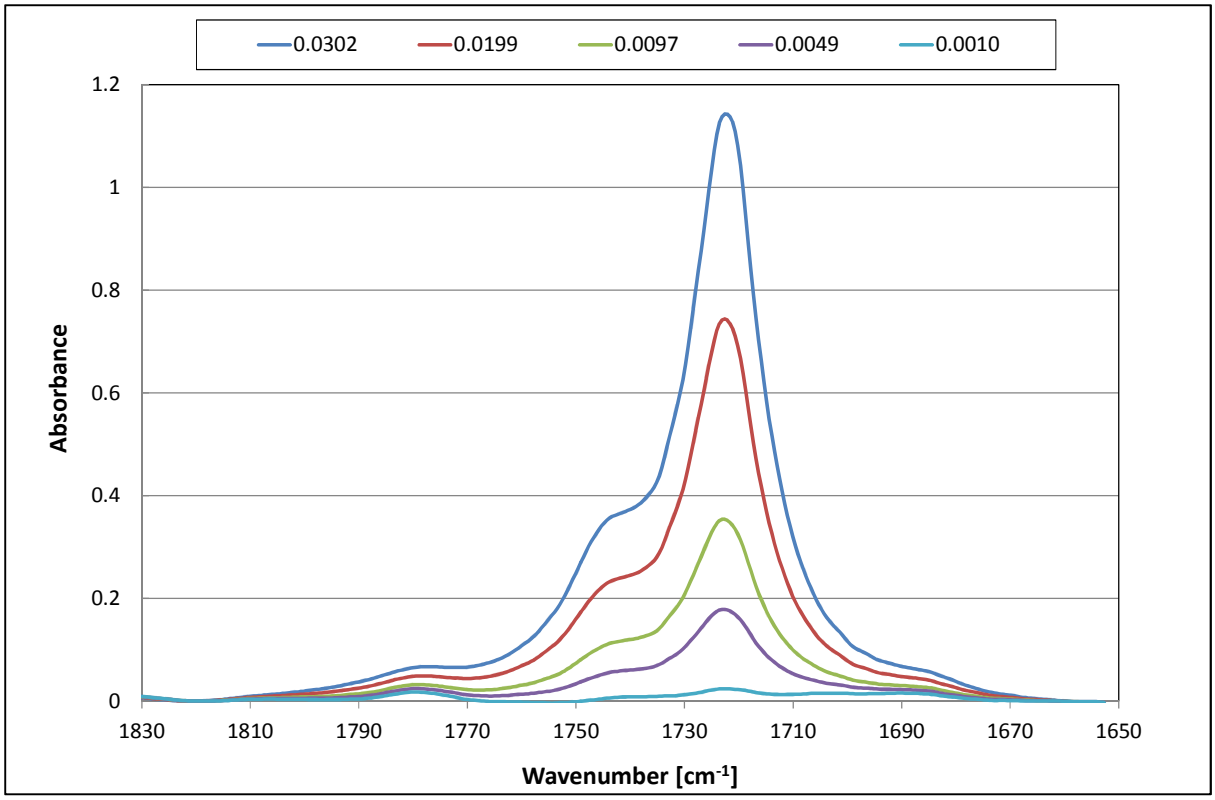

Figure 23: Baselined C=O spectra for dilute acetone in *n*-hexane at 25.6 °C

The spectra are then fitted with both Gaussian and Gauss-Lorentz (GL) functions, as seen in Figure 23. The area of the C=O is then calculated with the calculated values in Table 16.

Table 16: Gaussian and Gauss-Lorentz integrated absorbance areas calculated for C=O of acetone in *n*-hexane

	Integrated area [cm^{-1}]		Adj - R^2	
x	Gauss	GL	Gauss	GL
0.00102	0.3900	0.6943	0.891	0.922
0.00486	3.559	3.778	0.945	0.999
0.00970	6.677	8.046	0.969	0.998
0.0199	13.45	15.77	0.977	0.999
0.0302	20.64	24.27	0.979	0.999

Table 16 shows that the GL function gives a more accurate fit and thus it was decided to use Gauss-Lorentz functions for the spectral curve-fitting. It is however noted that for both functions the curve-fitting accuracy decreases at very low concentrations due to the increase of noise relative to the observed peaks. The data from Table 16 were now used to graphically test MCT detector-response linearity in Figure 24.

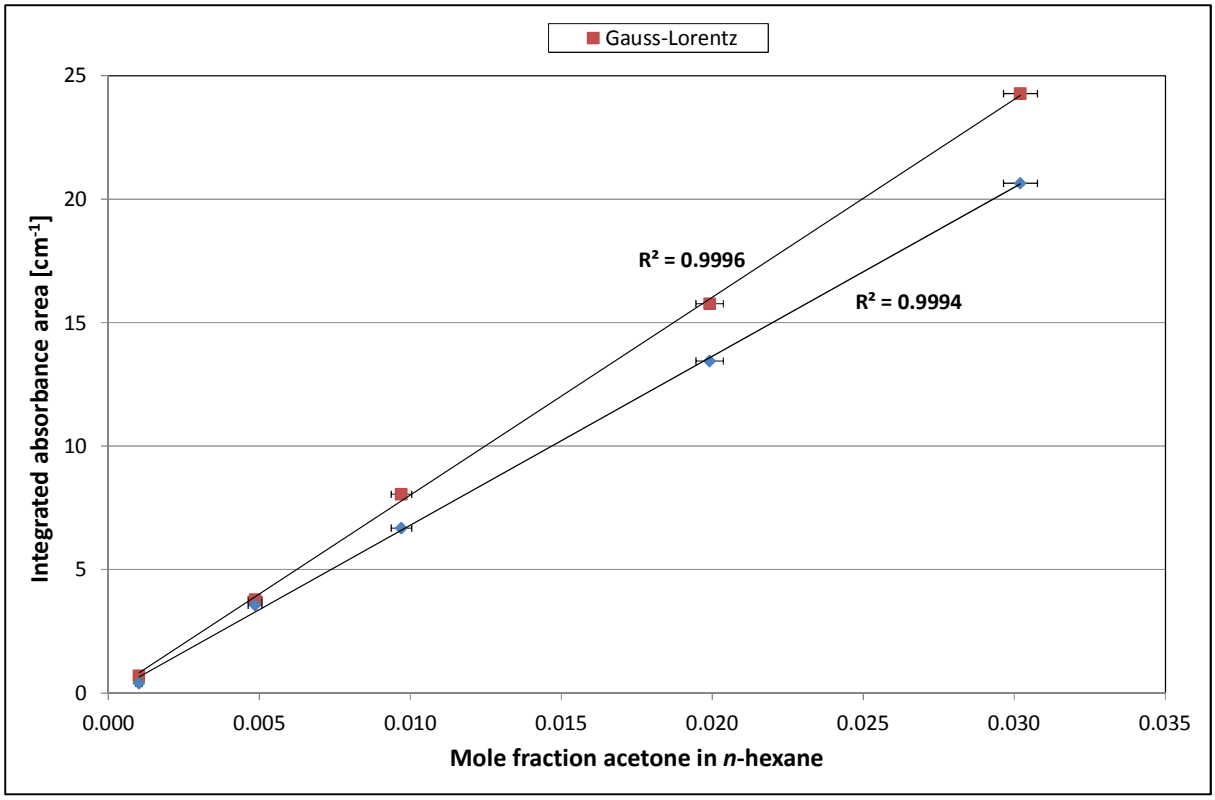

Figure 24: Absorbance area-concentration plot for acetone C=O peak confirming detector linearity for the MCT detector used in transmission mode

Figure 24 shows the Beer plot for the C=O acetone peak, using both Gaussian and Gauss-Lorentz functions to determine the peak area. Both methods prove to be very accurate, with the Gauss-Lorentz function providing a slightly more linear fit (R^2 = 0.9996 versus 0.9994). This is a very pleasing result and shows that MCT detector can be used with confidence up to an absorbance of at least 1 AU.

4.2 Verification using ethanol – *n*-hexane

Several IR spectra were measured for ethanol – n-hexane system in order to verify whether the FTIR setup can replicate literature values for the alcohol monomer fractions in these mixtures. The first step for the quantification of the monomer fractions was to determine the pathlength of the transmission cell used.

4.2.1 Cell pathlength determination

The cell pathlength is used in the determination of the absorption coefficients of the ethanol O-H peaks. The cell pathlength is specified as 0.2 mm, but this may not necessarily be 100% accurate.

Figure 25 shows the interference pattern generated from scanning the empty transmission cell along with peak positions as determined with the *Find Peaks…* function in the OMNIC package.

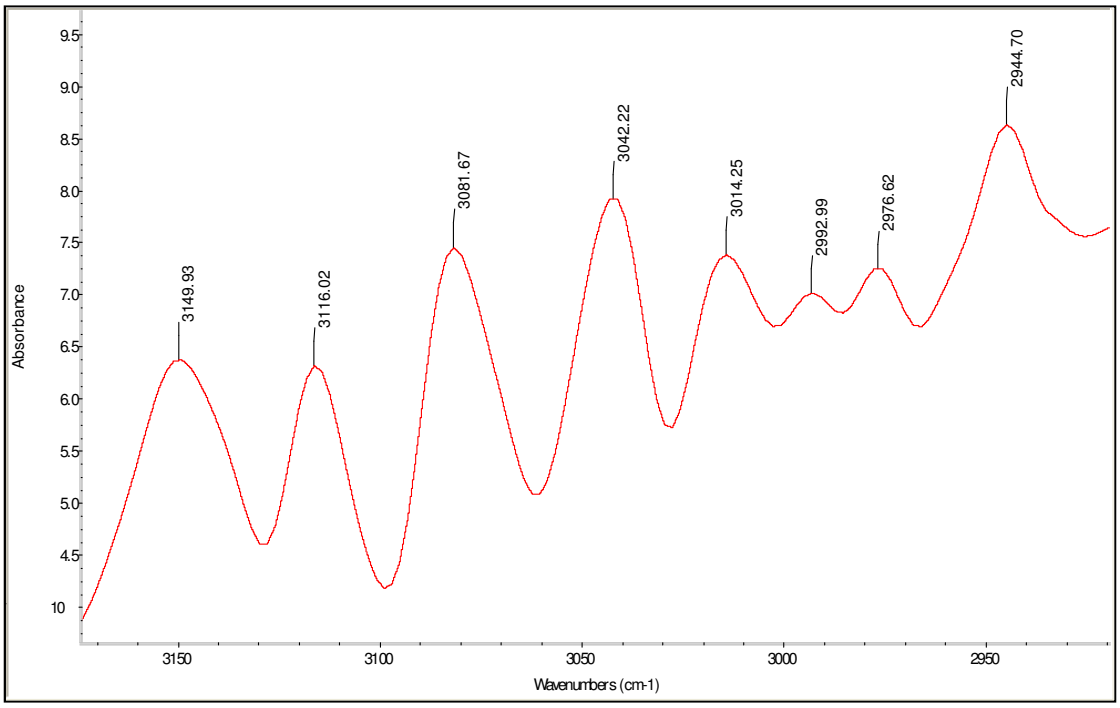

Figure 25 Interference pattern observed in a blank 0.2mm pathlength transmission cell

Using Figure 25 and EQ 2.85, one can more accurately calculate the pathlength as:

$$L = \frac{7}{2(3149.9 - 2944.7)}\left[\frac{1}{cm^{-1}}\right]$$
$$= 0.0171[cm]$$
$$= 0.171[mm]$$

The calculated value is slightly shorter than the value given by the manufacturer and was used in further calculations. The next step was to complete the spectral processing.

4.2.2 Spectral processing

After an experimental run, a set of raw unprocessed spectra is obtained as shown in Figure 26.

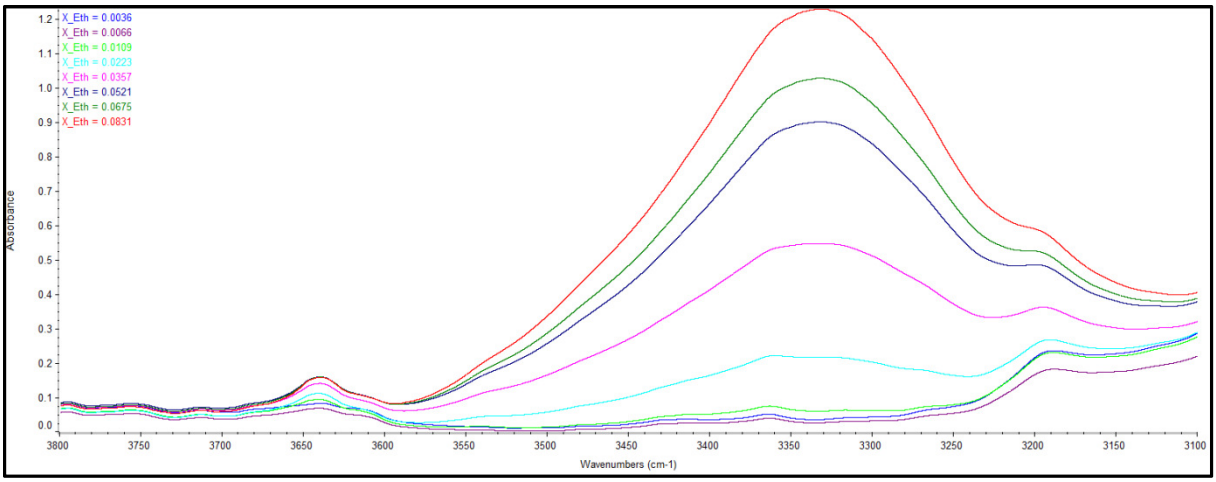

Figure 26: Common scale raw spectra for the ethanol (x ε [0.0036; 0.0831]) in *n*-hexane at 25.0 ± 0.5 °C

Figure 26 shows the unprocessed spectra for an ethanol – *n*-hexane system at 25.0 ± 0.5 °C. The mole fractions of ethanol range from 0.0036 to 0.0831, where the absorbance begins to stretch well above the recommended limited for Beer Law applicability. From Figure 27, it can be seen that spectra show roughly the same pattern between 3800 – 3700 cm^{-1} and this area provides an obvious region for which the baseline of the monomer peak may be fit. Figure 27 further emphasizes this point.

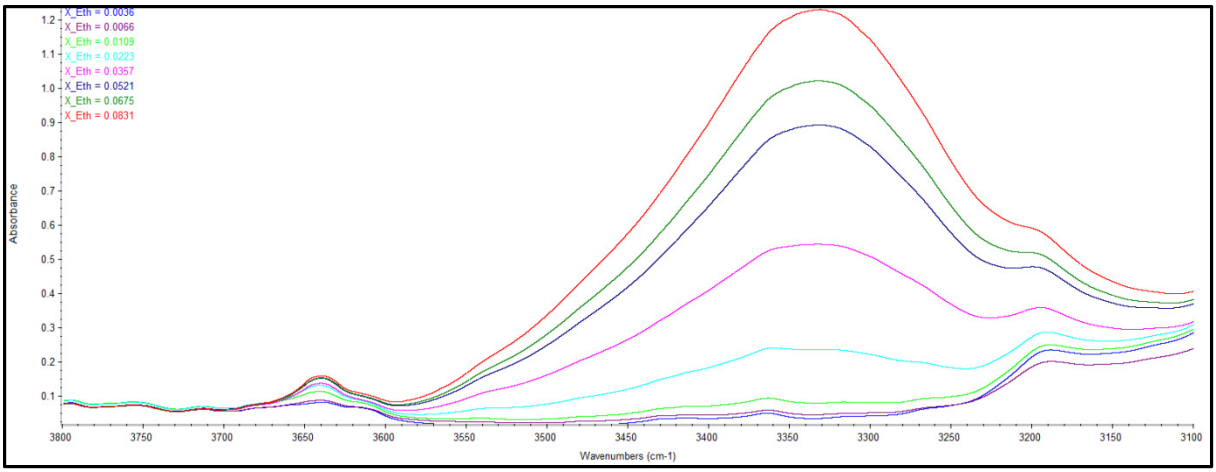

Figure 27: Common scale raw spectra for ethanol – *n*-hexane aligned between 3800-3700 cm^{-1}

Here the spectra have all been aligned in the region above 3700 cm^{-1} where a satisfactory agreement is seen. In this figure, the spectra show an ordered growth of absorbance with concentration. It is also evident that the curve-fitting process would necessarily need to account for the overlapping in the dimer region (around 3550 cm^{-1}) and below 3200 cm^{-1} where significant overlap from C-H peaks are seen. First linear baselines are used, after which a 5 component Gauss-Lorentz product curve (as per EQ 2.79) is fitted to each spectrum. Relatively few constraints were placed on the curves (barring

peak position) and as such these functions were in-effect the best-fit for each spectrum independent of each other. Subsequently the areas are calculated numerically (using EQ 2.80) and are shown in Table 17.

Table 17: Calculated areas for the 5GL fitted curves along with goodness of fit values

	O-H peak areas [cm^{-1}]			Adj - R^2	
X	Mono	Dimer	Poly	Baseline	5GL
0.00357	3.44	0.018	1.86	0.9104	0.9348
0.00660	2.60	0.349	2.06	0.9536	0.968
0.0109	3.34	0.482	3.65	0.9863	0.972
0.0223	3.67	0.064	13.62	0.9992	0.993
0.0357	2.66	0.394	48.07	0.9974	0.9837
0.0521	2.58	0.144	93.40	0.9982	0.9926
0.0675	2.46	4.311	117.20	0.998	0.9945
0.0831	2.54	6.346	157.06	0.9982	0.9964

In Table 17, the monomer and polymer areas are the sum of 2 GL curves each and the dimer area consists of a single peak. The growth of the polymer peak is most stable, as is the trend for the integrated absorbance areas shown by Asprion *et al.* (2001). The monomer peak growth is less smooth, whereas the dimer peak has very erratic development. This is due to difficulty in deconvoluting the dimer peak. The adjusted R^2-values in Table 17 indicate that the accuracy of fit generally increased with the mole fraction of ethanol.

The baselined and fitted spectra are shown in Figure 28.

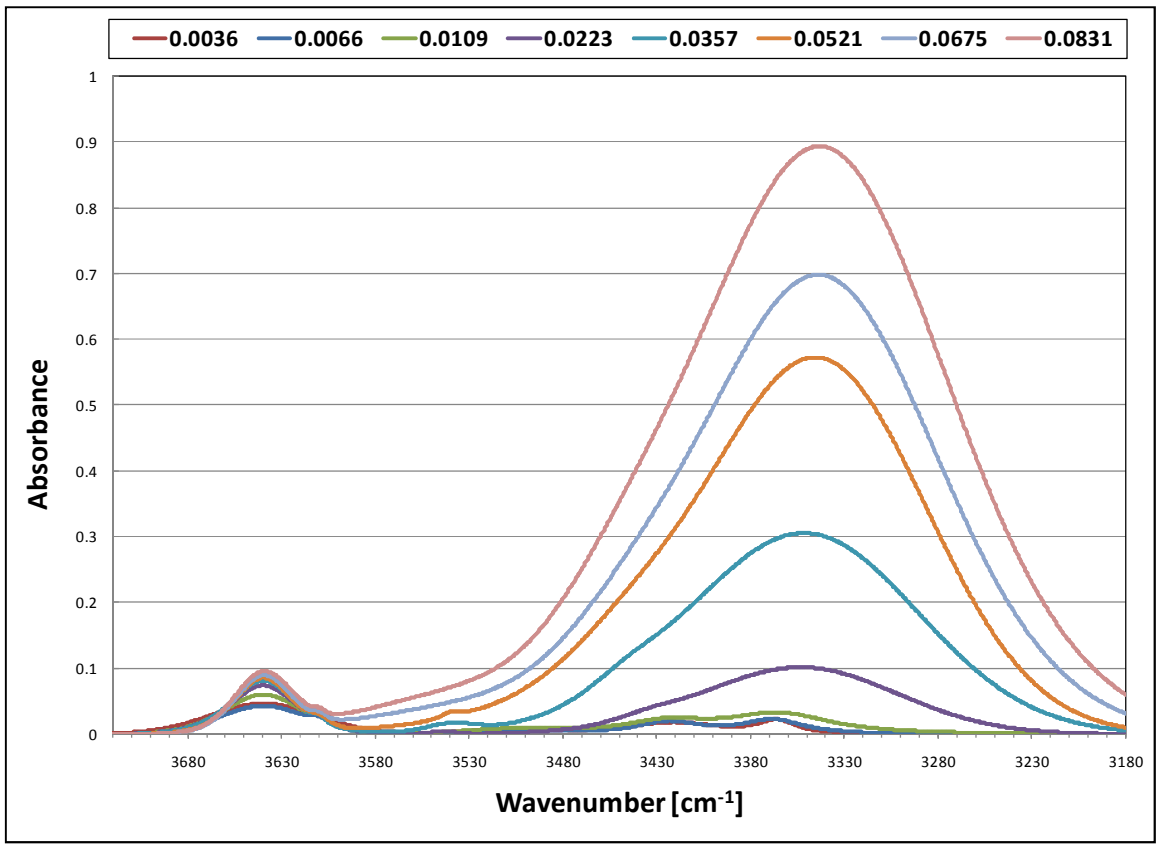

Figure 28: Baselined, fitted spectra for O-H peaks of ethanol in *n*-hexane

Figure 28 plots the processed spectral curves for the O-H peaks of ethanol. To the naked-eye, the resultant spectra look relatively similar to those seen in both literature sources. There is some narrowing present for the monomer peak. This is most likely due to the choice of curve and also causes some of the anomalies seen in the calculated monomer peak areas. The dimer peak is not necessarily as visible here (or in the von Solms *et al.* (2007) article) as it in Asprion *et al.* (2001) graphs. The next step in the process is to determine the absorption coefficients for the vS-method.

4.2.3 Monomer peak calibration

For the vS-method, the absorption coefficient is determined from EQ 2.82 using the calculated area for x_{EtOH} = 0.0036 and the cell pathlength calculated in Section 4.2.1 on page 68 to calculate an absorption coefficient[6] of 965 cm^{-2}. This absorption coefficient can then be used to calculate the monomer fractions which are then compared to literature values in Figure 29.

[6] The dimensionless units are omitted – the full unit set is AU cm^{-2} / mole fraction.

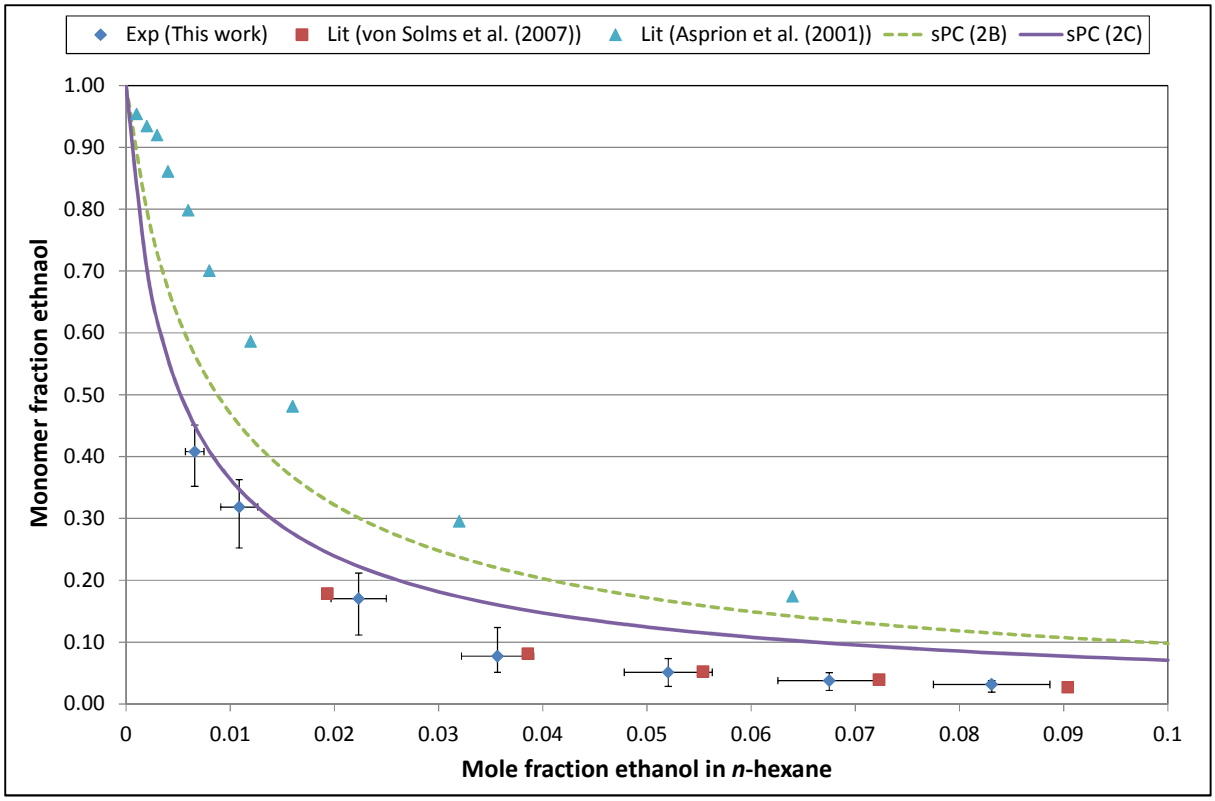

Figure 29: Comparison of verification data set to literature values and sPC-SAFT models

Figure 29 shows the experimental data compiled in this work, as well as literature values and two sPC-SAFT models. Horizontal and vertical error bars accompany the experimental data. These bars account for errors due to temperature variation and the mass measurement errors. In absolute (as opposed to percentage) terms, the vertical errors tend to be larger towards the lower mole fractions of ethanol, while horizontal errors become larger as the ethanol mole fraction increases. These data show very good agreement with that of von Solms *et al.* (2007), although these two data sets are at slightly different temperatures (23.3 °C vs. 25 °C). The Asprion *et al.* (2001) data were recorded at 25 °C.

The data sets are also compared to two sPC-SAFT models. The first is the 2B model used by von Solms *et al.* (2007) in their article[7] while the second (sPC (2C) in Figure 29) is the newly developed 2C association model, with the ethanol parameters as given by de Villiers *et al.* (2011b). The 2C model shows relatively good agreement with the experimental data, while slightly over-predicting the experimental values in this work and those of von Solms *et al.* (2007). Therefore the 2C model is used to adjust experimental values determined here, so that data sets may be compared at ("approximately") equal temperatures.

[7]Note the correct volume of association is 0.032384 rather than the 0.32384 shown in the source

In order to correct for this difference in temperature, a method is proposed whereby the sPC-SAFT 2C model is used to generate monomer fraction predictions for the ethanol – *n*-hexane system at 25.0 and 23.3 °C respectively. These two predictions are then subtracted from one another in order to estimate the temperature dependence (at these two temperatures at least) of ethanol monomer fractions in solution with *n*-hexane. The resultant function is shown in Figure 30.

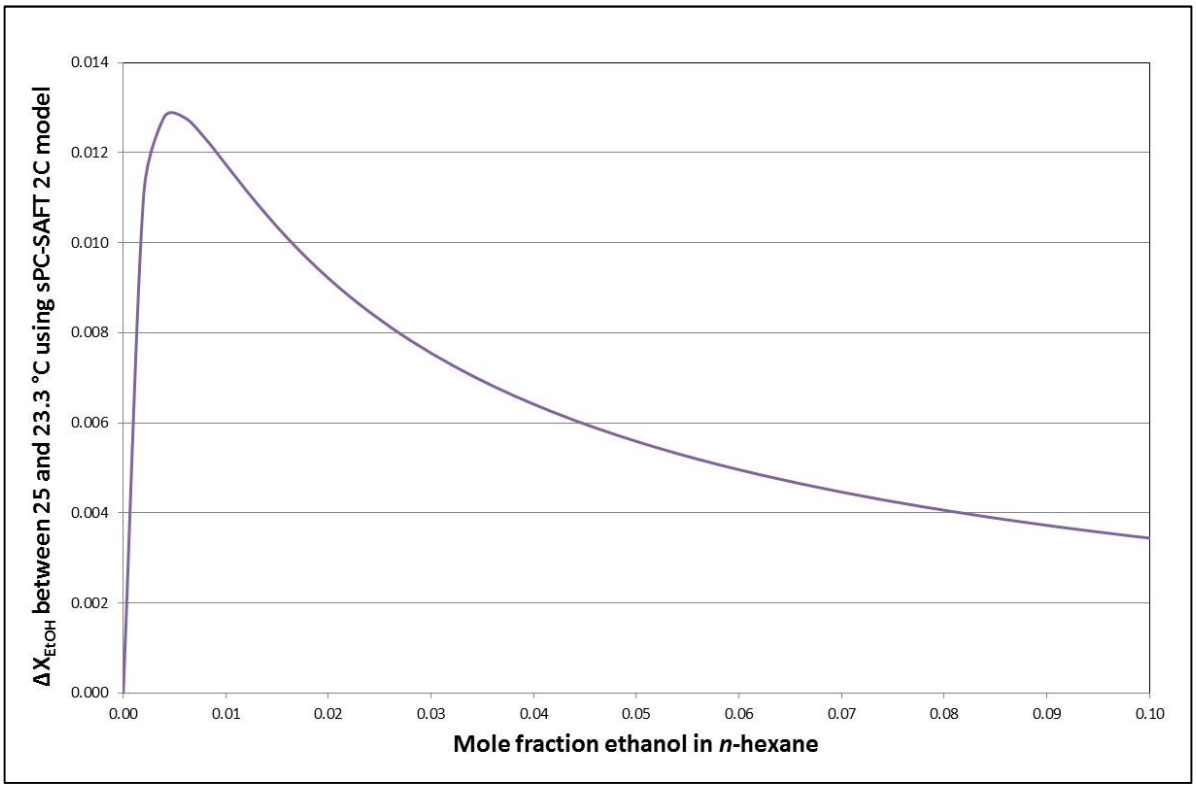

Figure 30: Temperature difference plot for ethanol monomer fraction prediction using the 2C model

The difference in predicted values does not exceed 1.4% mole (which predicts that the temperature difference has a negligible impact) and tends to decrease as ethanol monomer fraction increases. This graph necessarily begins at the origin increasing rapidly to a maximum before sloping gently downwards.

The points on this graph are used to generate interpolated values at each concentration in order to estimate how each data point must shift in order to account for the temperature difference between the data sets.

The results are shown in Figure 31.

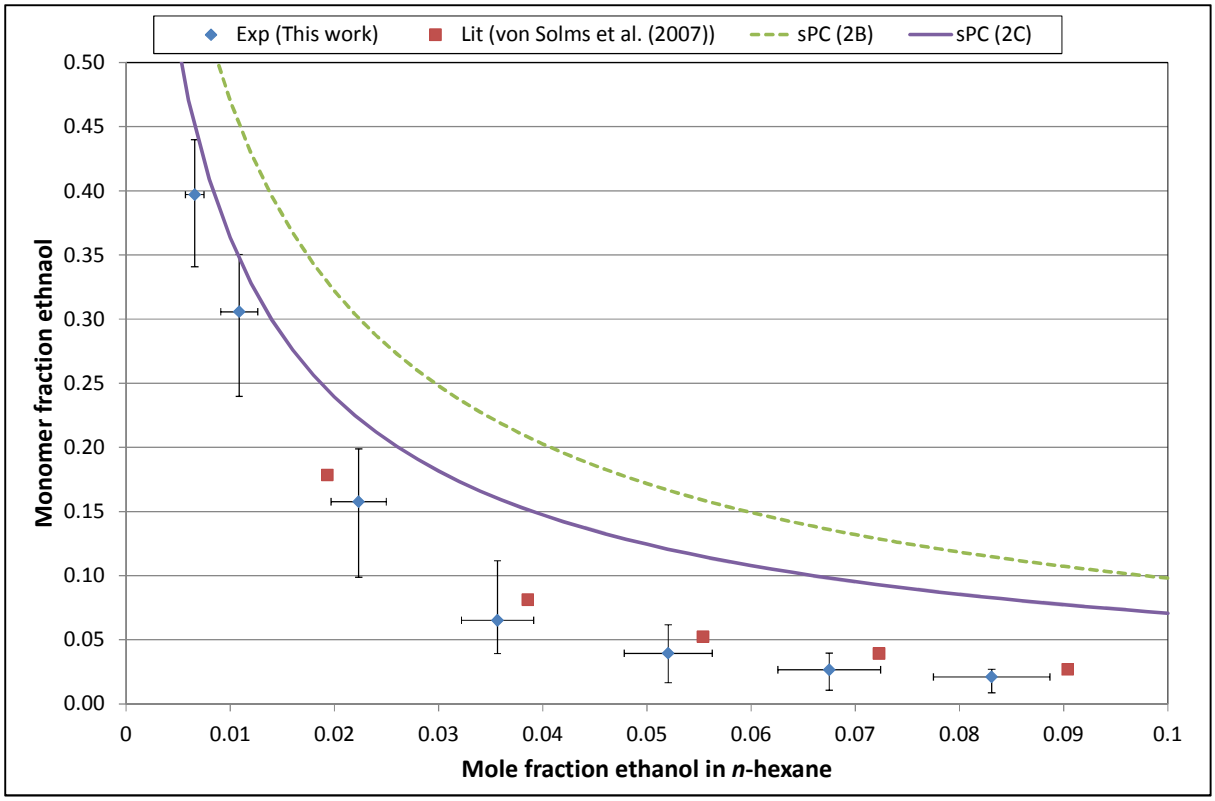

Figure 31: Temperature-adjusted comparison of verification data set to that of von Solms *et al.* (2007) at 23.3 °C

Here it can be seen that there is still good agreement between the data sets. The von Solms *et al.* (2007) data points generally reside within the error-space designated by the vertical and horizontal error bars, although the experimental data points of this work are in general slightly lower than those of von Solms *et al.* (2007). Similar monomer fraction results were obtained when pure Gaussian or Lorentzian curves were fitted. As a check, almost exactly the same monomer absorption coefficient was calculated during the minimization when using the As-method. However, due to the difficulty in accurately describing the dimer peak, a non-sensible absorption coefficient was calculated. This is similar to the result described in the report of Jensen & Kofod (2005). Further significant discussions on the differences between the literature data sets can be found in Chapter 10.6.

From the results shown in this section, it can be concluded that experimental apparatus function correctly and in such a way that reliable, spectroscopic, experimental data may be generated.

4.3 Sample analysis of dilute acetone in methanol

The dilute acetone in methanol system was chosen here for the sample analysis as there are two literature values for the monomer fraction of acetone at infinite dilution. These published values can be used to evaluate the calculated data:

- X_{mon} = 0.10 (Eamon & Symons (1985)) at 25 °C
- X_{mon} = 0.456 (Max & Chapados (2007)) at 27.3 °C

These values are very different. This discrepancy is discussed in Chapter 2.2.2.

4.3.1 Experimental conditions

The experimental mole fractions are calculated by using the quoted inaccuracy of the scale used to measure the solute and solvent, which are then combined to calculate the minimum and maximum possible mole fractions for each data point. This range is used to determine the horizontal error for each experimental data point. The temperature for each experimental run is calculated by using the average of the recorded FTIR temperatures, with a range of plus and minus three standard deviations.

Table 18: Concentrations and temperatures for an acetone – methanol system

	Acetone mole fraction			Temperature [°C]	
#	Measured	Low	High	Reactor	FTIR
1	0.000180	0.000147	0.000212	23.2	23.0
2	0.000429	0.000363	0.000494	23.0	23.2
3	0.000669	0.000571	0.000768	23.1	23.2
4	0.001030	0.000898	0.001161	23.1	23.2
5	0.001448	0.001283	0.001612	23.1	23.2
6	0.002014	0.001816	0.002211	23.1	23.4
7	0.002656	0.002425	0.002886	23.2	23.0
8	0.003364	0.003100	0.003628	23.1	23.3
9	0.004101	0.003804	0.004398	23.1	23.1
10	0.004683	0.004352	0.005013	23.1	23.1

For this system, the temperature is calculated as 23.2 ± 0.4 °C. The temperature range is slightly lower than the literature values, but not significantly so. A very dilute and narrow concentration range is used ranging from 0.018 mol% to 0.47 mol% of acetone in methanol. The range of mole fractions investigated here is substantially lower than those of the literature data sets, which begin at 0.3 mol% and 0.5 mol% respectively. One would thus expect to obtain very good data regarding

the interaction between acetone molecules at infinite dilution. It is thus reasonable to expect that even higher monomer fractions are obtained at these low concentrations of acetone.

4.3.2 Spectral processing

The raw spectra for the dilute acetone-methanol experimental run are shown in Figure 32.

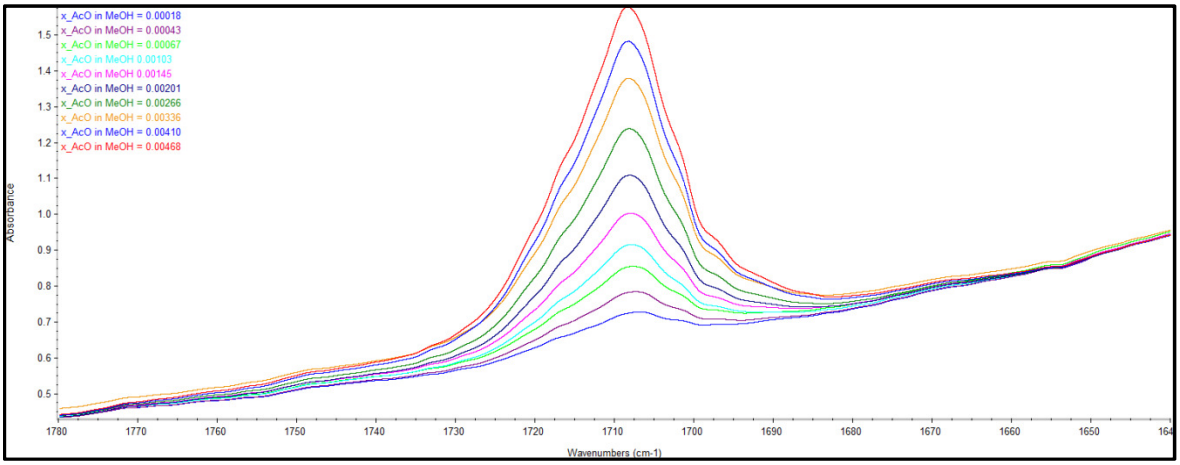

Figure 32: Unprocessed acetone C=O spectra in solution with methanol

In Figure 32, the smallest peak is representative of the lowest concentration of acetone and likewise for the largest peak as to the highest concentration. At X_{AcO} = 0.0047, the "net" height of the C=O peak is already nearing the 1 AU limit. It can also be seen that the spectral baseline is not necessarily linear. Therefore a composite exponential function is fitted to the spectral data with the spectral peaks removed for the baseline fit. The baselined data were then fitted with Gauss-Lorentz peaks. The fitted baseline spectrum for the most dilute sample is shown in Figure 33.

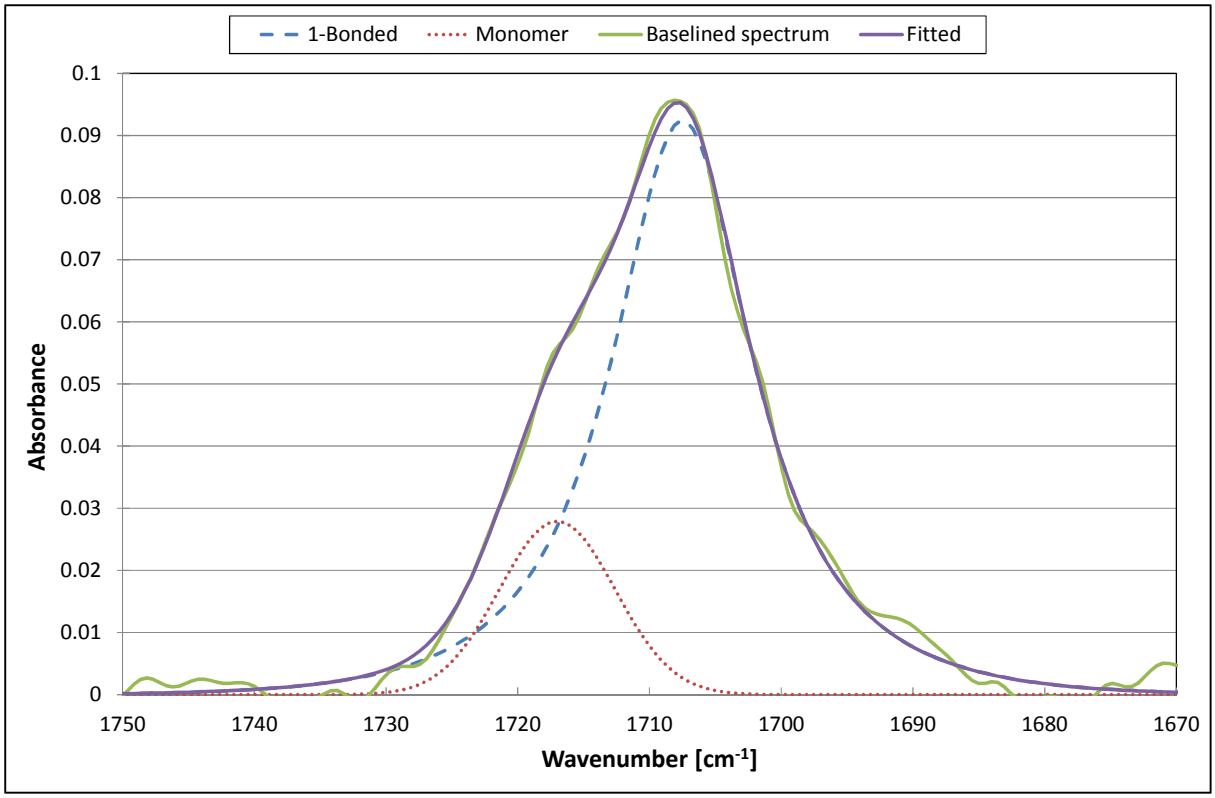

Figure 33: Low concentration (x = 0.00018) calibration spectra for acetone C=O peak in methanol

In Figure 33, the baselined acetone spectrum is fitted quite well using two GL-peaks with an adjusted-R^2 value of 0.996. The signal noise level is below 0.01 AU while the peak height is roughly 0.1 AU. The smaller monomer peak is located near 1717 cm^{-1} with the monohydrogen-bonded peak located near 1707.5 cm^{-1}. No acetone – acetone (dipole – dipole interaction) peak is seen at 1712 cm^{-1}, which is also expected due to the very low possibility of two acetone molecules being in close enough proximity to facilitate an interaction. Another interesting conclusion may be drawn from Figure 33 in that the monomer peak does not exist as a single entity even at very low concentrations. This immediately suggests that using the single low-calibration method for this system would not be viable.

Max & Chapados (2005) discuss a very weak shoulder, representative of the dihydrogen-bonded acetone molecules, at 1698 cm^{-1}. The result of incorporating a third peak into the fitting procedure is seen in Figure 34.

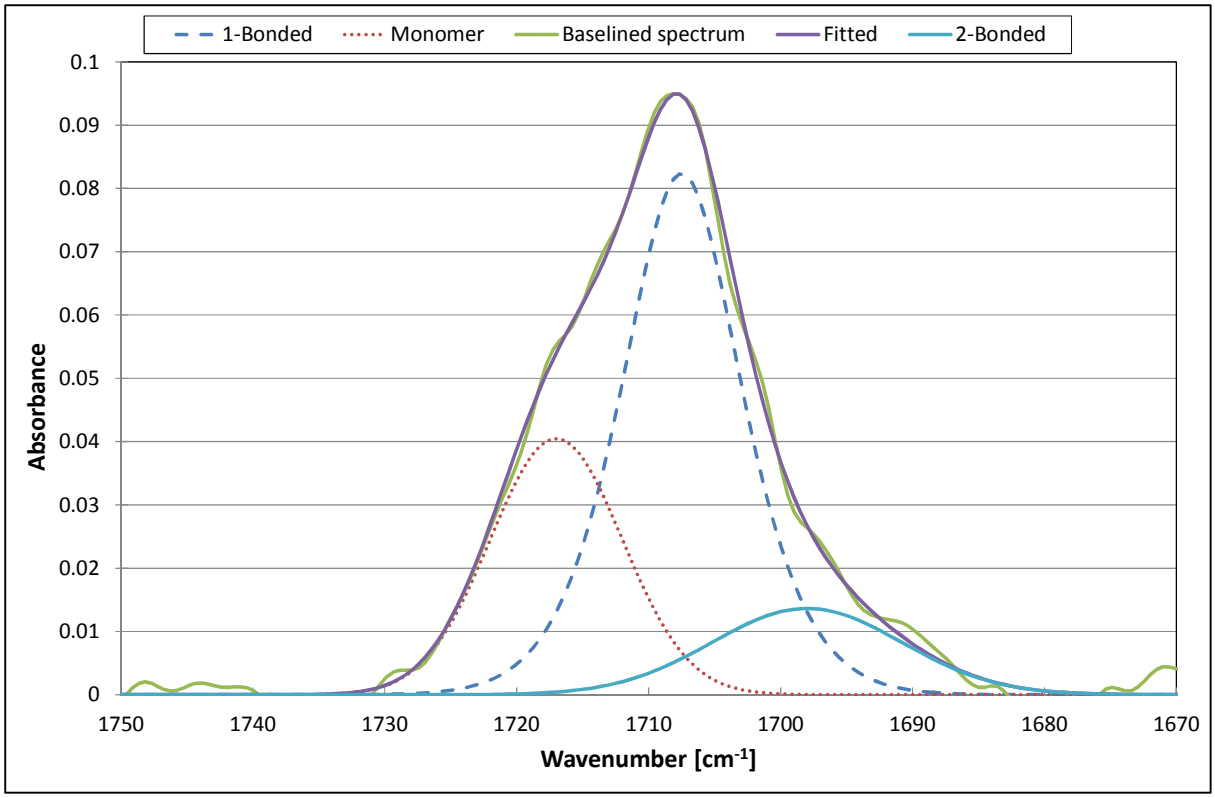

Figure 34: Low concentration (x = 0.00018) calibration spectra for acetone C=O peak in methanol with an additional peak assigned to dihydrogen-bonded acetone molecules

In Figure 34, the position parameters for the monomer and single hydrogen-bonded peaks are kept the same as in Figure 33 and a third peak is inserted at 1698 cm^{-1}. The adjusted-R^2 value is slightly improved at 0.9969 but this could be purely due to the additional parameters introduced into the fitting procedure.

When doing an "eye-test" on Figure 34, the weak shoulder does however seem to exist in the right-side tail of the spectral peak above. The fitted monomer peak has a significantly increased peak height as compared to the two-peak model. It will be of interest to see whether this translates into a larger calculated monomer fraction, or whether this effect is countered by the effect of the calculated absorption coefficient.

4.3.3 Monomer fraction calculations of acetone in methanol

The monomer fractions are calculated using the multiple-calibration method of Asprion *et al*. (2001), since in this case there is no pure low concentration peak with which to calculate the absorption coefficient. Monomer fractions are calculated for both the two-peak and three-peak acetone scenarios, with the results shown in Figure 35.

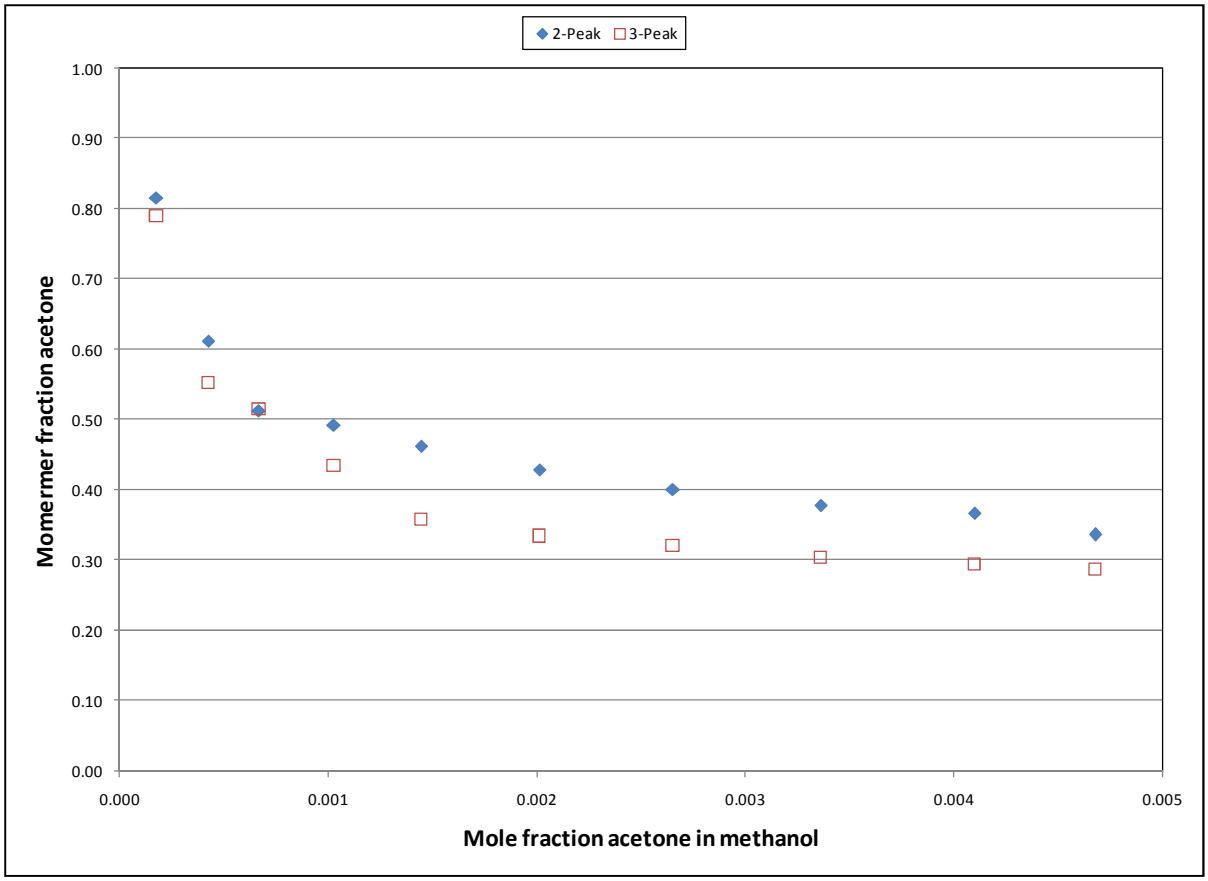

Figure 35: Monomer fractions for dilute acetone in methanol at 23.2 C using 2- and 3-peak fitting procedures

The data are shown here without error bars as the error bars overlap with one another resulting in an incomprehensible graph. The error bars are however presented in the experimental results on page 97. The data are relatively smooth but there are singular inconsistencies, specifically at x_{AcO} = 0.0007. These can be attributed to variance between individual fits within a given model. At these very low concentrations, some deviations are not unexpected.

The acetone monomer absorption coefficients are calculated as 1156.9cm^{-2} / mol% using the two-peak fit, with a summed square error (SSE) minimised to 4.5·10^{-6} for the 10 data points. Likewise, the absorption coefficient is calculated as 2092.6 cm^{-2} / mol% for the three-peak fit with the SSE calculated as 1.4·10^{-6}. For both models, the monomer fraction decreases from around 0.80 to 0.30 over the investigated range of concentrations.

From Figure 35 it is observed that the two-peak model consistently results in higher calculated monomer fractions as compared with the three-peak model. This difference is mainly due to the way absorbance “power” is distributed in each method. Both methods show very similar data for x_{AcO} > 0.0015, whereby the two data sets are offset (ΔX_{Mon} < 0.10). The magnitude of this offset is

significant. For $x_{AcO} < 0.0015$, a significant increase in gradient is observed for the 3-peak model relative to the 2-peak model. For this range, the difference between the calculated monomer fractions decreases significantly.

One can also conclude that the difference for measured experimental values of Max & Chapados (2005) compared to those of Eamon & Symons (1985) is not due to the presence of the shoulder peak representing dihydrogen-bonded acetone molecules. One can thus postulate that the reason for this observed difference in the literature values is due, as per the hypothesis given in Chapter 2 here, to the spectral analysis method employed by Eamon & Symons.

It is also noticeable from Figure 35 that both models predict monomer fractions approaching 1 as the mole fraction of acetone tends to 0. This result may initially seem drastically at odds with those published in the literature, but this difference can be placed in context by considering the following points:

- The concentrations tested here are at least an order of magnitude less than those of the two studies in the literature;
- A drastic increase is observed in the monomer fractions for acetone mole fractions below 0.0015.

The steepness of this increase is rather deceptive until one considers that the scale of the vertical axis is two orders of magnitude greater than that of the horizontal axis. To further investigate this point, exponential trends are fitted to the data for mole fractions greater than 0.0015.

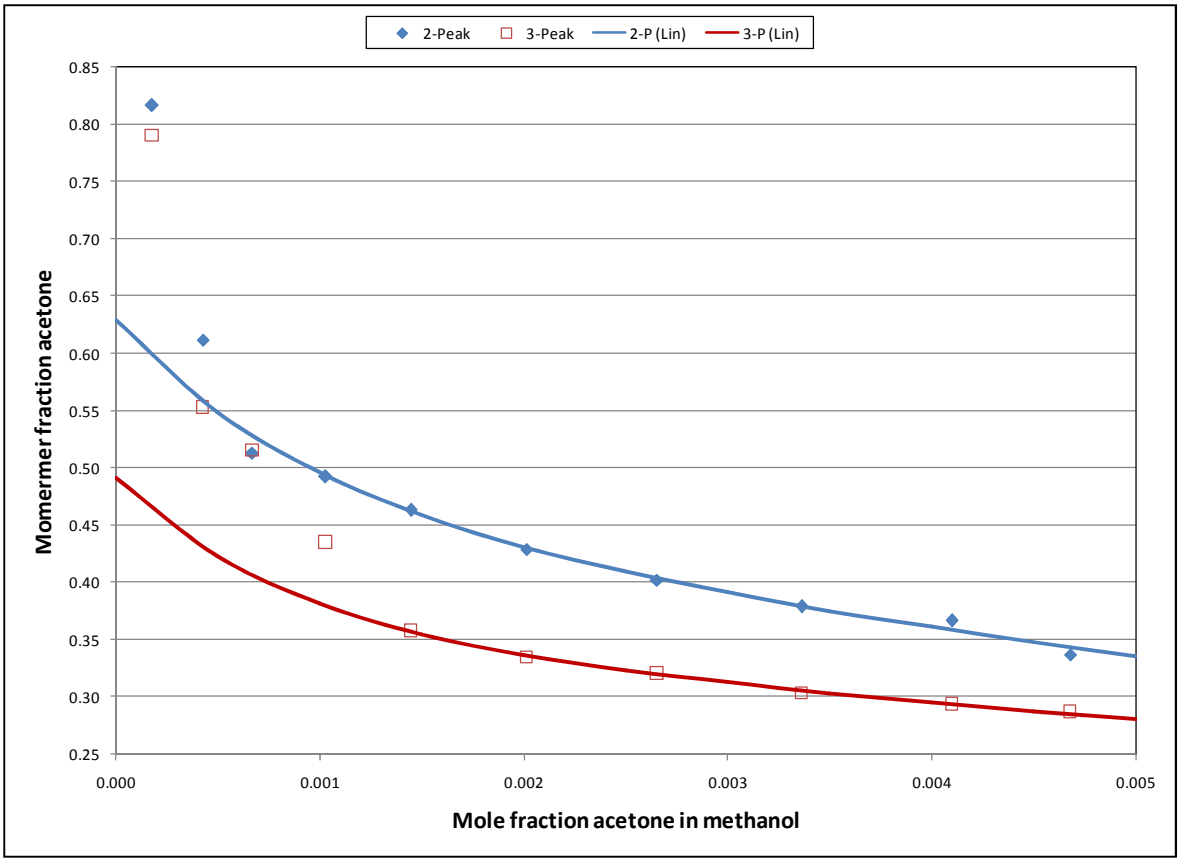

Figure 36: Analysis and explanation of the differences observed between this work and literature data

In Figure 36, the exponential trends are shown for demonstration purposes. A few interesting points are however exhibited when extrapolating the exponential functions to acetone mole fractions of zero. The extrapolated X_{Mon} value at $X_{AcO} = 0$ is 0.63 for the 2-peak model and 0.49 for 3-peak model. The three-peak model value is especially interesting here, as it is very close to that of Max & Chapados (2005). Figure 36 shows that without the super dilute concentration data points, one can obtain monomer fractions similar to those in the literature. The importance of these low concentration data points is clearly illustrated.

Since there exists a significant difference between the calculated monomer fractions, an informed choice must be made between the two methods. In physical terms, the 3-peak model is more realistic. Steric hindrance aside, acetone can form two hydrogen bonds via the lone electron pairs and the third peak representative of these interactions is visible in Figure 34. The counter argument can be made that third peak is not clearly visible and thus should not be considered in the analysis. Furthermore, steric hindrance can occur. In such dilute mixtures, with such an abundance of oxygen lone pairs available (from both the acetone and the solvent alcohol) for hydrogen-bonding, it is not realistic to consider that a single acetone molecule could penetrate the hydrogen-bonded alcoholic structure not just once but twice. Finally, the data generated from the 2-peak model is much

smoother and more consistent than those data calculated from the 3-peak model. This point indicates that the 2-peak model is less susceptible noise from the spectra. Thus, due to the points mentioned here, the 2-peak model is chosen to model the C=O bond spectra of acetone.

4.4 Sample analysis of dilute ethanol in acetone

4.4.1 Experimental conditions

The first step in the data analysis step is to determine the experimental conditions i.e. the mole fractions of the mixture and the temperatures as per Section 4.3.1. The mass of solute, in this case ethanol, is recorded at each injection into the reactor. The mass of mixture extracted from the reactor is also recorded along with the temperature of the reactor at that time. The sample is then transferred into the FTIR, where the temperature is also measured. Using these measurements, the data in Table 19 is drawn up.

Table 19: Concentration and temperature estimates for an ethanol – acetone system

#	Ethanol mole fraction			Temperature [°C]	
	Measured	Low	High	Reactor	FTIR
1	0.00092	0.00089	0.00096	24.8	24.2
2	0.00147	0.00139	0.00154	24.9	24.8
3	0.00224	0.00212	0.00235	24.9	24.9
4	0.00317	0.00302	0.00332	25.1	24.8
5	0.00426	0.00406	0.00445	25.1	24.8
6	0.00511	0.00488	0.00534	25.1	24.8
7	0.00613	0.00585	0.00639	25.1	24.9
8	0.00747	0.00714	0.00775	25.1	25.0

In Table 19, the error range for the mole fraction of ethanol is also calculated. This is done be using the estimated measurement error of the scale. The temperatures are also shown. The average temperature in the reactor is 25.0 °C with a standard deviation of 0.1 °C. The equivalent values for the FTIR temperatures are 24.8 and 0.2 °C. The FTIR temperature is used to estimate the temperature error, as it has greater variation as compared to the reactor temperature. Using three standard deviations, the temperature is estimated at 24.8 ± 0.6 °C.

4.4.2 Spectral processing

The second step involves the analysis of the spectra. Firstly a baseline needs to be fitted to each spectrum. The raw spectra for x_{EtOH} ε {0.00092; 0.0075} are shown in Figure 37.

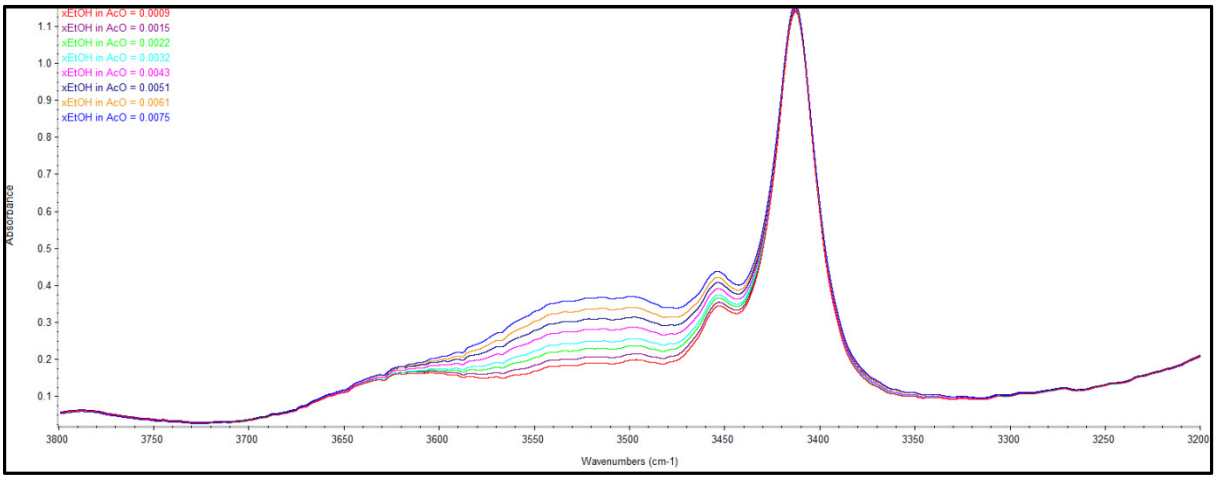

Figure 37: Multiple raw spectra for increasing ethanol in acetone at 24.8 ± 0.6 °C, as viewed in OMNIC spectral software

In Figure 37, the following features are observed:

- Constant peaks around 3415 cm^{-1} and 3455 cm^{-1}
- Developing around 3430 cm^{-1}, 3550 cm^{-1} and 3630 cm^{-1}

"Developing" is used here to make a distinction between peaks which are varying with concentration. As per the literature, the peak near 3415 cm^{-1} is assigned to the acetone C=O band. According to Figure 38 the peak at 3454 cm^{-1} can also be assigned to acetone (or at least some impurity in the acetone used in these experiments).

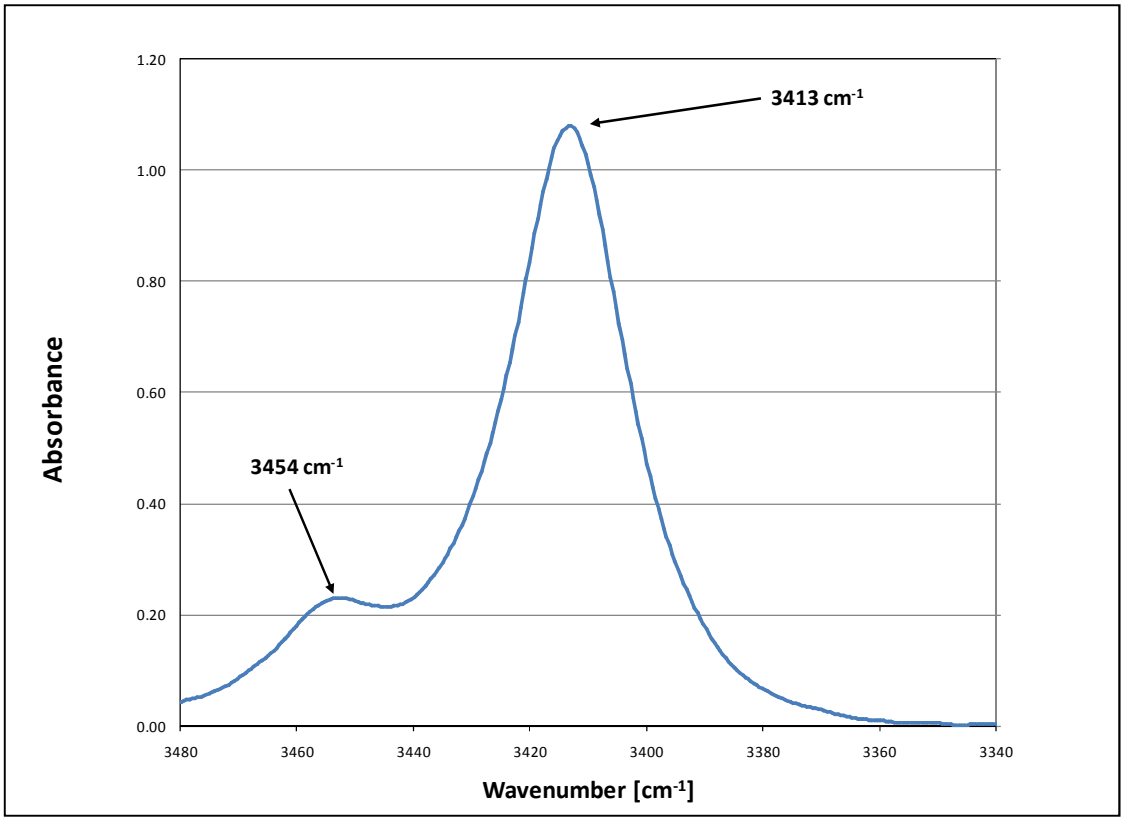

Figure 38: Pure acetone spectrum in the C=O overtone region

The peak near 3630 cm^{-1} is assigned to ethanol monomers and the peak development around 3500 cm^{-1} is naturally also assigned to hydrogen-bonded ethanol, in this case dimers. The final spectral assignment is with regard to the growth observed between the acetone peaks. While the position would be consistent with the first overtone of an acetone monomer peak shoulder, a visible peak is very unlikely for the high concentrations of acetone seen here. The peak is also consistent with the methanol-acetone O-H interaction peak described by Max & Chapados (2005). The “poly” or “combination” assignment is thus used to describe this spectral peak.

The growth of the ethanol peak with concentration is expected, but naturally the distribution of ethanol among various O-H peaks is of interest here. Also of interest is whether the acetone peaks have any discernible change due to the presence of ethanol. Each spectrum is fitted with a baseline as in the example here for x_{EtOH} = 0.00092.

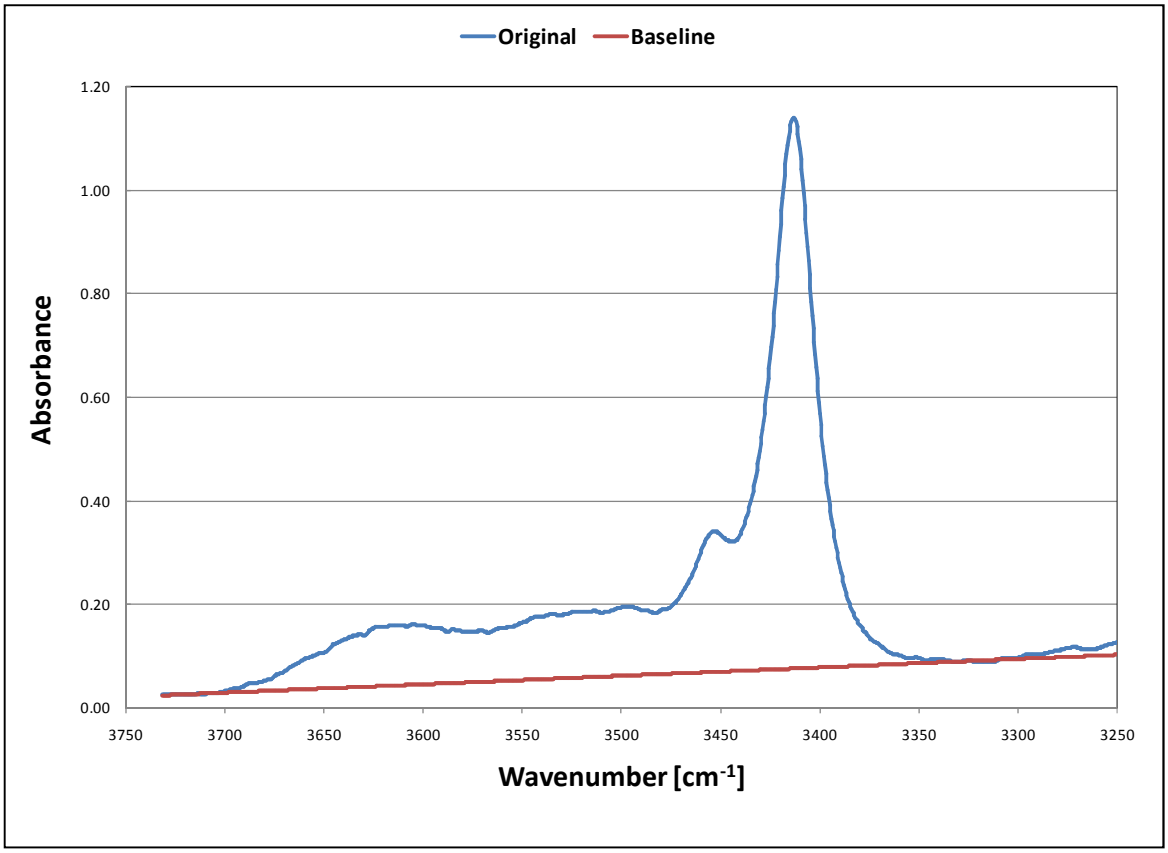

Figure 39: Baseline for ethanol (x = 0.00092) in acetone

As discussed in Section 2.5.1(B), the choice is baseline is very important. In Figure 39 it is shown that a linear baseline is fitted to data above 3700 cm^{-1} and at the lowest point to the right of the C=O peaks. A linear baseline is fitted and the adjusted-R^2 value is 0.9964 for the chosen data range, showing that the baseline aligns well on both ends of the peak range. The baselined spectrum is shown in Figure 40.

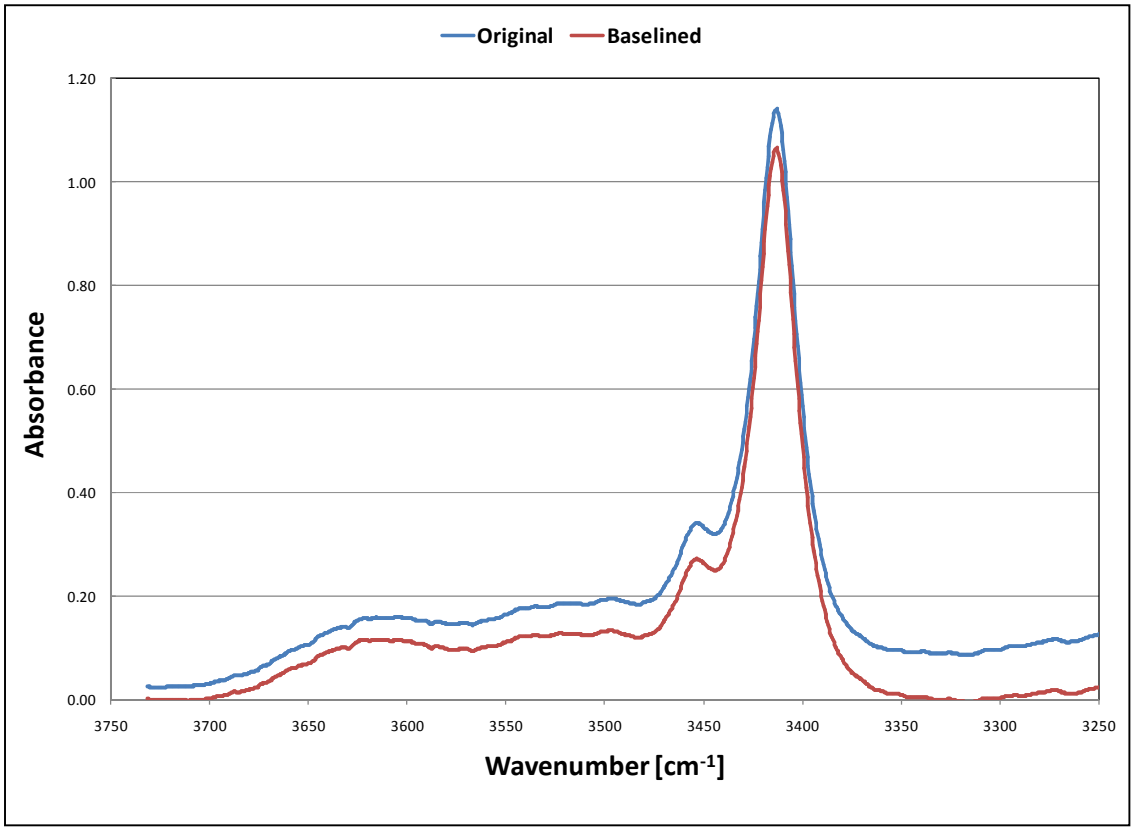

Figure 40: Raw and baselined data for ethanol (x = 0.00092) in acetone

The baseline has a very slight negative gradient and the O-H and C=O peaks are effectively zeroed at 3700 and 3280 cm^{-1}. The next step is to fit a series of Gauss-Lorentz curves to the baselined data. Asprion *et al.* (2001) used five component curves to describe alcohols diluted in alkanes whereas von Solms *et al.* (2007) only used three. In this case, three ethanol and two acetone curves are initially used to fit the data. A 5GL-function was fitted to the data with a resultant adjusted-R^2 value of 0.9988.

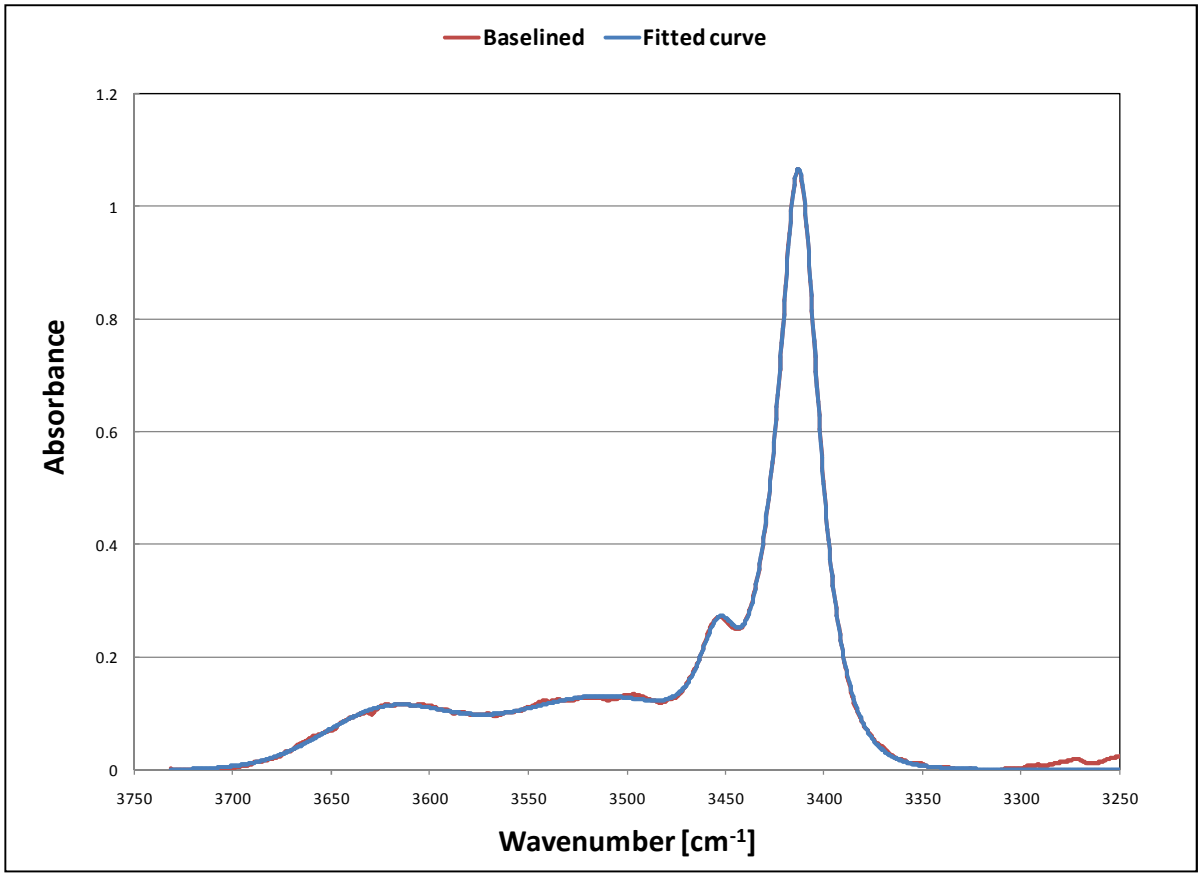

Figure 41: 5-peak Gauss-Lorentz function fitted to ethanol (x = 0.00092) in acetone with an adjusted-R^2 of 0.9988

As suggested by the adjusted-R^2 value, the five peaks fit the data very well.

The obtained equation parameters for the five fitted peaks are shown in Table 20.

Table 20: Parameters obtained for Gauss-Lorentz functions fitted to x_{EtOH} = 0.00092 in acetone

		A_{MAX}	a^2	b^2	v_{MAX}
AcO	Other	0.1654	0.005157	0.001181	3454
	C=O	1.032	0.005638	0.0006707	3413
EtOH	Mono	0.09133	1.757E-07	0.0004936	3623
	Dimer	0.1304	9.596E-05	8.457E-05	3513
	Poly	0.04283	0.007404	0.004525	3430

The component curves are shown Figure 42.

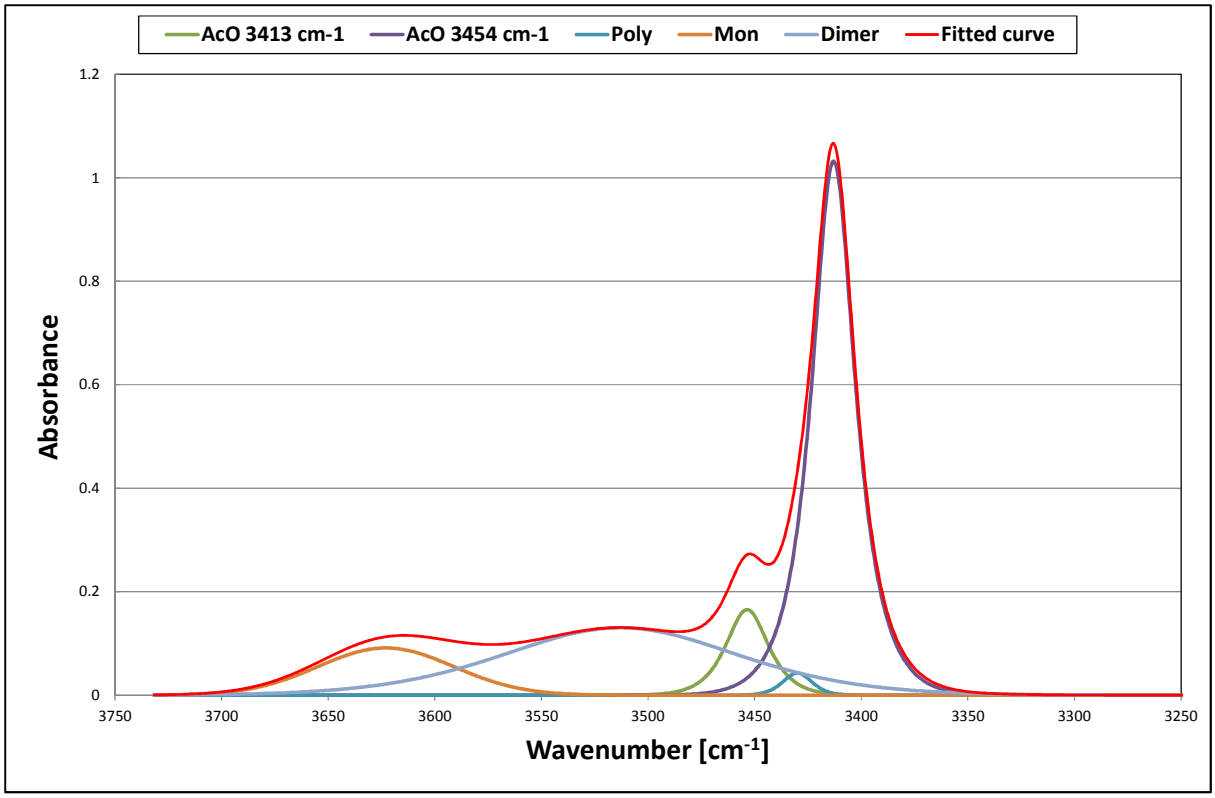

Figure 42: Individual curves fitted to ethanol (3 curves) in acetone (2 curves)

The acetone peaks are located at 3413 and 3454 cm^{-1}. The monomer peak of ethanol is found at 3623 cm^{-1}, with the dimer peak at 3513 cm^{-1}. A smaller peak, attributed to the ethanol polymer, is located at 3430 cm^{-1}.

(A) Ethanol peaks

The two fitted acetone peaks have been subtracted from the baseline data, which allows for a close-up view of the ethanol peaks in Figure 43.

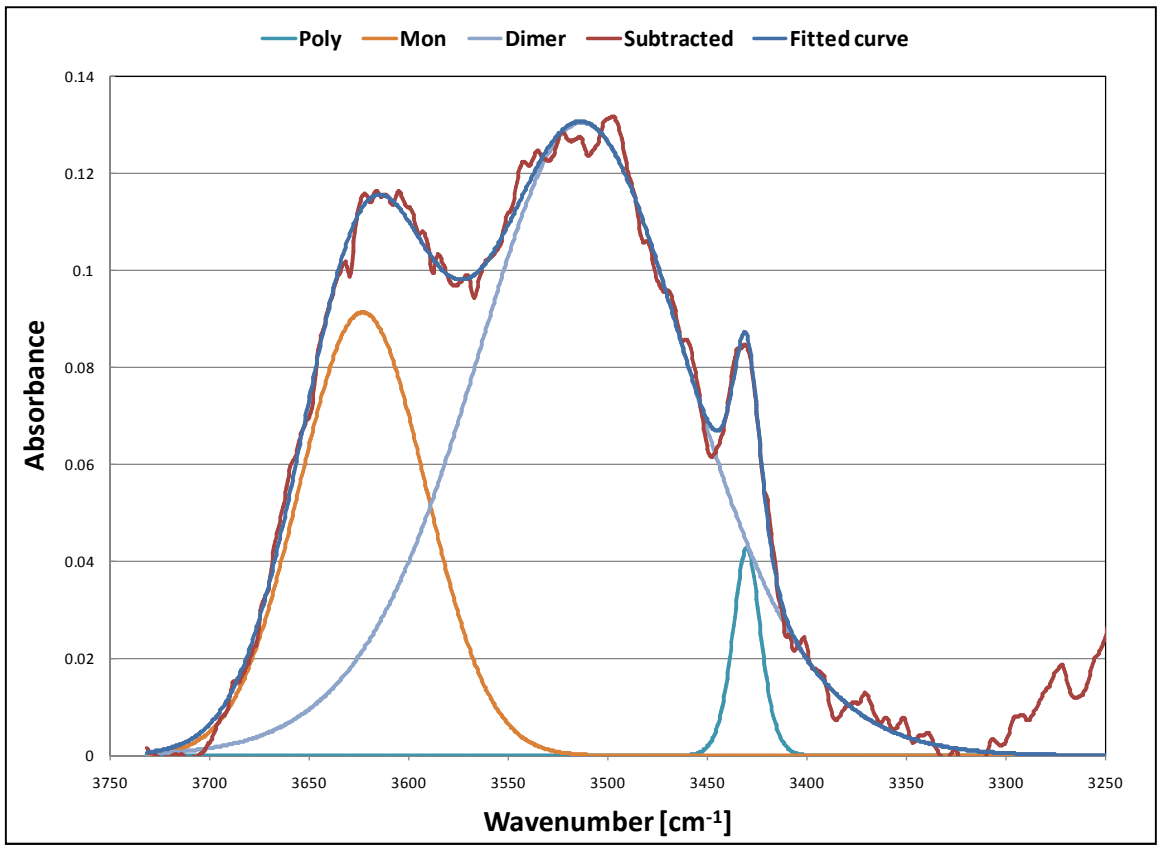

Figure 43: *n*-mer component curves of ethanol after the removal of acetone from the baseline data

Even to the naked-eye, the three fitted functions accurately describe the acetone-subtracted curve for the range 3700-3300 cm^{-1}. The monomer and dimer peaks are relatively large and convoluted, while the "poly" peak is small and relative sharp. In Figure 43, the monomer and dimer peaks are already well developed and of roughly equal size, despite the very low concentration of ethanol. Even at this super dilute ethanol concentration, a clear monomer peak is still not present and therefore the multiple calibration method must be used.

(B) Curve-fitting strategies

A few curve-fitting strategies were attempted in order to determine the best method for evaluating alchohol-acetone systems. For the Asprion-method, the position and width parameters are kept constant as per Table 20 with the A_{Max} parameter as a variable. The curves are also fitted with a best-fit methodology, where the fitting algorithm is allowed to vary all the parameters of the five fitted functions. The best-fit (with variable position and width parameters) results are shown in Figure 44.

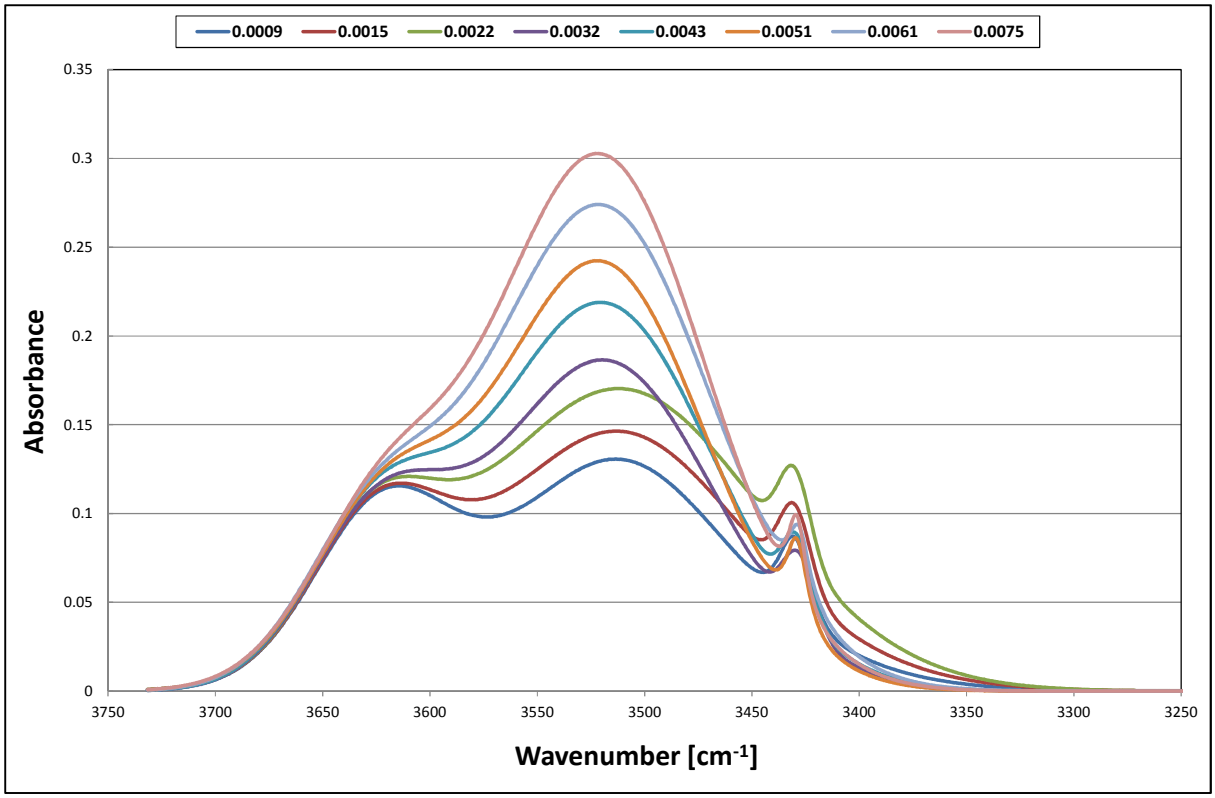

Figure 44: Free parameter functions for ethanol (X = 0.0009 - 0.0075) in acetone

Figure 44 highlights the issues described by Asprion *et al*. (2001). Using the best-fit method, the dimer and polymer peaks move randomly rather than showing a gradual progression toward lower wavenumbers. The inconsistent development of the peaks leads naturally to variability in the fitting parameters and calculated peak areas. This is undesirable.

Using the Asprion-method (with fixed position and width parameters) results in Figure 45.

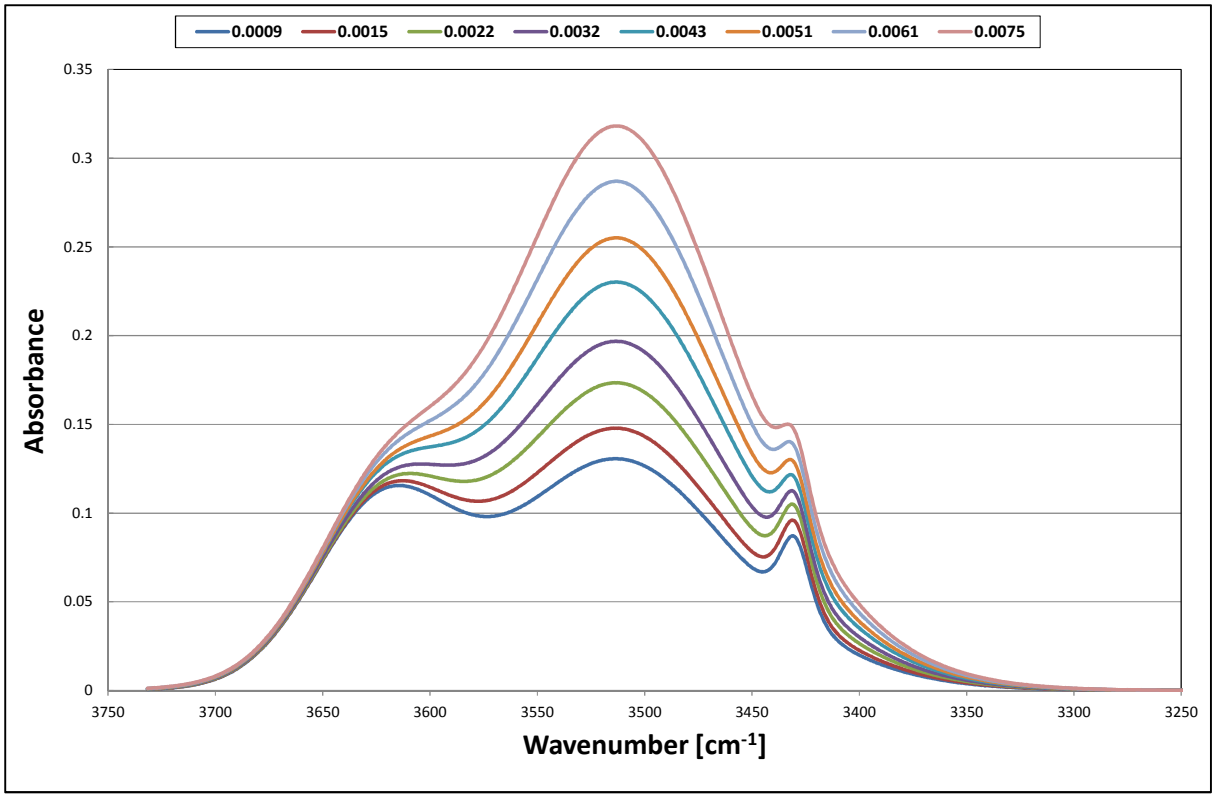

Figure 45: Fixed parameter functions for ethanol (X = 0.0009 - 0.0075) in acetone as per As-method

Comparing Figure 44 and Figure 45, there is a clear distinction between the two. Figure 45 shows a more consistent development as the alcohol mole fraction increase from 0.0009 to 0.0075.

Table 21: Adjusted-R^2 values for curves fitted to EtOH-AcO spectra

2AcO + 3EtOH FIT			
Baseline	Best-fit	Asprion-fixed	$\Delta_{best - fitted}$
0.9964	0.9998	0.9998	0
0.9978	0.9998	0.9998	0
0.9972	0.9991	0.9989	0.0002
0.9969	0.9998	0.9996	0.0002
0.9972	0.9997	0.9988	0.0009
0.9975	0.9996	0.9994	0.0002
0.9961	0.9996	0.9992	0.0004
0.9977	0.9995	0.9948	0.0047

Table 21 shows the performance of the fixed- and free-parameters fits, from which it is seen that the Asprion-method (fixed parameters) provided a comparatively good fit. In all cases, but one, the difference in percentage variance explained by fitted model is less than 0.1%. This is a very small loss

of accuracy and is easily offset by the consistency exhibited by the model in Figure 45 (as compared to Figure 44).

The next step in the fitting procedure is to calculate the areas of each fitted curve. Since GL product curves are used, the areas are calculated numerically in a spreadsheet using the ⅜th Simpson rule. The calculated areas are checked against values calculated with the quadl-function in Matlab. The ethanol peaks are calculated from 3750 – 3200 cm^{-1} with the acetone peaks fitted from 3550 – 3200 cm^{-1}.

Table 22: Calculated areas for ethanol fitted curves

	Best-fit (free parameter)			Asprion-fixed parameter fit		
x	$EtOH_{Mon}$	$EtOH_{Di}$	$EtOH_{Poly}$	$EtOH_{Mon}$	$EtOH_{Di}$	$EtOH_{Poly}$
0.0009	7.28	18.59	0.775			
0.0015	6.33	22.88	0.878	7.20	21.04	0.828
0.0022	5.62	28.19	0.873	7.04	24.69	0.832
0.0032	7.60	23.96	0.731	6.99	28.03	0.820
0.0043	7.41	28.43	0.697	6.95	32.79	0.770
0.0051	8.18	29.50	0.625	6.79	36.34	0.765
0.0061	7.24	35.41	0.715	6.68	40.89	0.740
0.0074	8.10	37.35	0.527	6.52	45.34	0.712

Table 22 gives a comparison of the calculated areas for each component curve fitted for ethanol in the ethanol-acetone mixture. When using the best-fit method, the monomer peak area can be described as erratic at best, with no discernible trend and a range of 5.62 to 8.18 $AU \cdot cm^{-1}$. The dimer peak area increases gradually from 18.6 to 37.4 cm^{-1}, apart from one serious anomaly at x_{EtOH} = 0.0022 → 0.0032. This anomaly is most likely due to shift in the position of the dimer curve relative to one another as observed in Figure 44. The polymer peak seems to increase initially before decreasing from 0.89 to 0.53 cm^{-1}. The anomalous behaviour of this peak may be due to the fact that it is located exactly between the two acetone peaks where the curves are deconvoluted.

4.4.3 Monomer fraction calculations of ethanol in acetone

The monomer fractions were then calculated from the area data, with the fixed parameter and free parameter peak areas. The results are shown in Figure 46.

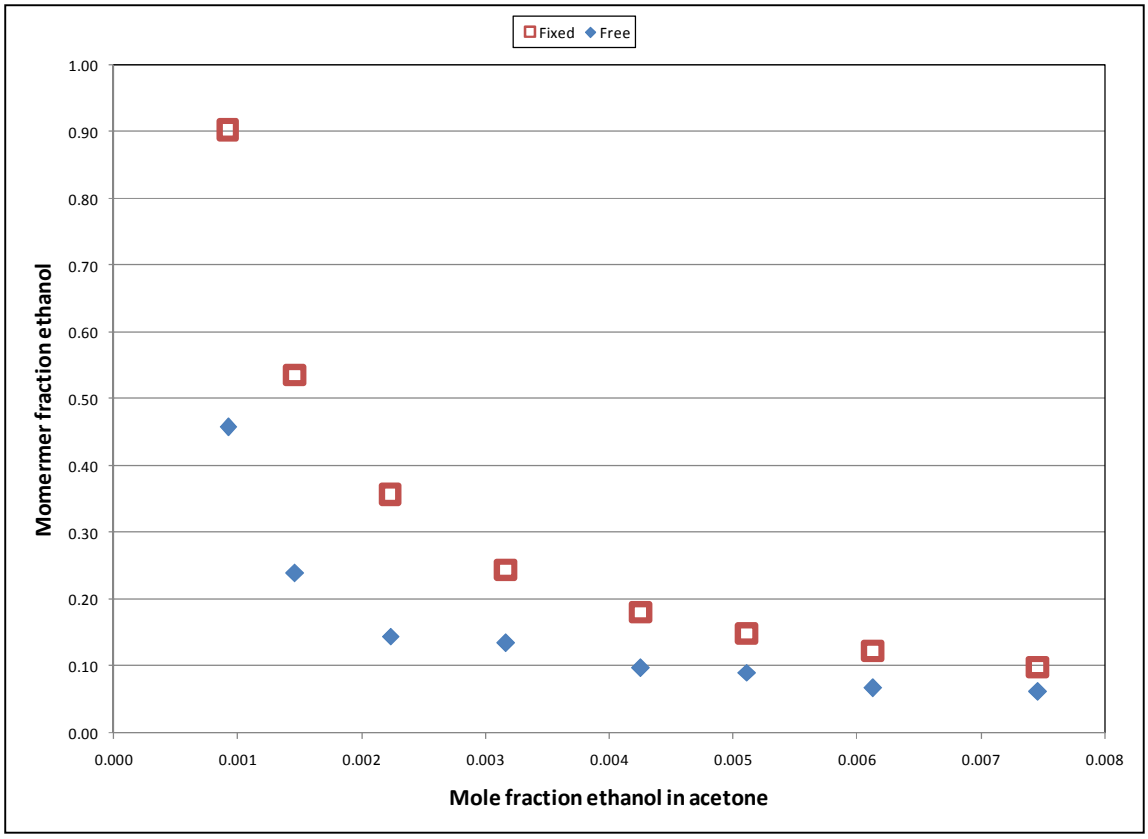

Figure 46: Comparison between free-parameter and fixed-parameter monomer fractions

Figure 46 displays the monomer fractions calculated from the peak areas. Both data sets follow an exponential decrease as ethanol mole fraction increases, but there is a significant difference calculated monomer fractions. The absorption coefficients are determined by regression as 10 322 and 5 244 cm^{-2} / mol% for the free and fixed cases respectively, with SSEs of $1.7 \cdot 10^{-5}$ and $2.4 \cdot 10^{-5}$ determined over 8 data points. While the fixed area data is much smoother than the free parameter data, the upward trend of the fixed area data are unrealistic at lower concentrations. Thus, by fixing the parameters, the areas become smoother but less realistic. Also, considering the super low concentrations some fluctuation is to be expected.

Thus the free parameters method will be used to model alcohol-acetone systems, with the corollary that the parameters be constrained somewhat to avoid gross variability in the data.

4.5 Summary of verification and sample analysis

In summary, the following conclusions are made:

With regard to the **experimental apparatus**:

- Transmission mode is necessary for obtaining low-concentration spectra.
- The MCT High-D* detector achieves a linear absorbance-concentration response.
- The experimental apparatus is able to reproduce the literature data of von Solms *et al.* (2007) for ethanol – *n*-hexane monomer fractions.

With regard to the **dilute acetone – methanol** system analysed here:

- The difference between Max & Chapados (2005) and Eamon & Symons (1985) is not due to the incorporation of a dihydrogen-bonded acetone peak. As hypothesized in the literature review, this difference is most likely due to basic spectral analysis employed by Eamon and Symons.
- Acetone monomer fractions escalate rapidly for mole fractions less than 0.0015.
- The difference between 2- and 3-peak models is significant i.t.o. the calculated monomer fractions. The 2-peak model was chosen for modelling the C=O bond spectra of acetone.

With regard to the **dilute ethanol – acetone** system analysed here:

- Acetone overtone peaks are assigned at 3414 and 3454 cm^{-1}.
- Ethanol harmonic O-H peaks are assigned around 3340, 3550 & 3630 cm^{-1}.
- The multiple calibration method of Asprion *et al.* (2001) is the preferred method for alcohols dissolved in acetone.
- Using free parameters for the curve-fitting models result in less smooth, but more realistic monomer fraction data, as compared to the fixed parameter method suggested by Asprion *et al.* (2001).
- Ethanol monomer fractions escalate rapidly for mole fractions less than 0.002 similarly to the observed effect for acetone with the monomer being almost completely enveloped by the polymer peaks, being visible as a weak shoulder at the highest measured mole fraction of 0.0075.

Chapter 5: Experimental results

This chapter will focus on graphically illustrating the experimental results obtained when applying the spectral analysis methods discussed in Chapter 4. Firstly, the results are shown for monomer fractions calculated for dilute acetone in mixtures with alcohols. Secondly, the results for dilute alcohol in solution with acetone are presented. The data tables are shown in Section 10.2.

5.1 Dilute acetone in alcohols

The various mixtures are shown first in isolation with error bars included, after which the results for Section 5.1 are consolidated into a single graph.

5.1.1 Acetone in methanol

As discussed in Section 4.3.3, the 2-peak model is used to model the acetone C=O interaction. The calculated monomer fraction of acetone in solution with methanol is shown in Figure 47.

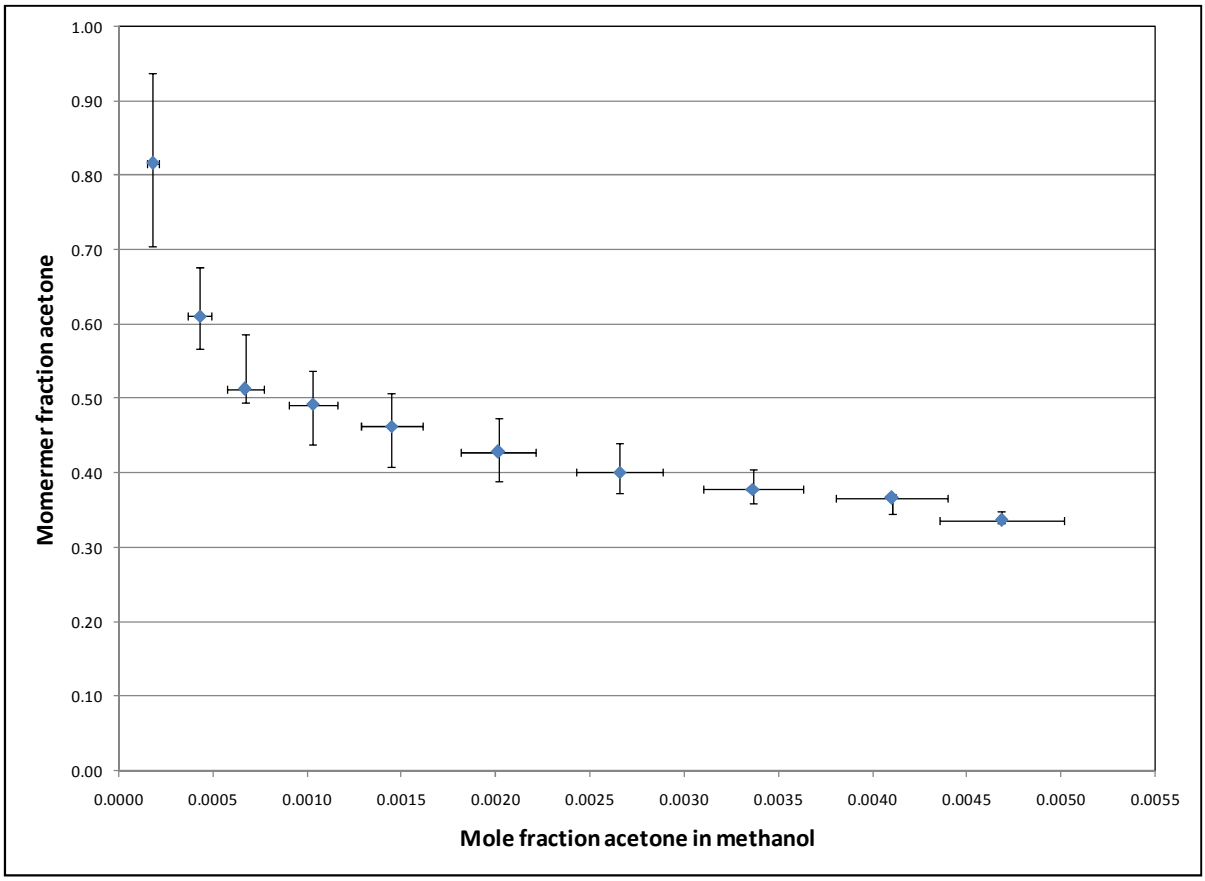

Figure 47: Acetone monomer fractions in methanol at 23.2 °C using the 2-peak model

Figure 47 shows the calculated monomer fractions of acetone in a super dilute mixture with methanol at 23.2 ± 0.4 °C. As per previous calculations, the absolute horizontal errors increase with acetone mole fraction while the vertical errors are greatest at very low acetone mole fractions. The horizontal error bars are calculated using the low and high acetone mole fraction estimates. The vertical error bars are calculated by plotting monomer fraction curves for the low and high acetone mole fractions estimates. The horizontal errors are most strongly affected by the uncertainty in the scale used to measure the mass of solute injected at each step in the experiment.

Double exponential curves are fitted to the low and high monomer estimates such that satisfactory fits (adjusted-R^2 values of 0.985 or better) are obtained. The exponential curves are then interpolated for the measured acetone mole fraction values to get the upper and lower vertical error values. Temperature error estimates are not incorporated here as the temperature deviation is only ± 0.4 °C and it is deemed that difference would be negligible when considering the differences observed for deviation of 1.7 °C in Figure 30. While the horizontal errors were affected directly by a single uncertainty parameter, the vertical errors incorporate the mass error into the error minimisation and curve-fitting procedure. These additional procedures cause the asymmetry seen in the vertical error in Figure 47.

The acetone monomer absorption coefficients are calculated as 1157 cm^{-2} / mol%. The estimated monomer fraction of acetone varies from around 0.90 to 0.30 and there is a clear trend towards a monomer fraction of 1 at infinite dilution.

5.1.2 Acetone in ethanol

Ethanol has a weaker hydrogen-bonding network compared to methanol (as evidenced by the hydrogen-bond strength calculated from spectroscopy) due to the fact that the –OH segment is somewhat more sterically hindered and therefore generally higher energy constants fitted for ε^{AB} within SAFT frameworks. Thus one would expect the acetone molecules to more easily penetrate the hydrogen-bonded ethanol as compared to methanol. The calculated acetone monomer fractions are shown in Figure 48.

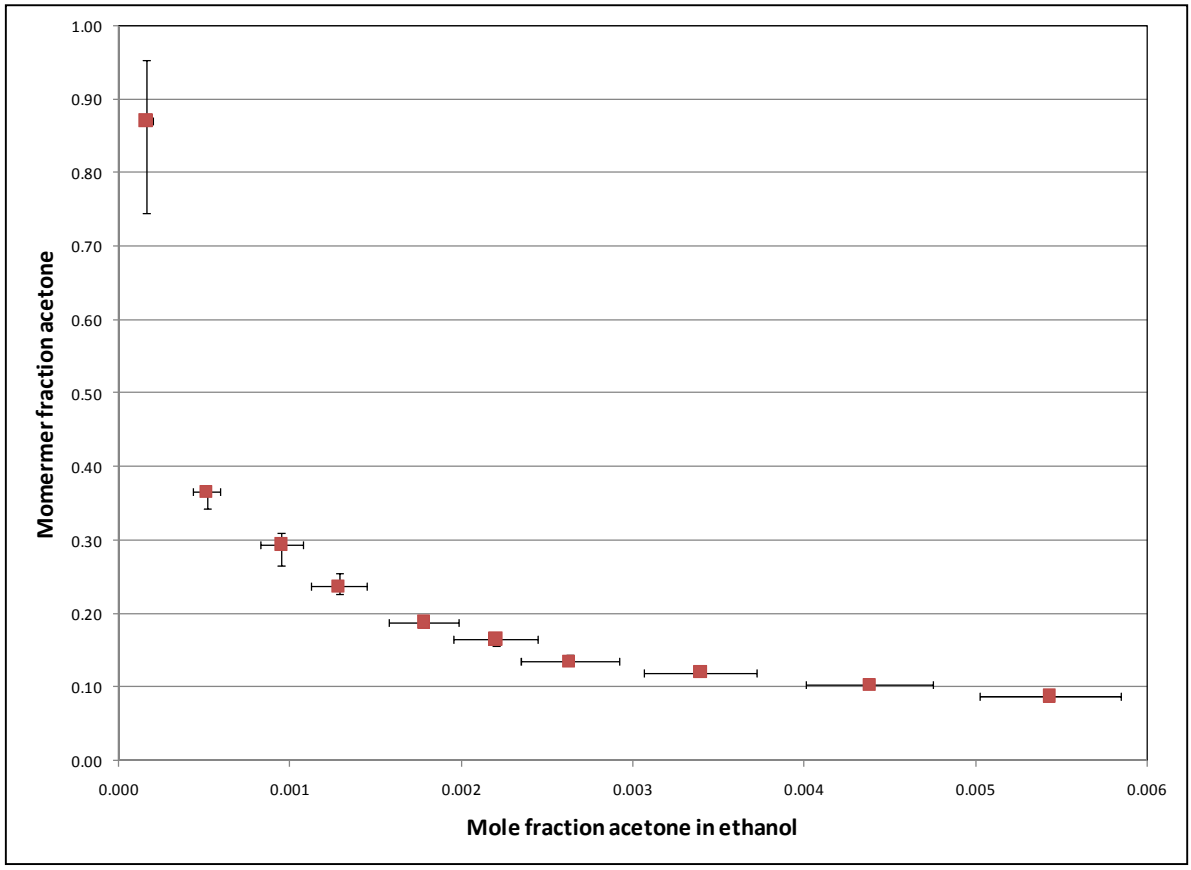

Figure 48: Acetone monomer fractions in ethanol at 23.2 °C

The monomer absorption coefficient is calculated as 6555 cm^{-2} / mol% with a SSE of $6.6 \cdot 10^{-7}$ calculated for 10 data points. Acetone monomer fractions range from 0.07 for $x_{AcO} \approx 0.005$, reaching 0.87 at $x_{AcO} = 0.00016$. As for acetone in methanol, there is a pronounced increase in observed monomer fractions for very dilute mixtures. This increase is noticeably steeper for acetone in ethanol in Figure 48, as compared to that seen for methanol in Figure 47. Thus acetone molecules do more easily hydrogen-bond with ethanol when compared to methanol.

A significant difference between Figure 47 and Figure 48 is the magnitude of the vertical error bars. Here the vertical error bars are much smaller and are negligibly small for $x_{AcO} > 0.002$. There is some overlap of the horizontal errors for $0.0015 < x_{AcO} < 0.003$, but the data points still follow a generally consistent exponential pattern.

5.1.3 Acetone in 1-propanol

As with ethanol, one would expect the acetone molecules to hydrogen-bond more easily in mixture with 1-propanol in comparison with methanol. For this experiment, a greater temperature deviation

was observed and thus a temperature correction is incorporated into the vertical error bar calculations. The calculated acetone monomer fractions are shown in Figure 49.

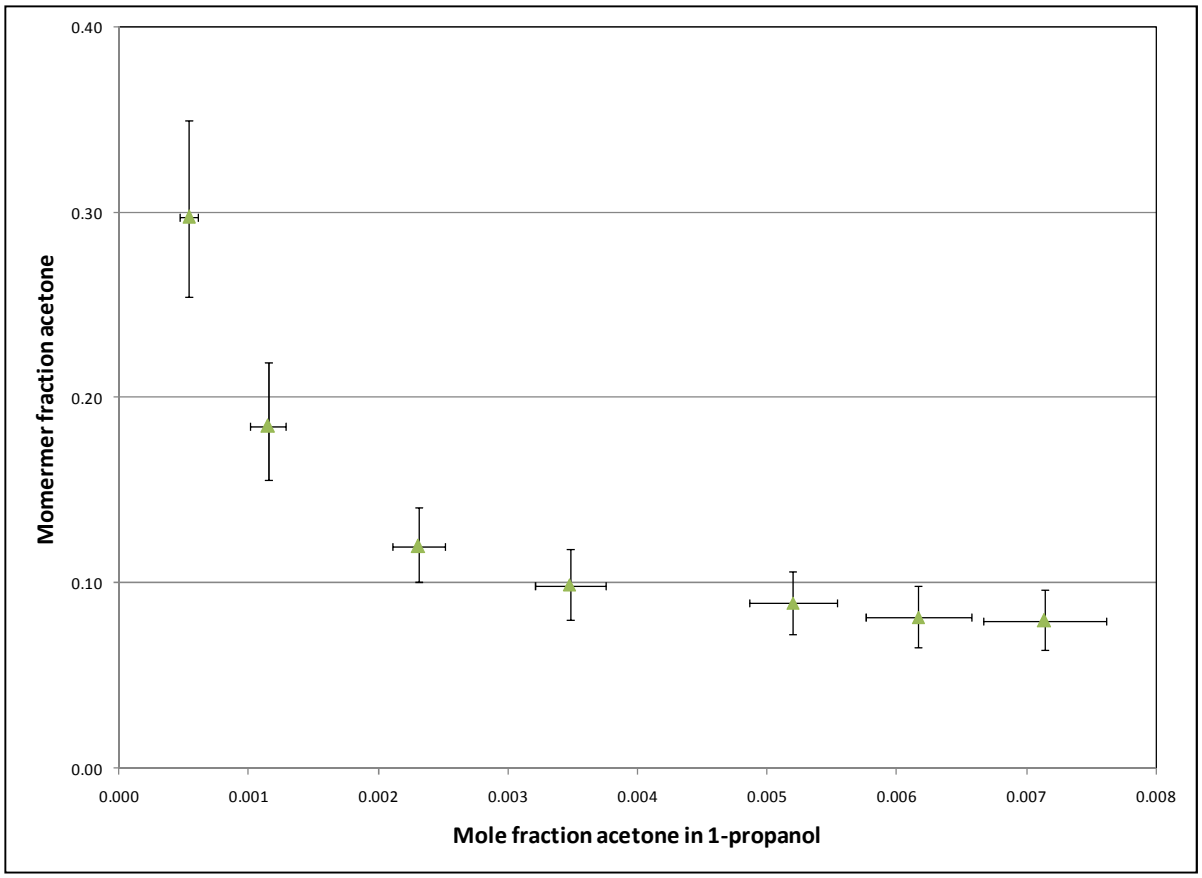

Figure 49: Monomer fraction of dilute acetone in 1-propanol at 22.8± 1.0 °C

The monomer absorption coefficient is calculated as 5232 cm^{-2} / mol%, with a SSE of $7.6 \cdot 10^{-6}$ calculated for a total of 7 data points. Due to the larger temperature deviation observed for these measurements, a temperature correction was incorporated into the error bars. For acetone dissolved in 1-propanol, the measured concentration range is not as low as for methanol and ethanol. A slightly different fitting technique was also employed, due to additional spectral noise around the C=O peak. Therefore the baseline and model peaks were fitted simultaneously, with the baseline and model subsequently split and evaluated separately. Figure 49 does however follow the same general trend observed before, where the acetone monomer fraction decreases sharply in the very dilute range before flattening out as the acetone mole fraction increases above 0.002.

5.1.4 Acetone in 2-propanol

For acetone dissolved in 2-propanol, a peak shoulder representing acetone monomers was not mentioned by Nyquist (1990). This study does however detect as weak shoulder around 1718 cm^{-1} (as is evidenced by Figure 50), but it is somewhat less pronounced than that seen acetone in the other alcohols studied here.

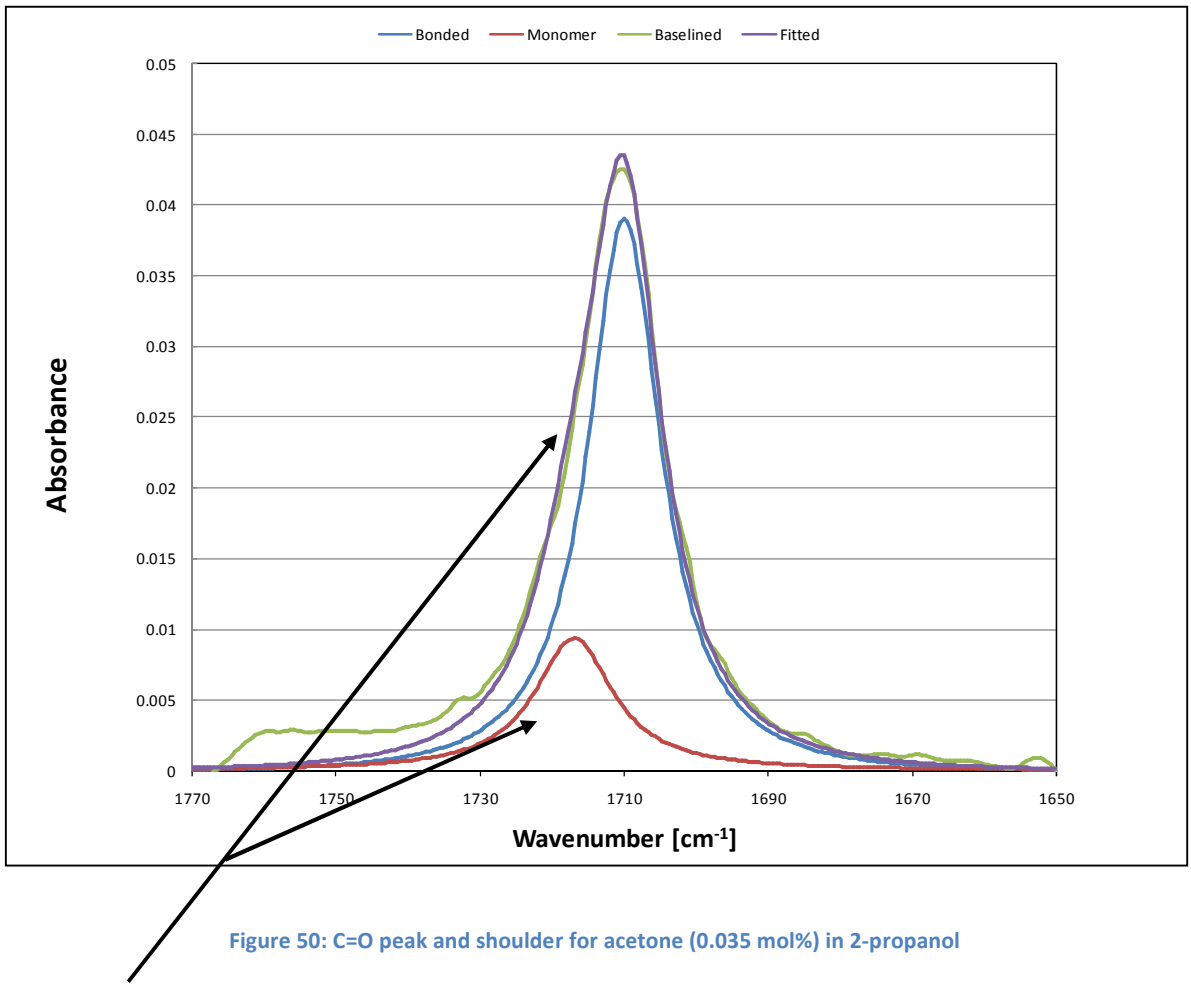

Figure 50: C=O peak and shoulder for acetone (0.035 mol%) in 2-propanol

As the shoulder in Figure 50 is much weaker than for the previous mixtures (analysed in this work) and was most likely not detected in other studies (e.g. Nyquist (1990)) specifically due to the lower concentration ranges considered in this work. Due to the weakness of the monomer peak, one would expect the resulting monomer fractions to be much lower. The monomer fractions for dilute acetone in 2-propanol are presented in Figure 51.

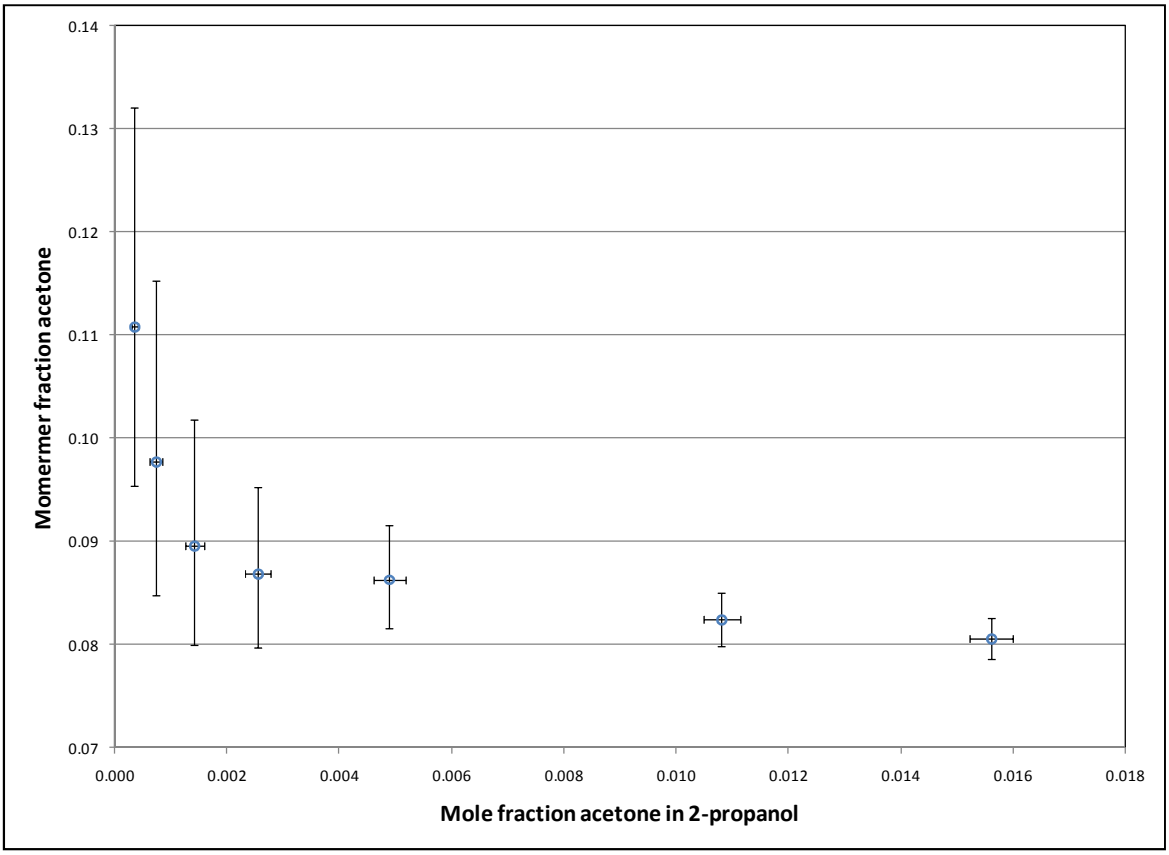

Figure 51: Monomer fraction data for acetone dissolved in 2-propanol at 23.0 °C

The monomer absorption coefficient is calculated as 2622 cm^{-2} / mol%. The SSE was calculated as $2.7 \cdot 10^{-5}$ for a total of 7 data points. This error is an order of magnitude larger than those previously calculated, but the increase is due to one large error in 10^{-5} range with the remaining errors being 10^{-6} or less. For the measured concentration range, monomer fractions are calculated between 0.12 and 0.07.

One would expect 1- and 2-propanol to yield very similar results, as the molecules are physically very similar. The proton donated in the hydrogen-bond is, however, more hidden for 2-propanol, and thus one would naturally expect a slightly weaker hydrogen bond network for 2-propanol compared to 1-propanol. This range is much narrower than seen that for the previously measured systems. The MCT-D* detector could not be used for these experiments and thus the DGTS detector was used, such that higher concentrations could be viewed. The cost, however, was that the spectral peaks were less accurately measured and fitted, due to signal-to-noise ratio at the very dilute concentrations. The characteristic upward trend is, however, visible at the lower end of the concentration spectrum.

5.1.5 Summary of dilute acetone-alcohol systems

The four data sets experimentally determined for dilute acetone (x_{AcO}< 0.005) in alcohols are plotted together in Figure 52.

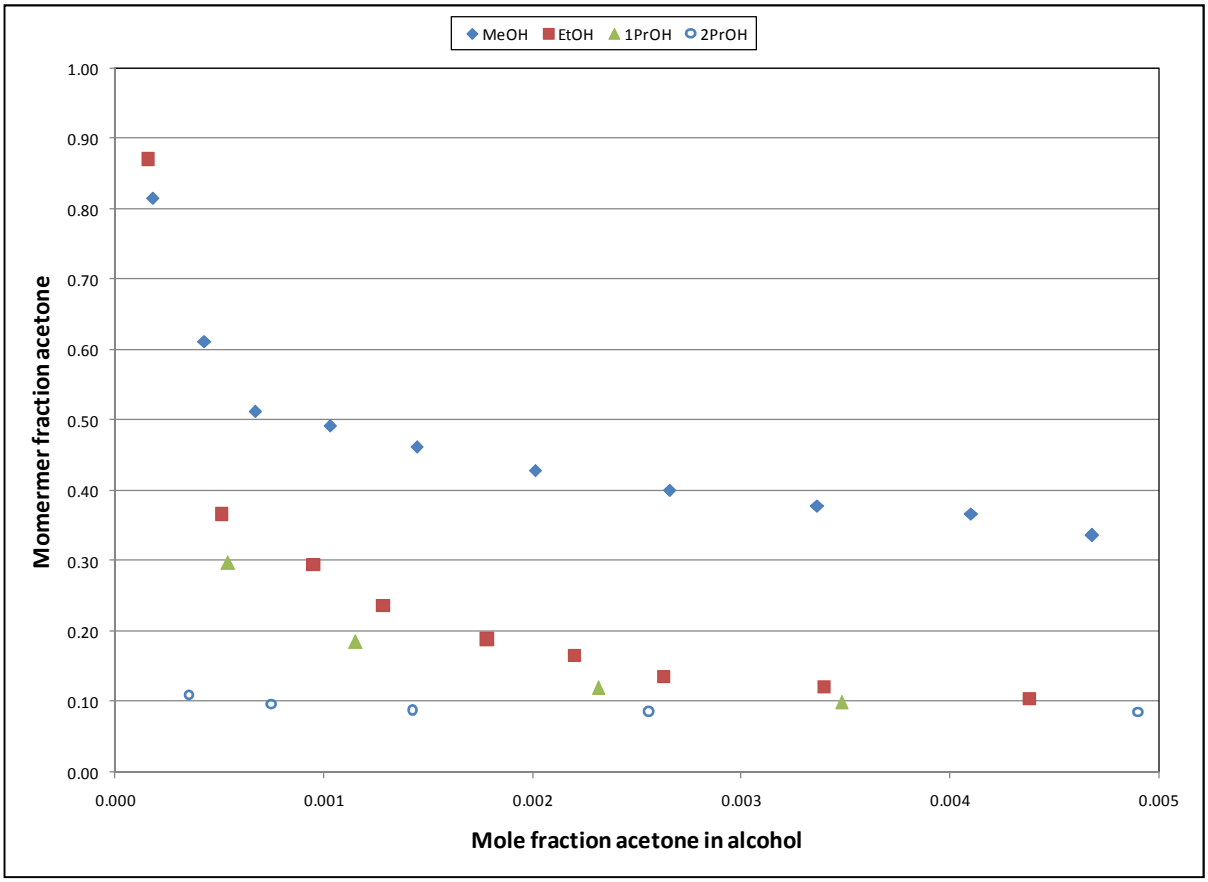

Figure 52: Acetone monomer fractions in various alcohols at super dilute concentrations and temperatures around 23 °C

In Figure 52 it can be seen that at roughly similar concentrations, acetone monomer fractions are highest for methanol, decreasing as alcohol chain-length increases. Acetone solvated in 2-propanol has the lowest comparative monomer fraction. The characteristic sharp increase is observed at low concentrations, although for acetone in 2-propanol the increase is not as clear here. The reasons for this deviation in the low concentration region have been discussed in Section 5.1.4.

5.2 Dilute alcohols in acetone

Monomer fractions were calculated from spectra of dilute methanol, ethanol, 1- and 2-propanol in mixtures with acetone. The data are shown in Section 10.2. The data are first evaluated individually and then are plotted on the same axis for comparison.

5.2.1 Methanol in acetone

The monomer fraction data for methanol in acetone are displayed in Figure 53.

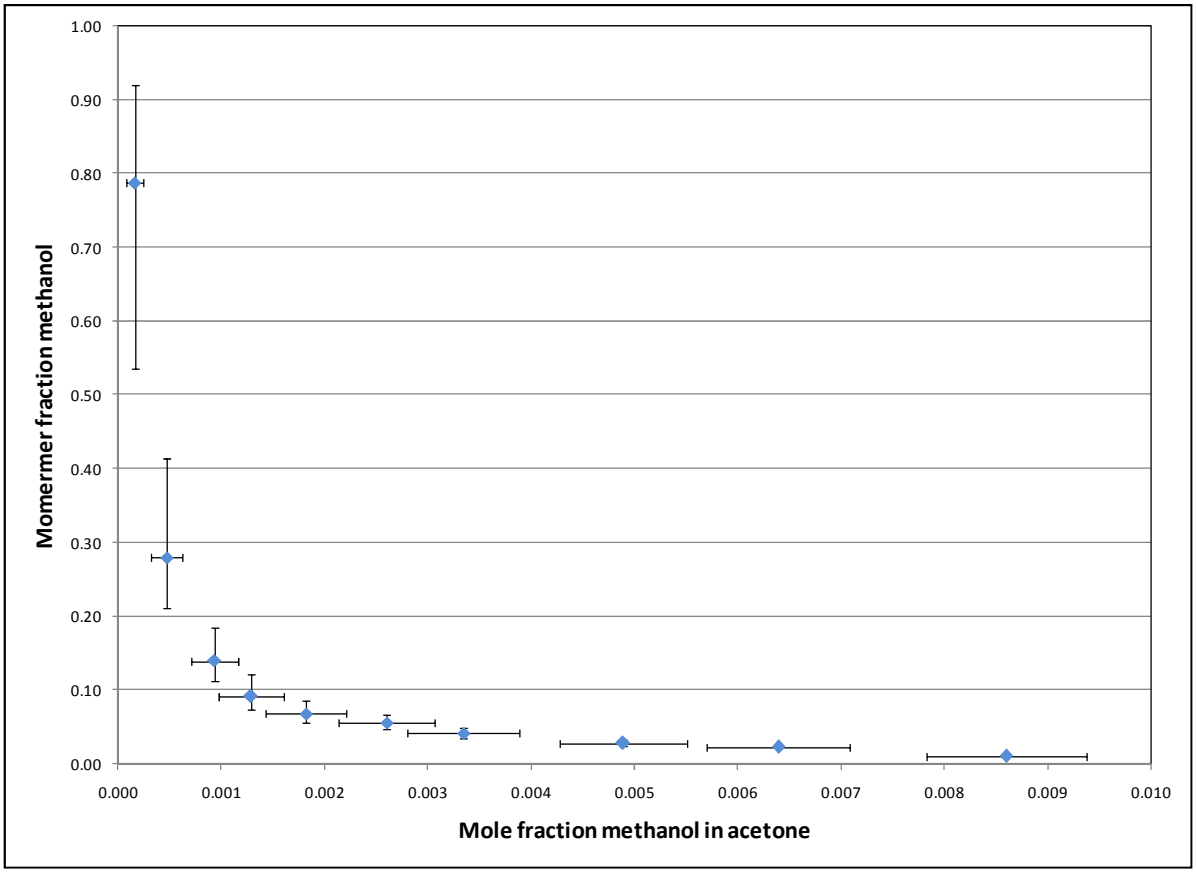

Figure 53: Methanol monomer fractions in acetone at 23.3 ± 0.2 °C

The methanol monomer absorption coefficient is calculated as 41 943 cm^{-2} / mol%. The SSE was determined to be $9.1 \cdot 10^{-6}$, summed for the 10 data points. With the proximity of the data points to each other and the lesser molar mass of methanol (as compared to the other solutes), there is some overlap between the horizontal error bars. The data do however still follow a consistent exponential shape, with the methanol monomer fraction tending to one as methanol concentration tends to zero. Methanol mole fractions are measured between 0.80 and approximately 0.01 for the observed concentration range. This is a rather precipitous drop over such a narrow concentration range, but is

not unexpected when considering the excess lone electron pairs (H-bond acceptors) available at these concentrations.

5.2.2 Ethanol in acetone

The ethanol-acetone spectra were collected at a temperature slightly offset from the alcohol-acetone data sets, due to higher atmospheric temperature. Therefore a temperature correction is done, similar to that applied for the ethanol – *n*-hexane verification data in Section 4.2. The free parameter data from Figure 46 are adapted to yield Figure 54.

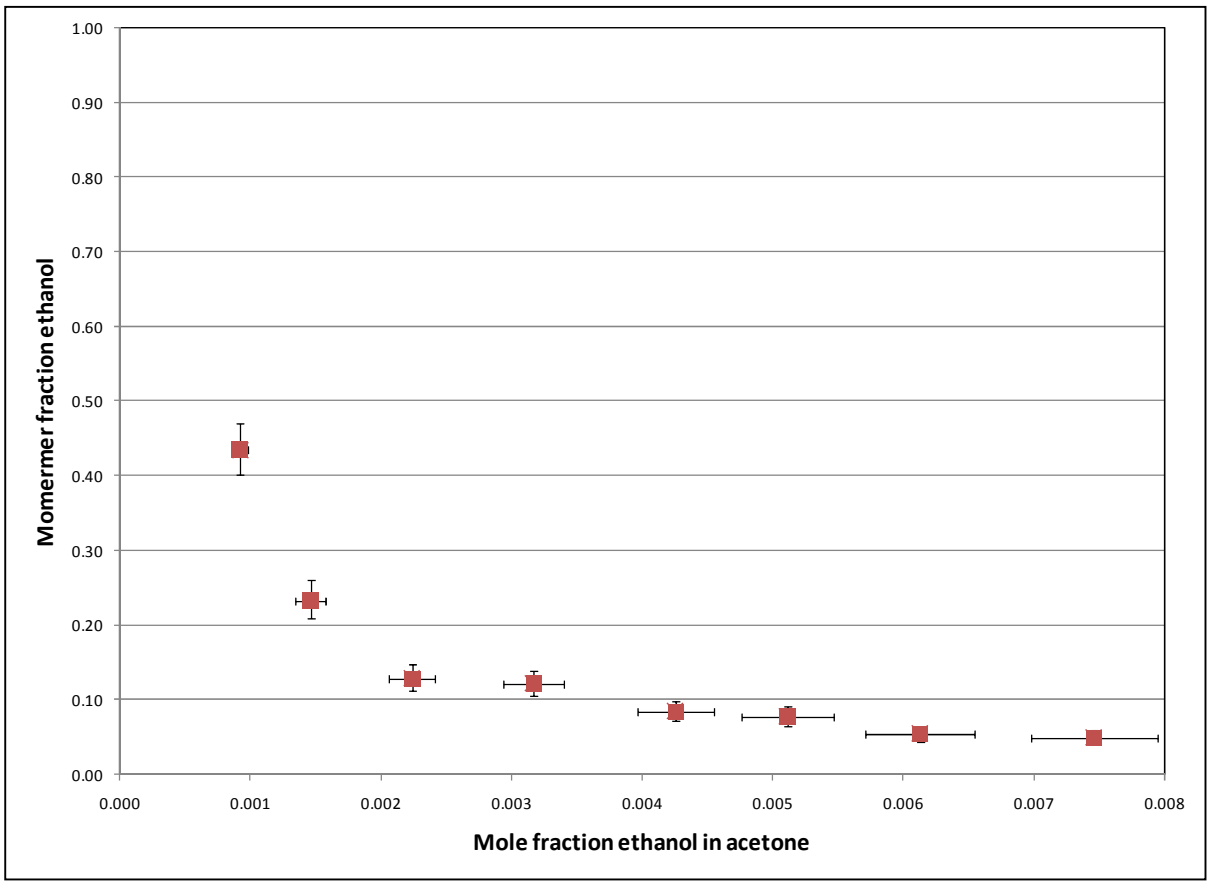

Figure 54: Ethanol monomer fractions in acetone adjusted to 23.0 ± 0.6 °C

Figure 54 shows the temperature-adjusted plot, with a temperature adjustment incorporated into the error bars as well. The effect of the temperature change is a minor change generally in the range of 0.01 mole fraction of ethanol.

As discussed in the sample analysis, the data are not smooth but a general exponential trend is again clear. For ethanol mole fractions below 0.002 the mole fraction begins to increase significantly from 0.13 to 0.43. The ethanol monomer absorption coefficient is calculated as 5 244 cm^{-2} / mol% with a

SSE of $1.7 \cdot 10^{-5}$ summed over 8 data points. This monomer absorption coefficient is significantly smaller than that calculated for methanol, but the measured concentration is also not as low. This has somewhat narrowed the error range.

5.2.3 1-Propanol in acetone

The 1-propanol – acetone system is demonstrated in Figure 55, with 1-propanol monomer fractions calculated for a range of alcohol mole fractions from 0.03 mol% to 0.6 mol%.

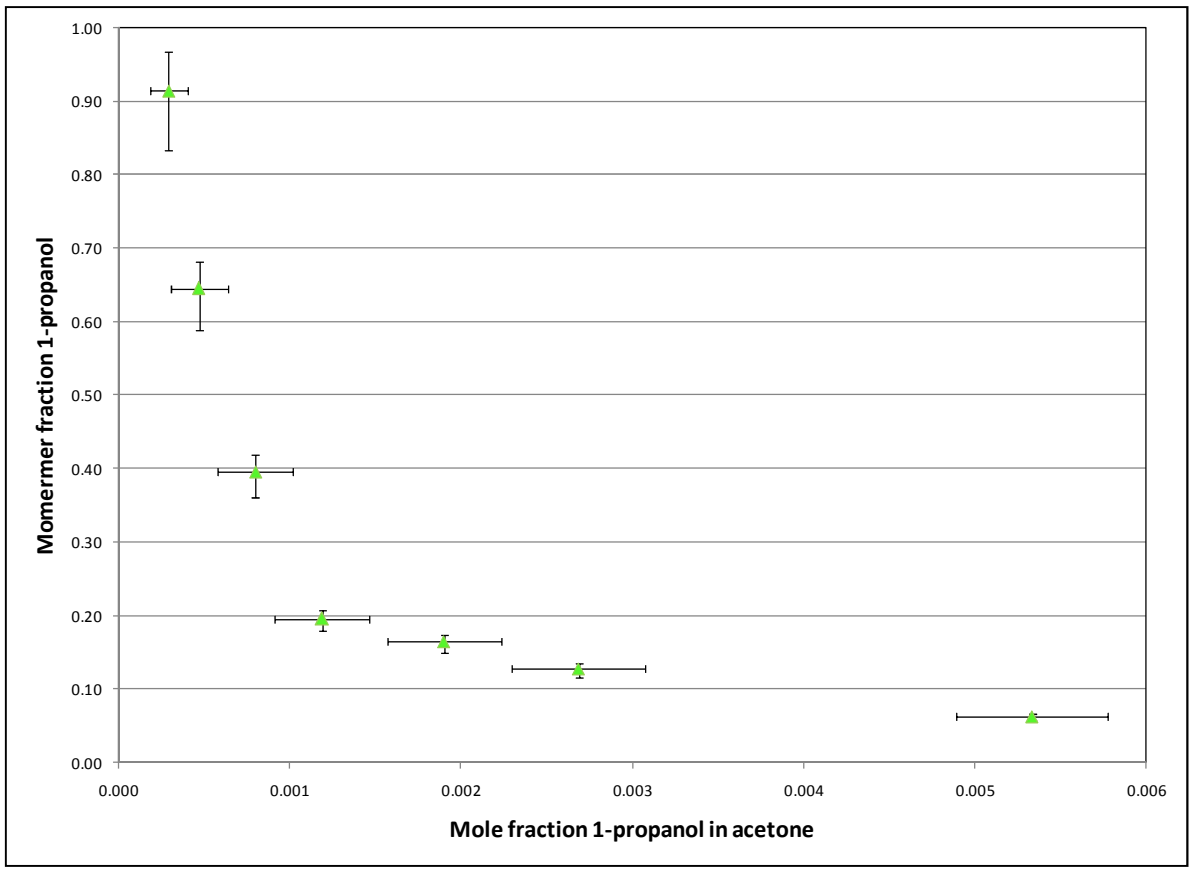

Figure 55: 1-Propanol monomer fraction in acetone to 23.1 ± 0.3 °C

Figure 55 displays a similar trend to that observed for methanol and ethanol in Figure 53 & Figure 54 with the error regions being relatively small. Once again a strong exponential increase is observed in the very dilute concentration range.

The monomer absorption coefficient is calculated as 17 678 cm^{-2} / mol%. The SSE, summed over 7 data points, was calculated as $2.1 \cdot 10^{-5}$.

5.2.4 2-Propanol in acetone

In Figure 56 the 2-propanol – acetone system is presented, with solute monomer fractions calculated for a range of alcohol mole fractions from 0.06 mol% to 0.9 mol%.

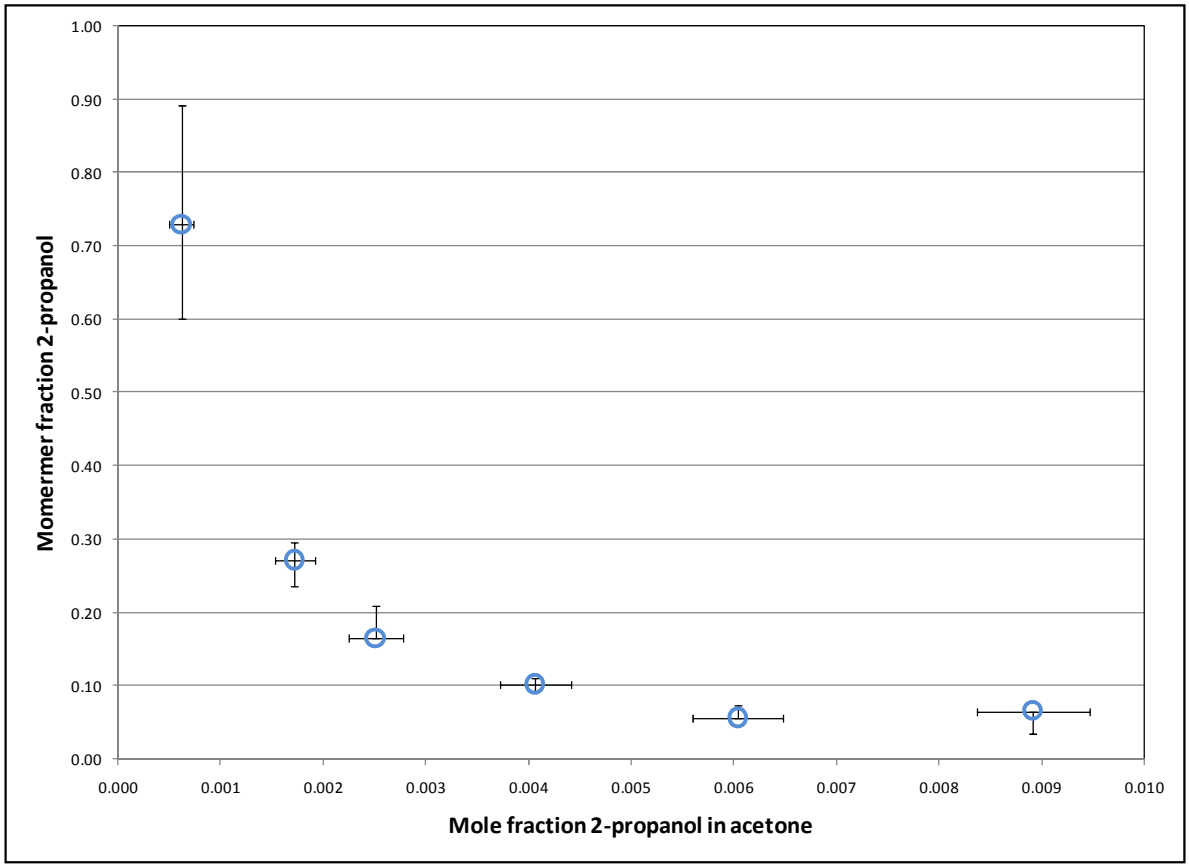

Figure 56: 2-Propanol monomer fractions dissolved in acetone at 23.3 ± 0.5 °C

Figure 56 follows on the exponential pattern seen for the other alcohols in this study. There is however considerably more "inconsistency" here as shown by the error bars. For several data, specific points are at the range of the calculated experimental error. Also, the experimental data trends upwards for x > 0.006, which is certainly a curve-fitting anomaly, rather than a physically real upward trend.

The monomer absorption coefficient is calculated as 10 381 cm^{-2} / mol% with the SSE calculated as $8.5 \cdot 10^{-6}$ for the 6 data points.

5.2.5 Summary of dilute alcohol-acetone systems

Finally it remains to compare the four data sets on the same set of axes in order to qualitatively assess their relative values.

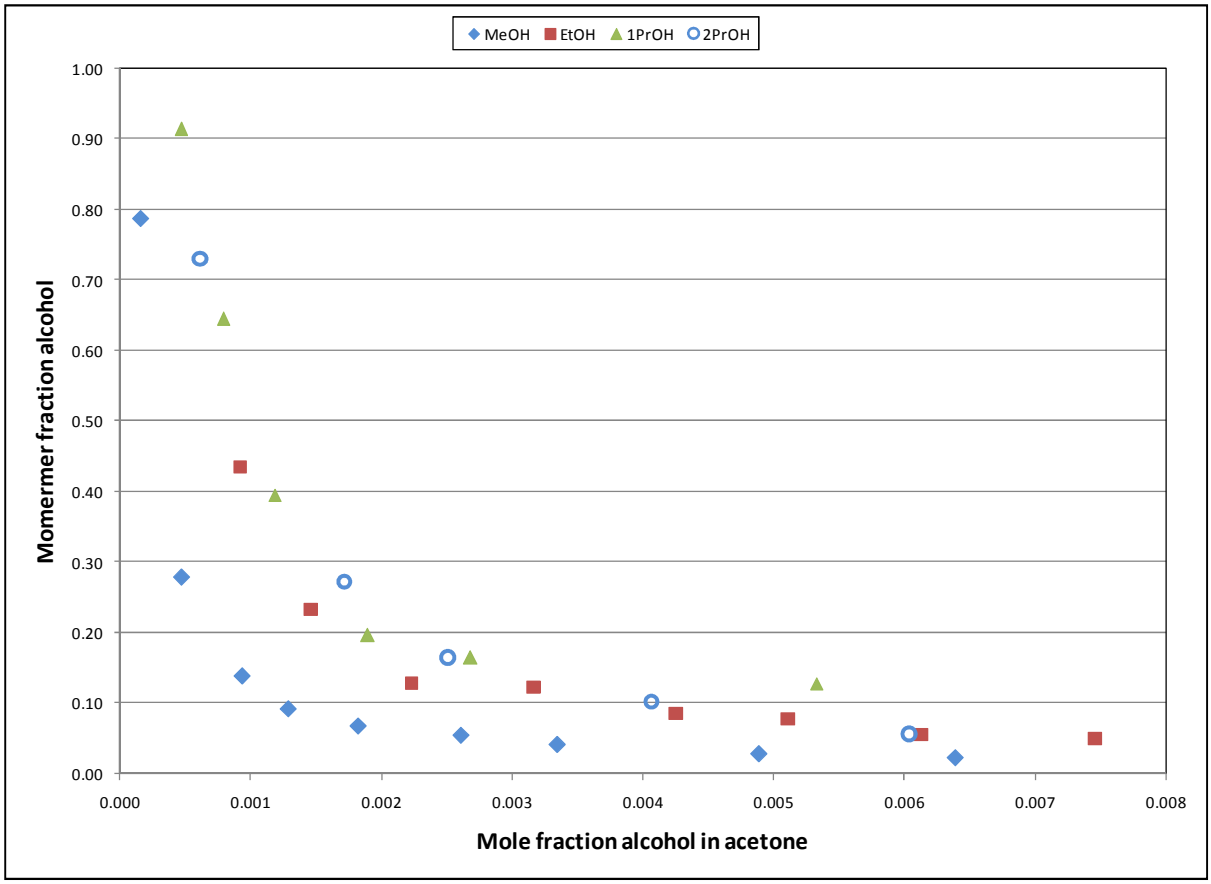

Figure 57: Alcohol monomer fractions in acetone at super dilute concentrations, with temperatures around 23 °C

Several trends are noted in the Figure 57:

- In the very dilute range, the propanols have the highest monomer fractions with ethanol in the middle and methanol having the lowest monomer fractions – this would be expected since methanol exhibits the strongest hydrogen-bonding, suggesting that it would be able to hydrogen bond more quickly in a given mixture.
- As solute concentration increases, the monomer fractions decrease exponentially and seemingly tend towards roughly the same values (especially the propanols and ethanol) which can be attributed to the excess hydrogen bond acceptors available in the mixtures.
- Some inconsistencies are apparent in the data, which can most likely be attributed to spectral analysis difficulties (since the temperature variation does not have a strong effect).

5.3 Summary of experimental results

Experimental results have been provided for various dilute acetone-alcohol and alcohol-acetone systems respectively.

Dilute mixtures of acetone in various alcohols have been examined, with acetone concentrations ranging from 0.01 to 0.15 mol% and temperatures around 23 °C. It was found that especially for methanol and ethanol there is a pronounced trend towards acetone monomer fractions of 1 at infinite dilution. This trend was not seen for the acetone – 2-propanol system, but a weak shoulder representative of the acetone monomers was still observed and quantified. This peak was not mentioned in other studies. Acetone monomer fractions are comparatively the highest in mixtures with methanol, while decreasing with increasing alcohol chain-length and pure component hydrogen bond strength.

For dilute mixtures of various alcohols in acetone, alcohol monomers are observed in the high dilution region below 0.1 mol% with temperatures around 23 °C. 1- and 2-propanol exhibit the highest monomer fractions, followed by ethanol and finally methanol with the lowest relative monomer fractions. This result is expected, and shows an inverse correlation to hydrogen bond strength. As seen for acetone, the alcohol monomer fractions tend to one at infinite dilution.

Chapter 6: Thermodynamic modelling

Chapters 4, 5 and 6 detail the experimental phase of this research, as related to the project deliverables described in Chapter 3, while Chapter 7 shows the thermodynamic modelling of the experimental data. The thermodynamic modelling presented here is related to the sPC-SAFT EoS and several variations thereof. A modified version of *TR Solutions*, developed by de Villiers *et al.* (2011a & 2011b), was used to calculate the model predictions. The application of polar variations and the 2C scheme have been mainly in terms of evaluating the prediction of phase equilibrium data. Here these variations of sPC-SAFT are applied to newly measured and existing monomer fraction data.

6.1 2C scheme performance for pure alcohol monomers

The 2C scheme has as yet not been used to model alcohol monomer fractions (at least not in any publications), whether for pure component or binary mixtures. For this reason it was decided to evaluate the 2C scheme performance using the parameters of de Villiers *et al.* (2011b). The performance of the 2C scheme is measured relative to the following models:

- sPC-SAFT (2B) [X] using the parameters of Kontogeorgis *et al.* (2010).
- sPC-SAFT (3B) [X] using the parameters of Kontogeorgis *et al.* (2010.
- sPC-SAFT (3B) using the parameters of Kontogeorgis *et al.* (2010).
- sPC-SAFT+JC Polar term (2B) using the parameters of of Al-Saifi *et al.* (2008).

The parameters used in these models can be found in Table 4 and Table 6, remembering that "[X]" denotes the use of monomer fraction data in the regression algorithm.

6.1.1 Methanol

A digitized version of Luck's (1980) data for monomeric methanol is presented in Figure 58, along with alcohol association scheme models usually employed for methanol.

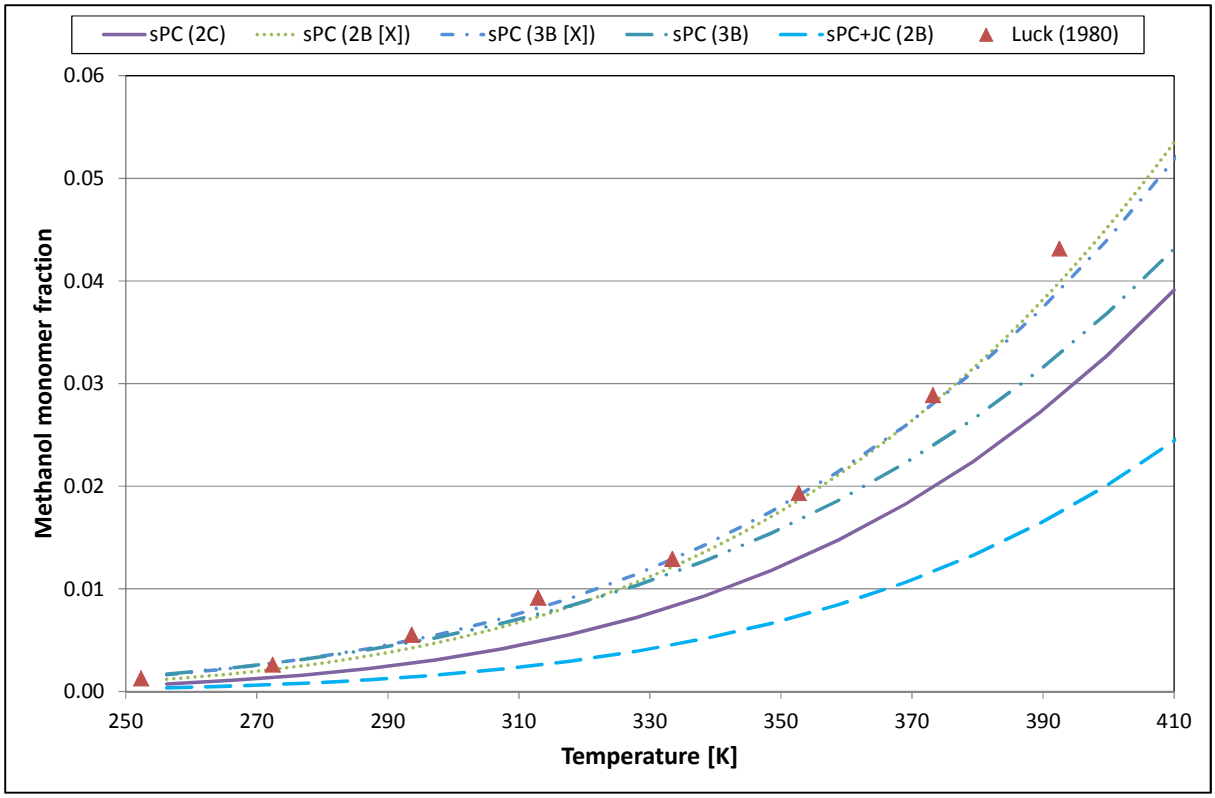

Figure 58: Pure methanol monomer fractions modelled with various association schemes

In Figure 58, the comparison is made between the model performance of the 2B, 3B and 2C association schemes. A fair comparison can be made however between the 3B (only VLE data used in the regression) and the 2C model. From Figure 58 it can be seen that the 3B more accurately predicts the methanol monomer fraction data of Luck (1980). The sPC-SAFT+JC-2B model of Al-Saifi *et al.* (2008) provides the worst prediction the pure methanol monomer fractions.

6.1.2 Ethanol

A similar model performance comparison was done using pure ethanol monomer fraction data of Luck (1986), using the following models:

- sPC-SAFT (2B) is modelled with the optimised parameters of Grenner *et al.* (2007)
- sPC-SAFT (2B [X]) from Kontageorgis *et al.* (2010)
- sPC-SAFT (2C) and sPC-SAFT (3B) from de Villiers *et al.* (2011b)
- sPC-SAFT+JC (2B) from Al-Saifi *et al.* (2008)

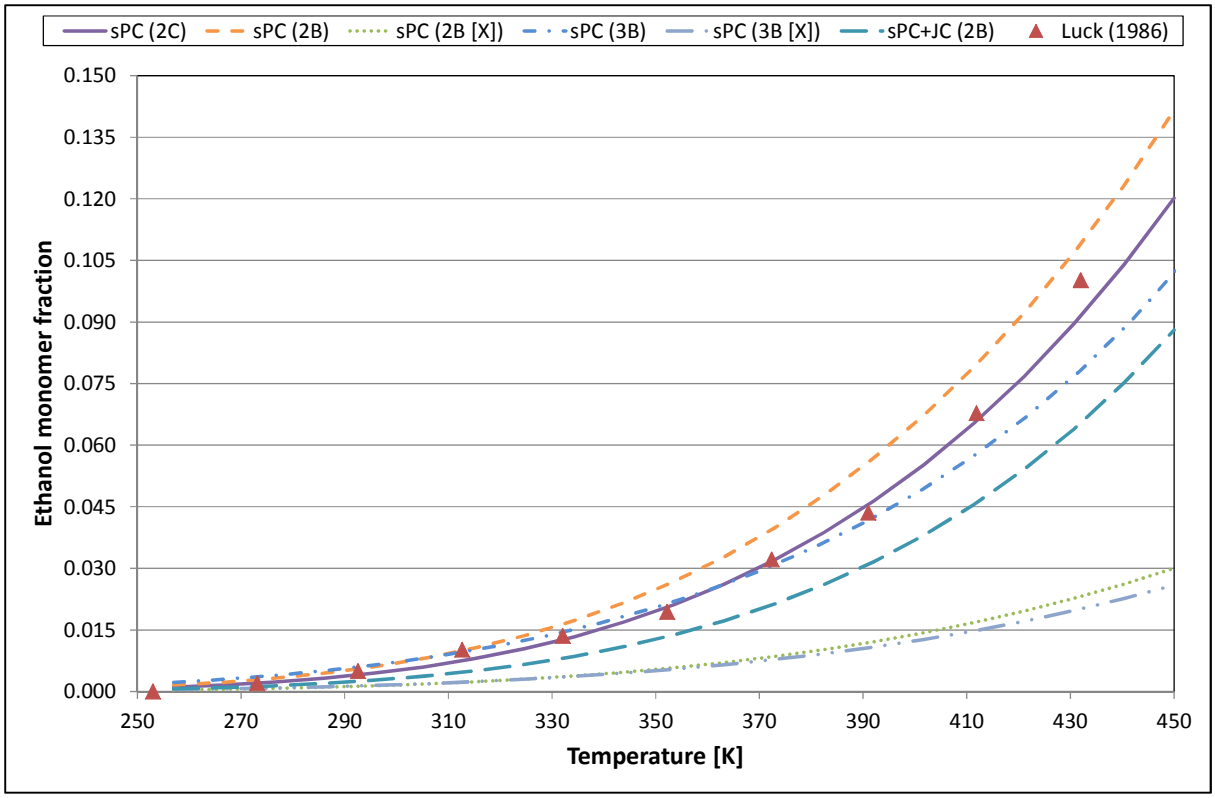

Figure 59: Pure Ethanol monomer fractions modelled with various association schemes

The 2C model predicts the pure ethanol monomer fractions the most accurately, although the model begins to deviate from 410 K onwards (roughly 80 % of the critical temperature of ethanol). Again, it should be noted that the literature (Kontogeorgis et al., 2010) is sceptical of the data produced by Luck in the sense that the methanol and ethanol data sets almost overlap with one another despite the different physical properties of the two substances.

6.2 Modelling strategy for binary alcohol-acetone systems

As these are new data sets which have not been modelled previously (at least not for monomer fraction predictions), several different approaches are taken towards modelling the experimental data. The SAFT framework allows the use of many different strategies for modelling of acetone-containing systems. To this end, various association schemes and sPC-SAFT theories (non-polar versus polar) were tested. Unless otherwise stated, the 2B alcohol parameters of Kontogeorgis *et al.* (2010) were used here, with Al-Saifi *et al.* (2008) providing the polar alcohol model constants and de Villiers *et al.* (2011b) the 2C model parameters. For acetone, the 2B association scheme has previously been implemented. Here, however, newly proposed single and double negative site association models were also evaluated for acetone. These two association models were given the designations N and 2N respectively.

The methanol-acetone system is used as test case, with several different strategies evaluated in terms of their ability to describe the experimental data. The methods producing the best results are then expanded to the other alcohol systems. The assumption is made that the four alcohols should behave relatively similarly. This assumption may be slightly dubious considering that methanol is more often than not modelled using the 3B association model, whereas longer-chain alcohols are usually modelled using the 2B model. Consider however the parameters and accuracy tables provided in Table 4, where the 2B parameters of Tyjberg *et al.* (2010) are perceived to be more accurate than the 3B parameters of Kontogeorgis *et al.* (2010) when the monomer fraction data have been omitted from the regression procedure. For the liquid density, the 2B parameters perform equally well compared to the 3B parameters even when monomer fraction data have been included in the regression routine. For the polar-2B alcohol parameters in Table 6, 2B-methanol performs similarly to 2B-ethanol, further supporting the assumption of alcohol group behaviour.

6.3 Methanol-acetone mixtures

As mentioned in the previous section, the methanol-acetone system is used as the test case for binary system modelling. Firstly, the model predictions for the entire mixture concentration range are examined. This is followed by sections zooming in on two dilute cases, so that an effective comparison can be made with the experimental data obtained in Chapter 6.

6.3.1 Selected binary modelling results for the full concentration range

Since the experimental concentration range is rather narrow, this section is included in order to provide a more holistic perception of the various models. This expanded view aids in decision-making process with respect to some of the SAFT-modelling strategies considered here.

Firstly, the model predictions are compared for the 2B-methanol model (Tyjberg *et al.* (2010)) versus those of the 3B-methanol association scheme (Kontogeorgis *et al.* (2010)) where monomer fraction data have been included (3B [X]) in the parameter regression or excluded (3B) from the regression.

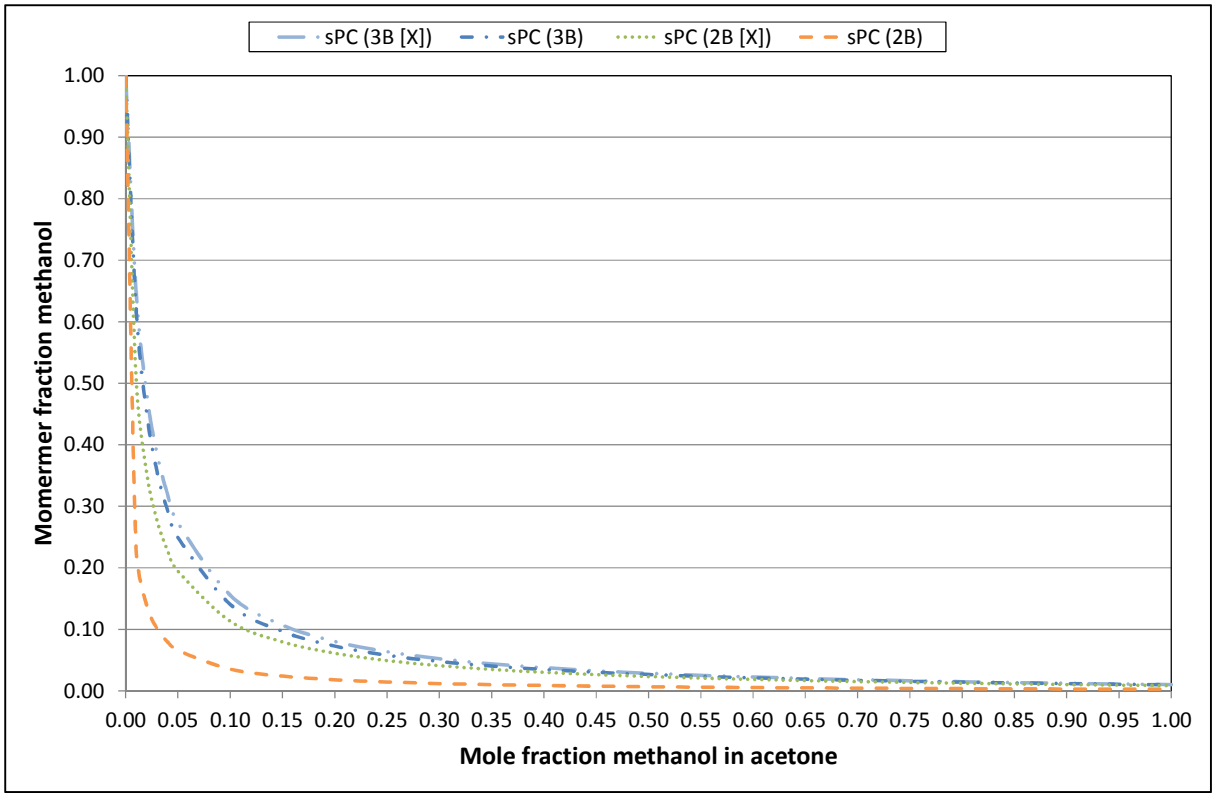

Figure 60: Comparison of 2B and 3B association scheme predictions for methanol in nonhydrogen-bonding acetone

Note that acetone is modelled as a nonhydrogen-bonding compound in Figure 60, using the parameters of Kouskoumvekaki *et al.* (2004). All the parameter sets predict the same exponentially-shaped curve, ranging from a value of 1 at infinite dilution down to near zero for pure methanol. For pure methanol the monomer fractions are calculated as 0.01031, 0.0098356, 0.00864 and 0.00260 for the 3B [X], 3B, 2B [X] and 2B models respectively. The full data are available in Table 55. The 2C models prediction are included in the table, but are not shown here since they are very similar to the 2B [X] models on this scale.

The 3B [X] and 3B models predict the highest monomer fractions and give very similar results. The 2B model predicts the lowest monomer fractions, with the 2B [X] model being in the middle. This result is somewhat counter-intuitive as one might expect fewer monomers to be present in a solution with two H-bond acceptors available on each methanol molecule.

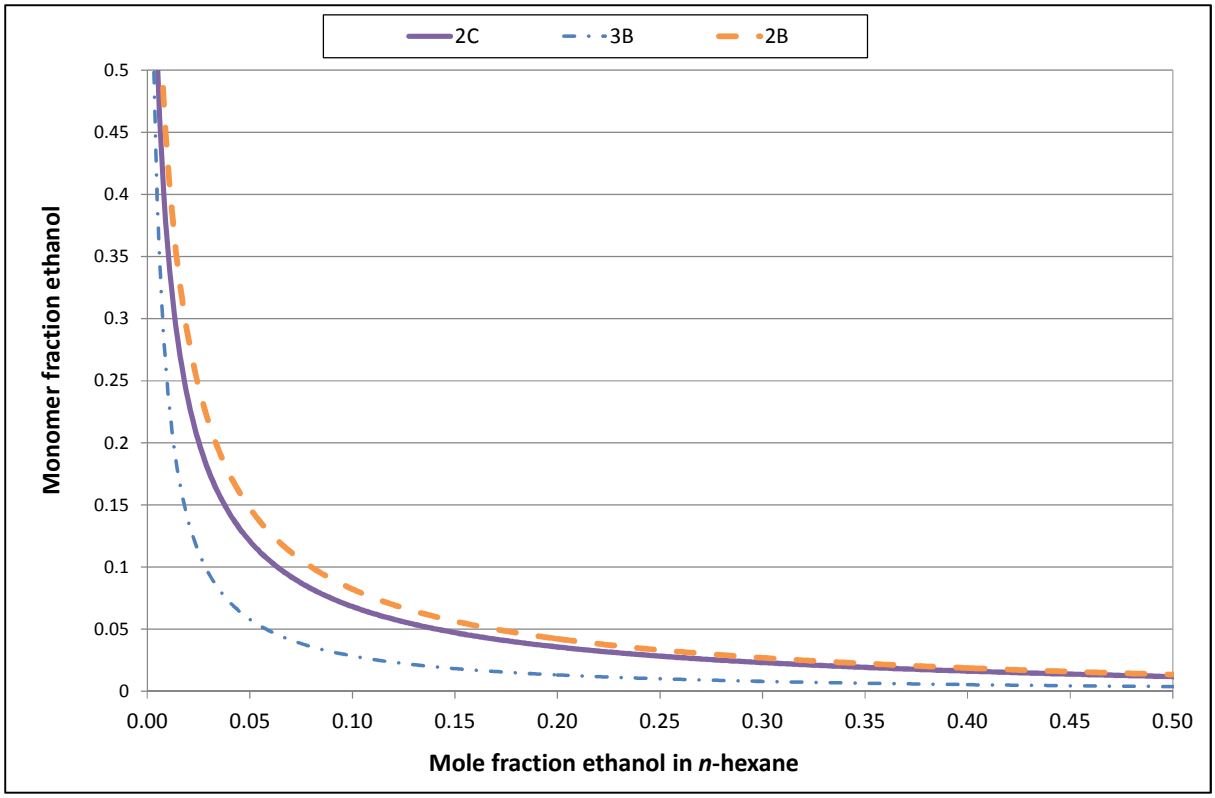

Figure 61: Examination on the effect of association scheme using ethanol (identical parameters), mixed with *n*-hexane

Figure 61 evaluates the effect of association scheme choice on a more equal footing than in Figure 60. Here the same ethanol parameter set is used, with only the association scheme varied in each instance. While ethanol and *n*-hexane are used here, the results would be qualitatively identical for methanol and **non-associating** acetone.

Figure 61 shows the expected relationship between the various association schemes, with the 3B scheme resulting in the lowest monomer fraction prediction and the 2B the highest. The 2C scheme appears between the two models, but it is closer to the 2B scheme which suggests that the bipolar site does more often than not act as positive association site. That the relative order of the 2B and 3B scheme is reversed in Figure 60 (as compared to Figure 61), serves to illustrate the strong effect of the EoS parameters on the monomer fraction predictions. The influence of the differing non-associating solvents would have no effect on the predicted monomer fractions since the exponent in EQ 2.46 would be equal to one, rendering the association strength between ethanol and the solvent equal to zero.

Superficially at least, the effect of an association scheme can be offset by a change in the parameters. Thus, consider the following parameters extracted from Table 4:

Table 23: Selected sPC-SAFT parameters for methanol

Model		m	σ [Å]	ε/k [K]	ε^{AB}/k [K]	κ	Reference	%AAD P_{sat}	%AAD ρ_{liq}
Methanol									
sPC-SAFT	3B	3.5841	2.411	163.2	1795.8	0.1715	Kontogeorgis *et al.* (2010)	0.5	0.2
sPC-SAFT	3B [X]	2.4573	2.805	198.8	2009.1	0.0465	Kontogeorgis *et al.* (2010)	1	2.5
sPC-SAFT	2B	2.877	2.5763	164.91	2304.11	0.3608	Tybjerg *et al.* (2010)	0.44	1.61
sPC-SAFT	2B [X]	1.8538	3.099	225.2	2383.1	0.0402	Kontogeorgis *et al.* (2010)	1.0	2.5

From Table 23, it can be seen that the 3B and 3B [X] models are offset from one another in terms of their association parameters:

- ε^{AB} is increased from 3B to 3B [X] while the κ value decreases for same model change. The strength of the association bonds increases as the range at which they can form decreases, which results in an overall approximately equivalent result as seen in Figure 60.

In a similarly qualitative sense, the 2B and 2B [X] models are evaluated where only the association volume changes. In this instance, a marked decrease is observed in Figure 60. This marked decrease can be explained by the fact that the parameter change is roughly a factor of 9.

From this sub-section it is shown that the effect of association scheme is secondary in importance to the EoS parameter set that is employed.

6.3.2 Dilute methanol

This section is divided into two parts whereby firstly the existing literature schemes and parameters sets are evaluated. Secondly, the performance of two newly defined schemes is considered.

(A) Evaluation of existing association schemes found in the literature

Working with literature parameter sets, the first approach is to model acetone as a non-associating compound while the traditional methanol association schemes are compared to one another. In Figure 62 the temperature is set at 23.3 °C for all the thermodynamic models.

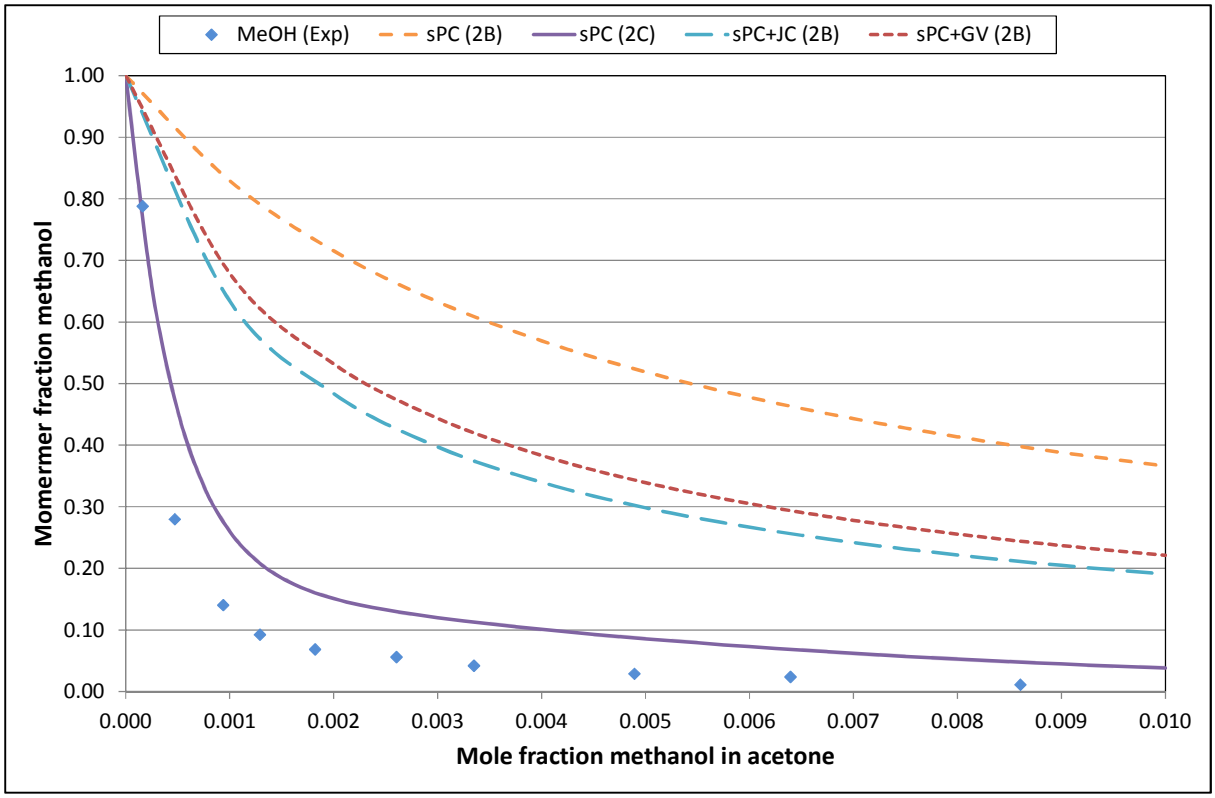

Figure 62: Various SAFT association schemes for methanol mixed with non-associating acetone

Figure 62 displays a very interesting trend. The methanol monomer fractions decrease steeply in the initial phase of solution. The 2B and polar-2B models simply cannot account for this. The 2C scheme, however, is able to capture this behaviour quite well, at least in terms of performance relative to the other models. When viewing the 2B models in isolation, using a polar model decreases the predicted monomer fractions as compared to the non-polar 2B models. The JC-model is more accurate than the GV-model, but here the JC-model has one more fitted parameter.

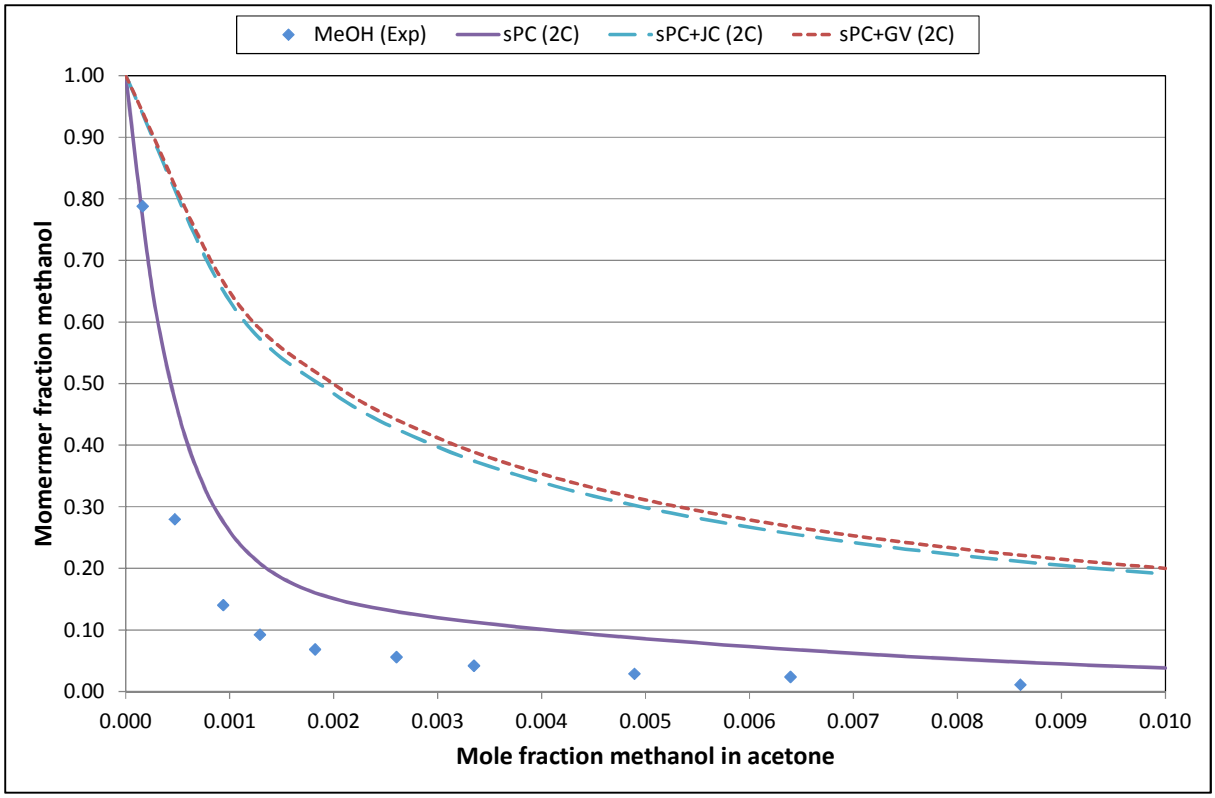

Figure 63: Methanol-acetone monomer predictions for polar and non-polar 2C models

In Figure 63, the JC- and GV-models provide very similar predictions for the methanol monomer fractions, while still predicting much higher values than those predicted by the 2C non-polar model. This is the opposite trend observed for the 2B models, where the polar models predicted lower monomer fractions. Closer inspection of the model parameters used here could provide some insight into the reasons for this.

Table 24: sPC-SAFT (2C) parameters used for the standard and non-polar models

	MeOH				AcO	
	2C	2C JC	2C GV	-	JC	GV
ε^{AB}	2535	2621	2466			
κ^{AB}	0.823	0.0639	0.1231			
ε_{ij}	197.23	192.4	179.1	253.4	245.5	210.1
m	2.1	1.69	1.97	2.774	2.187	2.786
σ	2.80	3.17	2.99	3.256	3.603	3.228
μ		1.7	1.7		2.72	2.88
x_p		0.2960			0.2969	
n_p			1			1.485

The GV-model used here has $n_p \neq 1$, which results in predictions very similar to those of the JC-model. In Table 24 it can be seen that the value for the association volume is significantly higher for the standard 2C model. Upon reflection of the model parameters given by de Villiers *et al.* (2011b), it is discovered that the κ^{AB} value was incorrectly given in the journal article and should have read 0.0823. This value is corrected with the new model predictions given in Figure 64.

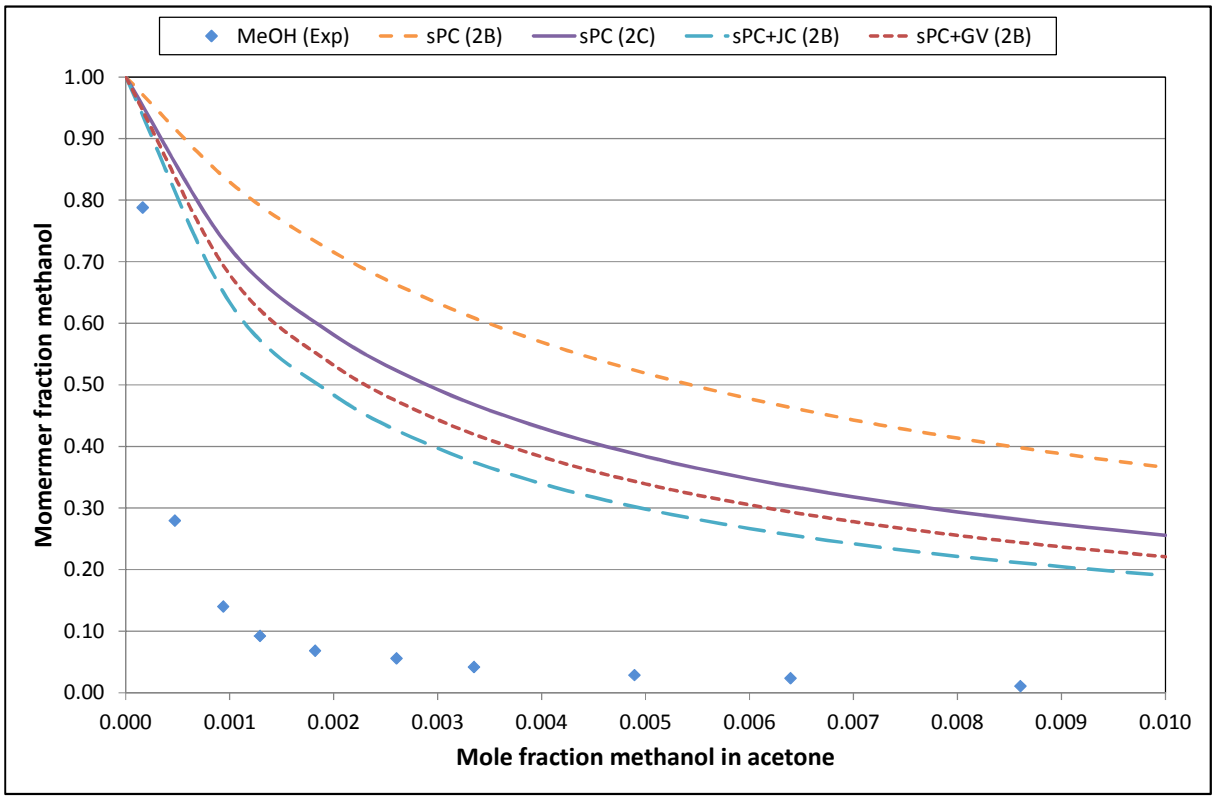

Figure 64: Corrected monomer fraction predictions for methanol in acetone

With the correct methanol 2C parameters used, the sPC-SAFT (2C) prediction falls into the region between the sPC-SAFT (2B) and the polar models. This correction serves to illustrate the influence of the association parameters on the predicted monomer fractions. By decreasing the association volume, the amount of molecules in close enough proximity to one another to hydrogen bond decreases dramatically. This in turn means that a larger fraction of unbonded molecules are present. The 2C scheme predicts monomer fractions significantly lower than the 2B scheme for the standard sPC-SAFT model, while this trend is reversed for the sPC-SAFT+JC model. Association scheme does however have a lesser effect on the monomer fraction prediction with the polar models.

In the end, the short-comings of the models presented here are however not due to the parameters used for each. Rather, the major short-coming is due to the fact that – in the model – acetone

cannot hydrogen bond, but in reality it is in fact forming hydrogen bonds via the lone electron pairs available on the oxygen atom.

Von Solms *et al.* (2004) assigned a 2B scheme to acetone and regression parameters were obtained accordingly. When using this association scheme, Figure 65 is obtained.

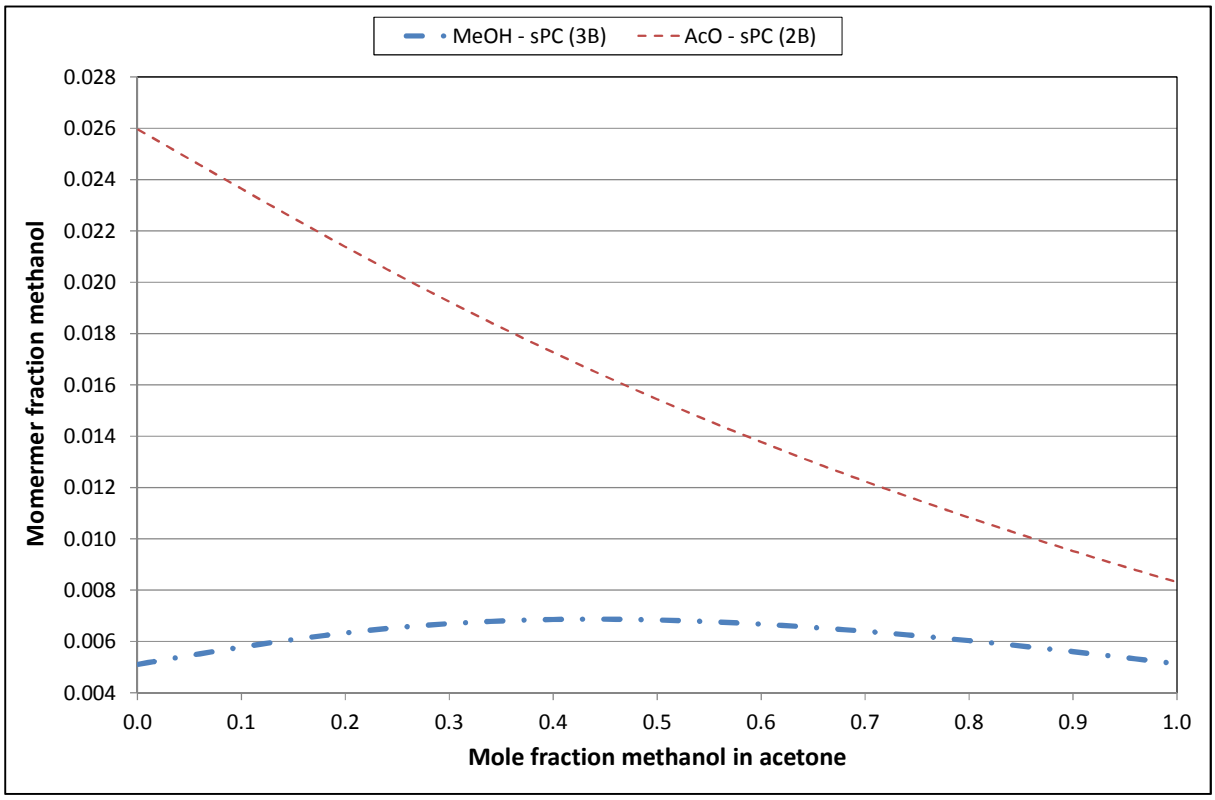

Figure 65: sPC-SAFT methanol(3B) – acetone(2B) monomer predictions at 23.3 °C

In Figure 65 monomer fraction predictions are shown for both methanol and acetone. Since acetone is assigned an association scheme, monomer fractions can be calculated for it. Methanol monomers begin at around 0.5 mol% increasing slowly with concentration to a maximum of 0.68 mol% at methanol mole fraction of 0.436, before decreasing back down to 0.5 mol% to form a dome shape.

For comparison with the data obtained in this study, Figure 66 is provided.

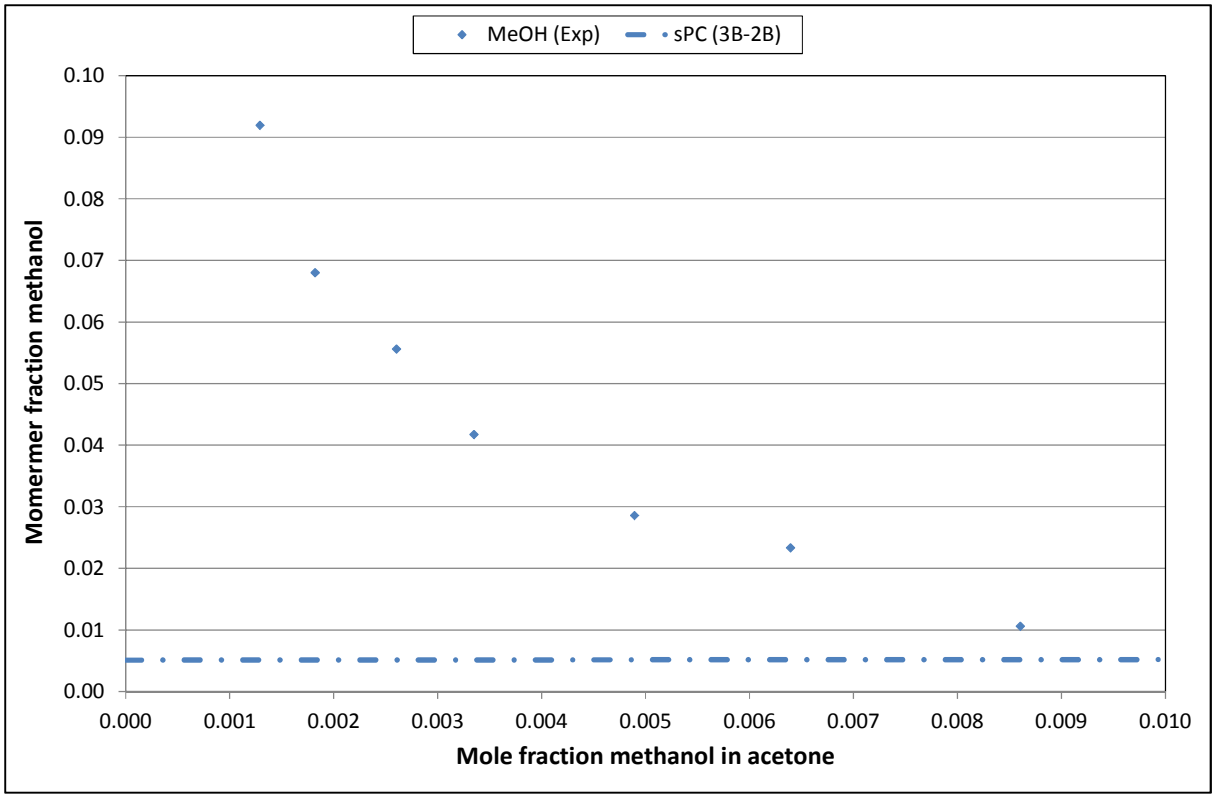

Figure 66: Comparison of experimental monomer fractions to predictions for methanol(3B) dissolved in acetone(2B)

Clearly these predictions do not correlate very well with the experimental methanol monomer fraction data obtained in this study. With acetone as a nonhydrogen-bonding compound, the models over predict monomer fraction values, whereas with the 2B acetone scheme monomer fractions are grossly under predicted. Due to the assignment of a positive association site to acetone, the acetone molecules now form hydrogen bonds with other acetone molecules, as well as the newly introduced methanol molecules. While the 2B scheme has been used to account for the polar interactions of acetone, it is not accurate in this case since the acetone-acetone polar interactions now become convoluted with the methanol-acetone hydrogen bonds.

(B) Evaluation of new association schemes for acetone

Two novel acetone association schemes are defined, in Figure 67, in order to more closely mimic the physical properties of acetone. Acetone cannot self-associate, but has the ability to form hydrogen bond via the two lone electron pairs on the oxygen atom. Therefore two negative association sites are assigned to acetone and this scheme is defined as the 2N scheme. It is felt, however, that considering the range in which the monomer fractions have been measured in this study one should evaluate a single negative association site scheme as well. The reasoning here is that with such low

alcohol concentrations, it is very unlikely for a single acetone molecule to form two hydrogen bonds with positive sites on alcohol molecules in the mixture.

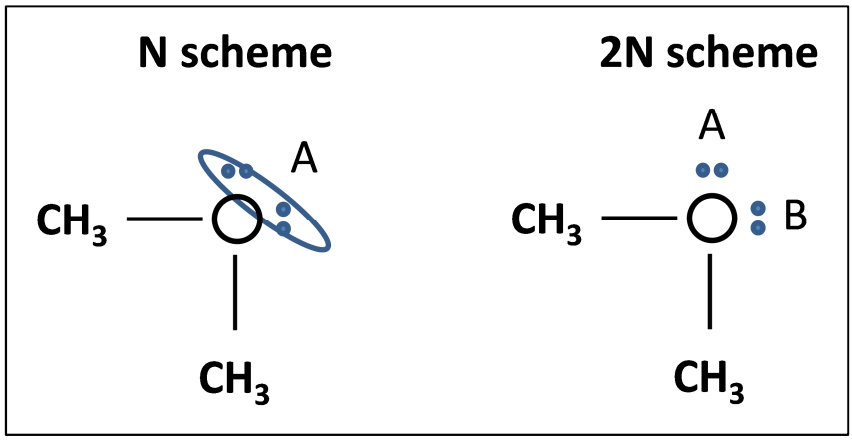

Figure 67: Presentation of the N and 2N schemes for acetone

Changing the 2B scheme for acetone to a N scheme yields Figure 68.

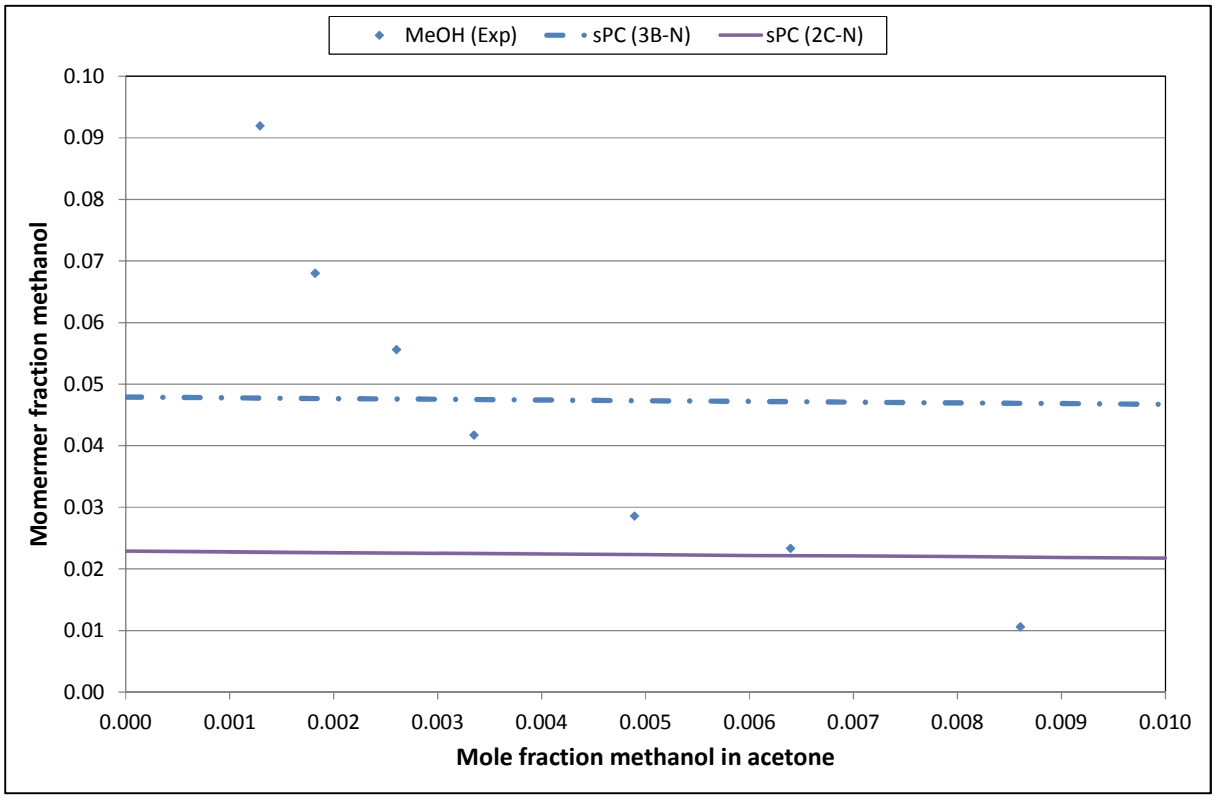

Figure 68: Comparison of experimental data to models for methanol dissolved a single negative association model for acetone

The single negative model used here uses the same parameters derived for the acetone(2B) model, with the positive association site removed from the simulation. For the methanol(3B) – acetone(N)

model, a methanol monomer fraction of 0.048 is predicted at infinite dilution, decreasing slowly as methanol concentration increases. For the methanol(2C) – acetone(N) model, a similar trend is followed, beginning with an infinite dilution monomer fraction of 0.023.

The overall trend of these models is shown in Figure 69.

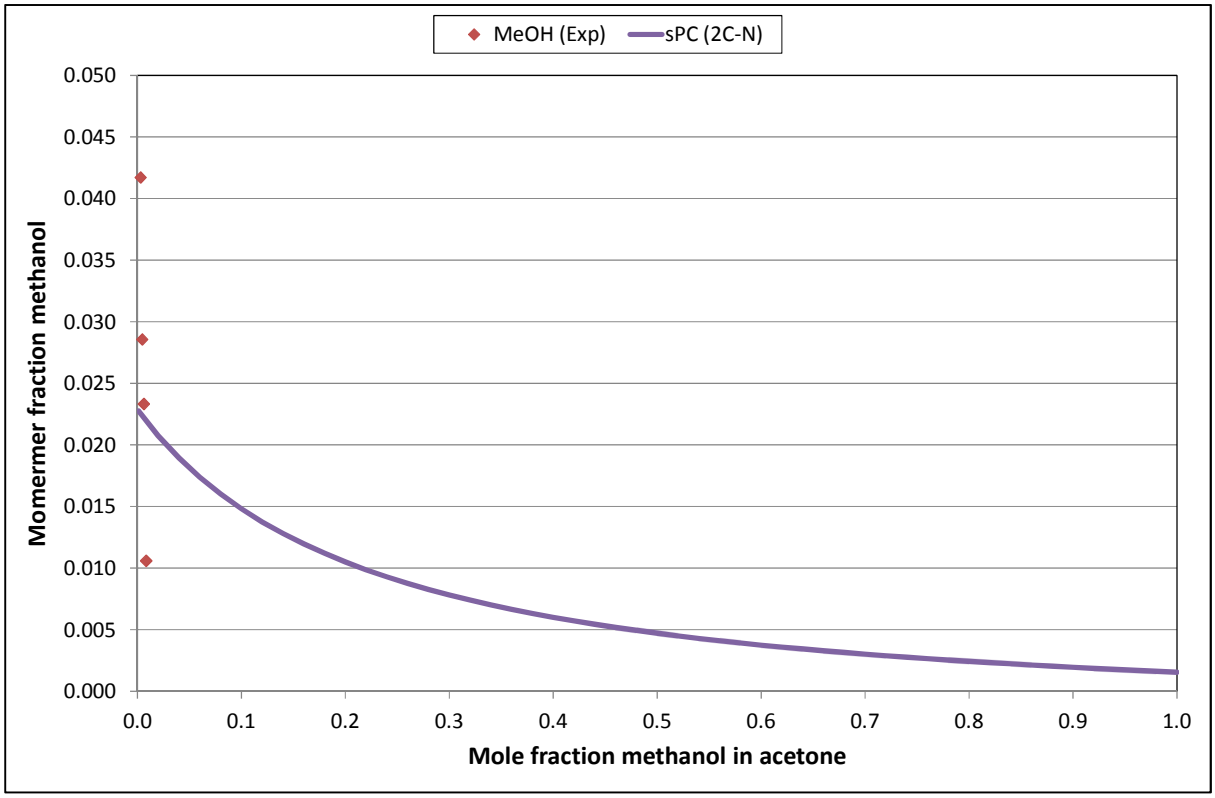

Figure 69: Expanded view of methanol(2C) - acetone(N) model predictions

Figure 69 shows the 2C-N methanol-acetone model at 23.3 °C predictions as per the standard sPC-SAFT model. The model predicts a slow exponential decrease starting at 2.3 mol% and decrease to 0.2 mol%. The general (exponential) shape of this graph is much more closely related to the experimental data – although at a significantly flatter slope – as compared with the case of acetone(2B) being used. A major difference compared with the experimental data is that the 2C-N model does not tend to 1 at infinite dilution and the gradient of the curve is not nearly as steep.

From Figure 69 it can be surmised that acetone is associating too strongly when using the N-scheme with the 2B parameters of von Solms *et al.* (2004). Thus the association parameters (ε^{AB} , κ) could be adjusted to achieve a better correlation with the experimental data. Therefore, the association parameters of acetone were adjusted in an attempt to obtain a better gauge of which parameter ranges should be used in the regression.

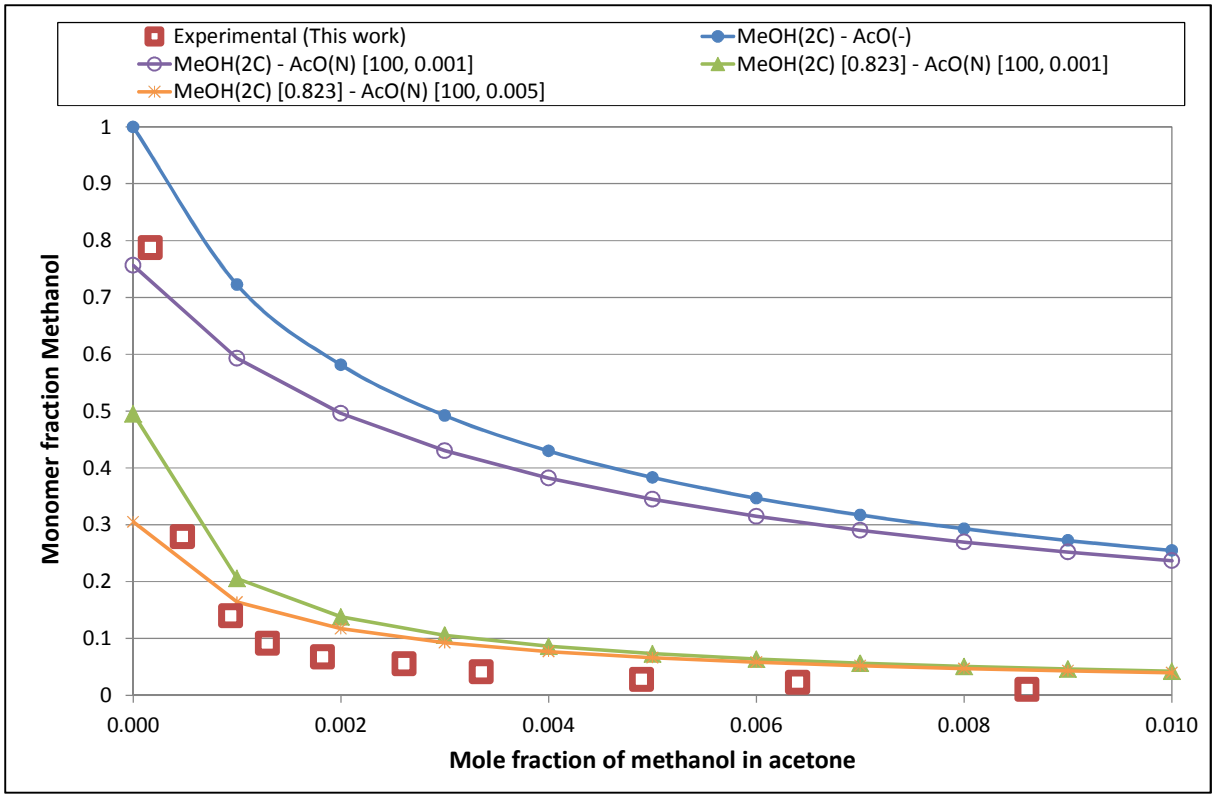

Figure 70: Comparison of experimental and 2C-N model predictions with adjusted association parameters[8]

Note that from Figure 70 onwards a different nomenclature is used in the legend of the graphs. The compound is shown first, with the association scheme in round brackets and values for the association parameters are presented in square brackets where they differ from the literature values. For methanol, κ-value of 0.0823 is used as the correct literature value, but the incorrectly reported value of 0.823 was also used. For associating acetone, however, both association parameters are modified. Firstly, the acetone(N) association parameters, parameters ε^{AB} and κ, are set to 100 and 0.001 (and later 0.005) respectively in order to assign a strength of association to acetone. This necessarily decreases the monomer fraction of methanol as some acetone molecules now become available to bond with. The effect is however more pronounced at lower mole fractions of methanol which suggests that methanol-methanol interactions quickly begin to dominate with a concentration increase. This would be expected, given the relatively weak association assigned to acetone.

In Figure 70, the increase of the alcohol κ to a value of 0.823 shows a much stronger effect than the changes to the acetone parameters. The weaker acetone parameters do however allow for a relatively close fit to the experimental data which allows for the following conclusion to be drawn:

[8] The model prediction points are connected with straight lines as a smooth line fit creates non-realistic inflection points at the lowest concentrations and also to assist in differentiating the models from one another.

By simultaneously weakening the acetone association and increasing the range of alcohol interactions, a relatively accurate fit of the experimental data may be achieved. Deviations are however observed at the lowest end of the concentration spectrum.

The relatively sharp initial decrease seen for the monomer fraction of the alcohol is similar to the trend observed in Figure 60. Referring back to Figure 60, the 2B model of Tyjberg *et al.* showed the lowest model predictions. This 2B model is adjusted and evaluated Figure 71.

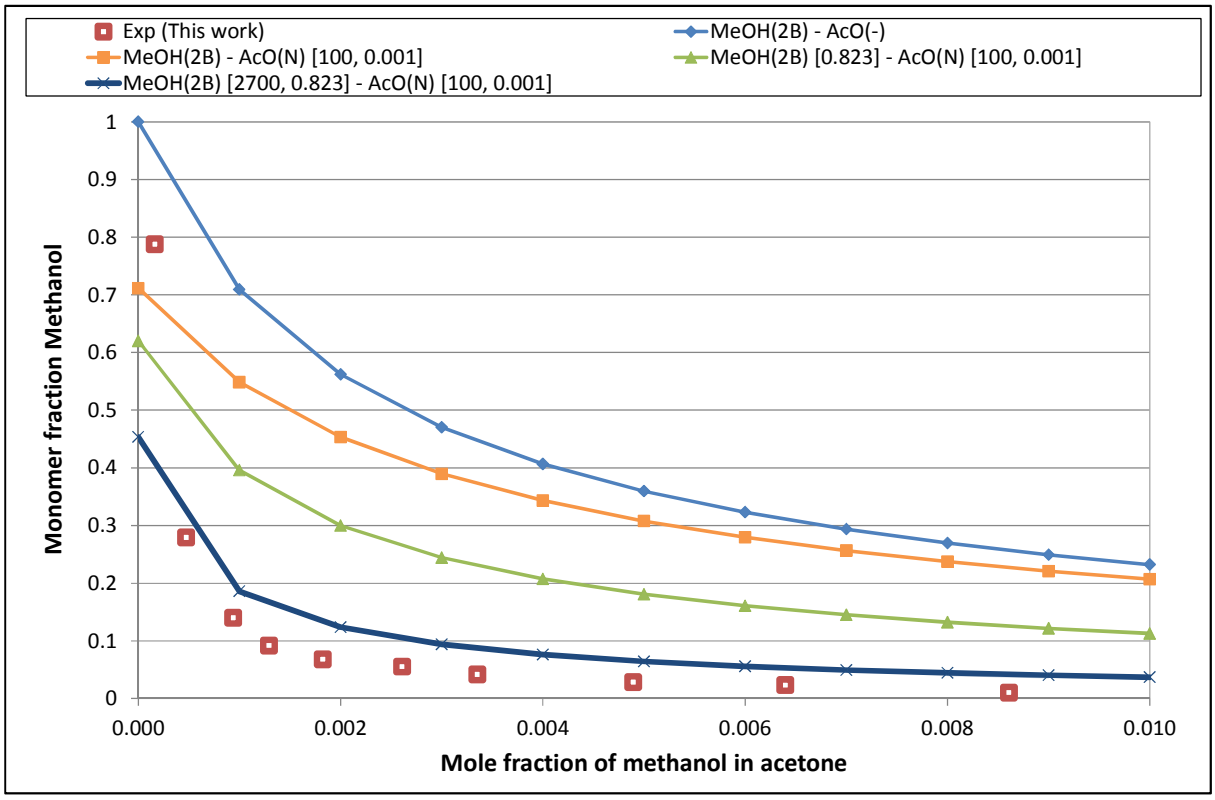

Figure 71: Manipulation of association parameters of 2B-methanol in order to more accurately approach the experimental values determined here

In Figure 71, a very similar trend is observed as in Figure 70. The graphs are plotted as per the descriptions in the legend, where the fluid, scheme and modifications to the association energy and volume are shown. As before, the increase of acetone from a non-associating compound to weakly associating single negative scheme has a relatively small effect in comparison to the changes made to the methanol association parameters. The model that most closely mimics the experimental data is the 2B-N model with the association energy and volume parameters set at 2700, 0.823, 100 and 0.001 respectively.

However, the 2B-N model still over-predicts the experimental data and thus one more modelling option is considered. Remembering that the 3B model exhibits a decrease in predicted monomer fraction as per the conclusions from Figure 61, the Figure 72 is developed.

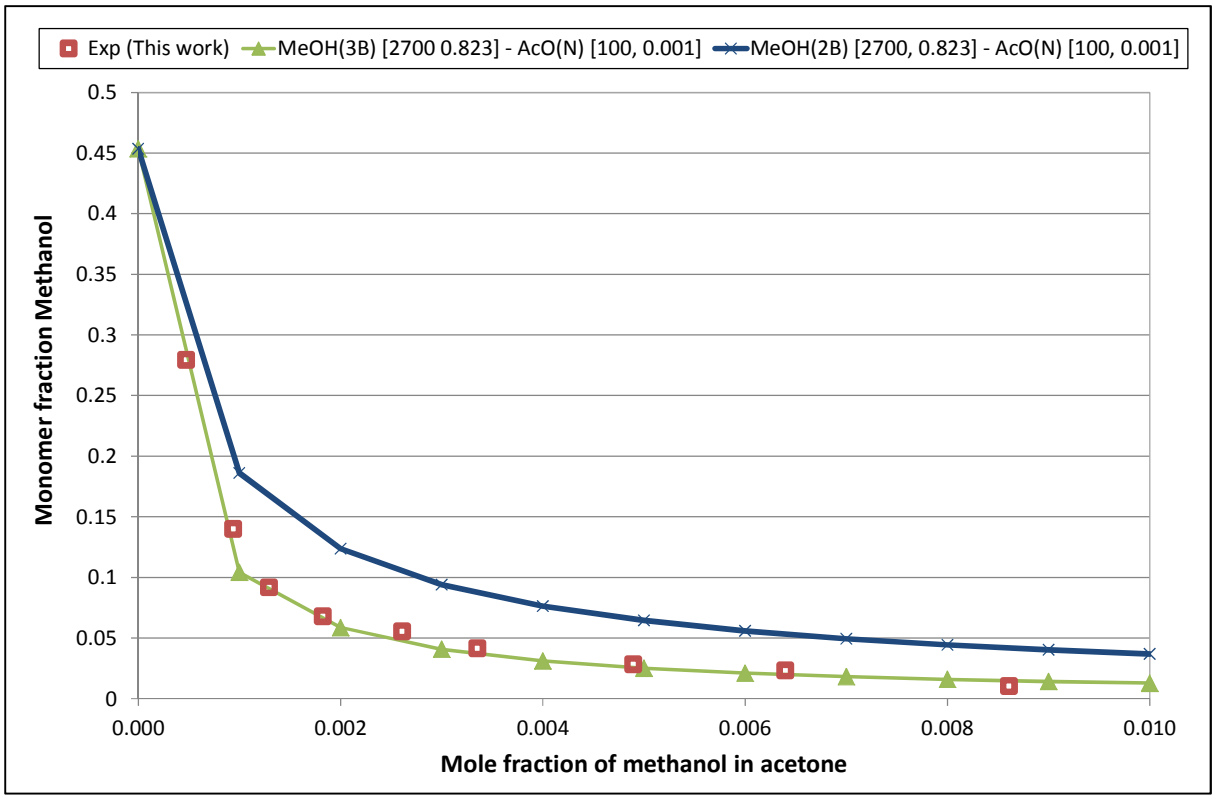

Figure 72: Comparison of the parameter adjusted 2B and 3B schemes for the modelling of experimental monomer fractions of methanol in acetone

In Figure 72, the optimised parameters of the 2B scheme are incorporated into a 3B scheme in order to decrease the predicted monomer fractions. This new 3B model almost exactly predicts the experimental methanol monomer fractions found at 23.3 °C. Only one deviation is found (although not visible on this graph), with the lowest monomer fraction point [0.00016, 0.788] not correlating with the model prediction. The model does, however, very accurately predict the increased slope for the two lowest concentrations of methanol in acetone shown in Figure 72. It is possible that the concentration deviation for the [0.00016, 0.788] experimental point is due to the fact that the spectrometer was simply unable to clearly differentiate the monomer peak at this very low concentration. The %AAD for the best fitting model was calculated as 15.5% when including the highly dilute range, while a value of 8.1% was attained when excluding it.

The data for the graphs drawn in this section are shown in Table 57 to Table 59.

6.3.3 Dilute acetone

(A) Evaluation of existing association schemes for acetone

Acetone is traditionally modelled as a non-associating compound, but as discussed it can partake in hydrogen-bonding via the lone electron pairs found on the oxygen atom. Acetone has previously been modelled using the 2B scheme, although this is not physically accurate. A C-H··O bond can form which would be representative of the positive site on a 2B molecule, but this bond is not in the same order of magnitude as the hydrogen bonds of interest here.

The acetone(2B) in methanol(2C/2B/3B) modelling data are used here for comparison with the experimental acetone monomer fractions.

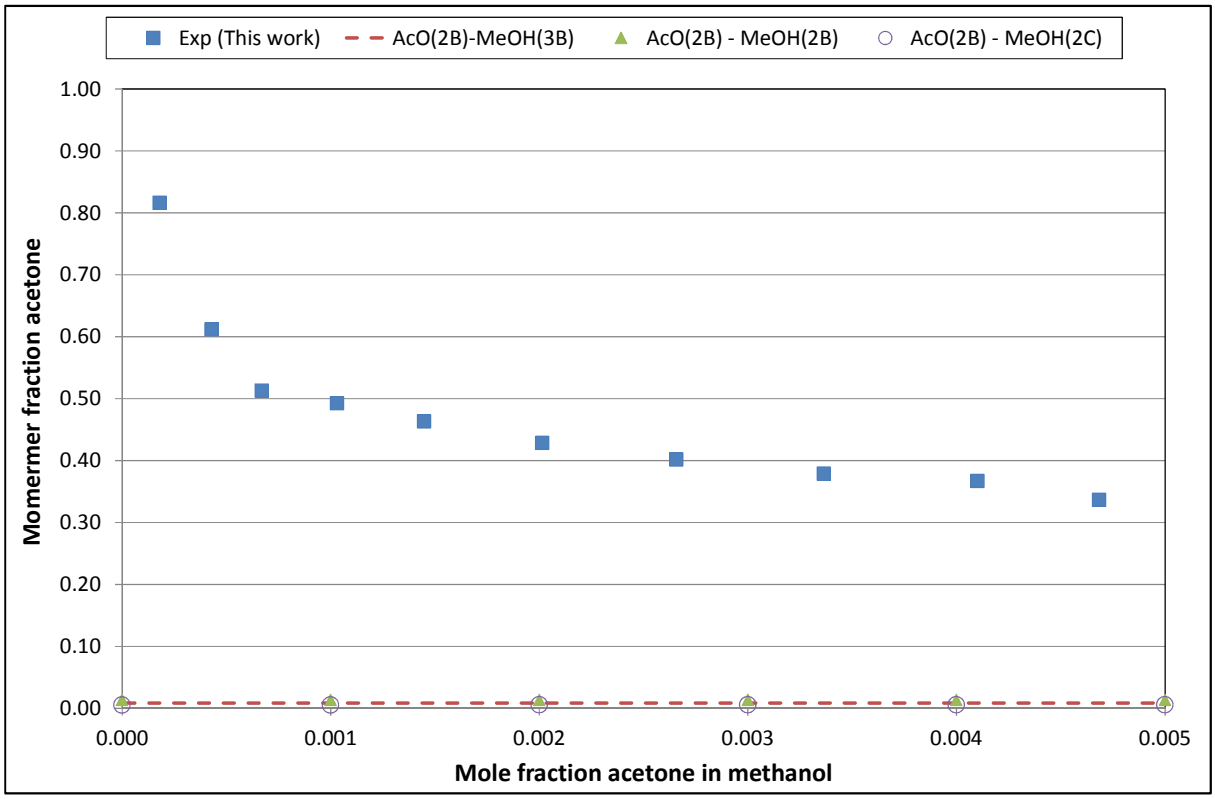

Figure 73: Comparison of acetone monomer fraction data in solution with methanol, with acetone (2B) modelling predictions

As seen in Figure 66, the use of a 2B scheme for acetone provides very inaccurate predictions of monomer fraction data in acetone containing systems. Here again (in Figure 73) the monomer fractions are grossly under-predicted due to increased hydrogen-bonding predicted with a positive association site attached to acetone and the comparatively large association volume parameter.

Due to the scale of the error in the prediction of the experimental data, the association schemes cannot be differentiated on the graph above.

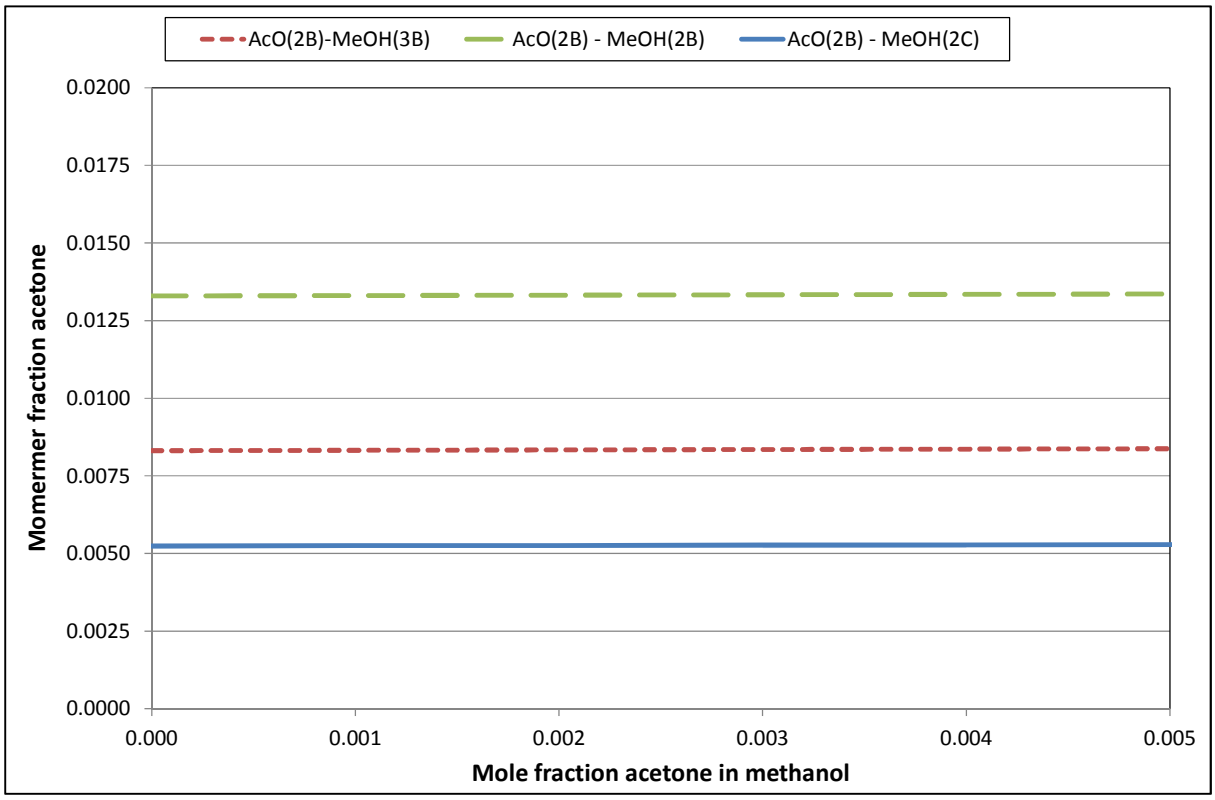

Figure 74: Zoomed in graphic of Figure 73, illustrated the differences of the AcO(2B) – MeOH (2B/3B/2C) standard models

Therefore, in Figure 74, the scale of the vertical axis is such that the various model predictions can be seen in isolation from one another. In this case the 2B-2B model predicts the highest monomer fraction, with the 2B-2C model giving the lowest predictions. The gradient of each of the models is almost zero and this is due to the strong association assigned to the acetone. For the sake of interest, the model prediction values are provided in Table 50.

The full spectrum is shown in Figure 75.

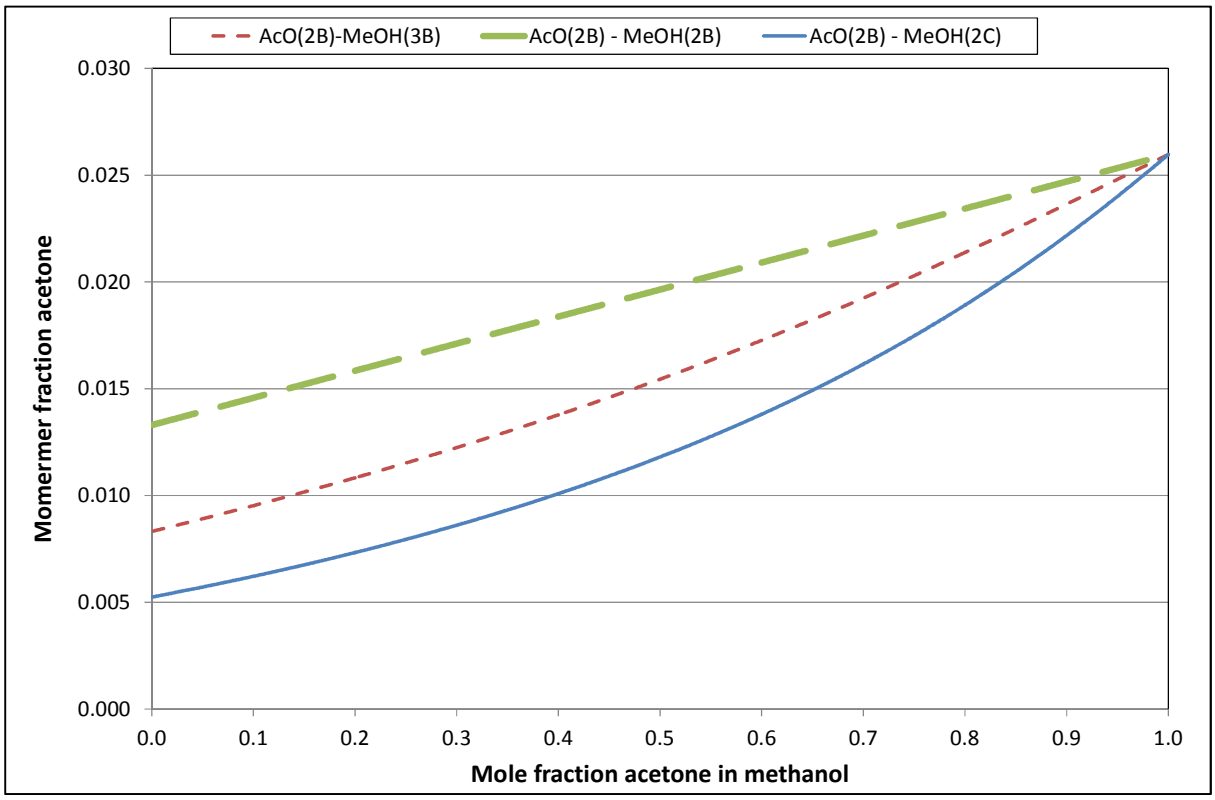

Figure 75: AcO(2B) - MeOH (2B/3B/2C) models for the entire concentration range at 23.3 °C

With the models shown for the entire concentration, it is clear that none of the models have a zero gradient. But none of the curves have a gradient sufficient to exceed a 2 mol% of monomers increase over the entire concentration range. The poor performance (in describing the experimental data) of the standard AcO(2B) model, which is the only association model available for acetone in the literature, necessitates modification of the AcO(2B) model parameters as well as the investigation of the newly proposed acetone schemes.

When using a 2B-2C model with modified association parameters, Figure 76 is generated.

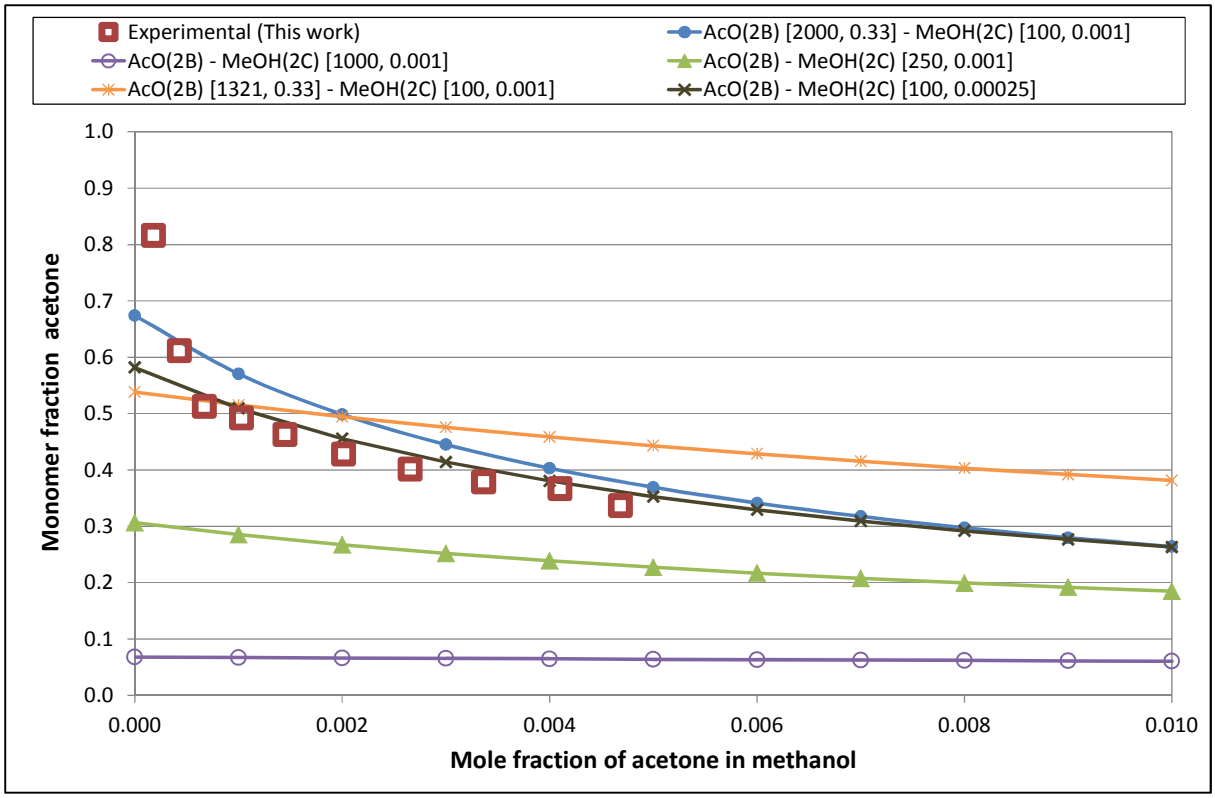

Figure 76: Predictions for various 2B-2C models with modified association parameters

Figure 76 shows various AcO(2B) – MeOH(2C) models. A relatively accurate fit (with a %AAD of 8.1%, or 5.4% when the highly dilute region is excluded) was obtained when using the standard 2B-acetone of von Solms *et al.* (2004) with a modified 2C-methanol molecule where the association energy and volume parameters are 100 and 0.00025 respectively. For this parameter set, a good fit is maintained except for the very low concentration measurements. In this low concentration region, the experimental data once again increase too steeply as compared to the model. And once more, this could also be due to an inaccuracy in the measurement for the highly diluted mixtures. A steeper gradient for the model curve can be achieved by increasing the acetone association energy parameter while decreasing the association volume parameter (as seen for the AcO(2B) [2000, 0.33] model) but this requires additional adjustments to the methanol parameters. Some model fine-tuning could result in a slightly more accurate fit. It should be noted that the methanol parameters that yield the best fit here do not correlate well with those published in the literature. It may be the case that the acetone molecules struggle to penetrate the methanol association network and thus when the methanol association strength is decreased (at least from the perspective of its interaction with acetone) a better fit is obtained. This could suggest the need for some form of a cooperativity/hindrance factor, which needs to be employed for systems where cross-association occurs. This additional factor is especially necessary when there is significant difference in association strengths of the two components.

(B) Evaluation of new association schemes for acetone

For this sub-section, the effect of a 2N scheme (see Figure 67) is also investigated. This scheme is defined as having two negative association sites and could be considered more physically representative of a dilute acetone solution where each lone electron pair has an opportunity of bonding with a hydrogen atom located on the –OH segment of methanol. However, the proposed N-scheme is still considered, since negative sites are in excess for acetone in a mixture with methanol (which is why it is generally well described by the 3B scheme).

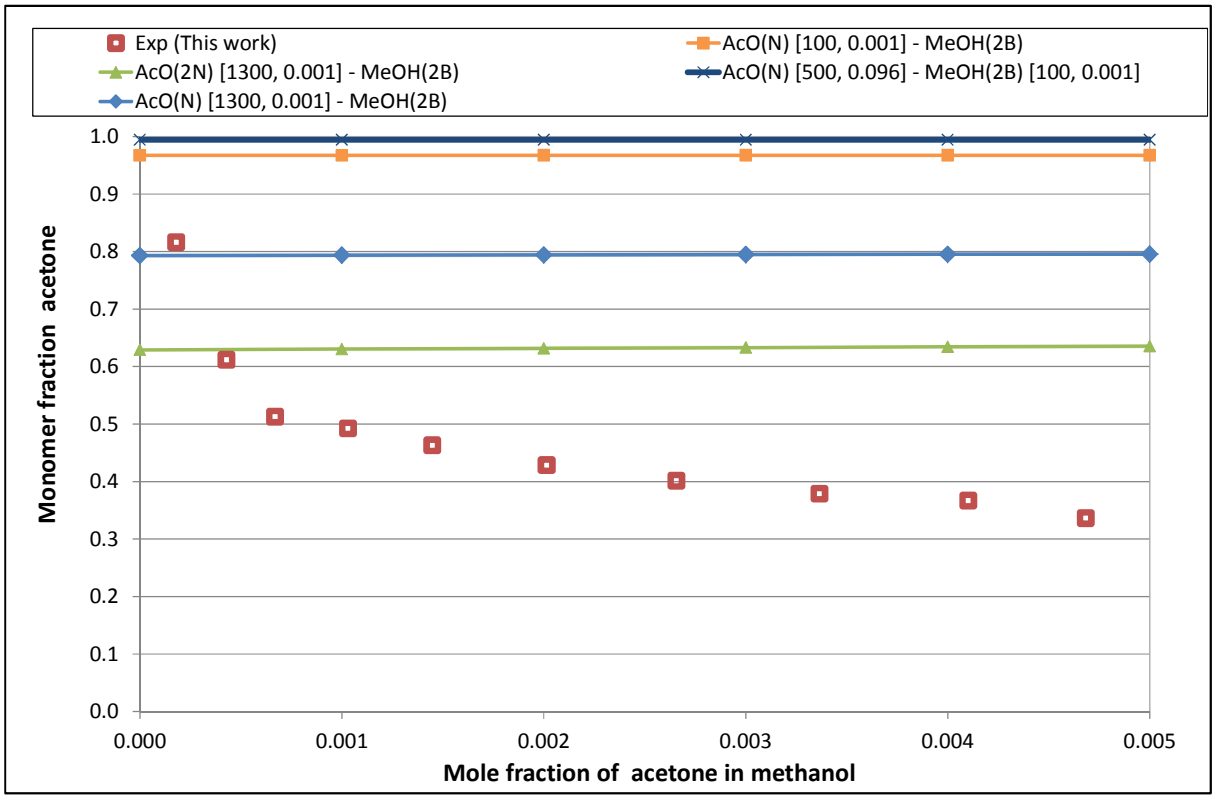

Figure 77: Evaluation of newly defined N and 2N schemes for the prediction of acetone monomer fractions in methanol

Figure 77 shows some of the scenarios tested for the modelling of acetone monomer fractions using the N and 2N schemes. In short, regardless of scheme (acetone or methanol) or parameters chosen, the trend of the experimental acetone monomer fractions cannot be replicated using the models/schemes proposed in this sub-section.

6.4 Ethanol-acetone mixtures

As the methanol-acetone mixture was used as a test case to examine all possible variations of schemes and parameters to model the experimental data accurately, the other sections of Chapter 7 will only show the most accurate modelling results rather than the entire progression as was seen in

Section 7.3. The lessons learnt in the modelling of the methanol-acetone mixtures are necessarily applied here and in the sections to come.

6.4.1 Dilute ethanol

The results for the dilute ethanol solution in acetone can be seen in Figure 78. The 2B-N model is shown, but in truth there is very little difference between the 2B and 2C predictions for the ethanol association scheme. As with the dilute methanol-acetone system, the model struggles to predict the increased gradient in the super dilute range. In the medium dilution range, good model predictions are obtained for both the following models:

- EtOH(2B) [2495, 0.825] – AcO(N) [50, 0.001]
- EtOH(2B) [2495, 0.85] – AcO(N) [100, 0.001]

These two models predicted monomer fractions with a %AAD of 20.3% and 18.0% respectively when including the highly dilute range, while the %AAD decreased to 12.8% and 10.6% when the highly dilute range was excluded.

Note that the base parameter system for the 2B model used here is that of Grenner *et al.* (2007). For both models, the predictions are very good in the range of 0.2 to 0.8 mol%.

Figure 78 shows that changing the acetone association energy parameter from 50 to 100 or 145 has very little impact (usually around 0.1 mol%) on the overall model prediction, while changing the ethanol association energy parameter from 2495 to 2050 has a much greater impact.

It can also be seen that using the 2N scheme for acetone has the undesirable effect of decreasing the model gradient and thus will not be a feasible solution to the modelling problem difficulty seen in the very dilute range.

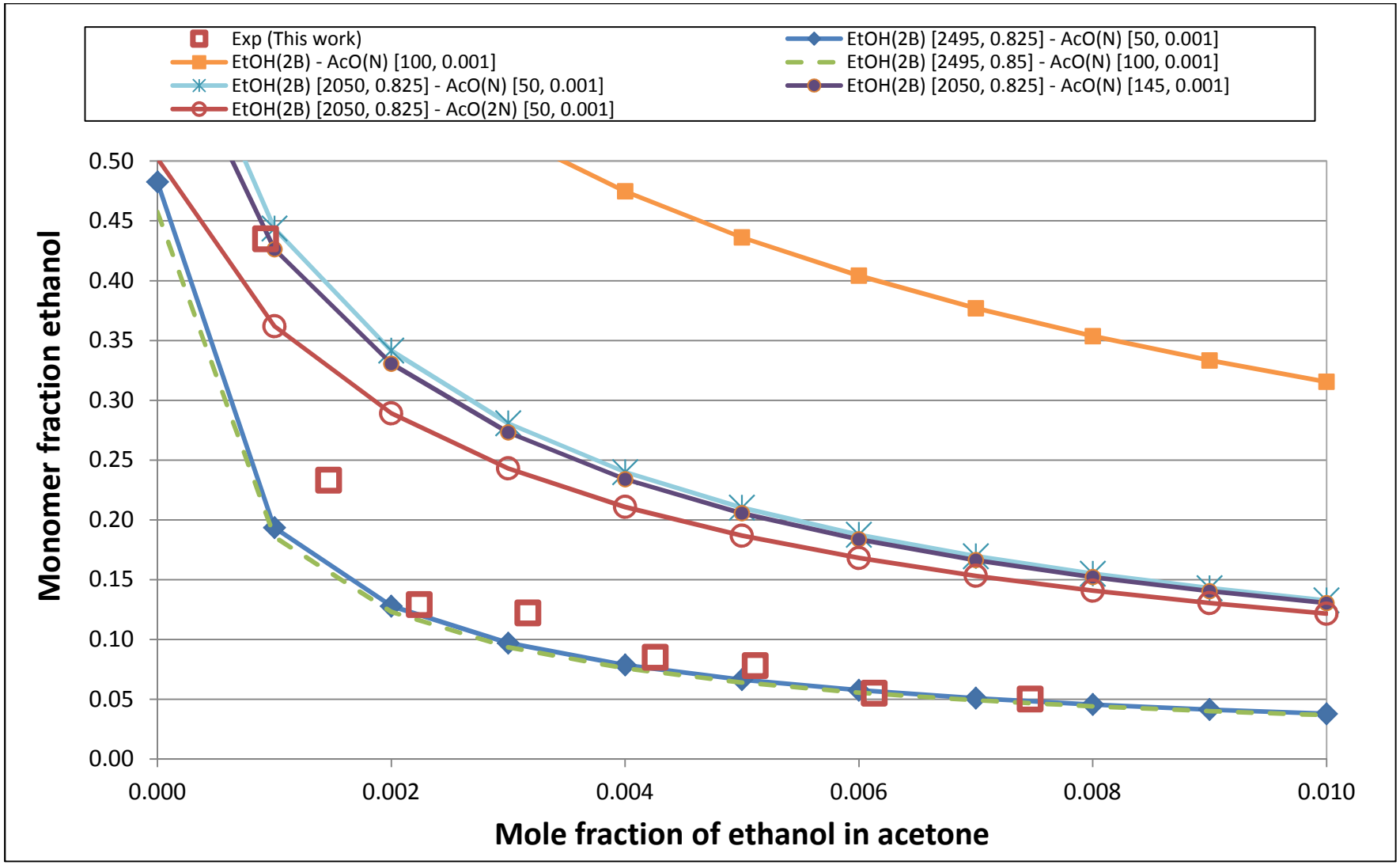

Figure 78: Experimental sPC-SAFT model fits for dilute ethanol-acetone mixtures

6.4.2 Dilute acetone

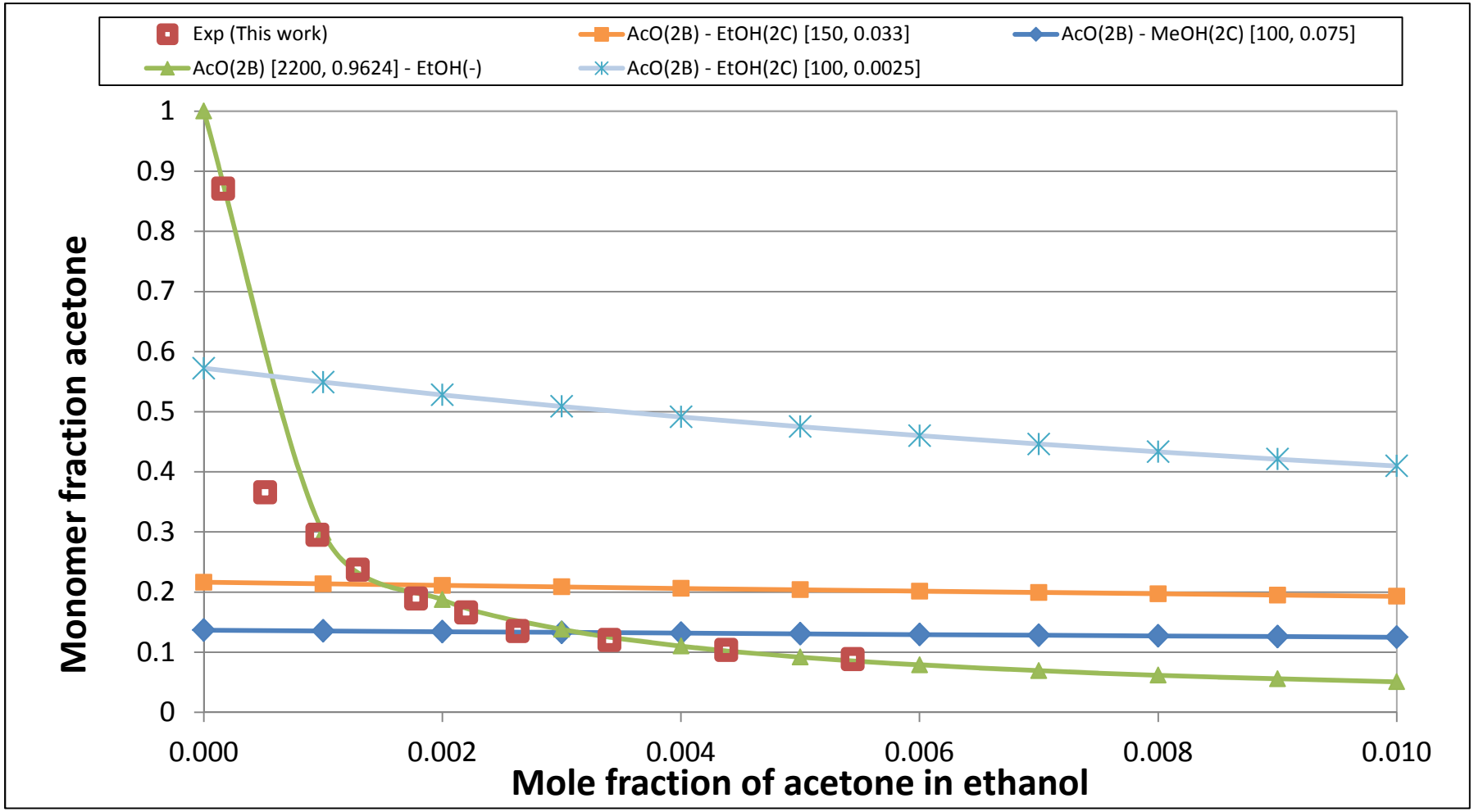

Figure 79: Comparison of various models for the prediction of acetone monomer fractions in solution with ethanol

Figure 79 shows the results for modelling of acetone monomer fractions in solution with ethanol at 23.2 °C. While it was possible to describe the dilute acetone-methanol system using a 2B-2C scheme, the same cannot be said for the acetone-ethanol system. The gradient observed in the experimental data does not allow for the easy modelling of the system, with several more scenarios presented in Table 52 in the appendices.

By modelling ethanol as non-associating and assigning very large association parameters to acetone, a satisfactory fit (yielding a %AAD of 14.5% or 8.6% depending on whether the highly dilute range is included or not) to the experimental data may be obtained. This result does however not seem physically feasible and is presented merely as part of the modelling and optimisation exercise. This result also casts some aspersions on either the accuracy of the experimental data for this particular system or the ability of the models to describe the rather complex behaviour of the acetone-ethanol interaction. A simple explanation for this may be that the acetone molecules struggle to penetrate the ethanol network and thus, from the perspective of the acetone molecules, ethanol does not associate.

6.5 1-Propanol – acetone mixtures

6.5.1 Dilute 1-propanol

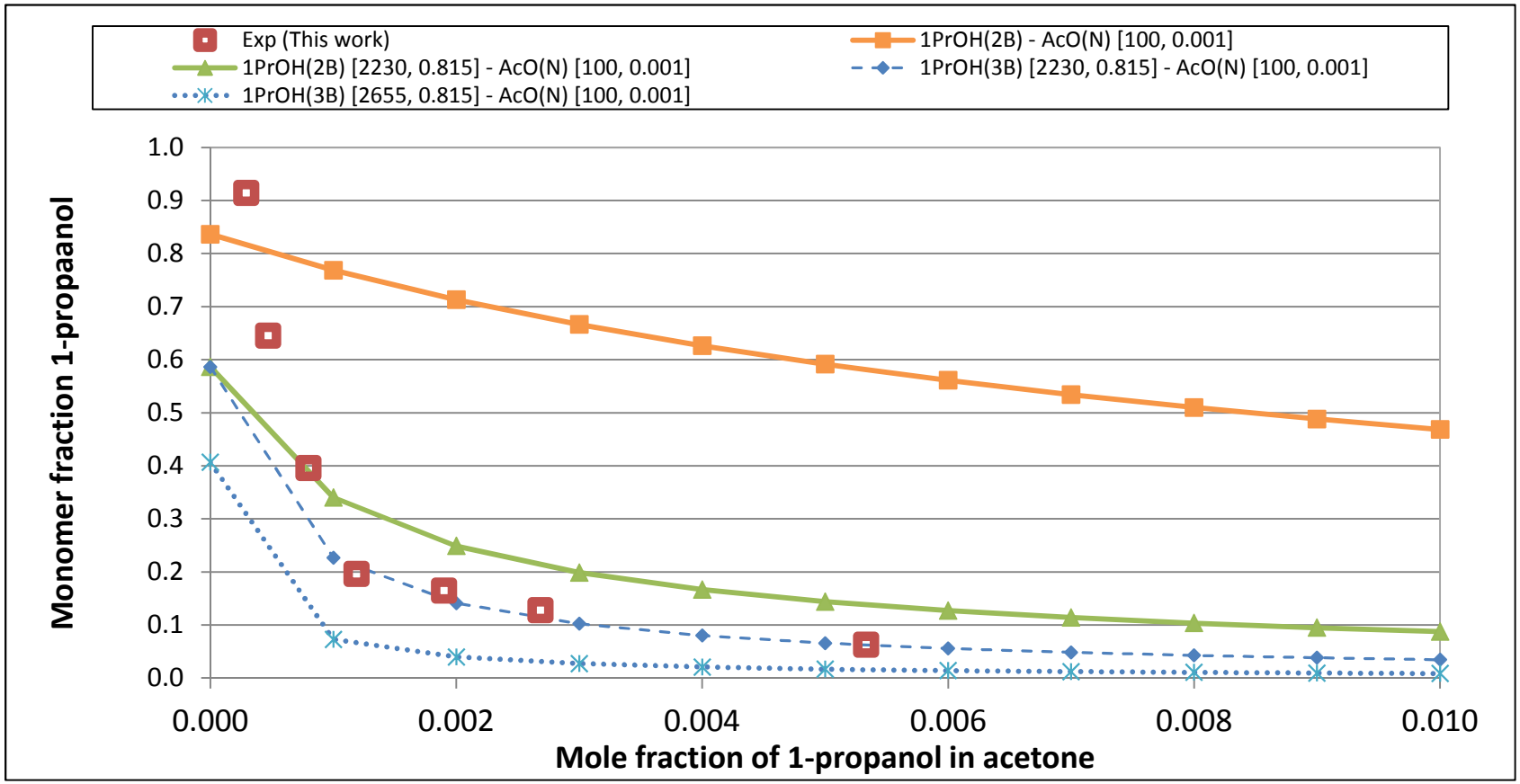

Figure 80: sPC-SAFT model predictions for the dilute 1-propanol - acetone system at 23.1 °C

Figure 80 shows the results for the dilute 1-propanol – acetone system. Here the 3B-N model is able to model the mid-range concentrations quite well by modifying the optimised volume of association parameter of Grenner *et al.* (2007) to 0.815. Acetone association parameters of 100 and 0.001 provide acceptable description of the data, with the %AAD calculated as 19.2% or 6.8% when the highly dilute region is excluded from the calculation. These parameters could be slightly improved, but since the effect of the acetone parameters was shown to have a relatively small effect, the parameters were kept as is. Modelling the very dilute mixture range once again poses a problem as the 3B-N model cannot describe the increase below 0.1 mol%. This once again is suggestive of either a mechanism change or an experimental discrepancy below this range. It should be noted however that the experimental spectra were not particularly noisy, even in the highly dilute range.

6.5.2 Dilute acetone

Figure 81 shows various sPC-SAFT model predictions for description of the monomer fraction data of a dilute acetone – 1-propanol mixture. For the very dilute range, below 0.3 mol% acetone, a 2B-2B scheme model is able to describe the data very well where a %AAD of 5.1%. In this case, the literature association energy for acetone is changed to 2532, while the 1-propanol parameters are set to 100 and 0.00025 for the energy and volume parameters respectively. This 2B-2B model however tends to under-predict the experimental data above 0.3 mol%. When using the entire experimental range, the %AAD increases to 16.6%. This model predicts a monomer fraction at infinite dilution of around 0.45 which interestingly is very similar to that predicted by Max & Chapados (2005) for acetone in methanol.

For more accurate modelling of concentrations above 0.3 mol% acetone, an improved fit is obtained for a 2B-3B model with the acetone association energy parameter decreased to 2319 and the 1-propanol volume parameter set to 0.001. In this narrowed range the %AAD is calculated as 6.5%, while the error increased to 10.5% when the entire experimental range is considered.

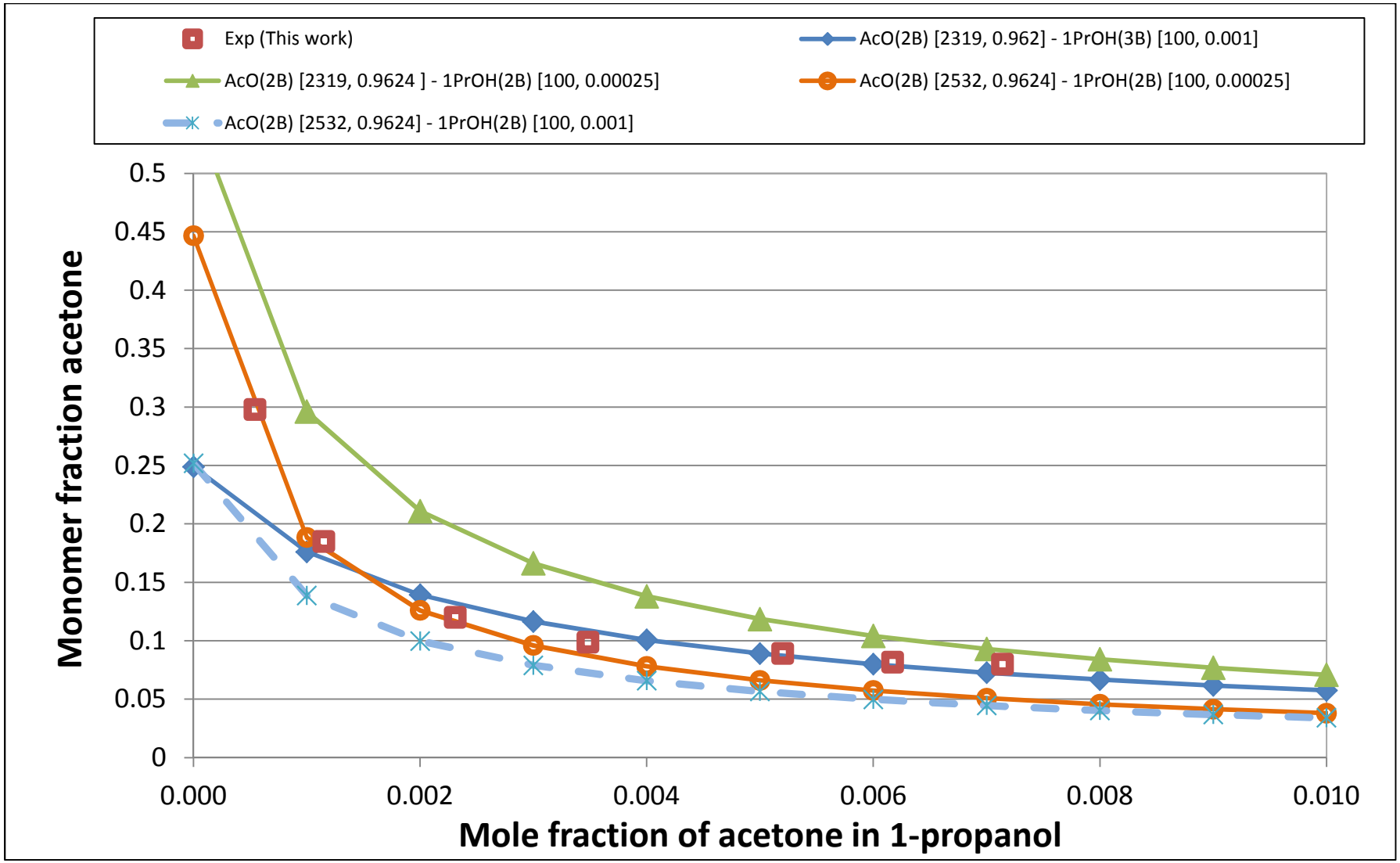

Figure 81: sPC-SAFT model predictions for dilute acetone – 1-propanol

6.6 2-Propanol – acetone mixtures

6.6.1 Dilute 2-propanol

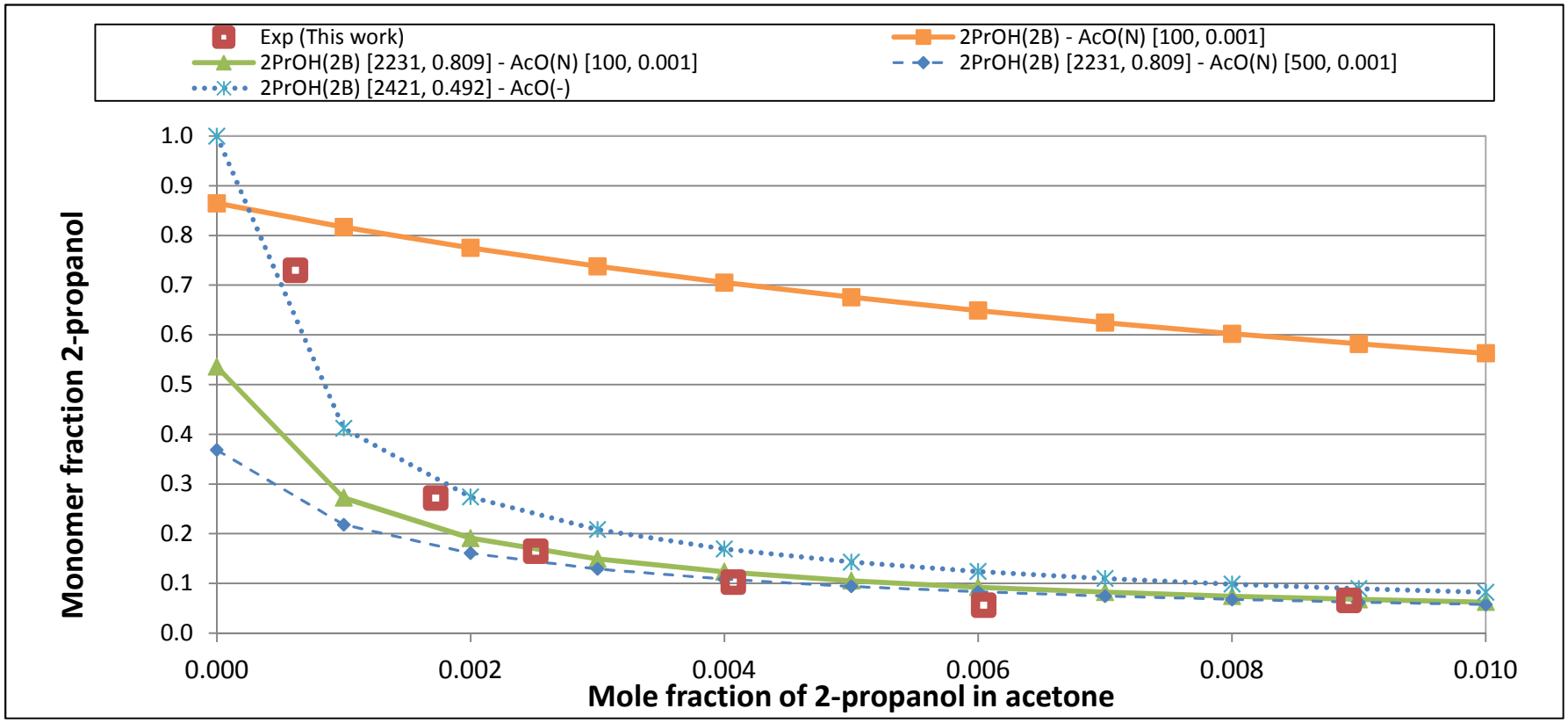

Figure 82: Model predictions for dilute 2-propanol - acetone mixtures

Figure 82 displays some interesting results for the modelling of a dilute 2-propanol – acetone mixture. Most interestingly, a modified version of Kouskoumvekaki *et al.* (2004) 2B model with non-associating acetone yields a good fit for the mixture in the dilute range, where 2421 and 0.492 are used for the association energy and volume parameters respectively. This method does however not describe the mid-concentration range very well, where the use of the N-scheme is necessary, as well as different association parameters for 2-propanol. When incorporating the N-scheme a %AAD value of 17.2% was calculated, although this value is somewhat skewed by the data point located at [0.00604, 0.056] and changes to 7.2% when that point is excluded.

An interesting interpretation of this result is that the association mechanisms change with concentration in cross-associating systems where there is a large discrepancy in the association strengths of the two components. In other words, in the high dilution range alcohol atoms do not interact extensively with acetone until a critical concentration is reached. This mechanism could be representative of the disruption of the polar interaction network between the acetone molecules. Judging from dilute alcohol-acetone figures shown in this work, the turning point is around 0.1 mol%.

6.6.2 Dilute acetone

Figure 83 shows several attempts to describe the experimental monomer fraction data of the dilute acetone – 2-propanol system. In all, a very poor description is obtained with the 2B-2B/3B models unable to describe the relatively flat trend of the data. From Figure 77 it follows that an N-2B model would be able to model a flat trend, but in this case the trend is flat but increasing, whereas the experimental data follow a negative gradient. This result, in terms of the overall lack model accuracy, is somewhat displeasing.

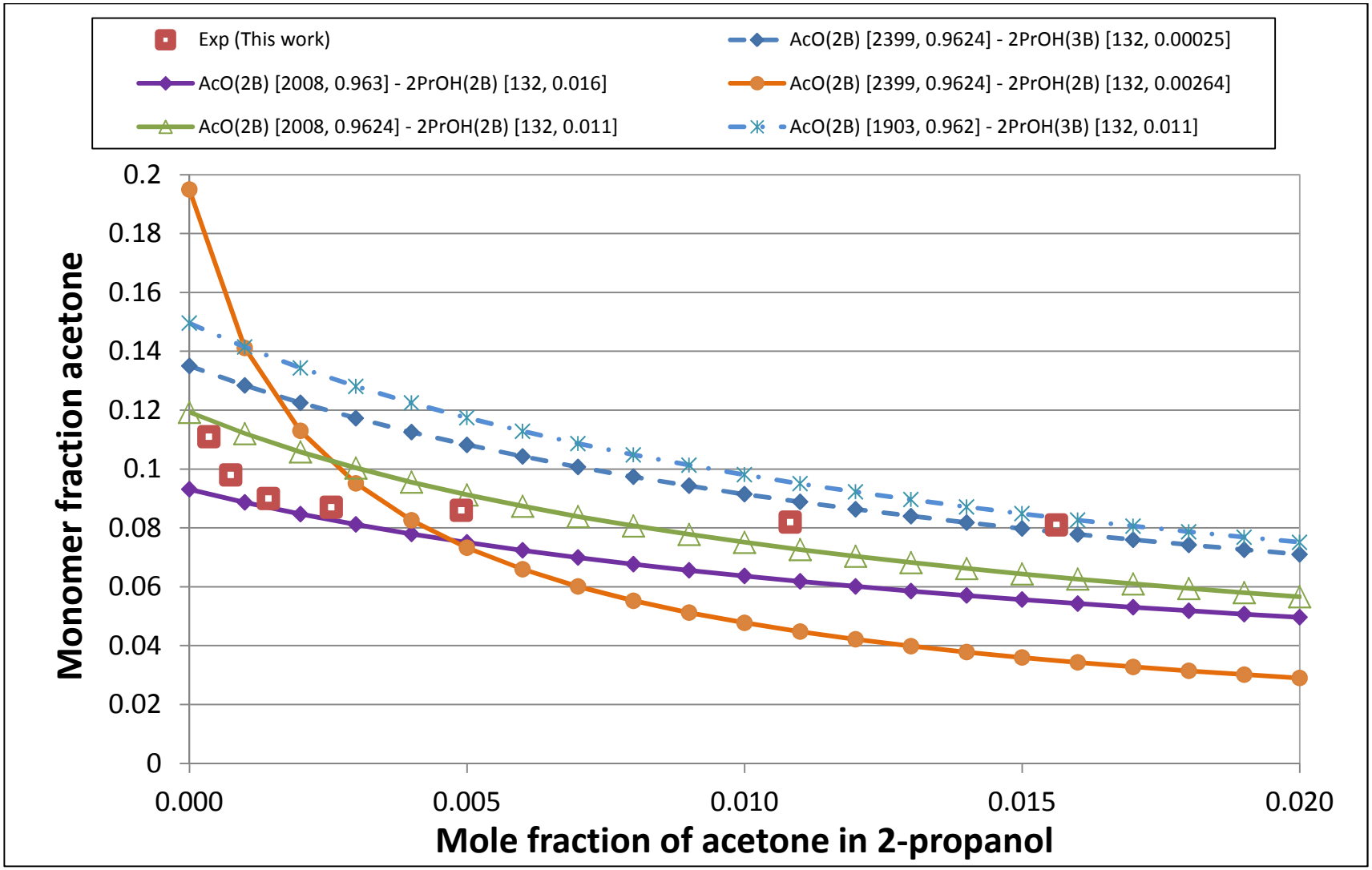

Figure 83: Modelling of dilute acetone - 2-propanol at 23 °C

6.7 Summary of thermodynamic modelling

Several evaluations were made of sPC-SAFT equation of state and its ability to describe monomer fraction data. The performance of the 2C association scheme (de Villiers et al., 2011b) was of specific interest during the investigation of alcohols, while two newly proposed (N and 2N) association schemes were considered for acetone. Pure monomer fraction data of methanol and ethanol were evaluated, the main focus was the description of dilute mixtures of alcohols with acetone.

For the modelling of pure methanol monomer fractions, it was found that the 3B scheme, using parameters of Kontogeorgis *et al.* (2010), provided superior modelling accuracy compared to the 2C scheme. However, for ethanol the 2C scheme was found to provide the best fit up to 410K.

When modelling binary systems it was typically found that all models struggled to describe the very dilute (below 0.1 mol%) range for alcohol-acetone system and it was necessary to modify the association parameters, which was shown to have a greater effect than association scheme, published in the literature in order to obtain satisfactory fits for the various systems. In general though, a good fit could be obtained for each of the systems except the dilute acetone – 2-propanol mixture. The best predications for were obtained using the following scheme and parameter sets:

- Dilute methanol in acetone: MeOH(3B) [2700, 0.823] – AcO(N) [100, 0.001];
  - %AAD: 8.1%
- Dilute ethanol in acetone: EtOH(2B) [2495, 0.825] – AcO(N) [50, 0.001]
  - %AAD: 10.6%
- Dilute 1-propanol in acetone: 1PrOH(3B) [2230, 0.815] – AcO(N) [100, 0.001]
  - %AAD: 6.8%
- Dilute 2-propanol in acetone: 2PrOH(2B) [2421, 0.492] – AcO(-)
  - %AAD: 7.2%
- Dilute acetone in methanol: AcO(2B) – MeOH(2C) [100, 0.00025]
  - %AAD: 5.4%
- Dilute acetone in ethanol: AcO(2B) [2200, 0.9624] – EtOH(-)
  - %AAD: 8.6%
- Dilute acetone in 1-propanol: AcO(2B) [2319, 0.962] – 1PrOH(3B) [100, 0.001]
  - %AAD: 6.5%

It was found that the newly proposed N scheme was effective when modelling acetone as the solvent, but in dilute acetone mixtures (i.e. when acetone was the solute) more accurate results were obtained using the 2B scheme to represent acetone.

Chapter 7: Conclusions

This chapter serves to highlight and contextualize the various conclusions derived earlier in this work.

7.1 Verification and experimental conclusions

ATR-FTIR was found to be unable to provide satisfactory experimental results within the constraints of the available setup and resources for this project. Thus a transmission-FTIR was used to measure monomer fractions in various dilute alcohol-acetone systems.

7.1.1 Verification

The transmission-FTIR setup was used to reproduce literature sources for the ethanol – *n*-hexane system. The data of von Solms *et al.* (2007) were recreated in Chapter 5, with replication of the work of Asprion *et al.* (2001) presented in the appendices. It was shown that the spectral processing and curve-fitting procedures were the most important factor influencing the calculated monomer fractions.

7.1.2 Sample analysis

Sample analyses have been completed and discussed for a dilute acetone-methanol and a dilute ethanol-acetone systems. These analyses are shown not only give insight into the spectral processing used for certain measurements and calculations, but also to substantiate why these methods were used.

For the acetone-methanol system, acetone monomer fractions were measured in the region near 1700 cm^{-1}. It is postulated that the difference in the observed literature values is due to spectral processing and analysis methods, rather the method of accounting for dihydrogen-bonded C=O peaks in acetone. Acetone monomer fractions were found to escalate rapidly for mole fractions below 0.0015 and this steep increase towards a monomer fraction of one was not observed previously.

For the ethanol-acetone system, ethanol monomers were observed near 3630 cm^{-1}, with several O-H and acetone overtone peaks in the region 3600 – 3300 cm^{-1}. The single calibration method was immediately eliminated due to the monomer peak not appearing in isolation. The multiple

calibration method predicted more realistic monomer fractions when a best-fit methodology was enforced, rather than fixed parameter methodology used by Asprion *et al.* (2001). The fraction of ethanol monomers present in the mixture was found to escalate rapidly for ethanol mole fractions less than 0.002. A similar phenomenon was observed for acetone. Notably, the ethanol monomer was effectively "absorbed" by the hydrogen-bonded peaks at concentrations as low as 0.75 mol%, which may explain why this peak has not been previously reported.

7.1.3 Dilute acetone mixtures

Four systems were examined, consisting of acetone in dilute mixtures with methanol, ethanol, 1- and 2-propanol. Acetone concentrations were in the range 0.01 – 1.6 mol%. Measurement of the acetone monomer fractions showed a steep increase for very dilute mixtures and it was observed that acetone monomer fractions were typically below 0.1 before an acetone concentration of 0.5 mol% was attained in the mixture, although in methanol the equivalent acetone monomer fraction was approximately 0.4. It was shown that acetone monomer fractions are higher for shorter alcohol chain-lengths when comparing mixtures at roughly equal concentrations. This correlates to higher monomer fraction observed for higher solvent hydrogen bond strength, which can be explained from fundamental principles.

For the acetone – 2-propanol system, a peak shoulder characteristic of acetone monomers was observed at 1718 cm^{-1}. This shoulder had not been noted in previous studies e.g. Nyquist (1990).

7.1.4 Dilute alcohol mixtures

For these measurements, dilute alcohol mixtures – in the range 0.01 – 0.9 mol% - were made with acetone as the solvent. As seen for the dilute acetone mixtures, solute monomer fractions trend towards one at infinite dilution. Alcohol monomer fractions were found to decrease below 0.3 for alcohol concentrations above 0.3 mol%.

Monomer fractions show an inverse correlation to hydrogen bond strength, with methanol having the lowest comparative monomer fractions, while 1- and 2-propanol exhibit the highest comparative monomer fractions. Some inconsistencies were observed within the data and were attributed mainly to curve-fitting difficulties. As solute concentration increases, the monomer fractions decrease exponentially and seemingly tend towards roughly the same values (especially the propanols and ethanol). This phenomenon can most likely be ascribed to the fact that there is an excess of hydrogen bond acceptors available in these mixtures.

7.2 Thermodynamic modelling

7.2.1 Pure component modelling

The 2C scheme, with parameters given by de Villiers *et al.* (2011b), was found to be inferior for modelling pure methanol experimental monomer fractions, when compared to the optimised 3B parameters of Grenner *et al.* (2007) where monomer fraction data were not included in the regression. For ethanol however, the 2C scheme provided a very accurate prediction of the monomer fraction data in the range 250 – 410 K and performs significantly better than any 2B scheme parameters. This evidence supports literature conjecture regarding the unlikely similarity between the methanol and ethanol monomer fraction data sets.

7.2.2 Alcohol-acetone modelling

In the initial study of alcohol association schemes, it was shown that the choice of parameters has predominant effect in shifting the monomer fraction predictions as compared to association scheme. It was found that the sPC-SAFT (2C) volume of association parameter was incorrectly reported as 0.823 in the journal article of de Villiers *et al.* (2011b) and should read 0.0823.

The use of existing association schemes for alcohol (2B/3B/2C) with published parameters tends to over-predict the experimental data. When using the 2B parameters of von Solms *et al.* (2004), the predicted alcohol monomer plot was very flat in comparison to the experimental. Not only was the gradient under-predicted, but also the actual experimental values.

The acetone(N) scheme is proposed, whereby a single negative association site is assigned to acetone. This scheme was initially implemented with the same parameters as the acetone(2B) scheme and was found to under predict the experimental data, while exhibiting the shape or trend of observed in the experimental data.

Simultaneous weakening the acetone association strength and range (using strength parameters in the order of 10^{2} and volume parameters in the order of 10^{-3}), and increasing the range of alcohol interactions allows for the simulation of the very acute decrease in alcohol monomer fractions observed in the experimental data. Deviations were however observed at the lowest end of the concentration spectrum. Using the methodology described here, it was found that the 3B-N model (with adjusted association parameters) is able to describe the behaviour of the experimental data of methanol monomer fractions (found in solution with acetone) very accurately.

For the dilute ethanol-acetone system, the best fit was obtained using a modified 2B-N model while interestingly the 3B-N model again presented the best results for 1- and 2-propanol. The generally very weak acetone parameters used, suggests that acetone does not play as strong a role in the association. For dilute alcohol-acetone systems the %AAD for the most accurate model predictions were in the range of 6-11% when the highly dilute region was not considered.

For the modelling of dilute acetone-alcohol systems, the use of adjusted association parameter 2B-2C/3B/2B models yields relatively accurate results, with %AAD in the range of 5-9% when the highly dilute range is excluded. Deviations in the very low concentration region were reported, where the model could not describe the gradient change of the experimental data. In this case however, the alcohol association had to be weakened significantly (with $\varepsilon^{AB} \approx 10^{2}$ and $\kappa \approx 10^{-3}$) while the acetone association parameters were increased to around 2500 and 1 respectively.

When using only negative sites (N and 2N schemes) to describe the association of acetone as a dilute solute in a mixture, the model could not describe even the trend of the experimental data. The N and 2N schemes were only successful when modelling acetone as the solvent in the mixture.

The fact that the model parameters differ so greatly when comparing the dilute alcohol-acetone models to the equivalent dilute acetone-alcohol model, suggests that a type of self-association dominates the interactions while cross-association interactions being less active. This phenomenon can be somewhat related to the concepts of hydrophobic effect and the co-operativity, and would be an interesting research topic in isolation.

Difficulty in modelling monomer fractions below 0.1 mol% was almost universally seen throughout this work, which highlights the difficulties in obtaining accurate data below this threshold. While this short-coming may relate to the experimental component of the work, it could potentially also be explained by a mechanism change in terms of the manner in which these very complex systems interact with one another.

Chapter 8: Recommendations

After the completion of the experimental work featured in this thesis, a new Nicolet spectrometer was purchased by the Department of Process Engineering. This spectrometer is now housed in a temperature-controlled laboratory and, judging from the results obtained for different FTIR study (carried out at both venues), is delivering superior results compared to the spectrometer at the Department of Geology. It is thus a recommendation of this study that the experimental work be expanded using this new resource. There is scope for expansion in terms of concentration and especially temperature, which was adjustable in ATR-mode but not in transmission mode.

Transmission FTIR should still be used in order to view super dilute concentrations, but a new transmission cell must be designed. This cell should incorporate, but not be limited to, the following:

- A sample chamber with an **adjustable pathlength**
- Design allowing for interchangeable spectral windows
- A heating jacket with integrated **temperature control** and probes
- A pressure sensor
- A stirring mechanism
- Injection ports
- A volume of at least 100 mL

With adjustable cell pathlengths, every data point could be adjusted such that peak height is high enough to model accurately while being kept small enough such that Beer's Law is observed. CaF_2 windows are very flexible in terms of their use and robustness, but one may wish to change spectral windows in certain cases. With the design of the transmission cell, the spectral window sealing gasket must be carefully considered. The strength of the spectral windows may limit experimental ranges in terms of the pressures that can be handled.

Depending on the wall thickness of the designed cell, it could be necessary to incorporate two temperature probes in the design. A relatively thick cell wall, with a temperature probe measuring only the sample temperature, creates difficulties for the temperature control unit (TCU) to gradually increase the temperature. The cell wall heats slowly initially, but as soon as it reaches higher temperatures the sample temperature spikes suddenly due to the vastly different heat capacities of the metal and liquid sample. A sample temperature overshoot occurs. This problem was solved by retracting the probe towards the edge of the sample vessel and severely limiting the maximum

power output of the heating jacket, but this meant having to constantly adjust the value depending on how high the desired temperature was. A more elegant solution would be to use two temperature probes, one penetrating ¾ the way through the cell wall to measure and control wall temperature. A second probe should then be placed near the sample point to measure the sample temperature. If possible, the design should allow for temperatures up 300 °C for comparison with pure alcohol sources in the literature.

By increasing the volume, as compared to the current setup, one would decrease the relative magnitude of the concentration error and thereby generate more accurate data. This may however be undesirable for systems which contain very expensive components, but here one could consider a design incorporating a piston mechanism to change the volume. As with any vessel design, the vessel cleaning process should also be considered. A simple design with fewer sharp edges would necessarily facilitate easy cleaning.

The IR pathway must be unobstructed by any of the fixtures and should ideally be completely isolated from the surroundings using commercially available parts. There should preferably be a physical mechanism for measuring the pathlength, for which the value can be compared to that determined from the spectral interference method. It could be feasible to construct a frame over the current baseplate to house a sample vessel with the necessary fixtures above the transmission cell with small pump to circulate fluid through. While a framework setup may work satisfactorily it is felt that a single well-engineered, temperature-controlled, variable pathlength transmission cell – while not being trivial to design – would add immense scope to any future work. While such cells are commercially available, they are very expensive may not be tailored to the specific requirement of a given experiment.

With an experimental apparatus set up as described above, one would be able to produce a full set of experimental data which could be used to iron out some of the issues described in at the end of the previous chapter. The polar models were not evaluated during the fitting of the experimental data, since they are almost identical when modelling monomer fractions. The polar component will only affect the molar volume calculation. But it is recommended that the polar models be used when evaluating the performance of the newly proposed association parameters in predicting other properties such as VLE, since a type of co-operativity/hinderance separation can be achieved.

Chapter 9: References

Adachi, D., Katsumoto, Y., Sato, H. & Ozaki, Y., (2002) **Near-Infrared Spectroscopic Study of Interaction Between Methyl Group and Water in Water-Methanol Mixtures**. *Appl. Spectrosc.*, 56(3), pp.357-61.

Al-Saifi, N.M., Hamad, E.Z. & Englezos, P., (2008) **Prediction of vapor–liquid equilibrium in water–alcohol–hydrocarbon systems with the dipolar perturbed-chain SAFT equation of state**. *Fluid Phase Equilibr.*, 2008, pp.82-93.

Armstrong, B.H., (1967) **Spectrum line profiles: The Voigt function**. *J. Quant. Spectrosc. Radiat. Transfer*, 7, pp.61-88.

Asprion, N., Hasse, H. & Maurer, G., (2001) **FT-IR spectroscopic investigations of hydrogen bonding in alcohol-hydrocarbon solutions**. *Fluid Phase Equilibr.*, 186, pp.1-25.

Barker, J.A. & Henderson, D., (1967) **Perturbation Theory and Equation of State for Fluids: The Square-Well Potential**. *J. Chem. Phys.*, 47, pp.2856-61.

Berthelot, D., (1898) **Sur le melange des gaz**. *Comptes rendus hebdomadaires des séances de l'Académie des sciences*, 126, pp.1703-855.

Bonner, O.D., (1972) **The Correspondence of Fundamental and Combination Bands in the Infrared Spectra of Liquid H2O and D2O**. *Infrared Phys.*, 12(2), pp.109-44.

Boublik, T., (1970) **Hard-sphere equation of state**. *J. Chem. Phys.*, 53, pp.471-72.

Carnahan, N.F. & Starling, K.E., (1969) **Equation of State for Nonattracting Rigid Spheres**. *J. Chem. Phys.*, 51(2), pp.635-36.

Chang, H.-C., Jiang, J.-C., Lin, S.H., Wang, N.-H. & Chao, M.-C., (2001) **Evidence for C-H-O interaction of acetone and deuterium oxide probed by high-pressure**. *J. Chem. Phys.*, 115(7), pp.3215-19.

Chaplin, M., (2007) *Water's Hydrogen Bond Strength*. [Online] Available at: http://arxiv.org/pdf/0706.1355 [Accessed June 2010].

Chapman, W.G., Gubbins, K.E., Jackson, G. & Radosz, M., (1989) **SAFT: Equation-of-State Solution Model for Associating Fluids**. *Fluid Phase Equilibr.*, 52, pp.31-38.

Chapman, W.G., Gubbins, K.E., Jackson, G. & Radosz, M., (1990) **New Reference Equation of State for Associating Liquids**. *Ind. Eng. Chem. Res.*, 29(8), pp.1709-21.

Chapman, W.G., Jackson, G. & Gubbins, K.E., (1988) **Phase equilibria of associating fluids. Chain molecules with multiple bonding sites**. *Mol. Phys.*, 65(5), pp.1057-79.

Chapra, S.C., (2008) **Applied Numerical Methods with Matlab for Engineers and Scientists**. 2nd ed. McGraw-Hill.

Chen, S.S. & Kreglewski, A., (1977) **Applications of the augmented van der Waals theory of fluids. I. Pure fluids**. *A. Ber. Bunsen-Ges. Phys. Chem.*, 81, p.1049–1052.

Clark, G.N.I., Haslam, A.J., Galindo, A. & Jackson, G., (2006) **Developing optimal Wetheim-like models of water for use in the Statistical Associating Fluid Theory (SAFT) and related approaches**. *Mol. Phys.*, 104, pp.3561-81.

Coates, J., (2000) **Interpretation of Infrared Spectra, A Practical Approach**. In R.A. Meyers, ed. *Encyclopedia of Analytical Chemistry*. John Wiley & Sons Ltd. pp.10815-37.

Coates, J., (2001) **Classical methods of quantitative spectroscopy**. In J. Chalmers & P.R. Griffiths, eds. *Handbook of Vibrational Spectroscopy: Volume 2*.

Czarnecki, M.A., Maeda, H., Ozaki, Y., Suzuki, M. & Iwahashi, M., (1998) **Resolution Enchancement and Band Assignments for the First Overtone of OH Stretching Mode of Butanols by Two-Dimensional Near-Infrared Correlation Spectroscopy. Part I: sec-Butanol**. *Appl. Spectrosc.*, 52(7), pp.994-1000.

Czarnecki, M.A. & Wojtkow, D., (2004) **Two-Dimensional FT-NIR Correlation Study of Hydrogen Bonding in the Butan-1-ol/Water System**. *J. Phys. Chem. A*, 108(13), pp.2411-17.

Czeslik, C. & Jonas, J., (1999) **Pressure and temperature dependence of hydrogen-bond strength in methanol clusters**. *Chem. Phys. Lett.*, 302, pp.633-38.

de Villiers, A.J., (2011) **Evalution and improvement of the sPC-SAFT equation of state for complex mixtures**. PhD Thesis. Stellenbosch University.

de Villiers, A.J., Schwarz, C.E. & Burger, A.J., (2011a) **Improving vapour–liquid-equilibria predictions for mixtures with non-associating polar components using sPC-SAFT extended with two dipolar terms**. *Fluid Phase Equilibr.*, 305, pp.174-84.

de Villiers, A.J., Schwarz, C.E. & Burger, A.J., (2011b) **New Association Scheme for 1-Alcohols in Alcohol/Water Mixtures New Association Scheme for 1-Alcohols in Alcohol/Water Mixtures**. *Ind. Eng. Chem. Res.*, 50, pp.8711-25.

Dellepiane, G. & Overend, J., (1966) **Vibrational spectra and assignment of acetone, acetone-d3 and acetone-d6**. *Spectrochim. Acta*, 22, pp.593-614.

Desseyn, H.O. *et al.*, (2001) **The effect of pressure and temperature on the vibrational spectra of different hydrogen bonded systems**. *Spectrochim. Acta A*, 57, pp.231-46.

Di Rocco, H.O., Iriarte, D.I. & Pomarico, J., (2001) **General expression for the Voigt function that is of special interest for applied spectroscopy**. *Appl. Spectrosc.*, 55, pp.822-26.

Diamantonis, N.I. & Economou, I.G., (2011) **Evaluation of Statistical Associating Fluid Theory (SAFT) and Perturbed Chain-SAFT Equations of State for the Calculation of Thermodynamic Derivative Properties of Fluids Related to Carbon Capture and Sequestration**. *Energ. Fuel.*, 25, p.3334–3343.

Dixit, S., Crain, J., Poon, W.C.K., Finney, J.L. & Soper, A.K., (2002) **Molecular segregation observed in a concentrated alcohol–water solution**. *Nature*, 416, pp.829-32.

Dodd, J.G. & DeNoyer, L.K., (2002) **Curve-fitting: Modelling Spectra**. In J. Chalmers & P. Griffiths, eds. *Handbook of Vibrational Spectroscopy: Volume 2*. New York: John Wiley & Sons Ltd. pp.2215-23.

Dry, M.E., (2002) **The Fischer-Tropsch process: 1950-2000**. *Catal. Today*, 71, p.227241.

Economou, I.G., (2002) **Statistical Associating Fluid Theory: A Succesful Model for the Calculation of Thermodynamic and Phase Equilibrium Properties of Complex Fluid Mixtures**. *Ind. Eng. Chem. Res.*, 41(5), pp.953-62.

Economou, I.G., Cui, Y. & Donohue, M.D., (1991) **Hydrogen Bonding in Polymer-Solvent Mixtures**. *Macromolecules*, 24, pp.5058-67.

Fabian, H. & Vogel, H.J., (2002) **Fourier Transform Infrared Spectroscopy of Calcium-Binding Proteins**. In H.J. Vogel, ed. *Methods in Molecular Biology Volume 173: Calcium-Binding Protein Protocols*. 2nd ed. Totowa, NJ: Humana Press. pp.57-74.

Falk, M. & Ford, T.A., (1966) **Infrared Spectrum and Structure of Liquid Water**. *Can. J. of Chem.*, 44, pp.1699-707.

Folas, G.K., Kontogeorgis, G.M., Michelsen, M.L. & Stenby, E.H., (2006) **Application of the Cubic-Plus-Association (CPA) Equation of State to Complex Mixtures with Aromatic Hydrocarbons**. *Ind. Eng. Chem. Res.*, 45, pp.1527-38.

Fujita, Y. & Ikawa, S.-i., (1989) **Effect of temperature on the hydrogen bond distribution in water as studied by infrared spectra**. *Chem. Phys. Lett.*, 159(2-3), pp.184-88.

Gilli, G. & Gilli, P., (2009) **The nature of the hydrogen bond: Outline of a comprehensive Hydrogen Bond Theory**. Oxford University Press.

Glew, D.N. & Rath, N.S., (1971) **H2O, HDO, and CH3OH Infrared Spectra and Correlation with Solvent Basicity and Hydrogen Bonding**. *Can. J. Chem*, 49, pp.837-56.

Grenner, A., Kontageorgis, G.M., von Solms, N. & Michelsen, M.L., (2007) **Modeling phase equilibria of alkanols with the simplified PC-SAFT equation of state and generalized pure compound parameters**. *Fluid Phase Equilibr.*, 258, pp.83-94.

Grenner, A., Tsivintzelis, I., Economou, I.G., Panayiotou, C. & Kontageorgis, G.M., (2008) **Evaluation of the Nonrandom Hydrogen Bonding (NRHB) Theory and the Simplified Perturbed-Chain-Statistical Associating Fluid Theory (sPC-SAFT). 1. Vapor-Liquid Equilibria**. *Ind. Eng. Chem. Res.*, 47, pp.5636-50.

Griffiths, P.R., (2002) **Beer's Law**. In J. Chalmers & P. Griffiths, eds. *Handbook of Vibrational Spectroscopy: Volume 2*. John Wiley & Sons Ltd. pp.2225-PUT IN.

Griffiths, P.R., (2005) **Infrared Spectroscopy - Overview**. pp.385-402.

Griffiths, P.R. & de Haseth, J.A., (2007) **Fourier Transform Infrared Spectrometry**. 2nd ed. Hoboken, NJ: John Wiley & Sons, Inc.

Gross, J. & Sadowski, G., (2000) **Application of perturbation theory to a hard-chain reference fluid: an equation of state for square-well chains**. *Fluid Phase Equilibr.*, 168, pp.183-99.

Gross, J. & Sadowski, G., (2001) **Perturbed-Chain SAFT: An Equation of State Based on a Perturbation Theory for Chain Molecules**. *Ind. Eng. Chem. Res.*, 40(4), pp.1244-60.

Gross, J. & Sadowski, G., (2002) **Application of the Perturbed-Chain SAFT Equation of State to Associating Systems**. *Ind. Eng. Chem. Res.*, 41(22), pp.5510-15.

Gross, J. & Vrabec, J., (2006) **An Equation-of-State Contribution for Polar Components: Dipolar Molecules**. *AIChE*, 52, pp.1194-204.

Guan, J., Hu, Y., Xie, M. & Bernstein, E.R., (2012) **Weak carbonyl-methyl intermolecular interactions in acetone clusters explored by IR plus VUV spectroscopy**. *Chem. Phys.*, 405, pp.117-23.

Gubbins, K.E. & Twu, C.H., (1978) **Thermodynamics of polyatomic fluid mixtures I.** *Chem. Eng. Sci.*, 33, pp.863-78.

Gulati, H.S. & Hall, C.K., (1997) **Fluids and fluid mixtures containing square-well diatomics: Equations of state and canonical molecular dynamics simulations**. *J. Chem. Phys.*, 107, pp.3930-46.

Guo, J.-H., Luo, Y., Augustsson, A., Kashtanov, S., Rubensson, J.-E., Shuh, D.K., Agrem, H. & Nordgren, J., (2003) **Molecular Structure of Alcohol-Water Mixtures**. *Phys. Rev. Lett.*, 91(15), pp.157401- 1-4.

Gupta, R.B. & Brinkley, R.L., (1998) **Hydrogen-bond coopertivity in 1-Alkanol+n-Alkane binary mixtures**. *AIChE*, 44(1), pp.207-13.

Hall, C.C., (1949) **Recent Research on the Fischer-Tropsch Synthesis**. In *The Industrial Chemist*. A Paper Presented to the 21st Congress of Industrial Chemistry, Brussels, Septemeber 1948.

Hsu, C.-P.S., (1997) **Infrared Spectroscopy**. In *Handbook of Instrumental Techniques for Analytical Chemistry*. Prentice Hall. Ch. 15.

Huang, S.H. & Radosz, M., (1990) **Equation of State for Small, Large, Polydisperse, and Associating Molecules**. *Ind. Eng. Chem. Res.*, 29(11), pp.2284-94.

Huang, S.H. & Radosz, M., (1991) **Equation of State for Small, Large, Polydisperse, and Associating Molecules: Extension to Fluid Mixtures**. *Ind. Eng. Chem. Res.*, 30(8), pp.1994-2005.

Ismail, A.A., van de Voort, F.R. & Sedman, J., (1997) **Fourier Transform Infrared Spectroscopy: Principles and Applications**. In Parè, J.R.J. & Bèlanger, J.M.R. *Instrumental Methods in Food Analysis*. Elsevier Science. Ch. 4.

Jensen, L. & Kofod, J.L., (2005) **Investigation of CPA and PC-SAFT EoS against IR-Spectroscopic data for Associating Compounds**. MSc Thesis. DTU.

Jog, P.K. & Chapman, W.G., (1999) **Application of Wertheim's thermodynamic perturbation theory to dipolar hard sphere chains**. *Mol. Phys.*, 97, pp.307-19.

Jog, P.K., Garcia-Cuellar, A. & Chapman, W.G., (1999b) **Extensions and applications of the SAFT equation of state to solvents, monomers, and polymers**. *Fluid Phase Equilibr.*, 158-160, pp.321-26.

Jog, P.K., Sauer, S.G., Blaesing, J. & Chapman, W.G., (2001) **Application of Dipolar Chain Theory to the Phase Behavior of Polar Fluids and Mixtures**. *Ind. Eng. Chem. Res.*, 40, pp.4641-48.

Kellner, R., Mermet, J.-M., Otto, M., Valcarcel, M. & Widmer, H.M., (2004) **Analytical Chemistry: A Modern Approach to Analytical Science**. 2nd ed. Wiley-VCH.

Kellner, R., Mermet, J.-M., Otto, M. & Widmer, H.M., (1998) **Analytical chemistry : the approved text to the FECS curriculum analytical chemistry**. Wiley-VCH.

Keutsch, F.M. & Saykally, R.J., (2001) **Water Clusters: Untangling the Mysteries of the Liquid, One Molecule at a Time**. In *Proceedings of the National Academy of Sciences of the United States of America*. National Academy of Sciences.

Kollman, P.A. & Allen, L.C., (1972) **The Theory of the Hydrogen Bond**. *Chem. Rev.*, 72(3), pp.283-303.

Kontogeorgis, G.M. & Folas, G.K., (2010) **Thermodynamic models for industrial applications: From classical and advanced mixing rules to association theories**. 1st ed. John Wiley & Sons.

Kontogeorgis, G.M., Tsivintzelis, I., von Solms, N., Grenner, A., Bogh, D., Frost, M., Kange-Rasmussen, A. & Economou, I.G., (2010) **Use of monomer fraction data in the parameterization of association theories**. *Fluid Phase Equilibr.*, 296, pp.219-29.

Kouskoumvekaki, I.A., von Solms, N., Michelsen, M.L. & Kontogeorgis, G.M., (2004) **Application of the perturbed chain SAFT equation of state to complex polymer systems using simplified mixing rules**. *Fluid Phase Equilibr.*, 215, pp.71-78.

Kraska, T., (1998) **Analytic and Fast Numerical Solutions and Approximations for Cross-Association Models within Statisical Association Fluid Theory**. *Ind. Eng. Chem. Res.* , 37, pp.4889-92.

Libnau, F.O., Kvalheim, O.M., Christy, A.A. & Toft, J., (1994) **Spectra of water in the near- and mid-infrared region**. *Vib. Spectrosc.*, 7, pp.243-54.

Lien, T., (1972) **A study of thermodynamic excess function of alcohol solutions by IR spectroscopy: application to chemical solution theory**. Thesis. [Toronto] (c) 1972.

Li, X.-S. & Englezos, P., (2004) **Vapor-liquid equilibrium of systems containing alcohols, water, carbon dioxide and hydrocarbons using SAFT**. *Fluid Phase Equilibr.*, 224, pp.111-18.

Lorentz, H.A., (1881) **Ueber die Anwendung des Satzes vom Virial in der kinetischen Theorie der Gase**. *Ann. Phys.*, 248(1), pp.127-36.

Luck, W.A.P., (1980) **A Model of Hydrogen-Bonded Liquids**. *Angew. Chem. Int. Ed. Engl.*, 19, pp.28-41.

Luck, W.A.P., (1986) **Caloric Properties of Liquid Alcohols - H-bonded liquids continuum or spectroscopic determined mixture model, is that really the question?** *J. Mol. Liq.*, 32, pp.41-51.

Luck, W.A.P., (1998) **The importance of coopertivity for the properties of liquid water**. *J. Mol. Struct.*, 448, pp.131-42.

Madsen, K., Nielsen, H.B. & Tingleff, O., (2004) *Methods for Non-Linear Least Squares Problems (2nd ed.)*. [Online] Informatics and Mathematical Modelling, Technical University of Denmark, DTU

Available at: http://www2.imm.dtu.dk/pubdb/views/publication_details.php?id=3215 [Accessed May 2011].

Mansoori, G.A., Carnahan, N.F., Starling, K.E. & Leland, T.W., (1971) **Equilibrium Thermodynamic Properties of the Mixture of Hard Spheres**. *J. Chem. Phys.*, 54(4), pp.1523-25.

Martinez, S., (1986) **Methanol/n-hexane systems - I. Infrared studies**. *Spectrochim. Acta A*, 42, pp.531-36.

Masters, C., (1979) **The Fischer-Tropsch Reaction**. In *Advances in Organometallic Chemistry*. Academic Press Inc. pp.61-100.

Matzopoulos, M., 2010. Model behaviour. *The Chemical Engineer*, February. pp.43-45.

Max, J.-J. & Chapados, C., (2005) **Infrared spectroscopy of acetone-methanol liquid mixtures: Hydrogen bond network**. *J. Chem. Phys.*, 122, pp.014504-1-18.

Max, J.-J. & Chapados, C., (2007) **Infrared spectroscopy of acetone-hexane liquid mixtures**. *J. Chem. Phys.*, 126, pp.154511-1-9.

Max, J.-J. & Chapados, C., (2008) **Infrared spectroscopy of methanol-hexane liquid mixtures. I. Free OH present in minute quantities**. *J. Chem. Phys.*, 128, p.224512.

McNaught, A.D. & Wilkinson, A., (1997) **Gold Book: IUPAC. Compendium of Chemical Terminology**. 2nd ed. Blackwell Scientific Publications.

Moorthi, K. & Nagata, I., (1991) **Properties of polar gases and their association in the liquid phase**. *Fluid Phase Equilibr.*, 63, pp.183-210.

Muller, E.A. & Gubbins, K.E., (2001) **Molecular-Based Equations of State for Associating Fluids: A Review of SAFT and Related Approaches**. *Ind. Eng. Chem. Res.*, 40, pp.2193-211.

Nakamoto, K., (2008a) **Infrared and Raman spectra of inorganic and coordination compounds. Part A. Theory and applications in inorganic chemistry**. 6th ed. Wiley-Blackwell.

Nakamoto, K., (2008b) **Infrared and Raman spectra of inorganic and coordination compounds. Part B. Applications in coordination, organometallic, and bioinorganic chemistry**. 6th ed. Wiley-Interscience.

Nyquist, R.A., (1990) **Infrared studies of ketones: Parameters affecting the induced carbonyl stretching vibration by solute/sovent interaction**. *Appl. Spectrosc.*, 44, pp.433-38.

Okada, T., Komatsu, K., Kawamoto, T., Yamanaka, T. & Kagi, H. (2005) **Pressure responce of Raman spectra of water and its implication to the change in hydrogen bond interaction**. *Spectrochim. Acta A*, 61, pp.2423-27.

Oliver, C., (2011) **Personal correspondence via e-mail**.

Pavia, D.L., Lampman, G.M. & Kriz, G.S., (1996) **Introduction to spectroscopy: a guide for students of organic chemistry**. 2nd ed. Harcourt Brace College.

Peery, T.B., (2003) **A Theoretical Description of Anisotropic Chemical Association and its Application to Hydrogen-bonded Fluids.** Doctaral dissertation. Oregon State University.

Peinado, A.C., van den Berg, F., Blanco, M. & Bro, R., (2006) **Temperature-induced variation for NIR tensor-based calibration**. *Chemometr. Intell. Lab.*, 83, pp.75-82.

Prausnitz, J.M., Litchtenthaler, R.N. & de Azevedo, E.G., (1999) **Molecular Thermodynamics of Fluid-Phase Equilibria**. 3rd ed. Prentice-Hall.

Press, W.H., Teulosky, S., Flannery, B.P. & Vetterling, W.T., (1988) **Numerical Recipes in C**. Cambridge University Press.

Rao, C.N.R., (1963) **Chemical Applications of Infrared Spectroscopy**. Academic Press.

Ree, F.H. & Hoover, W.G., (1964) **Fifth and Sixth Virial Coefficients for Hard Spheres and Hard Disks**. *J.Chem. Phys.*, 40(4), pp.939-50.

Richardson, R.L., Yang, H. & Griffiths, P.R., (1998) **Evaluation of a Correction for Photometric Errors in FT-IR Spectrometry Introduced by a Nonlinear Detector Response**. *Appl. Spectrosc.*, 52, pp.565-71.

Rospenk, M. & Zeegers-Huyskens, T., (1997) **FT-IR (7500-1800 cm-1) Study of Hydrogen-Bond Complexes between Phenols-OH(OD) and Pyridine. Evidence of Proton Transfer in the Second Vibrational Excited State**. *J. Phys. Chem. A*, 101, pp.8428-34.

Rull, F., (2002) **Structural investigation of water and aqueous solutions by Raman spectroscopy**. *Pure Appl. Chem.*, 74(10), pp.1859-70.

Rushbrooke, G.S., Stell, G. & Hoye, J.S., (1973) **Theory of polar liquids. I. Dipolar hard spheres**. *Mol. Phys.*, 26, pp.1199-215.

Sauer, S.G. & Chapman, W.G., (2003) **A Parametric Study of Dipolar Chain Theory with Applications to Ketone Mixtures**. *Ind. Eng. Chem. Res.*, 42, pp.5687-96.

Shao, L. & Griffiths, P.R., (2008) **Correcting Nonlinear Responce of Mercury Cadmium Telluride Dectectors in Open Path Fourier Transform Infrared Spectrometry**. *Anal. Chem.*, 80, pp.5219-24.

Silberberg, M.S., (2003) **Chemistry: The Molecular Nature of Matter and Change**. 3rd ed. McGraw-Hill.

Smith, B.C., (1998) **Infrared Spectral Interpretation: A systematic approach**. 1st ed. CRC Press.

Smith, B.C., (2011) **Fundamentals of Fourier Transform Infrared Spectroscopy**. 2nd ed. Boca Ranton, FL: CRC Press.

Soria, T.M., Sanchez, F.A., Pereda, S. & Bottini, S.B., (2010) **Modeling alcohol+water+hydrocarbon mixtures with the group contribution with the association equation of state GCA-EOS**. *Fluid Phase Equilibr.*. In press, corrected proof.

Specac, (2011) *Omni Cell System Datasheet*. [Online] Specac Inc. Available at: www.specac.com/userfiles/file/N35OmniCellSystem.pdf [Accessed November 2011].

Stuart, B., (2004) **Infrared spectroscopy: Fundamentals and applications**. John Wiley & Sons Ltd.

Symons, M.C.R. & Eaton, G., (1985) **Solvation of Acetone in Protic and Aprotic Solvents and Binary Solvent Mixtures**. *J. Chem. SOC., Faraday Trans. I* , 81, pp.1963-77.

Tamenori, Y., Takahashi, O., Yamashita, Y., Yamaguchi, T., Okada, K., Tabayashi, K., Gejo, T. & Honma, K., (2009) **Hydrogen bonding in acetone clusters probed by near-edge x-ray absorption fine structure spectroscopy in the carbon and oxygen K-edge regions**. *J. Chem. Phys.*, 131, pp.174311-1-9.

Tan, S.P., Adidharma, H. & Radosz, M., (2008) **Recent Advances and Applications of Statistical Associating Fluid Theory**. *Ind. Eng. Chem. Res.*, 47, pp.8063-82.

Thermo Fischer Scientific Inc., (2008) **Nicolet FT-IR User's Guide**. Equipment user guide.

Tucker, E.E. & Becker, E.D., (1973) **Alcohol Association Studies. II. Vapor Pressure, 220-MHz Proton Magnetic Resonance, and Infrared Investigations of tert-Butyl Alcohol Association in Hexadecane**. *J. Phys. Chem.*, 77(14), pp.1783-95.

Tumakaka, F. & Sadowski, G., (2004) **Application of the Perturbed-Chain SAFT equation of state to polar systems**. *Fluid Phase Equilibr.*, 217, pp.233-39.

Tybjerg, P.C.V., Kontogeorgis, G.M., Michelsen, M.L. & Stenby, E.H., (2010) **Phase equilibria modeling of methanol-containing systems with the CPA and sPC-SAFT equations of state**. *Fluid Phase Equilibr.*, 288, pp.128-38.

Venyaminov, S.Y. & Prendergast, F.G., (1997) **Water (H2O and D2O) Molar Absorptivity in the 1000-4000 cm-1 Range and Quantative Infrared Spectroscopy of Aqueous Solutions**. *Anal. Biochem.*, 248, pp.234-45.

von Solms, N., Jensen, L., Kofod, J.L., Michelsen, M.L. & Kontageorgis, G.M., (2007) **Measurement and modelling of hydrogen bonding in 1-alkanol + n-alkane binary mixtures**. *Fluid Phase Equilibr.*, 261, pp.272-80.

von Solms, N., Kouskoumvekaki, I.A., Michelsen, M.L. & Kontageorgis, G.M., (2006a) **Capabilities, limitations and challenges of a simplified PC-SAFT equation of state**. *Fluid Phase Equilibr.*, 241, pp.344-53.

von Solms, N., Michelsen, M.L. & Kontogeorgis, G.M., (2004) **Applying Association Theories to Polar Fluids**. *Ind. Eng. Chem. Res.*, 43, pp.1803-06.

von Solms, N., Michelsen, M.L., Passos, C.P., Derawi, S.O. & Kontageorgis, G.M., (2006b) **Investigating Models for Associating Fluids Using Spectroscopy**. *Ind. Eng. Chem. Res.*, 45(15), pp.5368-74.

von Solms, N., Michelson, M.L. & Kontageorgis, G.M., (2003) **Computational and Physical Performance of a Modified PC-SAFT Equation of State for Highly Assymetric and Associating Mixtures**. *Ind. Eng. Chem. Res.*, 42, pp.1098-105.

Walsh, J.M., Guedes, H.J.R. & Gubbins, K.E., (1992) **Physical Theory for Fluids of Small Associating Molecules**. *J. Phys. Chem.*, 96, pp.10995-1004.

Weisstein, E.W., (1999-2012) *Simpson's 3/8 Rule*. [Online] Available at: http://mathworld.wolfram.com/Simpsons38Rule.html [Accessed February 2011].

Weisstein, E.W., (1999-2013) **Derivative**. [Online] Available at: http://mathworld.wolfram.com/Derivative.html [Accessed February 2013].

Weisstein, E.W., (2002) *Gaussian Function*. [Online] Available at: http://mathworld.wolfram.com/GaussianFunction.html [Accessed February 2010].

Weisstein, E.W., (2004) *Lorentzian Function,*. [Online] Available at: http://mathworld.wolfram.com/LorentzianFunction.html [Accessed February 2010].

Wertheim, M.S., (1984a) **Fluids with Highly Directional Attractive Forces. I. Statistical Thermodynamics**. *J. Stat. Phys.*, 35, pp.19-34.

Wertheim, M.S., (1984b) **Fluids with Highly Directional Attractive Forces. II. Thermodynamic Perturbation Theory and Integral Equations**. *J. Stat. Phys.*, 35, pp.35-47.

Wertheim, M.S., (1986a) **Fluids with Highly Directional Attractive Forces. III. Multiple Attraction Sites**. *J. Stat. Phys.*, 42, pp.459-76.

Wertheim, M.S., (1986b) **Fluids with Highly Directional Attractive Forces. IV. Equilibrium Polymerization**. *J. Stat. Phys.*, 42, pp.477-92.

Wetzel, D.L.B., (1998) **Analytical Near Infrared Spectroscopy**. In Wetzel, D. & Chrarlambous, G. *Developments in Food Science*. Elsevier Science. pp.141-94. Instrumental Methods in Food and Beverage Analysis.

Widom, B., (2002) **Statistical Mechanics: A concise introduction for chemists**. Cambridge University Press.

Wolbach, J.P. & Sandler, S.I., (1998) **Using Molecular Orbital Calculations To Describe the Phase Behavior of Cross-associating Mixtures**. *Ind. Eng. Chem. Res.*, 37(8), pp.2917-28.

Workman Jr., J., (2001c) **Review of Near-Infrared and Infrared Spectroscopy**. In Workman Jr., J. *The Handbook of Organic Compounds*. Academic Press. pp.79-129.

Yelash, L., Muller, M., Paul, W. & Binder, K., (2005) **A global investigation of phase equilibria using the perturbed-chain statistical-associating-fluid-theory approach**. *J. Chem. Phys.*, 123, pp.014908-1-15.

Chapter 10: Appendices

10.1 Licensing agreements for reused figures and tables

Table 25: Licence agreements for literature figures and tables reprinted in this thesis

Referrence	Licence Number
Kontageorgis *et al.* (2010)	3020631380710
von Solms *et al.* (2007)	3020631038574
Asprion *et al.* (2001)	3021360606473
Guan *et al.* (2012)	3021490818796
Max & Chapados (2008)	3022410376256

Additionally, intellectual property from the following sources was also used in this dissertation:

Title: New reference equation of state for associating liquids
Author: Walter G. Chapman, Keith E. Gubbins, George Jackson, and MaciejRadosz
Publication: Industrial & Engineering Chemistry Research
Publisher: American Chemical Society
Date: Aug 1, 1990
Copyright © 1990, American Chemical Society

Title: New Association Scheme for 1-Alcohols in Alcohol/Water Mixtures with sPC-SAFT: The 2C Association Scheme
Author: Adriaan J. de Villiers, Cara E. Schwarz, and Andries J. Burger
Publication: Industrial & Engineering Chemistry Research
Publisher: American Chemical Society
Date: Jul 1, 2011
Copyright © 2011, American Chemical Society

The figures/tables are reprinted with the following conditions:

PERMISSION/LICENSE IS GRANTED FOR YOUR ORDER AT NO CHARGE

This type of permission/license, instead of the standard Terms & Conditions, is sent to you because no fee is being charged for your order. Please note the following:

- Permission is granted for your request in both print and electronic formats, and translations.
- If figures and/or tables were requested, they may be adapted or used in part.
- Please print this page for your records and send a copy of it to your publisher/graduate school.
- Appropriate credit for the requested material should be given as follows: "Reprinted (adapted) with permission from (COMPLETE REFERENCE CITATION). Copyright (YEAR) American Chemical Society." Insert appropriate information in place of the capitalized words.
- One-time permission is granted only for the use specified in your request. No additional uses are granted (such

as derivative works or other editions). For any other uses, please submit a new request.

If credit is given to another source for the material you requested, permission must be obtained from that source.

Licensed content publisher	Elsevier
Licensed content publication	Elsevier Books
Licensed content title	Infrared and Raman Spectroscopy
Licensed content author	Peter Larkin
Licensed content date	2011
Number of pages	28
Type of Use	reuse in a thesis/dissertation
Portion	figures/tables/illustrations
Number of figures/tables/illustrations	2
Format	both print and electronic

“Reprinted from Publication title, Vol /edition number, Author(s), Title of article / title of chapter, Pages No., Copyright (Year), with permission from Elsevier [OR APPLICABLE SOCIETY COPYRIGHT OWNER].” Also Lancet special credit - “Reprinted from The Lancet, Vol. number, Author(s), Title of article, Pages No., Copyright (Year), with permission from Elsevier.”

Complete versions of these licence agreements have been kept with the supervisors of this research and are available, should they be required.

10.2 Experimental data

10.2.1 Acetone in methanol

(A) 2 acetone peaks

Table 26: Data for error box calculations for the 2-peak acetone-methanol system

#	Acetone mole fraction			AcO monomer fraction		Temperature [°C]	
	Measured	Low	High	High	Low	Reactor	FTIR
1	0.000180	0.000147	0.000212	1.00	0.693	23.2	23.0
2	0.000429	0.000363	0.000494	0.724	0.533	23.0	23.2
3	0.000669	0.000571	0.000768	0.603	0.449	23.1	23.2
4	0.001030	0.000898	0.001161	0.566	0.438	23.1	23.2
5	0.001448	0.001283	0.001612	0.524	0.417	23.1	23.2
6	0.002014	0.001816	0.002211	0.477	0.392	23.1	23.4
7	0.002656	0.002425	0.002886	0.441	0.371	23.2	23.0
8	0.003364	0.003100	0.003628	0.413	0.353	23.1	23.3
9	0.004101	0.003804	0.004398	0.397	0.343	23.1	23.1
10	0.004683	0.004352	0.005013	0.363	0.316	23.1	23.1

Table 27: Acetone (2 peaks assigned) monomer data in solution with methanol at 23.2 °C

X_{AcO}	AcO Areas		Adjusted-R^2 Values		X_{mon}	err^2
	Bonded	Monomer	Baseline	AcO		
0.000180	2.03	0.291	0.9996	0.9934	0.816	8.6E-08
0.000429	3.11	0.521	0.9996	0.9969	0.612	1.1E-07
0.000669	4.14	0.682	0.9995	0.9983	0.513	1.1E-07
0.00103	5.31	1.01	0.9996	0.9988	0.492	1.1E-07
0.00145	6.65	1.33	0.9996	0.9990	0.463	8.5E-08
0.00201	8.77	1.71	0.9996	0.9991	0.429	6.7E-08
0.00266	10.8	2.12	0.9996	0.9992	0.402	2.4E-08
0.00336	12.4	2.53	0.9993	0.9993	0.379	8.4E-09
0.00410	15.1	2.99	0.9996	0.9992	0.367	3.0E-08
0.00468	16.8	3.13	0.9994	0.9992	0.337	1.7E-07

(B) 3 acetone peaks

Table 28: Data for error box calculations for the 3-peak acetone-methanol system

#	AcO mole fraction			AcO monomer fraction	
	Measured	Low	High	High	Low
1	0.000180	0.000147	0.000212	0.903	0.681
2	0.000429	0.000363	0.000494	0.654	0.539
3	0.000669	0.000571	0.000768	0.532	0.455
4	0.001030	0.000898	0.001161	0.446	0.383
5	0.001448	0.001283	0.001612	0.403	0.342
6	0.002014	0.001816	0.002211	0.374	0.316
7	0.002656	0.002425	0.002886	0.350	0.300
8	0.003364	0.003100	0.003628	0.328	0.288
9	0.004101	0.003804	0.004398	0.306	0.277
10	0.004683	0.004352	0.005013	0.290	0.269

Table 29: Acetone (3 peaks assigned) monomer data in solution with methanol at 23.2 °C

X_{AcO}	AcO Areas			Adjusted-R^2 Values		X_{mon}	err^2
	2-Bonded	1-Bonded	Monomer	Baseline	AcO		
0.000180	0.246	0.987	0.508	0.9996	0.9771	0.790	5.9E-08
0.000429	0.455	1.58	0.848	0.9996	0.9841	0.553	8.6E-08
0.000669	0.740	2.23	1.234	0.9995	0.9983	0.515	1.7E-07
0.00103	0.930	2.91	1.603	0.9996	0.9744	0.435	1.3E-07
0.00145	0.911	3.75	1.854	0.9996	0.991	0.358	1.5E-08
0.00201	1.16	4.84	2.413	0.9996	0.9907	0.335	1.2E-10
0.00266	1.43	6.11	3.048	0.9996	0.9905	0.321	1.4E-08
0.00336	1.68	7.33	3.653	0.9993	0.9902	0.304	1.2E-07
0.00410	2.04	8.50	4.314	0.9996	0.9907	0.294	2.7E-07
0.00468	2.28	9.41	4.813	0.9994	0.9911	0.287	4.9E-07

10.2.2 Acetone in ethanol

Table 30: Data for error box calculations for the acetone-ethanol system

#	AcO mole fraction			AcO monomer fraction		Temperature [°C]	
	Measured	Low	High	Low	High	Reactor	FTIR
1	0.000162	0.000122	0.000203	0.745	0.954	23.2	23
2	0.000515	0.000434	0.000597	0.344	0.369	23.1	23.2
3	0.000951	0.000829	0.00107	0.266	0.310	23.2	23.1
4	0.00129	0.00112	0.00145	0.228	0.255	23.1	-
5	0.00178	0.00158	0.00199	0.188	0.192	23.2	-
6	0.00220	0.00196	0.00245	0.1570	0.167	23.3	-
7	0.00263	0.00234	0.00292	0.1331	0.1447	23.2	-
8	0.00340	0.00307	0.00373	0.1157	0.1248	23.2	-
9	0.00438	0.00401	0.00475	0.1011	0.1041	23.1	-
10	0.00544	0.00502	0.00585	0.0883	0.0911	23.2	-

Table 31: Acetone monomer data in solution with ethanol at 23.2 °C

X_{AcO}	AcO Areas		Adjusted-R^2 Values		X_{mon}	err^2
	Bonded	Monomer	Baseline	AcO		
0.000162	1.00	1.02	0.9831	0.9929	0.871	1.6E-07
0.000515	1.50	1.36	0.9751	0.9937	0.366	3.6E-08
0.000951	2.09	2.02	0.9753	0.9945	0.295	2.3E-08
0.00129	3.04	2.20	0.9705	0.9977	0.237	6.7E-08
0.00178	4.08	2.43	0.9698	0.998	0.189	3.4E-08
0.00220	5.04	2.64	0.9647	0.9983	0.166	3.8E-08
0.00263	5.92	2.57	0.9623	0.9985	0.1352	1.9E-08
0.00340	7.48	2.95	0.9522	0.9986	0.1204	5.8E-09
0.00438	9.39	3.28	0.9384	0.9988	0.1038	3.7E-09
0.00544	11.0	3.47	0.9226	0.9988	0.0885	1.5E-07

10.2.3 Acetone in 1-propanol

Table 32: Data for error box calculations for the acetone – 1-propanol system

#	AcO mole fraction			AcO monomer fraction		Temperature [°C]	
	Measured	Low	High	High	Low	Reactor	FTIR
1	0.00054	0.000474	0.000609	0.350	0.255	22.5	22.2
2	0.00115	0.00102	0.00129	0.219	0.156	22.5	22.3
3	0.00231	0.00211	0.00252	0.141	0.101	23.0	22.5
4	0.00348	0.00321	0.00375	0.119	0.0806	23.6	23.0
5	0.00520	0.00486	0.00554	0.107	0.0725	23.9	23.1
6	0.00617	0.00576	0.00658	0.0986	0.0653	23.9	23.2
7	0.00714	0.00667	0.00762	0.0964	0.0640	22.5	23.3

Table 33: Acetone monomer data in solution with 1-propanol at 23.2 °C

X_{AcO}	AcO Areas		Adjusted-R^2 Values	X_{mon}	err^2
	Bonded	Monomer	Baseline + AcO		
0.000542	8.89	1.44	0.9966	0.298	2.2E-06
0.00115	11.2	1.91	0.9970	0.185	2.0E-06
0.00231	14.3	2.48	0.9973	0.120	9.8E-07
0.00348	17.7	3.08	0.9974	0.0989	3.5E-07
0.00520	21.3	4.15	0.9975	0.0892	5.9E-08
0.00617	23.3	4.50	0.9975	0.0816	5.6E-07
0.00714	25.4	5.10	0.9975	0.0799	1.5E-06

10.2.4 Acetone in 2-propanol

Table 34: Data for error box calculations for the acetone – 2-propanol system

#	2PrOH mole fraction			2PrOH monomer fraction		Temperature [°C]	
	Measured	Low	High	High	Low	Reactor	FTIR
1	0.000620	0.000500	0.000741	0.892	0.601	23.2	23.4
2	0.00173	0.00153	0.00192	0.296	0.236	23.2	23.0
3	0.00251	0.00225	0.00278	0.209	0.165	23.0	23.1
4	0.00407	0.00372	0.00442	0.111	0.0936	23.0	23.2
5	0.00604	0.00560	0.00648	0.0745	0.0563	22.5	23.5
6	0.00892	0.00838	0.00947	0.0657	0.0359	23.0	23.3

Table 35: Acetone monomer data in solution with 1-propanol at 23.0 °C

X_{AcO}	AcO Areas		Adjusted-R^2 Values	X_{mon}	err^2
	Bonded	Monomer	Baseline + AcO		
0.000353	0.65	0.18	0.9756	0.111	4.0E-10
0.000746	1.3	0.33	0.9945	0.098	1.2E-08
0.001422	2.5	0.57	0.9989	0.090	3.5E-08
0.002554	4.3	0.99	0.9932	0.087	1.5E-07
0.004896	8.0	1.89	0.9974	0.086	7.4E-07
0.010820	16.6	4.00	0.9984	0.082	6.1E-06
0.015618	21.9	5.64	0.9986	0.081	2.0E-05

10.2.5 Methanol in acetone

Table 36: Data for error box calculations for the methanol-acetone system

#	MeOH mole fraction			MeOH monomer fraction		Temperature [°C]	
	Measured	Low	High	High	Low	Reactor	FTIR
1	0.0001643	0.0000873	0.000241	0.921	0.536	23.1	23.2
2	0.0004735	0.000319	0.000628	0.415	0.211	23.0	23.3
3	0.000939	0.000707	0.00117	0.186	0.112	22.8	23.4
4	0.00129	0.000982	0.00160	0.121	0.0742	23.3	23.2
5	0.00182	0.00144	0.00221	0.0863	0.0561	23.4	23.2
6	0.00261	0.00214	0.00307	0.0677	0.0472	23.1	23.2
7	0.00335	0.00281	0.00389	0.0498	0.0359	23.5	23.3
8	0.00489	0.00427	0.00551	0.0327	0.0253	-	23.2
9	0.00640	0.00570	0.00709	0.0262	0.0210	23.0	23.3
10	0.00861	0.00783	0.00938	0.0116	0.00971	-	23.3

Table 37: Methanol monomer data in solution with acetone at 23.3 ± 0.2 °C

X_{MeOH}	MeOH Areas			Adjusted-R^2 Values	X_{mon}	err^2
	Monomer	Dimer	Poly	Baseline + fit		
0.000164	9.28	9.2	2.81	0.9988	0.788	2.9E-06
0.00047	9.49	7.1	1.71	0.9993	0.280	7.7E-07
0.00094	9.43	9.7	1.73	0.9993	0.140	5.0E-07
0.00129	8.52	8.4	4.04	0.9993	0.092	6.0E-07
0.00182	8.89	12.3	1.83	0.9993	0.068	1.7E-08
0.00261	10.40	7.8	5.42	0.9984	0.056	5.5E-08
0.00335	10.0	20.6	3.1	0.9993	0.042	2.0E-08
0.00489	10.0	18.3	10.6	0.9931	0.029	1.3E-09
0.00640	10.7	23.2	12.1	0.9989	0.023	3.8E-07
0.00861	6.5	27.0	14.1	0.9988	0.011	3.9E-06

10.2.6 Ethanol in acetone

(A) Fixed parameter fits

Table 38: Ethanol monomer data in solution with acetone calculated with fixed parameter areas at 24.8 °C

X_{EtOH}	EtOH Areas			Adjusted-R^2 Values		X_{mon}	err^2
	Monomer	Dimer	Poly	Baseline	Fit		
0.000925	7.28	18.6	0.775	0.9964	0.9998	0.878	4.6E-06
0.00147	7.20	21.0	0.828	0.9978	0.9998	0.548	3.3E-06
0.00224	7.04	24.7	0.832	0.9972	0.9989	0.351	1.5E-06
0.00317	6.99	28.0	0.820	0.9969	0.9996	0.246	2.2E-07
0.00426	6.95	32.8	0.770	0.9972	0.9988	0.182	1.9E-07
0.00511	6.79	36.3	0.765	0.9975	0.9994	0.148	1.3E-06
0.00613	6.68	40.9	0.740	0.9961	0.9992	0.122	3.7E-06
0.00747	6.52	45.3	0.712	0.9961	0.9992	0.097	9.5E-06

(B) Free parameter fits at 24.8 °C

Table 39: Data for error box calculations for the ethanol-acetone system

#	EtOH mole fraction			EtOH monomer fraction		Temperature [°C]	
	Measured	Low	High	High	Low	Reactor	FTIR
1	0.000925	0.000867	0.000983	0.476	0.420	24.8	24.2
2	0.00147	0.00135	0.00158	0.266	0.227	24.9	24.8
3	0.00224	0.00207	0.00241	0.154	0.132	24.9	24.9
4	0.00317	0.00294	0.00340	0.146	0.127	25.1	24.8
5	0.00426	0.00396	0.00454	0.106	0.092	25.1	24.8
6	0.00511	0.00476	0.00545	0.097	0.085	25.1	24.8
7	0.00613	0.00571	0.00652	0.072	0.063	25.1	24.9
8	0.00747	0.00699	0.00791	0.066	0.058	25.1	25.0

Table 40: Ethanol monomer data in solution with acetone calculated with free parameter areas

x_{EtOH}	EtOH Areas			Adjusted-R^2 Values		X_{mon}	err^2
	Monomer	Dimer	Poly	Baseline	Fit		
0.000925	7.28	18.6	0.775	0.8121	0.9998	0.446	3.7E-06
0.00147	6.33	22.9	0.878	0.9978	0.9991	0.245	3.6E-06
0.00224	5.62	28.2	0.873	0.9972	0.9991	0.142	3.2E-06
0.00317	7.60	24.0	0.731	0.9969	0.9998	0.136	1.7E-07
0.00426	7.41	28.4	0.697	0.9972	0.9997	0.0985	1.1E-08
0.00511	8.18	29.5	0.625	0.9975	0.9996	0.0905	6.1E-07
0.00613	7.24	35.4	0.715	0.9961	0.9948	0.0669	1.2E-06
0.00747	8.10	37.4	0.527	0.9961	0.9948	0.0614	4.4E-06

(C) Temperature-corrected free parameter fits at 23.0 °C

Table 41: Temperature-corrected ethanol monomer data in solution with acetone calculated with free parameter areas

x_{EtOH}	X_{mon}	EtOH monomer fraction	
		High	Low
0.000925	0.435	0.470	0.403
0.00147	0.233	0.260	0.210
0.00224	0.129	0.147	0.112
0.00317	0.122	0.140	0.106
0.00426	0.085	0.099	0.073
0.00511	0.078	0.091	0.066
0.00613	0.055	0.066	0.045
0.00747	0.050	0.060	0.041

10.2.7 1-Propanol in acetone

Table 42: Data for error box calculations for the 1-propanol – acetone system

#	1PrOH mole fraction			1PrOH monomer fraction		Temperature [°C]	
	Measured	Low	High	Low	High	Reactor	FTIR
1	0.000292	0.000182	0.000403	0.834	0.968	23.0	23.3
2	0.000470	0.000304	0.000636	0.589	0.683	23.0	23.1
3	0.000798	0.000577	0.00102	0.361	0.419	23.1	23.2
4	0.00119	0.00091	0.00147	0.179	0.208	23.1	23.0
5	0.00190	0.00157	0.00223	0.150	0.174	23.1	23.2
6	0.00269	0.00230	0.00307	0.117	0.135	23.3	23.2
7	0.00533	0.00489	0.00577	0.0573	0.0665	23.0	23.1

Table 43: 1-Propanol monomer data in solution with acetone calculated at °C

X_{1PrOH}	1PrOH Areas			Adjusted-R^2 Values	X_{mon}	err^2
	Monomer	Dimer	Poly	Baseline + fit		
0.000292	8.08	6.04	1.25	0.9994	0.914	6.7E-08
0.000470	9.17	8.14	1.87	0.9991	0.645	4.6E-08
0.000798	9.55	9.43	1.87	0.9993	0.396	1.6E-09
0.00119	7.05	14.5	2.34	0.9993	0.196	7.6E-08
0.00190	9.46	13.1	2.69	0.9994	0.165	9.4E-07
0.00269	10.37	13.6	8.05	0.9991	0.128	2.9E-06
0.00533	10.13	18.9	10.4	0.999	0.063	1.7E-05

10.2.8 2-Propanol in acetone

Table 44: Data for error box calculations for the 2-propanol – acetone system

#	2PrOH mole fraction			2PrOH monomer fraction		Temperature [°C]	
	Measured	Low	High	High	Low	Reactor	FTIR
1	0.000620	0.000500	0.000741	0.892	0.601	23.2	23.4
2	0.00173	0.00153	0.00192	0.296	0.236	23.2	23.0
3	0.00251	0.00225	0.00278	0.209	0.169	23.0	23.1
4	0.00407	0.00372	0.00442	0.111	0.0936	23.0	23.2
5	0.00604	0.00560	0.00648	0.0745	0.0644	22.5	23.5
6	0.00892	0.00838	0.00947	0.0406	0.0359	23.0	23.3

Table 45: 2-Propanol monomer data in solution with acetone calculated at 23.3 ± 0.5 °C

x_{2PrOH}	2PrOH Areas			Adjusted-R^2 Values	X_{mon}	err^2
	Monomer	Dimer	Poly	Baseline + fit		
0.000620	8.03	6.54	1.63	0.9993	0.730	5.6E-06
0.00173	8.35	3.35	7.30	0.9987	0.272	7.9E-07
0.00251	7.34	6.03	1.66	0.9988	0.165	6.3E-08
0.00407	7.41	8.82	2.40	0.9846	0.103	4.9E-08
0.00604	6.04	15.0	5.92	0.9993	0.056	1.4E-07
0.00892	10.4	17.6	5.75	0.9991	0.066	1.9E-06

10.3 Thermodynamic modelling data

10.3.1 Pure component modelling

(A) Methanol

Table 46: Digitized pure methanol monomer fraction data from Luck (1980)

T [K]	% OH Free	Frac	XA	X1
252.36	0.50	0.00501	0.503	0.00127
272.43	1.02	0.010	0.505	0.003
293.67	2.12	0.021	0.511	0.006
312.96	3.42	0.034	0.517	0.009
333.42	4.71	0.047	0.524	0.013
352.72	6.78	0.068	0.534	0.019
373.20	9.61	0.096	0.548	0.029
392.51	13.42	0.134	0.567	0.043
412.62	18.37	0.184	0.592	0.064
432.75	24.49	0.245	0.622	0.095
473.03	38.83	0.388	0.694	0.187
493.20	49.00	0.490	0.745	0.272
502.74	57.64	0.576	0.788	0.358
507.94	65.34	0.653	0.827	0.447
510.38	72.27	0.723	0.861	0.536
523.85	81.30	0.813	0.906	0.668
533.72	84.35	0.844	0.922	0.717
542.79	87.03	0.870	0.935	0.761
551.86	89.32	0.893	0.947	0.800
563.69	91.40	0.914	0.957	0.837
572.75	93.11	0.931	0.966	0.868
582.60	94.63	0.946	0.973	0.896
592.84	96.14	0.961	0.981	0.925
602.68	97.08	0.971	0.985	0.943
612.93	98.59	0.986	0.993	0.972
634.17	99.69	0.997	0.998	0.994

Table 47: Pure methanol model predicts from Figure 58 on page112

	3B		3B [X]		2B		2B [X]		2C		2B - JC	
T [K]	P [bar]	X_{MEOH}	P [bar]	X_{MEOH}	P [bar]	X_{MEOH}	P [bar]	X_{MEOH}	P [bar]	X_{MEOH}	P [bar]	X_{MEOH}
256.3	0.0236	0.00327	0.0237	0.00311	0.0129	0.00068	0.0230	0.00225	0.0000	0.00039	0.0130	0.00035
263.9	0.0407	0.00413	0.0408	0.00401	0.0222	0.00090	0.0395	0.00300	0.0000	0.00052	0.0222	0.00048
271.6	0.0678	0.00515	0.0677	0.00511	0.0368	0.00118	0.0657	0.00394	0.0000	0.00069	0.0367	0.00064
279.3	0.109	0.00636	0.109	0.00642	0.059	0.00153	0.106	0.00510	0.000	0.00090	0.059	0.00086
287.0	0.172	0.00778	0.171	0.00799	0.093	0.00195	0.166	0.00651	0.000	0.00115	0.092	0.00112
294.7	0.262	0.00942	0.260	0.00984	0.142	0.00247	0.253	0.00821	0.000	0.00146	0.140	0.00146
302.4	0.390	0.0113	0.387	0.0120	0.211	0.0031	0.376	0.0102	0.000	0.0018	0.209	0.0019
310.1	0.568	0.0135	0.564	0.0145	0.307	0.0038	0.547	0.0126	0.000	0.0023	0.304	0.0024
317.8	0.810	0.0160	0.804	0.0174	0.439	0.0047	0.780	0.0154	0.000	0.0028	0.435	0.0029
325.4	1.13	0.0189	1.12	0.0208	0.61	0.0057	1.09	0.0186	0.00	0.0034	0.61	0.0037
333.1	1.56	0.0221	1.55	0.0246	0.85	0.0068	1.49	0.0224	0.00	0.0041	0.84	0.0045
340.8	2.11	0.0257	2.09	0.0290	1.15	0.0082	2.02	0.0266	0.00	0.0048	1.14	0.0055
348.5	2.80	0.0298	2.78	0.0339	1.53	0.0097	2.68	0.0315	0.00	0.0057	1.52	0.0066
356.2	3.68	0.0343	3.65	0.0394	2.02	0.0115	3.51	0.0369	0.00	0.0067	2.01	0.0080
363.9	4.76	0.0394	4.73	0.0457	2.62	0.0135	4.53	0.0431	0.00	0.0079	2.62	0.0095
371.6	6.09	0.0451	6.06	0.0526	3.37	0.0157	5.78	0.0499	0.00	0.0091	3.36	0.0112
379.3	7.71	0.0514	7.66	0.0604	4.27	0.0182	7.29	0.0575	0.00	0.0105	4.28	0.0133
386.9	9.64	0.0584	9.58	0.0690	5.37	0.0211	9.10	0.0660	0.00	0.0120	5.38	0.0156
394.6	11.9	0.0661	11.9	0.0786	6.7	0.0243	11.2	0.0753	0.0	0.0136	6.7	0.0182
402.3	14.7	0.0747	14.6	0.0892	8.2	0.0279	13.8	0.0856	0.0	0.0155	8.3	0.0211
410.0	17.9	0.0842	17.7	0.1009	10.0	0.0319	16.7	0.0970	0.0	0.0174	10.1	0.0244

(B) Ethanol

Table 48: Digitized pure methanol monomer fraction data from Luck (1986)

T [K]	% OH Free	Frac	XA	X1
253.00	0.00	0	0.5	0
273.15	0.77	0.008	0.504	0.002
292.55	1.91	0.019	0.510	0.005
312.69	3.78	0.038	0.519	0.010
332.09	4.92	0.049	0.525	0.014
352.23	6.79	0.068	0.534	0.019
372.37	10.53	0.105	0.553	0.032
391.01	13.52	0.135	0.568	0.044
411.89	19.12	0.191	0.596	0.068
432.01	25.45	0.255	0.627	0.100
452.13	32.91	0.329	0.665	0.145
472.25	42.22	0.422	0.711	0.213
492.35	53.76	0.538	0.769	0.318
502.03	60.84	0.608	0.804	0.393
510.19	74.23	0.742	0.871	0.563
539.23	91.72	0.917	0.959	0.843
572.04	98.07	0.981	0.990	0.962
619.79	100.00	1	1	1

Table 49: Pure ethanol model predicts from Figure 59 on page 113

3B			3B [X]			2B Grenner *et al.*		2B [X]		2C		2B - JC	
T [K]	P [bar]	X_{EtOH}	T [K]	P [bar]	X_{EtOH}	P [bar]	X_{EtOH}	P [bar]	X_{EtOH}	P [bar]	X_{EtOH}	P [bar]	X_{EtOH}
257.0	0.0397	0.00221	257.0	0.0036	0.00046	0.0046	0.00155	0.0039	0.00038	0.0047	0.00106	0.0048	0.00064
267.3	0.0750	0.00302	266.7	0.0075	0.00063	0.0099	0.00226	0.0081	0.00054	0.0099	0.00158	0.0101	0.00095
277.6	0.1349	0.00403	276.3	0.0151	0.00085	0.0198	0.00320	0.0162	0.00075	0.0199	0.00228	0.0201	0.00139
287.8	0.232	0.00529	286.0	0.029	0.00113	0.038	0.00444	0.031	0.00102	0.038	0.00322	0.038	0.00197
298.1	0.382	0.00683	295.6	0.052	0.00146	0.068	0.00603	0.056	0.00137	0.068	0.00444	0.068	0.00274
308.4	0.607	0.00869	305.3	0.090	0.00188	0.118	0.00803	0.096	0.00181	0.118	0.00600	0.118	0.00373
318.7	0.934	0.0109	314.9	0.151	0.0024	0.198	0.0105	0.161	0.0023	0.197	0.0080	0.196	0.0050
329.0	1.397	0.0136	324.6	0.245	0.0030	0.318	0.0136	0.260	0.0030	0.317	0.0104	0.314	0.0066
339.2	2.032	0.0167	334.2	0.384	0.0037	0.496	0.0172	0.407	0.0038	0.494	0.0133	0.489	0.0085
349.5	2.89	0.0203	343.9	0.59	0.0045	0.75	0.0216	0.62	0.0047	0.75	0.0169	0.74	0.0109
359.8	4.01	0.0245	353.5	0.87	0.0054	1.11	0.0267	0.92	0.0058	1.10	0.0211	1.09	0.0138
370.1	5.47	0.0294	363.2	1.27	0.0065	1.59	0.0328	1.33	0.0070	1.58	0.0261	1.57	0.0172
380.4	7.32	0.0350	372.8	1.80	0.0078	2.23	0.0398	1.89	0.0085	2.22	0.0319	2.20	0.0213
390.6	9.63	0.0414	382.5	2.51	0.0092	3.07	0.0478	2.63	0.0102	3.06	0.0387	3.04	0.0260
400.9	12.48	0.0488	392.1	3.44	0.0108	4.15	0.0569	3.60	0.0121	4.14	0.0464	4.11	0.0316
411.2	15.95	0.0573	401.8	4.63	0.0127	5.51	0.0673	4.83	0.0143	5.50	0.0553	5.47	0.0381
421.5	20.13	0.0669	411.4	6.15	0.0148	7.21	0.0790	6.39	0.0168	7.19	0.0653	7.17	0.0455
431.8	25.10	0.0780	421.1	8.04	0.0171	9.28	0.0922	8.34	0.0196	9.27	0.0767	9.26	0.0541
442.0	31.0	0.0907	430.7	10.4	0.0197	11.8	0.1069	10.7	0.0227	11.8	0.0896	11.8	0.0639
452.3	37.8	0.1053	440.4	13.2	0.0226	14.8	0.1233	13.6	0.0262	14.8	0.1040	14.8	0.0752
462.6	45.8	0.1224	450.0	16.7	0.0259	18.4	0.1416	17.1	0.0300	18.4	0.1202	18.5	0.0880

10.3.2 Acetone-alcohol

(A) Acetone-methanol

Table 50: AcO(2B) monomer fractions in MeOH(2C/2B/3B) for Figure 73 on page 128

T [K]	P [bar]	x_{AcO}	x_{MeOH}	2B-3B	2B-2B	2B-2C
296.45	1.0132	1.00E-10	1	0.008312	0.013293	0.005240
296.45	1.0132	0.001	0.999	0.008324	0.013306	0.005249
296.45	1.0132	0.002	0.998	0.008336	0.013319	0.005258
296.45	1.0132	0.003	0.997	0.008347	0.013332	0.005267
296.45	1.0132	0.004	0.996	0.008359	0.013344	0.005276
296.45	1.0132	0.005	0.995	0.008371	0.013357	0.005285
296.45	1.0132	0.006	0.994	0.008382	0.013370	0.005294
296.45	1.0132	0.007	0.993	0.008394	0.013383	0.005304
296.45	1.0132	0.008	0.992	0.008406	0.013395	0.005313
296.45	1.0132	0.009	0.991	0.008417	0.013408	0.005322
296.45	1.0132	0.01	0.99	0.008429	0.013421	0.005331

Table 51: 2B-2C model data for Figure 76 on page 131

Scheme	2B-2C	2B-2C	2B-2C	2B-2C	2B-2C
AcO	[1321, 0.964]	[1321, 0.964]	[1321, 0.33]	[1321, 0.33]	[1321, 0.33]
MeOH	[100, 0.001]	[250, 0.001]	[100, 0.001]	[100, 0.00025]	[100, 0.001]
x_{AcO}			X_{AcO}		
1.00E-10	0.068	0.306	0.538	0.715	0.674
0.001	0.067	0.285	0.515	0.674	0.571
0.002	0.066	0.267	0.494	0.638	0.499
0.003	0.065	0.252	0.476	0.607	0.445
0.004	0.065	0.239	0.459	0.580	0.403
0.005	0.064	0.227	0.443	0.555	0.369
0.006	0.063	0.217	0.429	0.533	0.341
0.007	0.063	0.208	0.416	0.513	0.318
0.008	0.062	0.199	0.403	0.494	0.297
0.009	0.061	0.192	0.392	0.478	0.280
0.01	0.061	0.185	0.381	0.462	0.264

(B) Acetone-ethanol

Table 52: Several attempted model fits for the dilute acetone-ethanol system

		Scheme	2B-2C	2B-2C	2B-2C	2B-2C	2B-2C	2B-2C	2B-2C	2B-2C
		AcO association parameters	[1321, 0.96]	[1321, 0.96]	[1321, 0.96]	[1321, 0.96]	[1321, 0.96]	[1321, 0.33]	[1321, 0.52]	[1321, 0.96]
		EtOH association parameters	[150, 0.0327]	[150, 0.00025]	[150, 0.001]	[150, 0.01]	[75, 0.01]	[75, 0.01]	[100, 0.021]	[100, 0.0025]
T [K]	P [bar]	x_{AcO}					X_{AcO}			
296.35	1.01325	1.00E-10	0.216	0.821	0.686	0.370	0.409	0.556	0.377	0.572
296.35	1.01325	0.001	0.214	0.780	0.658	0.361	0.399	0.549	0.373	0.549
296.35	1.01325	0.002	0.211	0.745	0.633	0.354	0.390	0.543	0.368	0.528
296.35	1.01325	0.003	0.209	0.713	0.609	0.346	0.381	0.536	0.364	0.509
296.35	1.01325	0.004	0.206	0.684	0.588	0.340	0.373	0.530	0.360	0.491
296.35	1.01325	0.005	0.204	0.658	0.569	0.333	0.365	0.524	0.356	0.475
296.35	1.01325	0.006	0.202	0.634	0.551	0.327	0.357	0.518	0.352	0.460
296.35	1.01325	0.007	0.199	0.612	0.534	0.321	0.350	0.513	0.348	0.446
296.35	1.01325	0.008	0.197	0.592	0.518	0.315	0.343	0.507	0.345	0.433
296.35	1.01325	0.009	0.195	0.574	0.504	0.309	0.337	0.502	0.341	0.421
296.35	1.01325	0.01	0.193	0.556	0.490	0.304	0.330	0.497	0.338	0.410

2B-2C [1321, 0.96] [100, 0.025]	2B-2C [1321, 0.96] [100, 0.075]	2B-2B [1321, 0.96] [100, 0.075]	2B-3B [1321, 0.96] [100, 0.075]	2B-(-) [2200, 0.96] []	2B-(-) [2413, 0.96] []
0.250	0.137	0.209	0.135	1.000	1.000
0.246	0.135	0.206	0.134	0.448	0.299
0.241	0.134	0.203	0.133	0.304	0.187
0.237	0.133	0.200	0.132	0.233	0.138
0.233	0.132	0.197	0.130	0.191	0.110
0.230	0.131	0.195	0.129	0.162	0.092
0.226	0.129	0.192	0.128	0.141	0.079
0.222	0.128	0.190	0.127	0.125	0.069
0.219	0.127	0.187	0.126	0.112	0.062
0.216	0.126	0.185	0.125	0.102	0.056
0.213	0.125	0.182	0.124	0.093	0.051

(C) Acetone – 1-propanol

Table 53: Acetone - 1-propanol model predictions for 2B-2B/3B association schemes at 22.8 °C

Scheme			2B-2B	2B-2B	2B-2B	2B-2B	2B-3B
AcO association parameters			[1321, 0.962]	[2319, 0.962]	[2532, 0.962]	[2532, 0.962]	[2319, 0.962]
1PrOH association parameters			[100, 0.00025]	[100, 0.00025]	[100, 0.00025]	[100, 0.001]	[100, 0.001]
T [K]	P [bar]	x_{AcO}	X_{AcO}				
295.95	1.01325	1.00E-10	0.892	0.553	0.447	0.252	0.249
295.95	1.01325	0.001	0.846	0.296	0.188	0.139	0.176
295.95	1.01325	0.002	0.806	0.211	0.126	0.100	0.139
295.95	1.01325	0.003	0.770	0.166	0.096	0.079	0.117
295.95	1.01325	0.004	0.737	0.138	0.078	0.066	0.101
295.95	1.01325	0.005	0.708	0.119	0.066	0.057	0.089
295.95	1.01325	0.006	0.682	0.104	0.057	0.050	0.080
295.95	1.01325	0.007	0.658	0.093	0.051	0.045	0.073
295.95	1.01325	0.008	0.635	0.084	0.046	0.040	0.067
295.95	1.01325	0.009	0.615	0.077	0.042	0.037	0.062
295.95	1.01325	0.01	0.596	0.071	0.038	0.034	0.058

(D) Acetone – 2-propanol

Table 54: Model prediction data for dilute acetone – 2-propanol from Figure 83 on page 142

Scheme			2B-2B	2B-2B	2B-2B	2B-2B	2B-2B	2B-2B	2B-3B	2B-3B
AcO association parameters			[1321, 0.962]	[2399, 0.962]	[2399, 0.962]	[2147, 0.899]	[2008, 0.962]	[2008, 0.962]	[1903, 0.962]	[1903, 0.964]
2PrOH association parameters			[100, 0.00025]	[100, 0.00025]	[132, 0.00264]	[132, 0.00264]	[132, 0.011]	[132, 0.016]	[132, 0.011]	[132, 0.013]
T [K]	P [bar]	x_{AcO}	X_{AcO}							
296.15	1.0132	1.00E-10	0.898	0.534	0.195	0.311	0.119	0.093	0.150	0.135
296.15	1.0132	0.001	0.856	0.271	0.141	0.249	0.112	0.089	0.141	0.128
296.15	1.0132	0.002	0.819	0.190	0.113	0.211	0.106	0.085	0.134	0.123
296.15	1.0132	0.003	0.786	0.149	0.095	0.184	0.100	0.081	0.128	0.117
296.15	1.0132	0.004	0.755	0.123	0.083	0.164	0.096	0.078	0.122	0.113
296.15	1.0132	0.005	0.728	0.105	0.073	0.148	0.091	0.075	0.117	0.108
296.15	1.0132	0.006	0.702	0.092	0.066	0.135	0.087	0.072	0.113	0.104
296.15	1.0132	0.007	0.679	0.082	0.060	0.125	0.084	0.070	0.109	0.101
296.15	1.0132	0.008	0.658	0.074	0.055	0.116	0.081	0.068	0.105	0.097
296.15	1.0132	0.009	0.638	0.068	0.051	0.108	0.078	0.066	0.101	0.094
296.15	1.0132	0.01	0.619	0.062	0.048	0.102	0.075	0.064	0.098	0.091
296.15	1.0132	0.011		0.058	0.045	0.096	0.073	0.062	0.095	0.089
296.15	1.0132	0.012		0.054	0.042	0.091	0.070	0.060	0.092	0.086
296.15	1.0132	0.013		0.050	0.040	0.086	0.068	0.059	0.090	0.084
296.15	1.0132	0.014		0.047	0.038	0.082	0.066	0.057	0.087	0.082
296.15	1.0132	0.015		0.045	0.036	0.079	0.064	0.056	0.085	0.080
296.15	1.0132	0.016		0.042	0.034	0.075	0.063	0.054	0.083	0.078
296.15	1.0132	0.017		0.040	0.033	0.072	0.061	0.053	0.081	0.076
296.15	1.0132	0.018		0.038	0.031	0.070	0.059	0.052	0.079	0.074
296.15	1.0132	0.019		0.037	0.030	0.067	0.058	0.051	0.077	0.073
296.15	1.0132	0.02		0.035	0.029	0.065	0.057	0.050	0.075	0.071

10.3.3 Alcohol-acetone modelling

(A) Methanol-acetone

Table 55: sPC-SAFT 2B/3B/2C monomer fraction predictions at 23.3 °C for Figure 60 on pg. 115

x_{MeOH}	3B	2B	3B [X]	2B [X]	2C
1E-10	1	1	1	1	1
0.01	0.622	0.232	0.651	0.508	0.255
0.02	0.453	0.140	0.484	0.356	0.158
0.03	0.357	0.101	0.386	0.277	0.116
0.04	0.294	0.0797	0.320	0.228	0.0921
0.05	0.249	0.0659	0.273	0.195	0.0764
0.1	0.1406	0.0354	0.156	0.113	0.0409
0.15	0.0967	0.0241	0.1069	0.0797	0.0273
0.2	0.0729	0.0182	0.0804	0.0612	0.0201
0.25	0.0580	0.0145	0.0637	0.0493	0.0155
0.3	0.0478	0.0120	0.0523	0.0410	0.0124
0.35	0.0404	0.0102	0.0440	0.0349	0.0102
0.4	0.0347	0.00878	0.0376	0.0302	0.00848
0.45	0.0303	0.00768	0.0327	0.0264	0.00716
0.5	0.0267	0.00679	0.0286	0.0233	0.00610
0.55	0.0237	0.00606	0.0253	0.0208	0.00524
0.6	0.0212	0.00544	0.0226	0.0186	0.00452
0.65	0.0191	0.00491	0.0202	0.0168	0.00393
0.7	0.01725	0.00445	0.0182	0.0151	0.00342
0.75	0.01563	0.00405	0.0165	0.0137	0.00299
0.8	0.01421	0.00369	0.0149	0.0125	0.00261
0.85	0.01294	0.00337	0.0136	0.0114	0.00229
0.9	0.01180	0.00309	0.0124	0.0104	0.00201
0.95	0.01077	0.00283	0.0113	0.0095	0.00176
1	0.009836	0.00260	0.01031	0.00864	0.00154

Table 56: sPC-SAFT model predictions for methanol in acetone

				X_{mon}					
T [K]	P [bar]	x_{MeOH}	x_{AcO}	2B	2B JC	2B GV	2C	2C JC	2C GV
296.45	1.0132	1.00E-10	1	1.000	1.000	1.000	1.000	1.000	1.000
296.45	1.0132	0.001	0.999	0.829	0.610	0.679	0.257	0.634	0.649
296.45	1.0132	0.002	0.998	0.716	0.454	0.532	0.161	0.484	0.499
296.45	1.0132	0.003	0.997	0.633	0.366	0.444	0.119	0.397	0.412
296.45	1.0132	0.004	0.996	0.569	0.309	0.383	0.095	0.340	0.353
296.45	1.0132	0.005	0.995	0.519	0.268	0.339	0.080	0.298	0.311
296.45	1.0132	0.006	0.994	0.478	0.237	0.305	0.069	0.267	0.279
296.45	1.0132	0.007	0.993	0.443	0.213	0.278	0.061	0.242	0.253
296.45	1.0132	0.008	0.992	0.414	0.194	0.256	0.054	0.222	0.232
296.45	1.0132	0.009	0.991	0.388	0.178	0.237	0.049	0.205	0.215
296.45	1.0132	0.01	0.99	0.366	0.165	0.221	0.045	0.191	0.200

Table 57: Adjusted parameter 2C-N model data for Figure 70 on page 125

		Scheme	2C - (-)	2C -N	2C -N	2C -N
		MeOH association parameters	[2535 0.0823]	[2535 0.0823]	[2535 0.823]	[2535 0.823]
		AcO association parameters	[-]	[100 0.001]	[100 0.001]	[100 0.005]
T [K]	P [bar]	x_{MEOH}		X_{MEOH}		
296.45	1.01325	1.00E-10	1.000	0.756	0.495	0.305
296.45	1.01325	0.001	0.722	0.593	0.206	0.164
296.45	1.01325	0.002	0.581	0.496	0.138	0.117
296.45	1.01325	0.003	0.492	0.430	0.106	0.093
296.45	1.01325	0.004	0.430	0.382	0.086	0.077
296.45	1.01325	0.005	0.383	0.345	0.073	0.066
296.45	1.01325	0.006	0.347	0.315	0.064	0.058
296.45	1.01325	0.007	0.317	0.290	0.057	0.052
296.45	1.01325	0.008	0.293	0.270	0.051	0.047
296.45	1.01325	0.009	0.272	0.252	0.046	0.043
296.45	1.01325	0.01	0.255	0.237	0.042	0.040

Table 58: Adjusted parameter 2B-N model data for Figure 71 on page 126

Scheme			2B[X] - (-)	2B[X] -N	2B[X] -N	2B[X] -N
MeOH association parameters			[2304 0.3608]	[2304 0.3608]	[0.823]	[2700 0.823]
AcO association parameters			[-]	[100 0.001]	[100 0.001]	[100 0.001]
T [K]	P [bar]	x_{MEOH}	X_{MEOH}			
296.45	1.01325	1.00E-10	1.000	0.711	0.620	0.453
296.45	1.01325	0.001	0.709	0.548	0.396	0.186
296.45	1.01325	0.002	0.562	0.453	0.300	0.124
296.45	1.01325	0.003	0.470	0.390	0.244	0.094
296.45	1.01325	0.004	0.407	0.343	0.208	0.076
296.45	1.01325	0.005	0.360	0.308	0.181	0.064
296.45	1.01325	0.006	0.323	0.279	0.161	0.056
296.45	1.01325	0.007	0.294	0.256	0.145	0.049
296.45	1.01325	0.008	0.270	0.237	0.132	0.044
296.45	1.01325	0.009	0.249	0.221	0.122	0.040
296.45	1.01325	0.01	0.232	0.207	0.113	0.037

Table 59: Adjusted parameter 2B-N model data for Figure 72 on page 127

Scheme			2B[X] -N	3B -N
MeOH association parameters			[2700 0.823]	[2700 0.823]
AcO association parameters			[100 0.001]	[100 0.001]
T [K]	P [bar]	x_{MEOH}	X_{MEOH}	
296.45	1.01325	1.00E-10	0.453	0.453
296.45	1.01325	0.001	0.186	0.104
296.45	1.01325	0.002	0.124	0.059
296.45	1.01325	0.003	0.094	0.041
296.45	1.01325	0.004	0.076	0.031
296.45	1.01325	0.005	0.064	0.025
296.45	1.01325	0.006	0.056	0.021
296.45	1.01325	0.007	0.049	0.018
296.45	1.01325	0.008	0.044	0.016
296.45	1.01325	0.009	0.040	0.014
296.45	1.01325	0.01	0.037	0.013

(B) Ethanol-acetone

Table 60: Ethanol-acetone model data from Figure 78 on page 134

		Scheme	2B-N	2B-N	2B-N	2B-N	2B-N	2B-N	2B-2N
		EtOH association params	[2495, 0.05]	[2495, 0.85]	[2495, 0.825]	[2750, 0.825]	[2050, 0.825]	[2050, 0.825]	[2050, 0.825]
		AcO association params	[100, 0.001]	[100, 0.001]	[50, 0.001]	[50, 0.001]	[50, 0.001]	[145, 0.001]	[50, 0.001]
T [K]	P [bar]	x_{EtOH}				X_{EtOH}			
296.15	1.01325	1.00E-10	0.777	0.458	0.4826	0.3775	0.669	0.631	0.502
296.15	1.01325	0.001	0.663	0.186	0.1934	0.1058	0.444	0.426	0.362
296.15	1.01325	0.002	0.5827	0.123	0.1278	0.0656	0.341	0.331	0.289
296.15	1.01325	0.003	0.5222	0.093	0.097	0.048	0.281	0.273	0.243
296.15	1.01325	0.004	0.4747	0.076	0.079	0.038	0.240	0.234	0.211
296.15	1.01325	0.005	0.4362	0.064	0.066	0.032	0.210	0.205	0.187
296.15	1.01325	0.006	0.4041	0.056	0.057	0.027	0.188	0.184	0.168
296.15	1.01325	0.007	0.3770	0.049	0.051	0.024	0.170	0.166	0.153
296.15	1.01325	0.008	0.3537	0.044	0.046	0.021	0.155	0.152	0.141
296.15	1.01325	0.009	0.3333	0.040	0.041	0.019	0.143	0.140	0.130
296.15	1.01325	0.01	0.3155	0.037	0.038	0.018	0.133	0.130	0.122

(C) 1-Propanol – acetone

Table 61: Dilute acetone – 1-propanol model data from Figure 81 on page 139

	Scheme	2B-N	2B-N	3B-N	3B-N
	1PrOH association params	[2230, 0.0626]	[2230, 0.815]	[2230, 0.815]	[2655, 0.815]
	AcO association params	[100, 0.001]	[100, 0.001]	[100, 0.001]	[100, 0.001]
T [K]	P [bar]	x_{1PrOH}	X_{1PrOH}		
296.15	1.01325	1.00E-10	0.836	0.586	0.5864	0.4066
296.15	1.01325	0.001	0.769	0.340	0.2269	0.0728
296.15	1.01325	0.002	0.7131	0.249	0.1412	0.0398
296.15	1.01325	0.003	0.6663	0.199	0.102	0.027
296.15	1.01325	0.004	0.6263	0.167	0.080	0.021
296.15	1.01325	0.005	0.5916	0.144	0.066	0.017
296.15	1.01325	0.006	0.5611	0.127	0.056	0.014
296.15	1.01325	0.007	0.5341	0.114	0.048	0.012
296.15	1.01325	0.008	0.5099	0.103	0.043	0.011
296.15	1.01325	0.009	0.4882	0.095	0.038	0.009
296.15	1.01325	0.01	0.4684	0.088	0.035	0.008

(D) 2-Propanol – acetone

Table 62: Modelling data for 2-propanol - acetone with modified sPC-SAFT parameters

		Scheme	2B-N	2B-N	2B-N	2B-N	2B-(-)	2B-N	2B-2N
		1PrOH association params	[2231, 0.0246]	[2231, 0.809]	[2231, 0.809]	[2231, 0.809]	[2421, 0.492]	[2050, 0.825]	[2050, 0.825]
		AcO association params	[100, 0.001]	[100, 0.001]	[500, 0.001]	[1, 0.001]	[0, 0]	[145, 0.001]	[50, 0.001]
T [K]	P [bar]	x_{1PrOH}			X_{1PrOH}				
296.15	1.01325	1.00E-10	0.865	0.536	0.3683	0.5777	1.000	0.631	0.502
296.15	1.01325	0.001	0.817	0.272	0.2183	0.2837	0.412	0.426	0.362
296.15	1.01325	0.002	0.7750	0.191	0.1609	0.1971	0.274	0.331	0.289
296.15	1.01325	0.003	0.7381	0.149	0.129	0.153	0.208	0.273	0.243
296.15	1.01325	0.004	0.7052	0.123	0.109	0.126	0.169	0.234	0.211
296.15	1.01325	0.005	0.6757	0.106	0.094	0.108	0.143	0.205	0.187
296.15	1.01325	0.006	0.6490	0.092	0.083	0.094	0.124	0.184	0.168
296.15	1.01325	0.007	0.6246	0.082	0.075	0.084	0.110	0.166	0.153
296.15	1.01325	0.008	0.6024	0.074	0.068	0.076	0.099	0.152	0.141
296.15	1.01325	0.009	0.5819	0.068	0.062	0.069	0.090	0.140	0.130
296.15	1.01325	0.01	0.5630	0.062	0.057	0.063	0.082	0.130	0.122

10.4 Curve-fitting models

An ethanol – *n*-hexane data set is used to the various spectral profiles used for modelling liquids. The same data set (and the modelling procedures used in this section) is then also used to verify the linearity of the MCT detector. The data were baselined using the OMNIC *Autobaseline* function, before various profiles were fitted. Consider Figure 84:

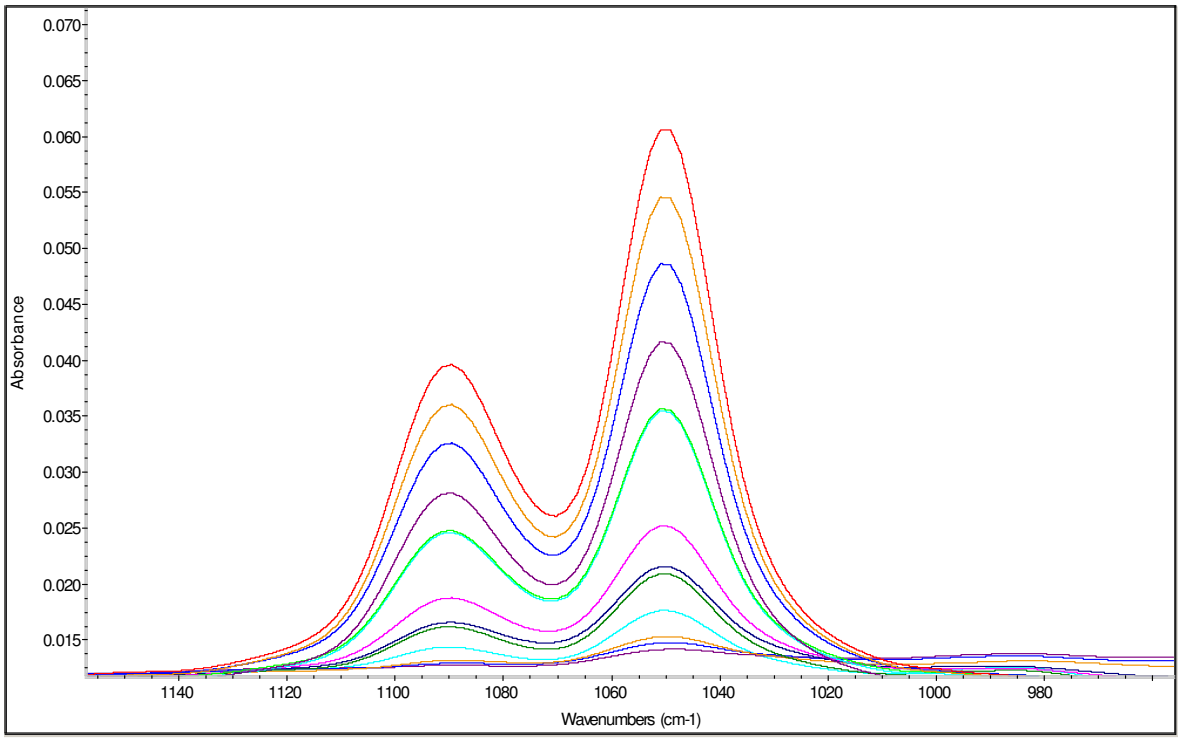

Figure 84: C-O bands for increasing ethanol concentration in *n*-hexane

According to Coates (2000), the C-O stretch band of a primary alcohol is located around 1050 cm^{-1}. Figure 84 provides the perfect opportunity to test the curve-fitting procedures. The area data can then also be used to test for Beer-law adherence

The two peaks at 1050 cm^{-1} and 1090 cm^{-1} are then fitted with the following functions:

- 2 Gaussian curves with a constant (2G+C)
  - $$A'\left(\tilde{\nu}\right) = A'_{1\max} \exp\left[-b_1^2\left(\tilde{\nu}-\tilde{\nu}_{1_{\max}}\right)^2\right] + A'_{2\max} \exp\left[-b_2^2\left(\tilde{\nu}-\tilde{\nu}_{2_{\max}}\right)^2\right] + C$$
- 2 Lorentzian curves with a constant (2L+C)
  - $$A'\left(\tilde{\nu}\right) = \frac{A'_{1\max}}{1+a_1^2\left(\tilde{\nu}-\tilde{\nu}_{1_{\max}}\right)^2} + \frac{A'_{2\max}}{1+a_2^2\left(\tilde{\nu}-\tilde{\nu}_{2_{\max}}\right)^2} + C$$

- 2 Gauss-Lorentz product curves with a constant (2GL+C)

$$A'(\tilde{\nu}) = \frac{A'_{1\max}}{1+a_1^2\left(\tilde{\nu}-\tilde{\nu}_{1_{\max}}\right)^2}\exp\left[-b_1^2\left(\tilde{\nu}-\tilde{\nu}_{1_{\max}}\right)^2\right]$$

$$+\frac{A'_{2\max}}{1+a_2^2\left(\tilde{\nu}-\tilde{\nu}_{2_{\max}}\right)^2}\exp\left[-b_2^2\left(\tilde{\nu}-\tilde{\nu}_{2_{\max}}\right)^2\right]+C$$

The equations are fitted with all equation constants as free parameters, using a trust region method.

10.4.1 2G+C model

The 2G+C fit is shown in Figure 85.

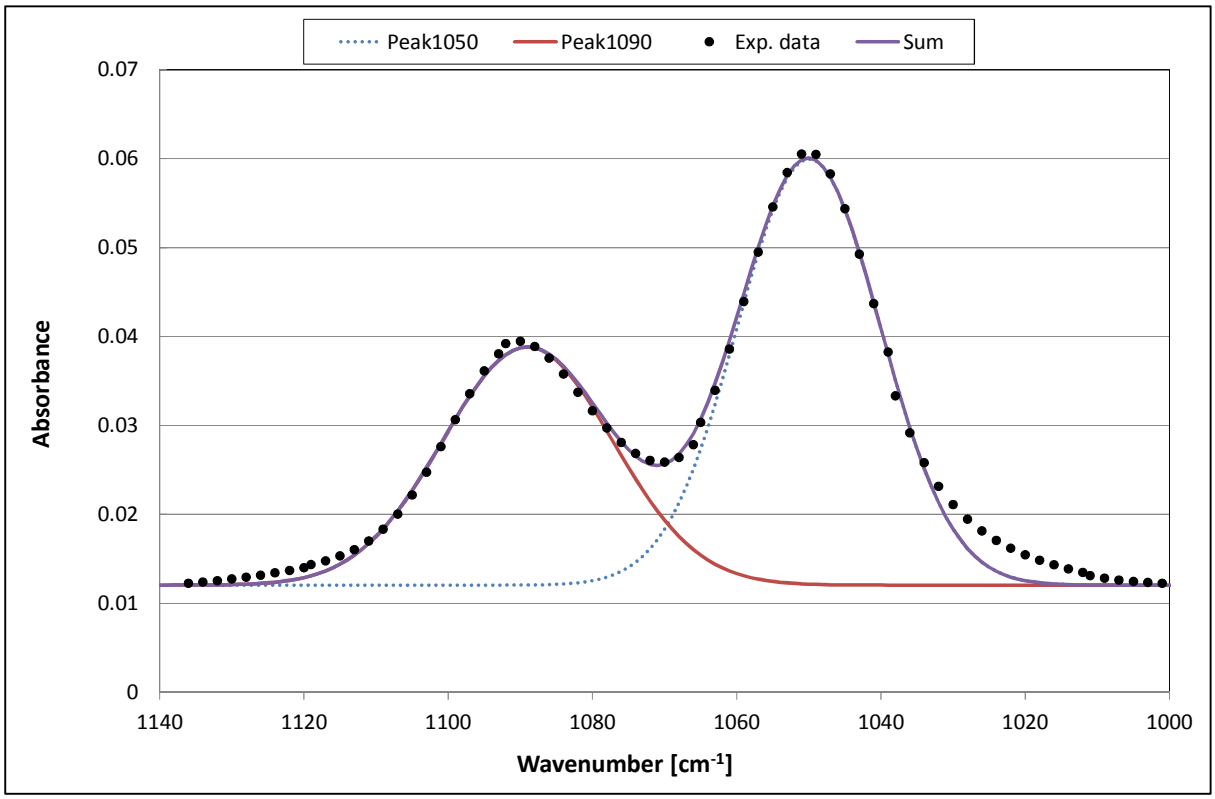

Figure 85: Two Gaussian curves fitted to the C-O stretch band of a 16.5 mol% ethanol in *n*-hexane mixture

The data were fitted from 960 – 1160 cm^{-1}. The adjusted-R^2 value is calculated as 0.9936. The Gaussian distribution succeeds in describing the convoluted area of the double peak, but fails to describe the general nature of the peaks as is seen on the edges of Figure 85. The centre of the 1090 cm^{-1} peak is also not fitted exactly, with the model predicting the peak centre at 1089 cm^{-1}.

10.4.2 2L+C model

When two Lorentz peaks are fitted, the adjusted-R^2 of 0.9963 is obtained, and the peak shape fit is visibly better. This can be seen in Figure 86.

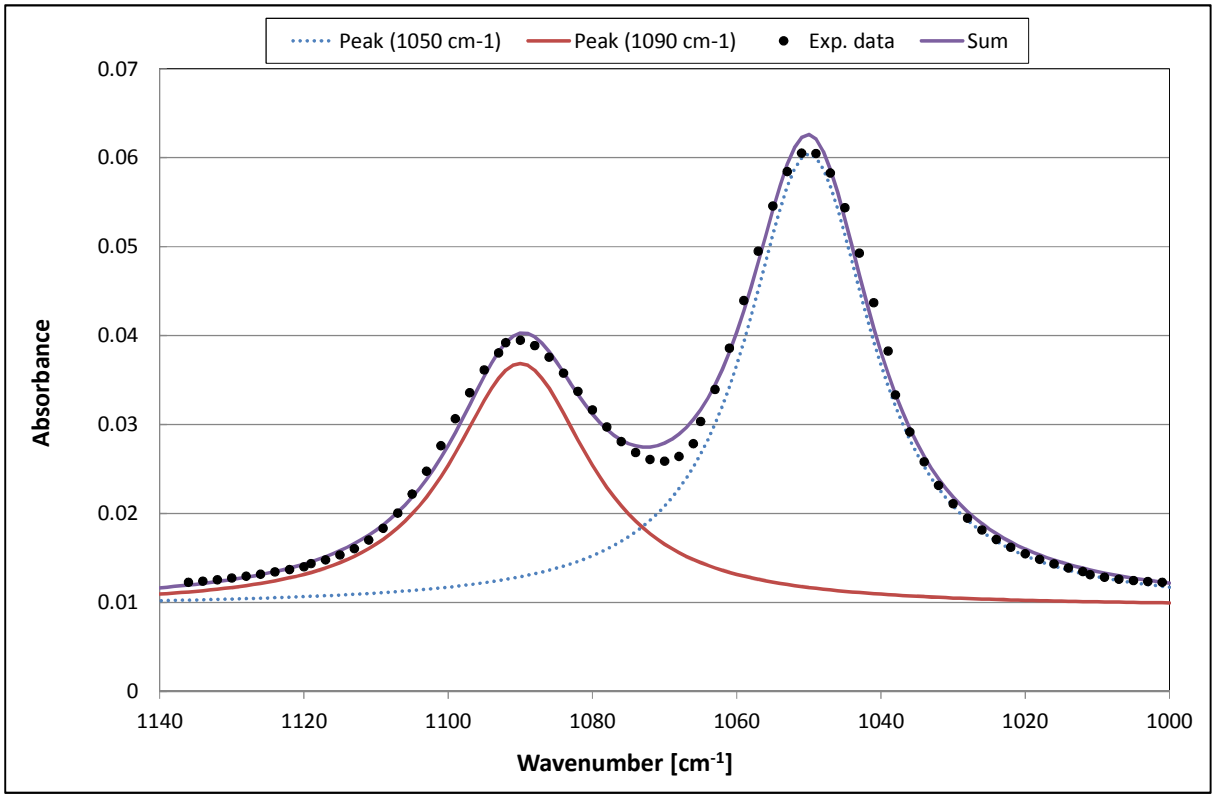

Figure 86: Two Lorentzian curves fitted to the C-O stretch band of a 16.5 mol% ethanol in *n*-hexane mixture

The Lorentzian functions do however not predict the overlap region as well as the Gaussian curves and there is a slight over-prediction on the 1050 cm^{-1} peak height.

10.4.3 2GL+C model

The product curve model is fitted in Figure 87.

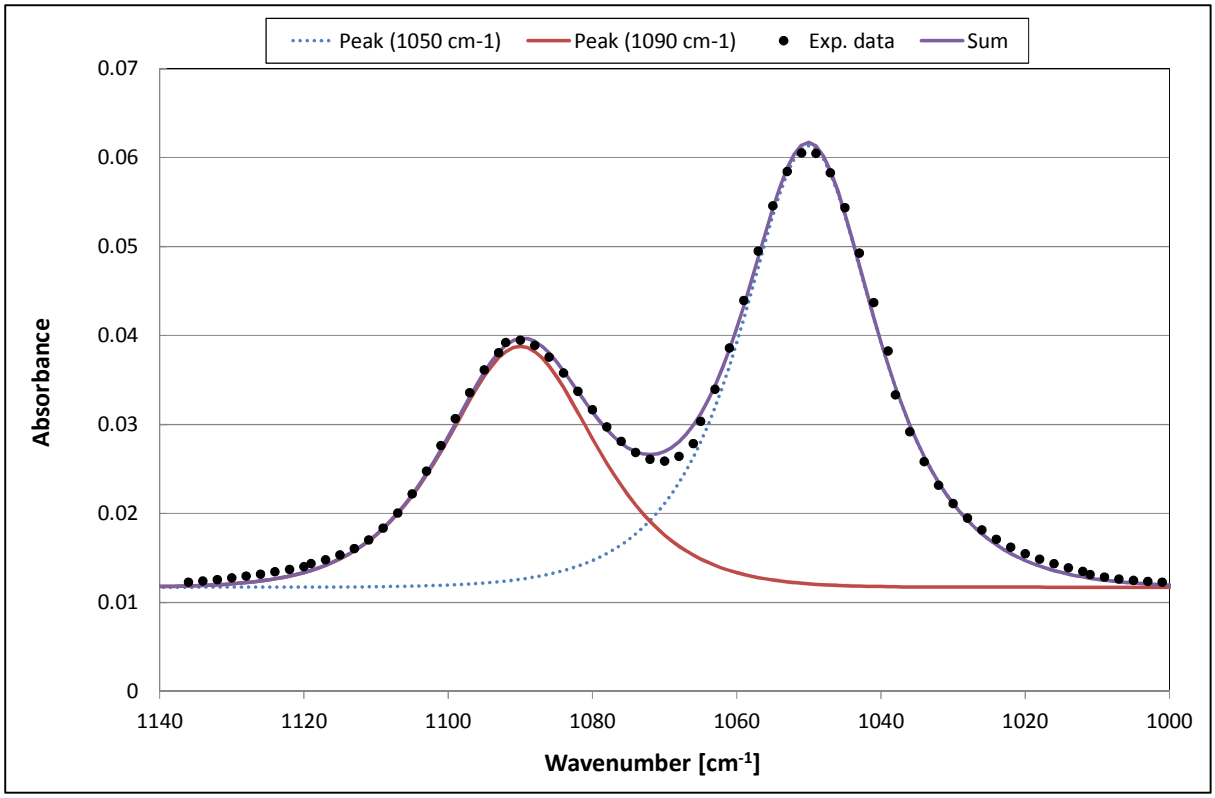

Figure 87: Gauss-Lorentz product curves fitted to the C-O stretch band of a 16.5 mol% ethanol in *n*-hexane mixture

The product curves achieve the best results, with an adjusted-R^2 value of 0.9972. The model simultaneously accounts for the broadening peak shape as well as the overlap area. Peak height and position are accurately modelled.

10.5 Linearity test for ATR mode with the MCT detector

The MCT detector response linearity in ATR mode is tested here. The test is done for an ethanol-*n*-hexane system, where pure *n*-hexane is used as the background of the spectrum, with progressively higher concentrations ethanol. The C-O stretch peak in Figure 84 is used for this calibration, as it is unaffected by hydrogen bonding (unlike the O-H stretch which is of interest in this investigation). To test the detector linearity, a calibration curve is drawn up using the absorbance areas calculated from the peak-fitting models.

By integrating the fitted curves for each data point, the absorbance areas can then be calculated. The integrals of the 2G+C and 2L+C models can be calculated using EQ 2.86 with α set to 0 for the Lorentzian curves and or 1 for the Gaussian curves. The integral of the product curve cannot be integrated analytically and must thus be calculated numerically. It should be noted that for the lower concentrations, it was necessary to fit linear trend (rather than a constant one) along with the

distribution functions in order to achieve a desirable fit. The models are accordingly denoted as 2Gmx+C, 2Lmx+C and 2GLmx+C. An indication of the fitting-accuracy of the various models is given by Table 63.

Table 63: Adjusted-R^2 values for various models fitted to C-O stretch band spectra

Mole fraction	Adjusted-R^2					
	2G+C	2L+C	2GL+C	2Gmx+C	2Lmx+C	2GLmx+C
0.1652	0.9924	0.9958	0.9973			
0.1466	0.9939	0.9958	0.9993			
0.1262	0.994	0.996	0.9993			
0.1041	0.9946	0.9956	0.9992			
0.0816	0.9934	0.9962	0.9991	0.9942	0.996	0.999
0.043	0.991	0.9962	0.9986	0.9933	0.9962	0.9986
0.0305	0.9877	0.9953	0.9976	0.9929	0.9961	0.9984
0.02	0.9933	0.9863	0.9953	0.9902	0.9851	0.9966
0.009	0.9126	0.9381	0.9525	0.9881	0.9789	0.9909
0.0064	0.7938	0.8209	0.8397	0.9874	0.9813	0.9875
0.0041	0.6147	0.6805	0.6369	0.9717	0.9553	0.9521

In Table 63 it can be seen that the additional parameter m only begins to make a marked difference somewhere in the range $0.009 < X_{ethanol} < 0.02$. At mole fractions of 0.009 and less, the additional parameter is required in order to account for the slope observed in the data. What is also of interest is that the Gaussian model (2Gmx+C) achieves a better fit at the lowest concentrations. The GL functions however provide the best fits over the greatest range.

Once all the absorbance areas determined, a Beer plot of the spectral absorption versus concentration could be made. A linear trend was fitted to the data with an adjusted-R^2 value of 0.9987 for the curve $A = 9.3315 \cdot v$ seen in Figure 88.

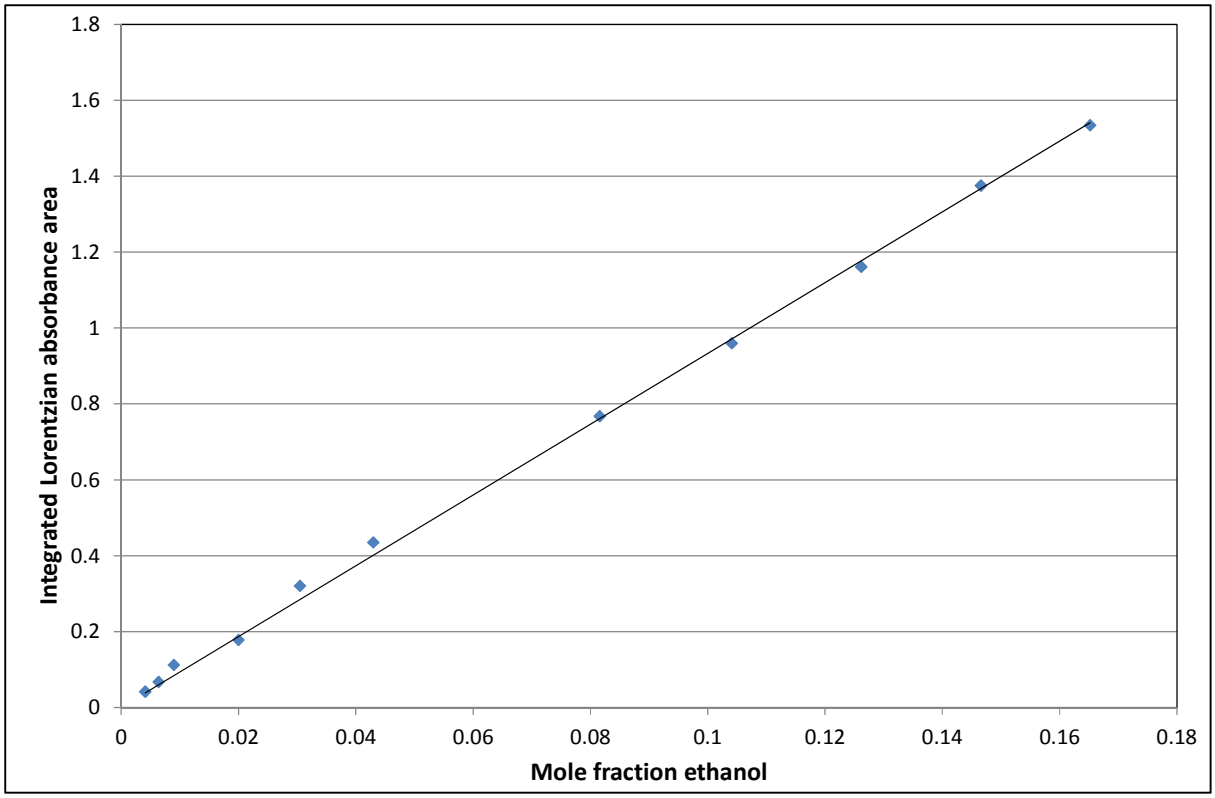

Figure 88: Beer plot for the MCT detector on the C-O stretch band (1050 cm^{-1}) of ethanol in n-hexane

From Figure 88 it is seen that the linearity of the Beer plot is very good. The larger errors are toward the lower end of the concentration scale, which is to be expected as concentration determination becomes more difficult and signal noise has a greater effect. The result is expected since the absorbance is well below the prescribed limit of 0.7AU but is nonetheless very satisfactory. These data suggests that the MCT detector achieves a linear response for absorbance versus concentration and thus the system can be used to determine the monomer fractions in the O-H stretch band.

10.6 Discussion of literature monomer fraction data for the ethanol – *n*-hexane system

Asprion *et al*. (2001) provide their A/d data as a function of mole fraction. These data were used here to re-calculate the adsorption coefficients and monomer fractions.

Table 64: Re-calculated monomer percentages for the data of Asprion *et al.* (2001)

EtOH mol%	A/d [cm^{-2}]			Calculated % molarities			% monomer			
	Mono	Dimer	Poly	Mono	Dimer	Poly	As	Beer	Err^2	% AErr
0.101	11.1	1.24	0.97	0.078	0.012	0.000	86.5	77.2	0.0001	10.79
0.2	20.6	3.41	2.24	0.145	0.032	0.001	81.3	72.3	0.0005	11.04
0.299	29.8	5.57	7.88	0.209	0.053	0.003	78.9	70.0	0.0011	11.26
0.402	38.7	11.2	33.5	0.272	0.106	0.014	69.4	67.6	0.0001	2.56
0.597	52.5	19.7	98.3	0.369	0.187	0.040	61.9	61.7	0.0000	0.23
0.8	61.9	28.0	272	0.435	0.266	0.111	53.6	54.3	0.0001	1.39
1.196	77.2	41.8	667	0.542	0.397	0.271	44.8	45.3	0.0002	1.18
1.6	85.1	57.6	1210	0.597	0.547	0.492	36.5	37.3	0.0013	2.27
3.198	109	96.0	3880	0.765	0.912	1.58	23.5	23.9	0.0032	1.76
6.4	132	137	9980	0.927	1.301	4.06	14.7	14.5	0.0133	1.80
10.02	157	227	17500	1.102	2.156	7.11	10.6	11.0	0.1235	3.51
12.8	148	197	23500	1.039	1.871	9.55	8.3	8.1	0.1142	2.64
16.03	165	253	30800	1.158	2.403	12.52	7.2	7.2	0.0026	0.32

In Table 64, the molar percentage of ethanol and area-over-pathlength data is taken from Asprion *et al.* (2001) and is used to derive new absorption coefficients. The “As” monomer percentage is calculated using as a fraction of the total calculated % molarities. The second monomer fraction (referred to as “Beer” in the table) is calculated using the Beer law directly with the monomer peak area and absorption coefficient. The two sets of calculated monomer percentages differ at low concentration values, but give almost identical results for ethanol molar percentages above 0.5%.

EQ 2.83 is used to calculate the squared-error term, which is minimized to obtain the absorption coefficients. The SSE is calculated as 0.2609 with a %AAD of 3.9%. The following absorption coefficients were obtained:

- Monomer: 142.4 cm^{-2} / mol%
- Dimer: 105.3 cm^{-2}/ mol%
- Polymer: 2460 cm^{-2}/ mol%

When minimizing for average absolute percentage error, the following absorption coefficients are obtained at a minimum SSE of 0.316 and a %AAD error of 1.7%:

- Monomer: 111.6 cm^{-2} / mol%
- Dimer: 217.4 cm^{-2} / mol%
- Polymer: 2223 cm^{-2} / mol%

The monomer absorption coefficient can be compared to that calculated directly from the Beer law, using the single calibration method of von Solms. Here α_{mono} = 109.9 cm^{-2} / mol%, which is very similar to the value obtained when minimising the %AAD. Asprion *et al.* (2001) give an absorption coefficient of 1529.8 cm^{-2} L / mol which, assuming very dilute ideal mixture, is converted to 116.3 cm^{-2} / mol%. One may naturally assume that since three of these calculated coefficients are relatively close together, that they may be the more correct values to use. However, a very interesting discovery is made upon comparing the newly calculated As-data to sPC-SAFT model predictions.

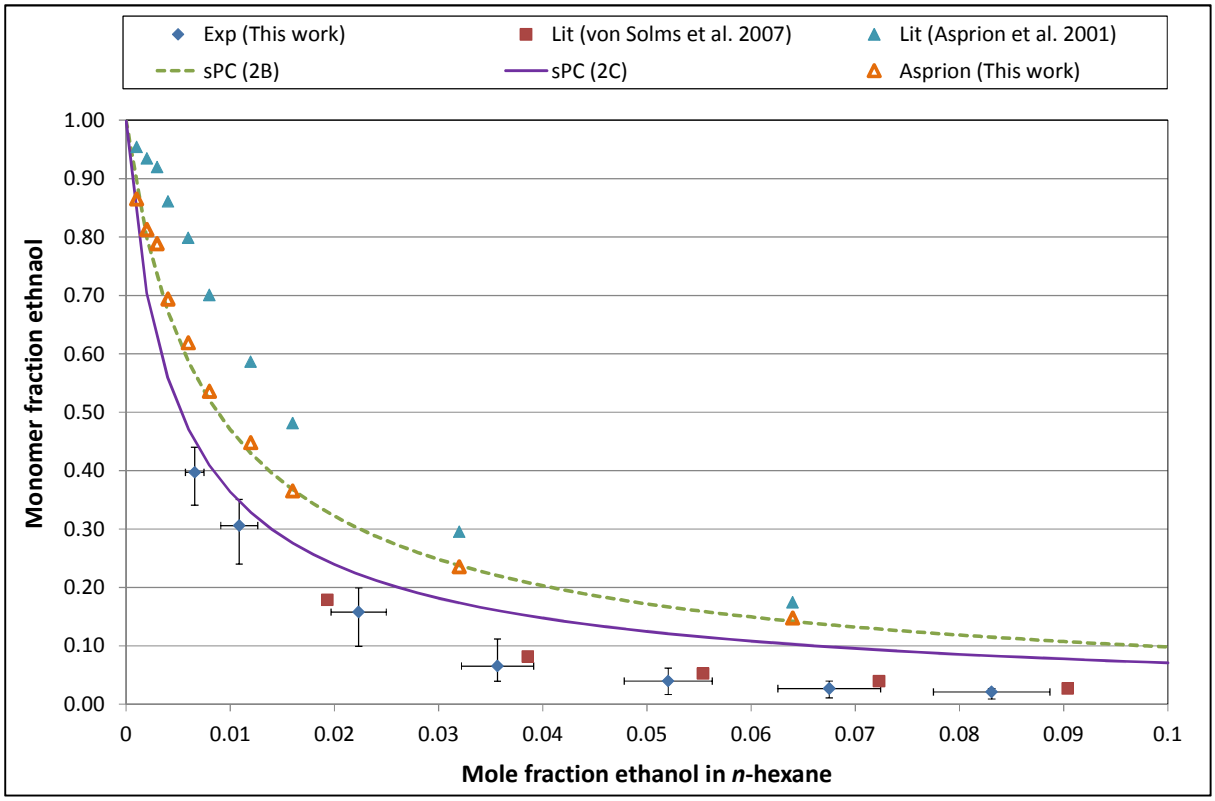

Figure 89: Various data sets for ethanol monomer fractions in *n*-hexane

Figure 89 shows the two literature data sets for the monomer fractions of ethanol in *n*-hexane, as well as the temperature adjusted data set calculated in Chapter 4.2. Also included, are the data

calculated under the head "As % monomer" in Table 64 and two sPC-SAFT model predictions (incorporating the 2B and 2C association schemes). Most interestingly, the modified Asprion data calculated in this work lies almost exactly on the model prediction for the sPC-SAFT-2B equation of state. This raises some interesting questions regarding the fitting procedures. Using the exact same absorption area, two relatively different monomer fraction data sets are obtained. The difference most likely arises due to the incorporation of thermodynamic predictions into the fitting algorithm.

Differences in calculated monomer fractions are also caused by the spectral processing. A subset of the ethanol – *n*-hexane was manipulated using the Autobaseline function in the OMNIC software package. Using the "eye" test, linear baselines are added as necessary. By following Asprion's fitting method, without incorporating thermodynamic model predictions, the data in Figure 90 can be obtained.

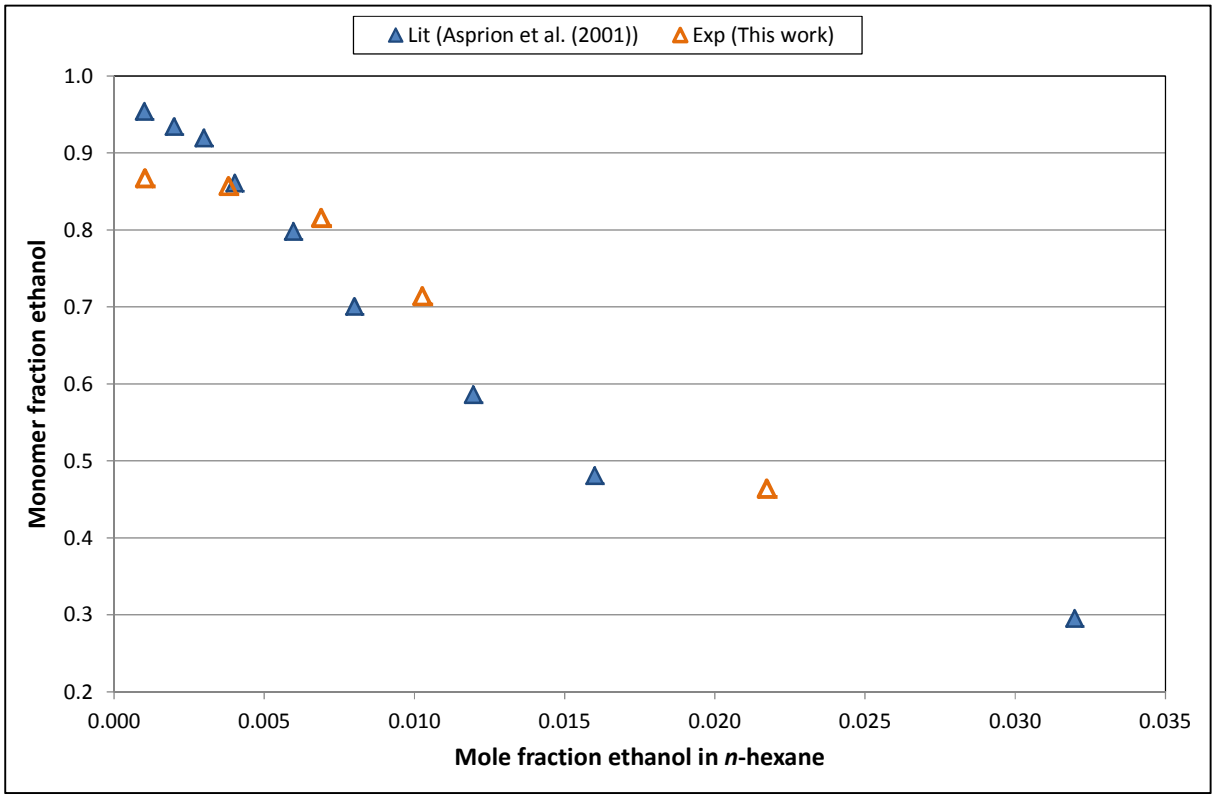

Figure 90: Monomer fraction data obtained by modified spectral processing procedures in for comparison with the data of Asprion *et al.* (2001)

Figure 90 shows that it is possible to obtain data similar to that given by Asprion *et al.* (2001). Both data sets have a characteristic tail-off towards ethanol mole fractions of zero. This curve shape is somewhat counter-intuitive as one could expect monomers to decrease exponentially with an increased concentration of ethanol molecules. This shape may be an artefact of the spectral

processing procedures whereby some significant portion of noise has been incorporated with the processed monomer signal. This would result in a relatively constant error being added to the area terms used in the regression. By adjusting the spectral processing, Figure 91 is developed.

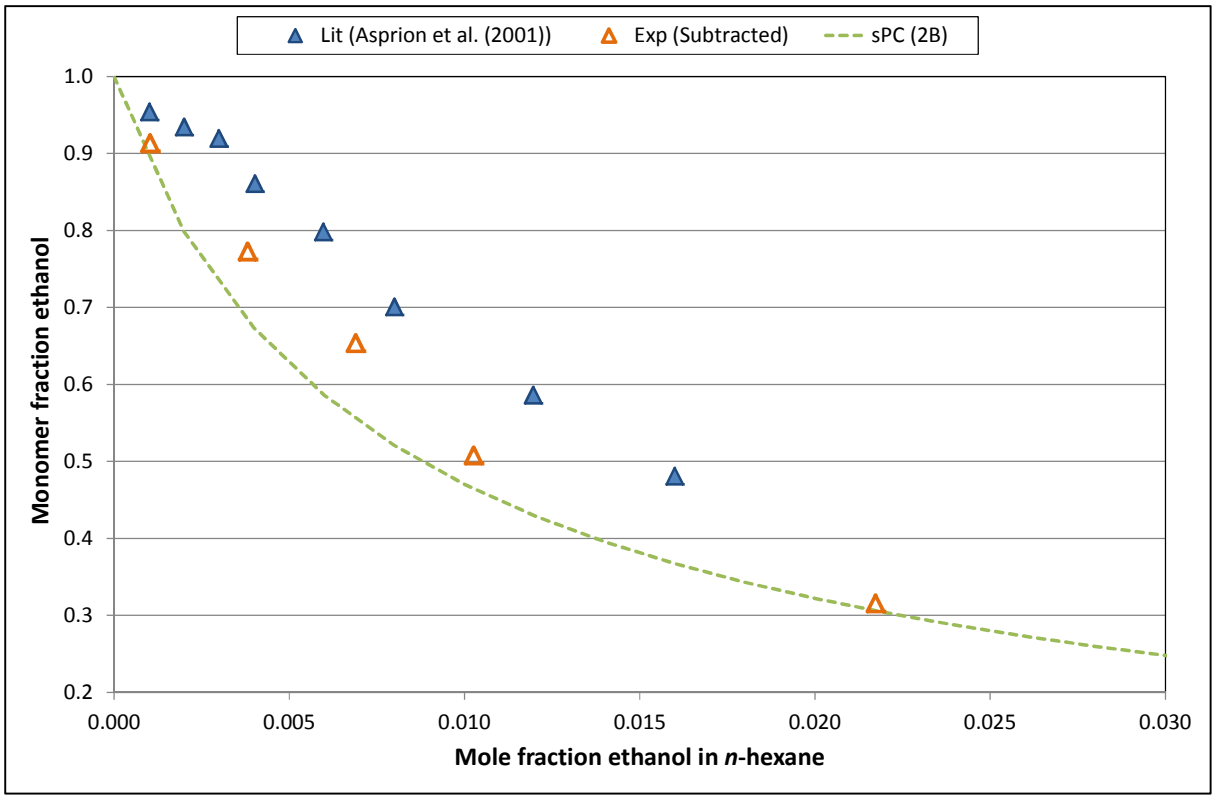

Figure 91: Noise-subtracted, re-fitted ethanol - *n*-hexane monomer fractions

Here the experimental data predict lower monomer fractions than that of Asprion *et al.* (2001) in a manner which is relatively similar to that observed in Figure 89. The newly calculated monomer fractions relatively closely follow the sPC-SAFT-2B association model. There is however still a degree of tailing-off (flattening out) as the ethanol mole fraction tends to zero and this may be an inherent short-coming of spectroscopy (or at least the apparatus as used) at the very dilute concentrations.

The data and calculations here in Chapter 10.6 and also in Chapter 4.2 show the impact of the spectral processing and curve-fitting procedures on the final monomer fraction calculations. It is most likely these procedures which have resulted in the observed discrepancy in literature data, rather than any major differences in the raw spectra.

10.7 Sample presentation vessel design

10.7.1 O-ring groove to seal on the probe

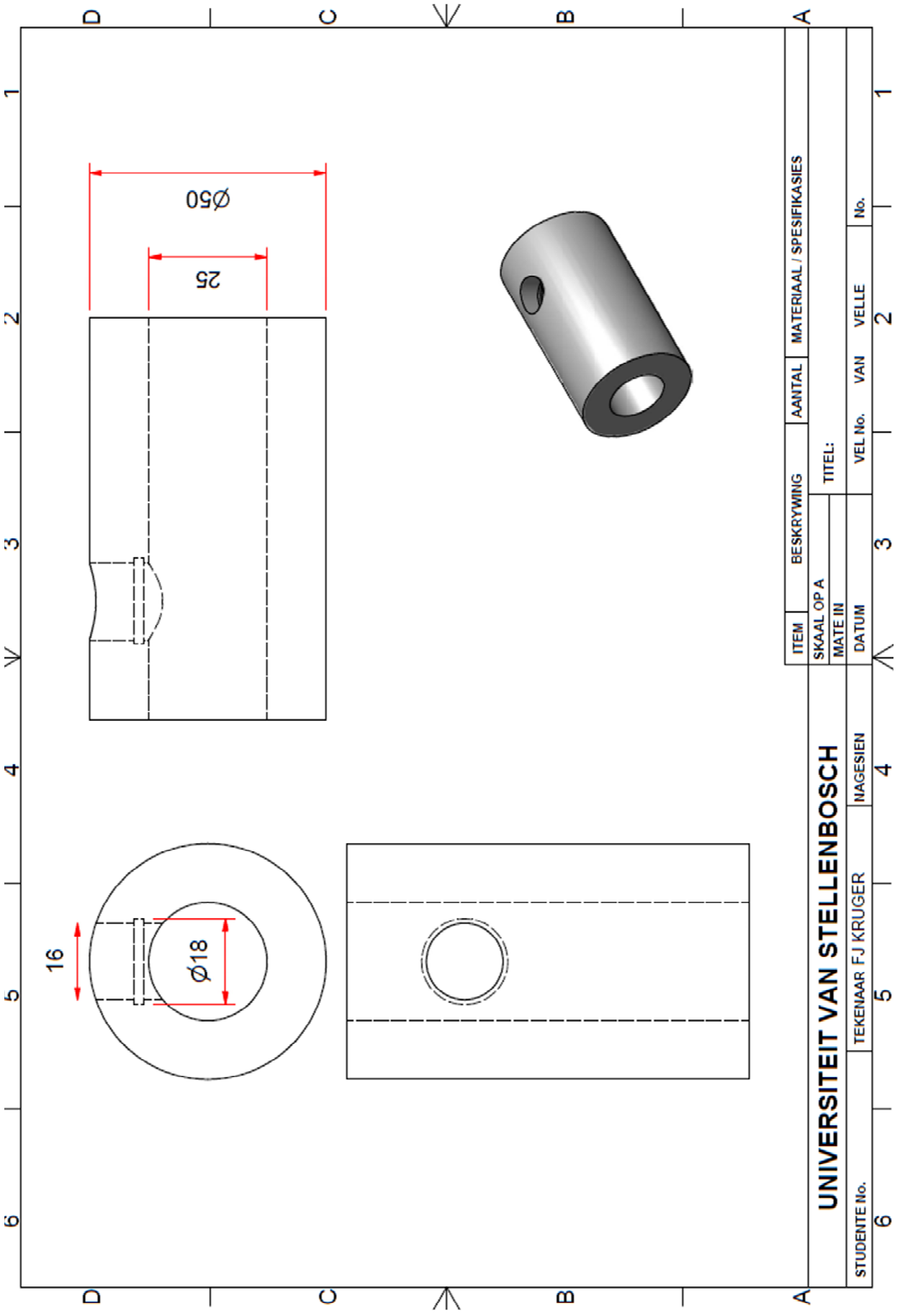

10.7.2 The main vessel section

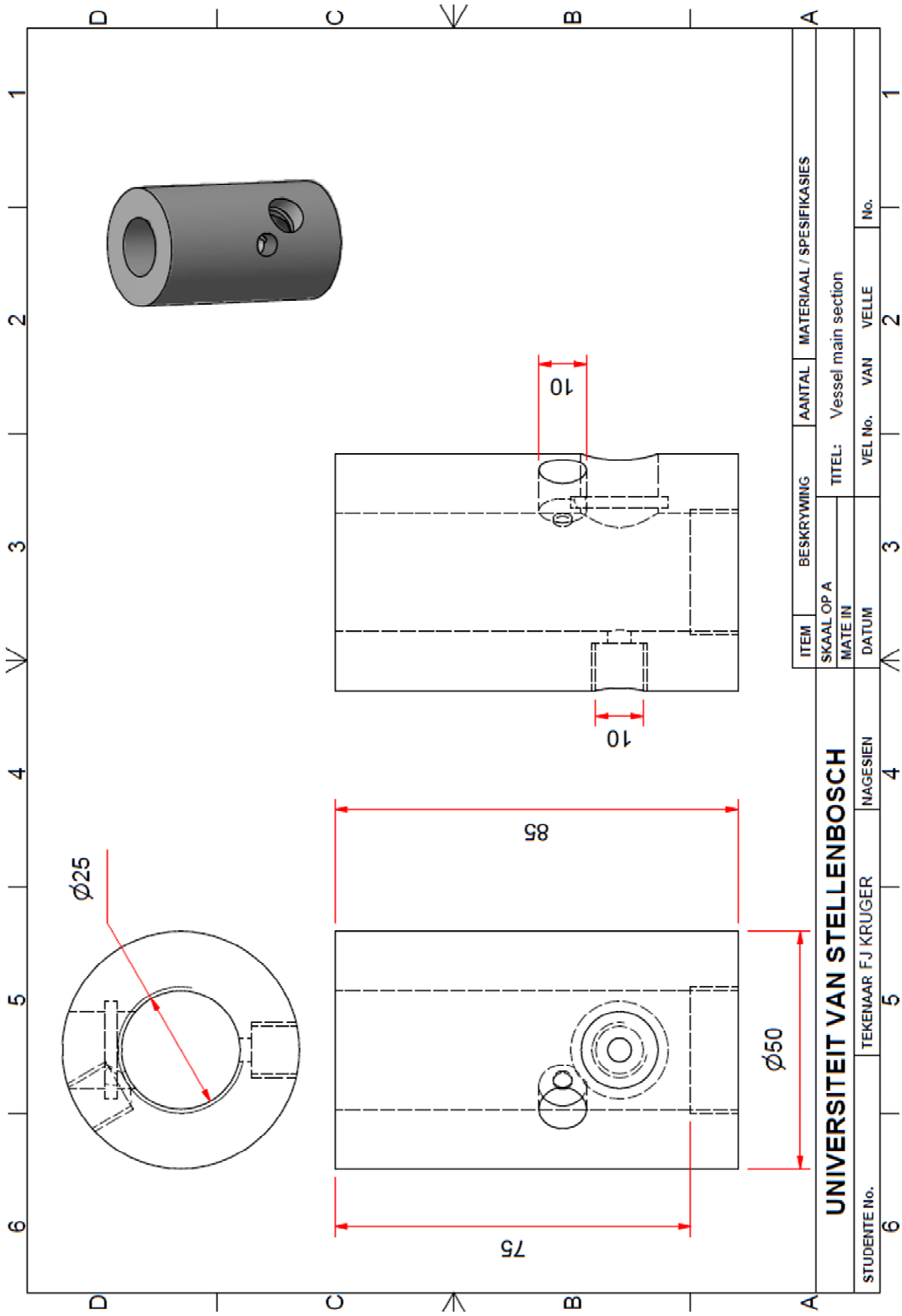

10.7.3 Vessel internals

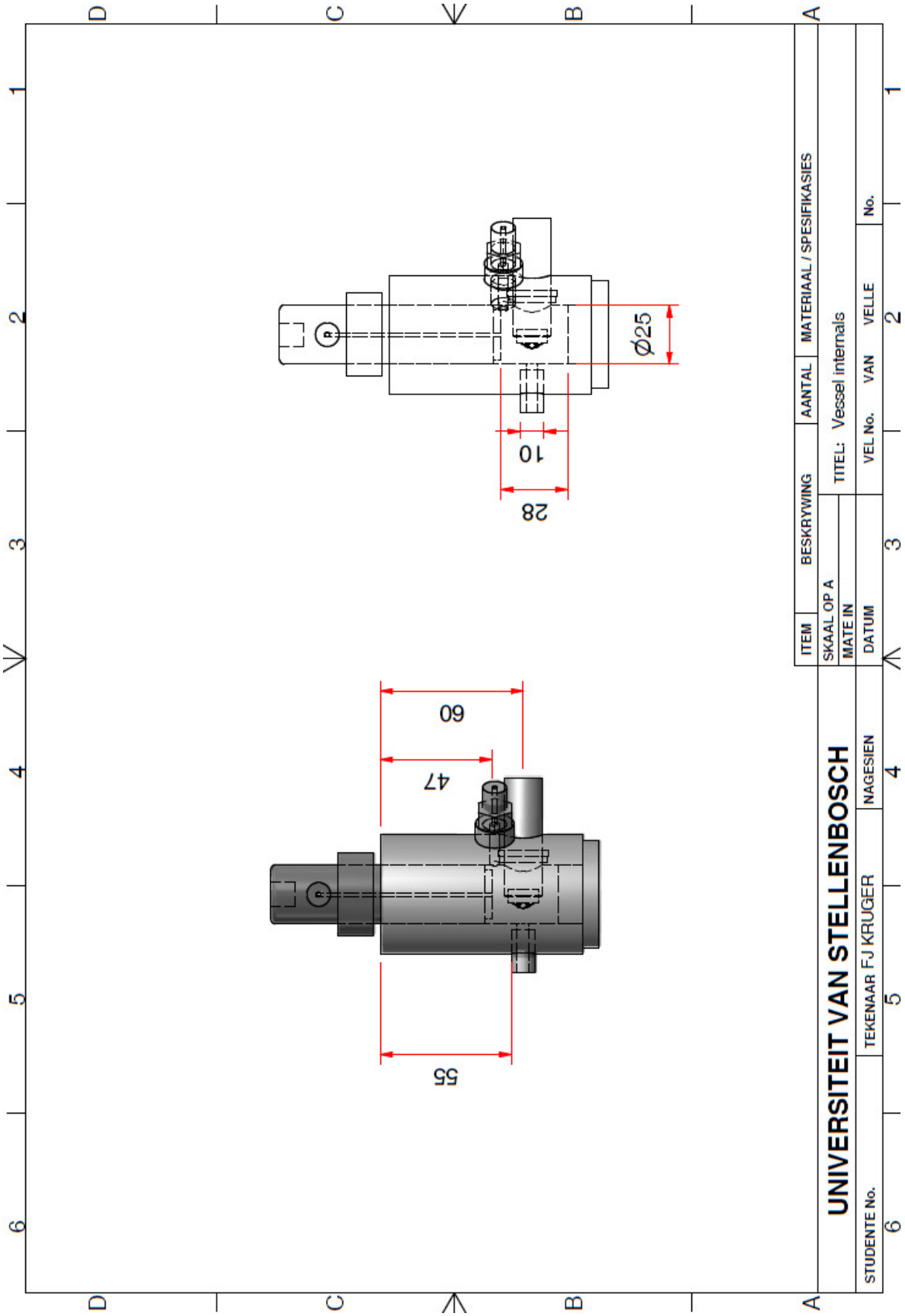

10.7.4 The final assembly

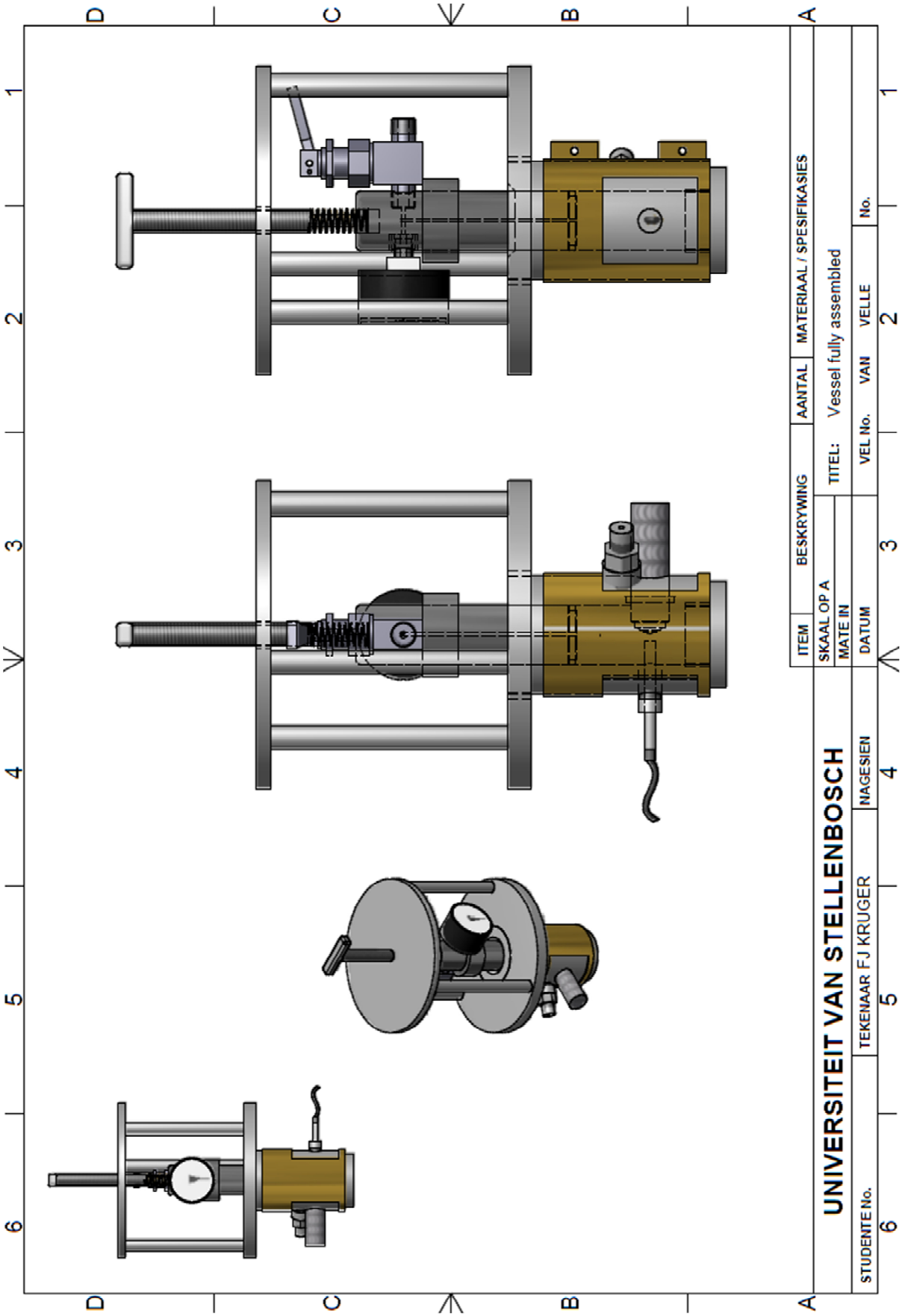

10.8 Methodology for the determination of new EoS parameters using a 2B-alcohol 1N-acetone model within the sPC-SAFT framework

With the system temperature (T) and pressure (P) known, a solution for the volume is determined via an iterative process in which the system volume is manipulated until the calculated pressure is equal to the known system pressure. The calculated pressure is determined by (de Villiers, 2011):

$$P = -RT\left(\frac{\partial F}{\partial V}\right)_{T,n} + \frac{nRT}{V}$$

EQ 10.1

Here F is given as the sum of reduced residual Helmholtz energy terms for the system. First order partial derivatives from each of the hard sphere, chain and dispersion are given by de Villiers (2011) with only the partial derivative for the association term developed here. The following equations are required and developed for the determination of the association term and partial derivatives:

The reduced density partial derivative is calculated by:

$$\eta = \frac{N_{AV} \cdot \pi \cdot n \cdot d_{mix}^3}{6V \cdot m_{mix}}$$

EQ 10.2

$$\frac{\partial \eta}{\partial V} = -\frac{\eta}{V}$$

EQ 10.3

The radial distribution (EQ 2.42 on page 16) is derived in terms of the reduced density:

$$\frac{\partial g}{\partial V} = \frac{\left(-0.5(1-\eta)^3 + 3(1-0.5\eta)(1-\eta)^2\right)}{(1-\eta)^6}$$
$$= \frac{-0.5(1-\eta) + 3(1-0.5\eta)}{(1-\eta)^4}$$

EQ 10.4

With association strength as a linear function of the radial distribution function, the partial derivative is given by:

$$\frac{\partial \Delta}{\partial g} = \frac{\Delta}{g}$$

EQ 10.5

The volume partial derivative of association strength is then given by a simple application of the chain rule:

$$\frac{\partial \Delta}{\partial \mathrm{V}} = \frac{\partial \Delta}{\partial \mathrm{g}} \cdot \frac{\partial g}{\partial \eta} \cdot \frac{\partial \eta}{\partial \mathrm{V}}$$

EQ 10.6

10.8.1 Analytical solution of the association term

The basic building blocks are now available to calculate the association term given by EQ 2.43 and EQ 2.44 and the partial derivatives thereof:

$$\tilde{a}^{assoc} = \sum_i x_i \left[\sum_{A=1}^{M} \left[\ln X^{A_i} - \frac{X^{A_i}}{2} \right] + \frac{M_i}{2} \right] = F^{assoc}$$

and

$$X^{A_i} = \left(1 + N_{AV} \sum_j \sum_{B_j} \rho_j X^{B_j} \Delta^{A_i B_j} \right)^{-1}$$

Since only one association model is evaluated here, the analytical approach proposed by Kraska (1998) is used. A solution is achieved as follows:

Kraska's Model II describes component 1 with sites A^+ and B^- with component having a single negative site, C^-. This model is akin to the 2B-alcohol 1N-acetone model described in this work. Continuing the development by accounting for the possible site-site interactions, three equations are obtained for the fraction of alcohol/acetone not bonded at sites A, B and C:

$$X_A = \frac{1}{1 + \frac{1}{V}\left(x_1 X_B \Delta^{AB} + x_2 X_C \Delta^{AC} \right)}$$

EQ 10.7

$$X_B = \frac{1}{1 + \frac{1}{V} x_1 X_A \Delta^{AB}}$$

EQ 10.8

$$X_C = \frac{1}{1 + \frac{1}{V} x_1 X_A \Delta^{AC}}$$

EQ 10.9

Note that the number density has been replaced by 1/V, with Avogadro's number assimilated into the association strength as compared to EQ 2.44 above. By using a basis of 1 mole mixture, the x_i

notation of Kraska (1998) becomes equivalent to n_i used in this work. Kraska goes on to rearrange and combine the above equations to yield an analytically solvable cubic polynomial in X_C:

$$X_C^3 + pX_C^2 + qX_C + r = 0$$

EQ 10.10

with

$$p = \frac{\left(\Delta^{AB} - \Delta^{AC}\right) - \frac{n_1}{V}\left(\Delta^{AC}\right)^2 + \frac{n_2}{V}\Delta^{AC}\left(\Delta^{AC} - 2\Delta^{AB}\right)}{\frac{n_2}{V}\Delta^{AC}\left(\Delta^{AB} - \Delta^{AC}\right)}$$

EQ 10.11

$$q = \frac{\Delta^{AC} - 2\Delta^{AB} + \frac{n_2}{V}\Delta^{AC}\Delta^{AB}}{\frac{n_2}{V}\Delta^{AC}\left(\Delta^{AB} - \Delta^{AC}\right)}$$

EQ 10.12

$$r = \frac{\Delta^{AB}}{\frac{n_2}{V}\Delta^{AC}\left(\Delta^{AB} - \Delta^{AC}\right)}$$

EQ 10.13

EQ 10.10 can be solved for analytically by employing Cardano's method, usually yielding only one valid solution such that $X_C \in [0, 1]$. Cardano's method revolves around solving a depressed cubic removing the squared term via a substitution and not covered in depth here. The equations necessary for the solution of EQ 10.10 are given here as derived from the method described by Press *et al.* (1988, p.157):

$$Q = \frac{p^2 - 3q}{9}$$

EQ 10.14

$$R = \frac{2p^3 - 9pq + 27r}{54}$$

EQ 10.15

10.8.2 Case I: Three real solutions

A cubic polynomial will always have at least one real root, but when $Q^3 - R^2 \geq 0$, three real roots are obtained by using:

$$\theta = \arccos\left(\frac{R}{\sqrt{Q^3}}\right)$$

EQ 10.16

$$X_{C1} = -2\sqrt{Q}\cos\left(\frac{\theta}{3}\right) - \frac{p}{3}$$

EQ 10.17

$$X_{C2} = -2\sqrt{Q}\cos\left(\frac{\theta + 2\pi}{3}\right) - \frac{p}{3}$$

EQ 10.18

$$X_{C3} = -2\sqrt{Q}\cos\left(\frac{\theta + 4\pi}{3}\right) - \frac{p}{3}$$

EQ 10.19

10.8.3 Case II: One real solutions

If however $Q^3 - R^2 < 0$, the one real root is given by:

$$X_C = -sign(R)\left(S + \frac{Q}{S}\right) - \frac{p}{3}$$

EQ 10.20

with

$$sign(R) = \begin{cases} +1 & if\ R > 0 \\ -1 & if\ R < 0 \\ 0 & if\ R = 0 \end{cases}$$

EQ 10.21

and

$$S = \sqrt[3]{\sqrt{R^2 - Q^3} + |R|}$$

EQ 10.22

10.8.4 Calculation of volume partial derivative of F^{Assoc}

Once a valid solution for X_C is obtained, it can be substituted into EQ 10.9 to solve for X_A and then into EQ 10.8 to solve for X_B. The association term is subsequently solved but in order to iteratively solve for the volume EQ 10.1, the volume partial derivatives also need to be determined. Therefore:

$$p\left(\Delta^{AB},\Delta^{AC},V\right)=\frac{\left(\Delta^{AB}-\Delta^{AC}\right)-\frac{n_1}{V}\left(\Delta^{AC}\right)^2+\frac{n_2}{V}\Delta^{AC}\left(\Delta^{AC}-2\Delta^{AB}\right)}{\frac{n_2}{V}\Delta^{AC}\left(\Delta^{AB}-\Delta^{AC}\right)}$$

$$\therefore \frac{\partial p}{\partial V}=\left[\left(\frac{\partial p}{\partial \Delta^{AB}}\right)_{\Delta^{AC},V}\frac{\partial \Delta^{AB}}{\partial V}\right]+\left[\left(\frac{\partial p}{\partial \Delta^{AC}}\right)_{\Delta^{AB},V}\frac{\partial \Delta^{AC}}{\partial V}\right]+\left[\left(\frac{\partial p}{\partial V}\right)_{\Delta^{AB},\Delta^{AC}}\right]$$

EQ 10.23

$$\begin{aligned}\left(\frac{\partial p}{\partial V}\right)_{\Delta^{AB},\Delta^{AC}}&=\frac{\partial}{\partial V}\left(\frac{\left(\Delta^{AB}-\Delta^{AC}\right)-\frac{n_1\left(\Delta^{AC}\right)^2}{V}+\frac{n_2\Delta^{AC}\left(\Delta^{AC}-2\Delta^{AB}\right)}{V}}{\frac{n_2\Delta^{AC}\left(\Delta^{AB}-\Delta^{AC}\right)}{V}}\times\frac{V}{V}\right)\\&=\frac{\partial}{\partial V}\left(\frac{\left(\Delta^{AB}-\Delta^{AC}\right)V}{n_2\Delta^{AC}\left(\Delta^{AB}-\Delta^{AC}\right)}-\frac{n_1\left(\Delta^{AC}\right)^2}{n_2\Delta^{AC}\left(\Delta^{AB}-\Delta^{AC}\right)}+\frac{n_2\Delta^{AC}\left(\Delta^{AC}-2\Delta^{AB}\right)}{n_2\Delta^{AC}\left(\Delta^{AB}-\Delta^{AC}\right)}\right)\\&=\frac{1}{n_2\Delta^{AC}}\end{aligned}$$

EQ 10.24

$$\begin{aligned}\left(\frac{\partial p}{\partial \Delta^{AB}}\right)_{\Delta^{AC},V}&=\frac{\partial}{\partial \Delta^{AB}}\left(\frac{\left(\Delta^{AB}-\Delta^{AC}\right)-\frac{n_1\left(\Delta^{AC}\right)^2}{V}+\frac{n_2\Delta^{AC}\left(\Delta^{AC}-2\Delta^{AB}\right)}{V}}{\frac{n_2\Delta^{AC}\left(\Delta^{AB}-\Delta^{AC}\right)}{V}}\times\frac{\left(\Delta^{AB}-\Delta^{AC}\right)}{\left(\Delta^{AB}-\Delta^{AC}\right)}\right)\\&=\frac{\partial}{\partial \Delta^{AB}}\left(\frac{1-\frac{n_1\left(\Delta^{AC}\right)^2}{V\left(\Delta^{AB}-\Delta^{AC}\right)}+\frac{n_2\Delta^{AC}\left(\Delta^{AC}-2\Delta^{AB}\right)}{V\left(\Delta^{AB}-\Delta^{AC}\right)}}{\frac{n_2\Delta^{AC}}{V}}\right)\\&=\frac{V}{n_2\Delta^{AC}}\times\frac{\partial}{\partial \Delta^{AB}}\left(1+\frac{n_1\left(\Delta^{AC}\right)^2+n_2\left(\Delta^{AC}\right)^2-2n_2\Delta^{AC}\Delta^{AB}}{V\Delta^{AB}-V\Delta^{AC}}\right)\end{aligned}$$

using the quotient rule, this becomes:

$$\left(\frac{\partial p}{\partial \Delta^{AB}}\right)_{\Delta^{AC},V} = \frac{V}{n_2\Delta^{AC}} \times \left(\frac{-2n_2\Delta^{AC}V\left(\Delta^{AB}-\Delta^{AC}\right) - \left(n_1\left(\Delta^{AC}\right)^2 + n_2\left(\Delta^{AC}\right)^2 - 2n_2\Delta^{AC}\Delta^{AB}\right)V}{V^2\left(\Delta^{AB}-\Delta^{AC}\right)^2} \right)$$

$$= \frac{-2n_2\left(\Delta^{AB}-\Delta^{AC}\right) - n_1\left(\Delta^{AC}\right) + n_2\left(\Delta^{AC}\right) - 2n_2\Delta^{AB}}{n_2\left(\Delta^{AB}-\Delta^{AC}\right)^2}$$

$$= \frac{\Delta^{AC}\left(3n_2 - n_1\right)}{n_2\left(\Delta^{AB}-\Delta^{AC}\right)^2}$$

EQ 10.25

$$\left(\frac{\partial p}{\partial \Delta^{AC}}\right)_{\Delta^{AC},V} = \frac{\partial}{\partial \Delta^{AC}} \left(\frac{\left(\Delta^{AB}-\Delta^{AC}\right) - \frac{n_1\left(\Delta^{AC}\right)^2}{V} + \frac{n_2\Delta^{AC}\left(\Delta^{AC}-2\Delta^{AB}\right)}{V}}{\frac{n_2\Delta^{AC}\left(\Delta^{AB}-\Delta^{AC}\right)}{V}} \times \frac{\Delta^{AC}\left(\Delta^{AB}-\Delta^{AC}\right)}{\Delta^{AC}\left(\Delta^{AB}-\Delta^{AC}\right)} \right)$$

$$= \frac{\partial}{\partial \Delta^{AC}} \left(\frac{\frac{1}{\Delta^{AC}} - \frac{n_1\Delta^{AC} - n_2\Delta^{AC} + 2n_2\Delta^{AB}}{V\left(\Delta^{AB}-\Delta^{AC}\right)}}{\frac{n_2}{V}} \times \frac{\frac{n_2}{V}}{\frac{n_2}{V}} \right)$$

$$= \frac{\partial}{\partial \Delta^{AC}} \left(\frac{V}{n_2\Delta^{AC}} - \frac{n_1\Delta^{AC} - n_2\Delta^{AC} + 2n_2\Delta^{AB}}{n_2\left(\Delta^{AB}-\Delta^{AC}\right)} \right)$$

$$= -\frac{V}{n_2\left(\Delta^{AC}\right)^2} - \frac{\left(n_1-n_2\right)n_2\left(\Delta^{AB}-\Delta^{AC}\right) - n_2\left(n_1\Delta^{AC} - n_2\Delta^{AC} + 2n_2\Delta^{AB}\right)}{n_2\left(\Delta^{AB}-\Delta^{AC}\right)}$$

$$= -\frac{V}{n_2\left(\Delta^{AC}\right)^2} - \frac{\left(n_1-n_2\right)\left(\Delta^{AB}-\Delta^{AC}\right) - \Delta^{AC}\left(n_1+n_2\right) + 2n_2\Delta^{AB}}{\left(\Delta^{AB}-\Delta^{AC}\right)}$$

$$= -\frac{V}{n_2\left(\Delta^{AC}\right)^2} - \frac{n_1\Delta^{AB} - n_1\Delta^{AC} - n_2\Delta^{AB} + n_2\Delta^{AC} - \Delta^{AC}\left(n_1+n_2\right) + 2n_2\Delta^{AB}}{\left(\Delta^{AB}-\Delta^{AC}\right)}$$

$$= -\frac{V}{n_2\left(\Delta^{AC}\right)^2} - \frac{n_1\left(\Delta^{AB}-2\Delta^{AC}\right) + n_2\Delta^{AB}}{\left(\Delta^{AB}-\Delta^{AC}\right)}$$

EQ 10.26

Using EQ 10.24, EQ 10.25 and EQ 10.26 and substituting into EQ 10.6 such that

$$\frac{\partial \Delta^{AB}}{\partial \mathrm{V}} = \frac{\partial \Delta^{AB}}{\partial \mathrm{g}} \cdot \frac{\partial g}{\partial \eta} \cdot \frac{\partial \eta}{\partial \mathrm{V}}$$

And then volume partial derivative of p is found by EQ 10.23

Similarly, q derived by:

$$q\left(\Delta^{AB},\Delta^{AC},V\right)=\frac{\Delta^{AC}-2\Delta^{AB}+\frac{n_2}{V}\Delta^{AC}\Delta^{AB}}{\frac{n_2}{V}\Delta^{AC}\left(\Delta^{AB}-\Delta^{AC}\right)}$$

$$\therefore \frac{\partial q}{\partial V}=\left[\left(\frac{\partial q}{\partial \Delta^{AB}}\right)_{\Delta^{AC},V}\frac{\partial \Delta^{AB}}{\partial V}\right]+\left[\left(\frac{\partial q}{\partial \Delta^{AC}}\right)_{\Delta^{AB},V}\frac{\partial \Delta^{AC}}{\partial V}\right]+\left[\left(\frac{\partial q}{\partial V}\right)_{\Delta^{AB},\Delta^{AC}}\right]$$

EQ 10.27

With the summarised formulas given here:

$$\left(\frac{\partial q}{\partial V}\right)_{\Delta^{AB},\Delta^{AC}}=\frac{1}{n_2\left(\Delta^{AB}-\Delta^{AC}\right)}$$

EQ 10.28

$$\left(\frac{\partial q}{\partial \Delta^{AB}}\right)_{V,\Delta^{AC}}=\frac{V-n_2\Delta^{AC}}{n_2\left(\Delta^{AB}-\Delta^{AC}\right)^2}$$

EQ 10.29

$$\left(\frac{\partial q}{\partial \Delta^{AC}}\right)_{V,\Delta^{AB}}=\frac{V}{n_2}\times\left(\frac{1+\left(n_2\right)^2\Delta^{AB}+2\left(\frac{\Delta^{AB}}{\Delta^{AC}}\right)^2-4\frac{\Delta^{AB}}{\Delta^{AC}}}{\left(\Delta^{AB}-\Delta^{AC}\right)^2}\right)$$

EQ 10.30

And r is derived by:

$$r\left(\Delta^{AB},\Delta^{AC},V\right)=\frac{\Delta^{AB}}{\frac{n_2}{V}\Delta^{AC}\left(\Delta^{AB}-\Delta^{AC}\right)}$$

$$\therefore \frac{\partial r}{\partial V}=\left[\left(\frac{\partial r}{\partial \Delta^{AB}}\right)_{\Delta^{AC},V}\frac{\partial \Delta^{AB}}{\partial V}\right]+\left[\left(\frac{\partial r}{\partial \Delta^{AC}}\right)_{\Delta^{AB},V}\frac{\partial \Delta^{AC}}{\partial V}\right]+\left[\left(\frac{\partial r}{\partial V}\right)_{\Delta^{AB},\Delta^{AC}}\right]$$

EQ 10.31

$$\left(\frac{\partial r}{\partial V}\right)_{\Delta^{AB},\Delta^{AC}}=\frac{\Delta^{AB}}{n_2\Delta^{AC}\left(\Delta^{AB}-\Delta^{AC}\right)}$$

EQ 10.32

$$\left(\frac{\partial r}{\partial \Delta^{AB}}\right)_{V,\Delta^{AC}}=\frac{-V}{n_2\left(\Delta^{AB}-\Delta^{AC}\right)^2}$$

EQ 10.33

$$\left(\frac{\partial r}{\partial \Delta^{AC}}\right)_{V,\Delta^{AB}} = \frac{V\Delta^{AB}}{n_2}\frac{2\Delta^{AC}-\Delta^{AB}}{\left(\Delta^{AC}\right)^2\left(\Delta^{AB}-\Delta^{AC}\right)^2}$$

EQ 10.34

With the volume partial derivatives of p, q and r known, the following derivatives are calculated:

$$\frac{\partial Q}{\partial V} = \frac{2p}{9}\frac{\partial p}{\partial V} - \frac{1}{3}\frac{\partial q}{\partial V}$$

EQ 10.35

$$\frac{\partial R}{\partial V} = \frac{6p^2-9q}{54}\left(\frac{\partial p}{\partial V}\right) - \frac{p}{6}\left(\frac{\partial q}{\partial V}\right) + \frac{1}{2}\left(\frac{\partial r}{\partial V}\right)$$

EQ 10.36

If $Q^3 - R^2 \geq 0$

The derivative of arc cos (x) is given by (Weisstein, 1999-2013):

$$\frac{d}{dx}\left(\arccos(x)\right) = -\frac{1}{\sqrt{1-x^2}}$$

EQ 10.37

Therefore the partial derivatives for θ is calculated by:

$$\frac{\partial \theta}{\partial R} = -\frac{1}{\sqrt{Q^3-R^2}}$$

EQ 10.38

$$\frac{\partial \theta}{\partial Q} = \frac{3R}{2\sqrt{Q^5-Q^2R^2}}$$

EQ 10.39

The partial derivatives for EQ 10.17, EQ 10.18 and EQ 10.19 are calculated by:

$$\frac{\partial X_{C1}}{\partial V} = \frac{-1}{\sqrt{Q}}\cos\left(\frac{\theta}{3}\right)\cdot\frac{\partial Q}{\partial V} + \frac{2}{3}\sqrt{Q}\sin\left(\frac{\theta}{3}\right)\cdot\frac{\partial \theta}{\partial V} - \frac{1}{3}\cdot\frac{\partial p}{\partial V}$$

EQ 10.40

$$\frac{\partial X_{C2}}{\partial V} = \frac{-1}{\sqrt{Q}}\cos\left(\frac{\theta+2\pi}{3}\right)\cdot\frac{\partial Q}{\partial V} + \frac{2}{3}\sqrt{Q}\sin\left(\frac{\theta+2\pi}{3}\right)\cdot\frac{\partial \theta}{\partial V} - \frac{1}{3}\cdot\frac{\partial p}{\partial V}$$

EQ 10.41

$$\frac{\partial X_{C3}}{\partial V} = \frac{-1}{\sqrt{Q}}\cos\left(\frac{\theta+4\pi}{3}\right)\cdot\frac{\partial Q}{\partial V} + \frac{2}{3}\sqrt{Q}\sin\left(\frac{\theta+4\pi}{3}\right)\cdot\frac{\partial \theta}{\partial V} - \frac{1}{3}\cdot\frac{\partial p}{\partial V}$$

EQ 10.42

EQ 10.40, EQ 10.41 and EQ 10.42 are quite similar. For the sake of argument, assume that X_{C1} is the solution in this case. Then the analytical volume partial derivative of the reduced residual Helmholtz energy is given by:

$$F^{assoc}\left(X_A, X_B, X_C\right) = n_1\left(\ln X_A - \frac{X_A}{2} + \ln X_B - \frac{X_B}{2} + 1\right) + n_2\left(\ln X_C - \frac{X_C}{2} + \frac{1}{2}\right)$$

$$\therefore \left(\frac{\partial F}{\partial V}\right) = n_1\left(\frac{1}{X_A} - \frac{1}{2}\right)\frac{\partial X_A}{\partial V} + n_1\left(\frac{1}{X_B} - \frac{1}{2}\right)\frac{\partial X_B}{\partial V} + n_2\left(\frac{1}{X_C} - \frac{1}{2}\right)\frac{\partial X_C}{\partial V}$$

EQ 10.43

Finally, in order to solve EQ 10.43 two more partial derivatives are required:

$$\frac{\partial X_A}{\partial V} = \frac{-n_2\Delta^{AC}}{V\left(1 + \frac{1}{V}\left(n_1 X_B \Delta^{AB} + n_2 X_C \Delta^{AC}\right)\right)^2}\cdot\frac{\partial X_C}{\partial V} + \frac{n_1 X_B \Delta^{AB} + n_2 X_C \Delta^{AC}}{\left(V + n_1 X_B \Delta^{AB} + n_2 X_C \Delta^{AC}\right)^2}$$

$$-\frac{V}{n_2\left(\Delta^{AC}\right)^2}\left(\frac{1}{X_C} - 1\right)\cdot\frac{\partial \Delta^{AC}}{\partial V}$$

EQ 10.44

$$\frac{\partial X_B}{\partial V} = \frac{-n_1\Delta^{AB}}{V\left(1 + \frac{1}{V}\left(n_1 X_A \Delta^{AB}\right)\right)^2}\cdot\frac{\partial X_A}{\partial X_C}\cdot\frac{\partial X_C}{\partial V} + \frac{n_1 X_A \Delta^{AB}}{\left(V + n_1 X_A \Delta^{AB}\right)^2} + \frac{n_1 X_A \Delta^{AB}}{\left(V + n_1 X_A \Delta^{AB}\right)^2}\cdot\frac{\partial \Delta^{AB}}{\partial V}$$

EQ 10.45

Alternatively if $Q^3 - R^2 < 0$, the following calculations are required after EQ 10.36

$$\frac{\partial S}{\partial R} = 2R\left(\frac{1}{2\sqrt{R^2 - Q^3}} + 1\right)\left(\sqrt{R^2 - Q^3} + |R|\right)^{-2/3}$$

EQ 10.46

$$\frac{\partial S}{\partial Q} = \frac{-Q^2}{2\sqrt{R^2 - Q^3}}\left(\sqrt{R^2 - Q^3} + |R|\right)^{-2/3}$$

EQ 10.47

And as before, EQ 10.46 and EQ 10.47 are combined with EQ 10.35 and EQ 10.36 to yield:

$$\frac{\partial S}{\partial V} = \frac{\partial S}{\partial R}\frac{\partial R}{\partial V} + \frac{\partial S}{\partial Q}\frac{\partial Q}{\partial V}$$

EQ 10.48

The new volume partial derivative of X_c is then obtained by:

$$\frac{\partial X_C}{\partial V} = -sign(R)\left(1 - \frac{Q}{S^2}\right)\frac{\partial S}{\partial V} - \frac{sign(R)}{S}\frac{\partial Q}{\partial V} - \frac{1}{3}\frac{\partial p}{\partial V}$$

EQ 10.49

EQ 10.49 is then substituted into EQ 10.43 as for the previous case.

10.8.5 Brief description of the method for calculating the volume and regression of new parameters

Since the monomer fraction can now be calculated directly, a single iterative loop can be established to immediately calculate the volume for a given temperature and pressure. For this loop, volume is iterated until the calculated pressure is equal to the experimental pressure.

To fit new regression parameters, a second outer iterative loop is set up with the chosen parameters for the regression used as variables. In this case, the chosen experimental data were then used in the error calculation.

This analytical method can necessarily be expanded for any combination of association schemes, although more general iterative methods have proven to be successful.

10.9 Nomenclature

10.9.1 General symbols

Table 65: Important symbols

Symbol	Description
A	Absorbance area OR Helmholtz free energy
a^{assoc}	Part of a^r due to site-site interactions such as hydrogen bonds
a^{chain}	Part of a^r due to chain forming bonds between segments
a^{disp}	Dispersion interactions segments
a^{hs}	A type of segment-segment interaction between hard spheres
a_i ; b_i; c_i	Fitted parameters used polar term or dispersion term integrals
a, b	Lorentzian and Gaussian widths
a^r	Residual Helmholtz energy
a^{seg}	Part of a^r made up of segment to segment interactions
C	Concentration OR a constant set to 0.12 for T-dependent diameter
$\hat{c}_A$	Stoichiometric alcohol concetration
d	distance OR diameter
d_P	Penetration depth for an ATR evanescent wave
g(d)	Radial distribution function
h	Segment width in Simpson's Rule
ii	Refers to an interaction between components of the same type
ij	Refers to an interaction between components of different types
I_1	First integral in a^{disp}
I_2	Second integral in a^{disp}
$\underline{K}$	Equilibrium constants
k	Boltzman's constant
m	Segment number parameter OR number of peak-to-peak fringes
M	Number of association sites per molecule
N	Number of molecules
n	Material refractive index
n_P	Number of polar segments (GV formulation)
r	Radius
s	Soft repulsion parameter with CK formalism
T	Temperature
u(r)	Pair potential function
v^0	Close-packed hard core volume
v^∞	Temperature-independent soft-core volume
$\tilde{\nu}$	Wavenumber
v_i	Regression weights
v_1	Asymmetric stretch spectral assignment
v_3	Symmetric stretch spectral assignment
x	Mole fraction (usually refers to that of the solute)
X_P	Fraction of polar segments (JC formulation)

X_1	Monomer fraction of component 1
X^A	Fraction molecules not bonded at site A
Z	Compressibility factor
α	Absorbance coefficient OR Gaussian fraction
Δ^{AB}	Association strength between sites A and B
ε^{AB}	Association energy parameter between sites A and B
ε_i	Dispersion energy parameter
η	Reduced density
κ^{AB}	Association volume parameter
ρ	Molar density
λ	Reduced well width within CK formalism OR wavelength
σ	Segment diameter parameter
μ^0	Dispersion energy parameter in SAFT-HR
ξ	Quasi-packing factor for mixtures of hard spheres
···	Intermolecular hydrogen bond
-	Single intramolecular bond
=	Double intramolecular bond

10.9.2 Acronyms

Table 66: List of acronyms used in this research

Acronym	Description
1PrOH	1-propanol
2PrOH	2-propanol
2B	Association scheme with 1 positive and 1 negative site
2C	Association scheme with 1 negative and 1 bipolar site
2D	Two-dimensional
3B	Association scheme with 1 positive and 2 negative sites
5GL	Function: sum of 5 Gauss-Lorentz functions
%AAD	Percentage average absolute deviation
AcO	Acetone
Adj - R^2	Adjusted coefficient of determination
As	Refers to the method/data of Asprion *et al.* (2001)
ATR	Attenuated Total Reflectance
AU	Absorbance units
BACK	Boublik-Alder-Chen-Kreglewski EoS
CK-SAFT	SAFT (Chen and Kreglewski)
DGTS	Deuterated triglycine sulphate
EN	electronegativity
EQ	Equation
EoS	Equation of State
EtOH	Ethanol
FIR	far-infrared

FT	Fourier Transform
FTIR	Fourier Transform Infrared spectroscopy
GL	Gauss-Lorentz from
GV	Gross and Vrabec: refers to a polar term in SAFT
H-bond	Hydrogen bond
IR	Infrared
JC	Jog and Chapman: refers to a polar term in SAFT
LJ	Lennard-Jones
MCT	Mercury Cadmium Telluride (detector)
MCT High-D*	Specific type of MCT detector with a very good resolution
MeOH	Methanol
MIR	mid-infrared
N	Association scheme with 1 negative site
2N	Association scheme with 2 negative sites
NIR	near-infrared
NRHB	Non-random hydrogen bonding (EoS)
OMNIC	Spectral processing package from Nicolet
PCP-SAFT	Polar PC-SAFT (uses JC term)
PC-PSAFT	PC – Polar SAFT (used GV term)
PC-SAFT	Perturbed Chain - Statistical Associating Fluid Theory
RDF	Radial distribution function
SAFT	Statistical Associating Fluid Theory
SAFT-HR	Statistical Associating Fluid Theory (Huang and Radosz)
sPC-SAFT	Simplified PC-SAFT
sPC-SAFT+GV	Combination EoS with GV polar term
sPC-SAFT+JC	Combination EoS with JC polar term
SSE	Summed squared error
TPT	Thermodynamic Perturbation Theory
vS	Refers to the method/data of von Solms *et al.* (2007)